Cardiac-Sympathetic Dysfunction in Hypertension

Emma N. Bardsley



Thesis presented for the degree of

Doctor of Philosophy

at the University of Oxford

Supervisor: David J. Paterson

Merton College

Trinity Term 2018

Abstract

Cardiac-Sympathetic Dysfunction in Hypertension
Thesis presented for the degree of *Doctor of Philosophy* at the University of Oxford.
Emma Nicole Bardsley, Merton College, Trinity Term, 2018.

The work presented in this thesis examined the cellular and molecular phenotypes associated with sympathetic over-activity in the initiation and progression of hypertension in the prehypertensive spontaneously hypertensive rat (preSHR) and spontaneously hypertensive rat (SHR), with validation of key molecular pathways in human stellate ganglia.

Chapter One provided an overview of the short and long-term regulation of arterial blood pressure. This chapter focussed specifically on the role of the sympathetic nervous system as a primary causative factor in the aetiology of hypertension, and presented evidence highlighting a critical role for impaired cyclic nucleotide signalling in sympathetic over-activity.

Chapter Two detailed the methodology utilised in each chapter of this thesis. Specifically, sympathetic neuronal culturing and Förster Resonance Energy Transfer (FRET) were used to measure intracellular cyclic nucleotide generation and protein kinase activity. This chapter also included a comprehensive description of an RNA sequencing analysis pipeline, intracellular Ca^{2+} imaging, immunofluorescence, protein assays, enzyme activity assays, electrical field stimulation and high-pressure liquid chromatography with electrochemical detection.

Chapter Three examined the transcriptome of the stellate ganglia from the SHR compared to its normotensive Wistar counterpart. Differentially expressed genes were reported and individual genes were grouped into gene families and enriched pathways to provide functional relevance. The over-represented molecular function gene ontology families included ligand-gated ion channels and regulation of phosphodiesterase signalling. The expression of key genes was confirmed in human stellate ganglia for physiological context.

Chapter Four investigated the role of presynaptic beta-adrenergic signalling as a mediator of elevated neurotransmission in the preSHR stellate ganglia. Neuronal cAMP-PKA-Ca^{2+} signalling pathways coupled to beta-adrenergic receptors were measured and found to be elevated in prehypertension. The beta-2-adrenoceptor was shown to play a dominant role. The expression of presynaptic beta adrenoceptors was also observed in human stellate ganglia.

Chapter Five examined the profile of catecholamines synthesised in the cardiac-sympathetic stellate ganglia of preSHR and their healthy counterparts. Noradrenaline released from the preSHR ganglia was elevated compared to Wistar. Moreover, the synthesis of adrenaline was observed, where the concentration of adrenaline released from the preSHR ganglia was also elevated. The enzyme involved in adrenaline synthesis was observed in human stellate ganglia.

Chapter Six highlighted a role for intracrine angiotensin synthesis in the cardiac-sympathetic stellate ganglia of preSHR and SHR alongside their healthy counterparts. The receptors for AngII and Ang1-7 were identified on rat and human stellate ganglia. In preSHR stellate ganglia, the synthesis of AngII and Ang1-7 were elevated, whereas in young preSHR stellates, electrically-evoked concentrations of AngII were not elevated compared to Wistar. In adult SHR stellate ganglia, the synthesis of AngII was elevated, however, the synthesis of the Ang1-7 peptide was no longer increased. This occurred alongside a concomitant elevation in electrically-evoked AngII from adult SHR stellate ganglia.

Chapter Seven provided a concluding discussion and summarised the main observations in this thesis with a focus on wider physiological context. Chapter seven also discussed the implications of the findings described, with an emphasis on the potential future avenues of research within the field of neurogenic hypertension.

List of Publications

Original Manuscripts Contributing to this Thesis

1. **Bardsley EN**, Davis H, Buckler KJ, Paterson DJ. Neurotransmitter switching coupled to β-adrenergic signaling in sympathetic neurons in prehypertensive states. *Hypertension*. 2018;71(6):1226-1238 doi:10.1161/HYPERTENSIONAHA.118.10844
2. **Bardsley EN**, Davis H, Ajijola OA, Buckler KJ, Ardell JL, Shivkumar K, Paterson DJ. RNA Sequencing Reveals Novel Transcripts from Sympathetic Stellate Ganglia During Cardiac Sympathetic Hyperactivity. *Sci Rep*. 2018;8:8633 doi:10.1038/s41598-018-26651-7.
3. **Bardsley EN**, Larsen HE, Paterson DJ. Impaired cAMP-cGMP cross-talk during cardiac sympathetic dysautonomia. *Channels (Austin)*. 2017;11(3):178-180. doi:10.1080/19336950.2016.1259040.
4. Larsen HE, **Bardsley EN**, Lefkimmiatis K, Paterson DJ. Dysregulation of neuronal Ca^{2+} channel linked to heightened sympathetic phenotype in prohypertensive states. *J Neurosci*. 2016;36(33):8562-8573. doi:10.1523/JNEUROSCI.1059-16.2016.
5. Davis H, **Bardsley EN**, Paterson DJ. Transcriptional profiling of stellate ganglia from normotensive and spontaneously hypertensive rat strains.*Sci Data*.2018;5:18023. doi:10.1038/sdata.2018.123.
6. **Bardsley EN**, Paterson DJ. Neurocardiac regulation: From Cardiac Mechanisms to Novel Therapeutic Approaches. *J Physiol (Lond)* 2018. doi:10.1113/JP276962.
7. **Bardsley EN**, Paterson DJ. Sympathetic Neurons Synthesize Angiotensins. Implications for Cardiac Excitability. *JMCC*. 2019 (*in Review*)

Awards and Conference Abstracts

Merton College Graduate Prize Scholarship: 2017

OXION Wellcome Trust Annual Symposium: Poster award first place 2016

BHF CRE Annual Research Symposium: Poster award runner up 2016

MSDTC Annual Research Symposium: Poster award runner up 2015

Merton College Travel Award Recipient: 2015, 2016, 2017, 2018

British Pharmacological Society Travel Award Recipient: 2016, 2017

British Pharmacological Society Travel Award Recipient: 2016, 2017

1. **Bardsley EN**, Davis H, Buckler KJ, Paterson DJ. Neurotransmitter switching in sympathetic neurons coupled to beta-adrenergic signalling in hypertensive states. *The FASEB Journal*. 2018. doi:10.1096/fasebj.2018.32.1_supplement.591.1.
2. **Bardsley EN**, Davis H, Bayles R, Habecker BA, Paterson DJ. Stellate transcriptomics reveal consistent patterns of gene expression across species. *The FASEB Journal*. 2018;32(1_supplement):918.3-918.3. doi:10.1096/fasebj.2018.32.1_supplement.918.3.
3. **Bardsley EN**, Davis H, Ajijola OA, et al. Identification of novel mRNA transcripts in the sympathetic stellate ganglia using RNA sequencing. *The FASEB Journal*. 2018;32(1_supplement):596.4-596.4. doi:10.1096/fasebj.2018.32.1_supplement.596.4.
4. **Bardsley E**, Paterson DJ. Impaired cyclic nucleotide signalling in pre-hypertensive spontaneously hypertensive rats: a dichotomy of pathways? *The FASEB Journal*. 2016;30(1 Supplement):1006.5-1006.5. doi:doi/10.1096/fasebj.30.1_supplement.1006.5.

5. **Bardsley EN**, Paterson DJ. Sympathetic beta-adrenergic signalling exacerbates dysautonomia in hypertension. BHF Centre of Research Excellence and EPSRC Centre for Mathematics of Precision Healthcare. The Heart - Models, Measurements, Medicine. 2017.
6. **Bardsley EN**, Davis H, Paterson DJ. Identification of novel signalling pathways in the sympathetic stellate ganglia from the spontaneously hypertensive rat by RNA-seq. *British Heart Foundation Centre of Research Excellence Annual Research Symposium*. 2017.
7. **Bardsley EN**, Davis H, Paterson DJ. Impaired adrenergic signalling exacerbates dysautonomia in hypertension. *Sherrington Talks*. 2017.
8. **Bardsley EN**, Davis H, Paterson DJ. Do beta adrenergic blockers also work via the peripheral sympathetic nervous system? *International Union Of Physiological Sciences (IUPS)*. 2017.
9. **Bardsley EN**, Paterson DJ. Impaired cyclic nucleotide signalling. Does pathway divergence drive disease? *UCLA Sparc Seminar*. 2016.
10. **Bardsley EN**, Paterson DJ. Presynaptic beta-adrenergic signalling exacerbates neuronal calcium dysfunction in hypertension. *OXION Wellcome Trust Annual Symposium*. 2016.
11. **Bardsley EN**, Lefkimmiatis K, Paterson DJ. Impaired cyclic nucleotide signalling in pro-hypertensive spontaneously hypertensive rats: a dichotomy of pathways. *Medical Science Doctoral Training Centre DPhil Day*. 2016.
12. **Bardsley EN**, Paterson DJ. Beta adrenergic blockers affect the peripheral sympathetic nervous system. *British Heart Foundation Centre of Research Excellence Annual Research Symposium*. 2016.
13. **Bardsley EN**, Paterson DJ. cAMP and PKA hyperactivity in sympathetic stellate neurons from pre- and pro- spontaneously hypertensive rats: a molecular marker? *International Society for Autonomic Neuroscience (ISAN)*. 2015.

Acknowledgements

There are so many people who deserve my thanks and gratitude for enabling me to complete my DPhil.

I would like to acknowledge the Wellcome Trust and in particular the OXION programme for funding my four-year DPhil studentship and for supporting this research. Thanks also to Merton College and the British Pharmacological Society for awarding me funding and grants to attend several international conferences to present the work described herein.

My sincerest thanks to Professor David J. Paterson, who gave me the opportunity to join his research group, and for making it possible for me to come to Oxford. I would like to express my sincerest gratitude for the freedom you gave me to explore numerous different research questions, as well as the insight you provided that helped to explain the often-unexpected results. I thoroughly enjoyed working together and without your unwavering support, patience and laid-back approach to life and work, my Dphil would not have been possible.

To Peter, my partner and best friend, whom I would never have met if I hadn't come to Oxford. Thank you for the love and kindness you show every day. For the many hours you have spent listening to me and offering advice. For your relentless sense of humour and optimism that never fail to cheer me up. Most of all, thank you for believing in me.

To my parents, for encouraging me to follow my dreams. I wouldn't be here today without your unwavering love and support.

Dedication

For my Mum and Dad

Thesis Contributions

Statement of Contributions to this Thesis

The planning, design, experimental work, analysis and interpretation of the results in this thesis were carried out by me. I would, however, like to acknowledge the help provided by others.

Chapter Two

I would like to thank Dr. Julia A. Shanks for sharing her expertise and for teaching me the neuronal culture protocol. I would like to acknowledge Dr. Dan Li for teaching me how to use the OptoFluo software utilised for recording the FRET data in this thesis. In addition, I would like to acknowledge Dr. Andreas Koschinski for his technical advice and assistance involving the initial setup for the FRET rig and for showing me how to align the DV2 beam splitter. Dr. Koschinski also provided the Chinese Hamster Ovary cells used to investigate the dynamic range of Epac1-H187, corresponding to Figure 2.6. I would like to thank Dr. Konstantinos Lefkimmiatis for developing the Epac1-H187 vector that was used throughout this thesis. In addition, I would like to acknowledge the UCLA Autonomic Group, Dr. K. Shivkumar, Dr. J. Ardell and Dr. A. Olujimi, for extracting and shipping the human donor stellates.

Chapter Three

The RNA sequencing parameters were based on recommendations by the Wellcome Trust Centre for Human Genomics (WTCHG). The WTCHG also conducted the library preparation and the RNA sequencing. The RNA sequencing analysis pipeline was planned by me and Harvey Davis, for which he is second author on a paper published in Scientific Reports (2016). In order to optimise this protocol, Harvey Davis carried out a comprehensive optimisation of the analysis protocol, trialling and troubleshooting the Tuxedo suite comprising Bowtie, TopHat and Cufflinks. We both tested an alternative analysis involving HiSat2, Stringtie and Ballgown. Upon release of the Salmon quasi-mapping tool, Harvey and I independently carried out the Salmon quasi-mapping pipeline and DESeq2 differential expression analysis to ensure accurate results. Harvey also contributed to troubleshooting this analysis and helped to sterilise my instruments during the RNA extractions. I would also like to acknowledge Dr. Konstantinos Lefkimmiatis for his technical advice regarding the phosphodiesterase FRET experiments carried out in this chapter.

Chapter Four

In Chapter Four, Harvey Davis used FRET microscopy to measure cAMP in four of the cells stimulated by salbutamol, contributing to Figure 4.8. I would also like to acknowledge Dr. Andrew Jefferson of the Micron Facility in the Biochemistry Department for his technical training that enabled me to use the Confocal Microscope and Zen Software for capturing the immunofluorescence images.

Chapter Five

In Chapter Five, Harvey Davis conducted the electrical stimulation experiments and total catecholamine experiments corresponding to Figures 5.4 and 5.5. In addition, Harvey optimised the mobile phase to detect both noradrenaline and adrenaline within the same stellate samples using HPLC-EC. I would also like to thank Dr. Sarah Threlfell for her technical advice regarding the optimisation of the HPLC-EC protocol, for her expertise using the CLARITY software, and for sharing equipment and consumables. I would also like to acknowledge Dr. Keith J. Buckler for teaching me how to measure intracellular Calcium with Indo-1AM using the Nikon microscope, and for instructing me how to conduct the ionomycin calcium calibration, as well as providing me with full use of his lab.

Chapter Six

In Chapter Six, Peter M. Sloan helped me to carry out the RNA extractions for young and adult rats, corresponding to Figures 6.2, 6.7 and 6.12.

List of Abbreviations

αAR	Alpha Adrenergic Receptor
AC	Adenylyl Cyclase
ACE	Angiotensin Converting Enzyme
Adr	Adrenaline
Agt	Angiotensinogen
ANS	Autonomic Nervous System
Ang1-7	Angiotensin 1-7
AngII	Angiotensin II
ATR	Angiotensin II Receptor
βAR	Beta Adrenergic Receptor
BP GO	Biological Processes Gene Ontology
Ca^{2+}	Calcium
$[Ca^{2+}]_i$	Intracellular Calcium
cAMP	3',5'-Cyclic Adenosine Monophosphate
CC GO	Cellular Component Gene Ontology
cGMP	3,'5'-Cyclic Guanosine Monophosphate
cN	Cyclic Nucleotide
CNS	Central Nervous System
CO	Cardiac Output
CVLM	Caudal Ventrolateral Medulla
DBH	Dopamine Beta Hydroxylase
DDC	L-DOPA Decarboxylase
DOB	Dobutamine
EDRF	Endothelium Derived Relaxing Factor
EIA	Enzyme Immunoassay
ELISA	Enzyme-Linked Immunosorbent Assay
eNOS/NOS3	Endothelial Nitric Oxide Synthase
ER	Endoplasmic Reticulum
FRET	Förster Resonance Energy Transfer
GO	Gene Ontology
GPCR	G-Protein Coupled Receptor
GWAS	Genome Wide Association Studies
IBMX	3-Isobutyl-1-Methylxanthine
I_{CaN}	N-Type Calcium Channel
iNOS/NOS2	Inducible Nitric Oxide Synthase
IML	Intermediolateral Column
ISO	Isoprenaline

KEGG	Kyoto Encyclopedia of Genes and Genomes
2K1C	Two-Kidney One-Clip
MET	Metoprolol
MF GO	Molecular Function Gene Ontology
N.A	Nucleus Ambiguus
NA	Noradrenaline
NET	Norepinephrine Transporter
nNOS/NOS1	Neuronal Nitric Oxide Synthase
NO	Nitric Oxide
NOS	Nitric Oxide Synthase
NTS	Nucleus Tractus Solitarius
PAG	Periaqueductal Gray
PDE	Phosphodiesterase
PGSN	Post-Ganglionic Sympathetic Neuron
PKA	Protein Kinase A
PKG	Protein Kinase G
PNMT	Phenylethanolamine N-Methyltransferase
preSHR	Prehypertensive Spontaneously Hypertensive Rat
qRT-PCR	Quantitative Real-Time Polymerase Chain Reaction
RAAS	Renin-Angiotensin-Aldosterone System
RAS	Renin-Angiotensin System
Ren	Renin
RVLM	Rostral Ventrolateral Medulla
rVRG	Rostral Ventral Respiratory Group
SAL	Salbutamol
sGC	Soluble Guanylyl Cyclase
SHR	Spontaneously Hypertensive Rat
SNA	Sympathetic Nerve Activity
SG	Stellate Ganglion
SNS	Sympathetic Nervous System
TH	Tyrosine Hydroxylase
WKY	Wistar Kyoto Rat

List of Figures

Figure 1.1. The Autonomic Nervous System and Peripheral Innervation 4
Figure 1.2. Baroreceptor Reflex Control of Autonomic Outflow 5
Figure 1.3. Chemoreceptor Reflex Control of Autonomic Outflow 6
Figure 1.4. Primary sites of action for common anti-hypertensive therapeutics 11
Figure 1.5. Animal Models of Hypertension 15
Figure 1.6. The Neuro-Cardiac Axis 17
Figure 1.7. Elevated Calcium Conductance in preSHR Sympathetic Neurons 22
Figure 1.8. cGMP Reduces Calcium Conductance in preSHR Neurons 24
Figure 1.9. Voltage-gated Calcium Channel Regulation by Cyclic Nucleotides 27
Figure 2.1. Anatomical and Morphological Characteristics of Stellate Ganglia 34
Figure 2.2. Epac1-H30 FRET Biosensor Construct and Mechanism 38
Figure 2.3. Epac1-H187 FRET Biosensor Construct and Mechanism 39
Figure 2.4. AKAR4 FRET Biosensor Construct and Mechanism 40
Figure 2.5. Epac1-H30 FRET Sensor Dynamic Range 47
Figure 2.6. Epac1-H187 FRET Sensor Dynamic Range 48
Figure 2.7. AKAR4 FRET Sensor Dynamic Range 50
Figure 2.8. Emission Ratio from Cells Loaded with Indo-1AM 54
Figure 2.9. RNA Integrity and Quantity Validation 60
Figure 2.10. Stellate RNA Extraction Optimisation Parameters 62
Figure 2.11. RNA-seq SMARTer cDNA Library Preparation 64
Figure 2.12. RNA to cDNA Library Preparation for RNA Sequencing 65
Figure 2.13. Directional RNA Sequencing Library 67
Figure 2.14. ELISA Protocol Summary 76
Figure 3.1. MA plot and PCA plot confirm validity of RNA-seq analysis. 88
Figure 3.2. Differentially Expressed Genes in SHR Stellate Ganglia. 90
Figure 3.3. Over-represented Cellular Component Gene Ontology Group Hierarchy 92
Figure 3.4. Over-represented Biological Processes Gene Ontology Group Hierarchy. 95
Figure 3.5. Over-represented Molecular Function Gene Ontology Group Hierarchy 97
Figure 3.6. Extracellular Ligand-Gated Ion Channel Activity (GO:0005230) 99
Figure 3.7. Phosphoric Ester Hydrolase Activity (GO:0042578) 101
Figure 3.8. KEGG Differentially Expressed Functional Enrichment Pathways 104
Figure 3.9. Cytosolic cAMP and PKA Activity are Not Altered in SHR Neurons 106

Figure 3.10. Phosphodiesterase Impairment in preSHR Sympathetic Neurons. 108
Figure 4.1. RNA-seq Depicts β-Adrenergic Receptors on Rat Stellate Ganglia 127
Figure 4.2. Human and Rat Stellate Ganglia Express β-Adrenergic Receptors 128
Figure 4.3. β- and α-Adrenergic Receptor Expression on Rat Stellate Neurons 130
Figure 4.4. Rat and Human Stellate Ganglia Express β-Adrenergic Receptors 132
Figure 4.5. βAR Stimulation Increases cAMP-PKA in PreSHR Neurons 134
Figure 4.6. Raw Traces Representing CFP and YFP Emission Wavelength 135
Figure 4.7. βAR Signalling Enhances Intracellular Ca^{2+} in preSHR Neurons 136
Figure 4.8. Contribution of β_1AR and β_2AR Signalling to Neuronal cAMP Generation 139
Figure 4.9. β_2AR Signalling Plays a Dominant Role in Neuronal cAMP Generation 140
Figure 4.10a. Intracellular Signalling in Healthy Neurons 148
Figure 4.10b. Intracellular Signalling in Diseased Neurons 149
Figure 5.1. RNA-seq Highlights Catecholamine Synthesis Pathway 157
Figure 5.2. Catecholamine Synthesising Enzyme mRNA Validation by qRT-PCR 158
Figure 5.3. Rat and Human Stellate Ganglia Express PNMT 160
Figure 5.4. Total Catecholamine Concentration in Rat Stellate Ganglia 162
Figure 5.5. Evoked Catecholamine Release from Rat Stellate Ganglia 163
Figure 5.6a. Intracellular Signalling in Healthy Neurons 171
Figure 5.6b. Intracellular Signalling in Diseased Neurons 172
Figure 6.1. RNA-seq Highlights Angiotensin synthesis in Rat Stellate Ganglia 183
Figure 6.2. Angiotensin II Synthesising Enzyme mRNA in Stellate Ganglia. 184
Figure 6.3. Rat Stellate Ganglia Express Angiotensin II Synthesising Enzymes 186
Figure 6.4. Human Stellates Express AngII Synthesising Enzymes and Precursors 187
Figure 6.5. Angiotensin II Content in Stellate Ganglia 189
Figure 6.6. Angiotensin Converting Enzyme 2 Expression in Stellate Ganglia 192
Figure 6.7. ACE2 Activity is Elevated in the Hypertensive Rat Stellate Ganglia 194
Figure 6.8. Angiotensin 1-7 is Synthesised in Human and Rat Stellate Ganglia 196
Figure 6.9. AT_{1A}R Expression on Rat Stellate Ganglia 198
Figure 6.10. AngII and Ang1-7 Receptor mRNA in Rat Stellate Ganglia 199
Figure 6.11. AngII and Ang1-7 Receptor mRNA in Human Stellate Ganglia 200
Figure 6.12a. Angiotensin Synthesis in Sympathetic Stellate Neurons 210
Figure 6.12b. Angiotensin Synthesis in Stellate Neurons in Hypertension 211
Figure 7.1a. Model Figure: Cardiac-Sympathetic Neurotransmission 224
Figure 7.1b. Model Figure: Cardiac-Sympathetic Dysfunction in Hypertension 225
Figure 8.6. ΔC_T values for qRT-PCR in Rat Stellate Ganglia. 277

List of Tables

Table 1.1 Common Anti-hypertensive Therapeutics Categorised by Class 11
Table 1.2. Phosphodiesterase Isoforms and Cyclic Nucleotide Substrates 26
Table 2.1. Neuronal Blocking and Plating Media 33
Table 2.2. List of Primary and Secondary Antibodies and Optimal Dilutions 36
Table 2.3. HEK293T Growth and Infection Media 44
Table 2.4. Buffers and Solutions 55
Table 2.5. Human Stellate Donor Characteristics 57
Table 2.6. RNA Extraction Protocols for Rat and Human Stellate Ganglia 58
Table 2.7. Stellate RNA Extraction Optimisation Parameters. 62
Table 2.8. Salmon-Quasi Mapping Rates 68
Table 2.9. List of Primers and Dilutions for Optimal qRT-PCR Reactions 71
Table 2.10. List of Protein and Enzyme Assays and Optimal Sample Dilutions 77
Table 3.1. Highest Abundance Gene Transcripts in Wistar and SHR Ganglia 89
Table 3.2. Differentially Expressed Gene Transcripts in Stellate Ganglia 90
Table 3.3. Over-represented Cellular Component Gene Ontology Groups 93
Table 3.4. Over-represented Biological Processes Gene Ontology Groups 94
Table 3.5. Over-represented Molecular Function Gene Ontology Groups 96
Table 3.6. Extracellular Ligand-gated Ion Channel GO Group (GO:0005230) 100
Table 3.7. Phosphoric Ester Hydrolase Activity GO Group (GO:0042578). 102
Table 3.8. Over-represented KEGG groups 103
Table 6.1. The KEGG Group ‘Renin Secretion’ (rno04924) 182
Table 6.2. Differentially Expressed Genes in KEGG Group ‘Renin Secretion’ 182
Table 8.1. Cellular Component Gene Ontology Gene List 272
Table 8.2a. Biological Processes Gene Ontology Gene List 273
Table 8.2b. Biological Processes Gene Ontology Gene List 274
Table 8.2c. Biological Processes Gene Ontology Gene List 275
Table 8.3. Molecular Function Gene Ontology Gene List 275
Table 8.4. KEGG Functional Enrichment Analysis Gene List 276

Table of Contents

Abstract ii

List of Publications iii

Awards and Conference Abstracts iv

Acknowledgements vi

Dedication vii

Thesis Contributions viii

List of Abbreviations x

List of Figures xii

List of Tables xiv

Table of Contents xv

Chapter One: Introduction 1

1.1 Hypertension: Prevalence and Cause 2

1.2 Essential Hypertension: Origins and Risk Factors 2

1.3 Arterial Blood Pressure Regulation and Hypertension 3

1.3.1 Acute Blood Pressure Regulation 3

1.3.2 Long-term Blood Pressure Regulation 7

1.3.3 Clinical Anti-hypertensive Agents and Therapeutic Strategies 7

1.3.3.1 β-Adrenergic Receptor Blockers 8

1.3.3.2 Diuretics 8

1.3.3.3 Angiotensin Converting Enzyme Inhibitors 9

1.3.3.4 Angiotensin II Receptor Blockers 9

1.3.3.5 Calcium Channel Blockers 10

1.3.3.6 α_1 Adrenergic Receptor antagonists 10

1.4 Animal Models of Hypertension 13

1.5 The Autonomic Nervous System 16

1.5.1 Overview of Autonomic Regulation 16

1.5.2 Key Milestones in Neuroscience Research: A Brief Historical Perspective 16
1.5.3 Autonomic Dysfunction in Hypertension 19
1.5.4 Cardiac-Sympathetic Over-Activity in Hypertension 20
1.5.5 Intrinsic Excitability: Regulators of Cardiac-Sympathetic Activity 21
1.5.6 Phosphodiesterase Enzymes: Regulation of Cyclic Nucleotides 26

1.6 Conclusion 28

1.7 Thesis Aims 29

Chapter Two: General Methods 30

2.1 Introduction 31

2.2 Animals 31

2.3 Isolation of Rat Sympathetic Stellate Neurons 32
2.3.1 Cardiac-Sympathetic Stellate Ganglia Dissection 32
2.3.2 Neuronal Isolation from Rat Sympathetic Cardiac-Stellate Ganglia 32
2.3.3 Preparation of Culturing Media 33
2.3.4 Preparation of Poly-D-Lysine / Laminin Coated Coverslips 35

2.4 Immunocytochemistry 35

2.5 Förster Resonance Energy Transfer (FRET) 36
2.5.1 FRET Overview 36
2.5.2 cAMP FRET Sensors 37
2.5.3 PKA FRET Sensor 40
2.5.4 Generation and Amplification of FRET Sensors 41
2.5.4.1 Epac1-H187 41
2.5.4.2 AKAR4 41
2.5.4.3 Epac1-H30 41
2.5.4.4 HEK293T Cell Culture 42
2.5.4.5 Ad-CMV-Epac1-H30 Amplification 42
2.5.4.6 Ad-CMV- Epac1-H30 Harvest and Purification 42
2.5.4.7 Ad-CMV-Epac1-H30 Titration and Quantification 43
2.5.4.8 HE293T Cell Media 43
2.5.5 FRET Experimental Setup 44
2.5.5.1 FRET Sensor Expression 44
2.5.5.2 Microscope Setup for FRET Imaging 44
2.5.5.3 FRET Imaging Protocol 45

2.5.6 Establishing the Dynamic Range of the FRET Sensors 46
2.5.6.1 Dynamic Range of Epac1-H30 46
2.5.6.2 Dynamic Range of Epac1-H187 46
2.5.6.3 Dynamic Range of AKAR4 49
2.5.7 FRET Experimental Protocol 51
2.5.8 FRET Statistical Analysis 51

2.6 Intracellular Calcium Imaging 52
2.6.1 Calcium Imaging Protocol 52
2.6.2 Calcium Imaging Experimental Protocol 53
2.6.3 Ionomycin Calibration of Indo-1AM 53

2.7 Buffers and Solutions 55
2.7.1 HEPES-buffered Tyrode's Solution 55
2.7.2 Carbon Dioxide / Bicarbonate-buffered Tyrode's Solution 55
2.5.3 High K^+ Carbon Dioxide / Bicarbonate-buffered Tyrode's Solution 55
2.5.4 Zero Ca^{2+} HEPES-buffered Tyrode's Solution 55
2.5.5 High Ca^{2+} HEPES-buffered Tyrode's Solution 55

2.8 RNA Sequencing 56
2.8.1 Stellate Ganglia Tissue Preparation for RNA Extraction 56
2.8.2 Rat and Human Stellate Ganglia RNA Extraction Protocol 57
2.8.3 RNA Integrity Validation 59
2.8.4 Optimisation of Stellate Tissue Preparation and RNA Extraction 61
2.8.5 RNA Extractions for RNA Sequencing and qRT-PCR 63
2.8.6 Transcript Mapping 66
2.8.7 Differential Expression Analysis 68
2.8.8 Gene ontology and KEGG Pathway Analysis 68

2.9 Validation of the RNA-seq Dataset 69
2.9.1 cDNA Library Preparation 69
2.9.2 Two-Step Quantitative Real-Time Polymerase Chain Reaction 70
2.9.3 qRT-PCR Statistical Analysis 72

2.10 Measurements of Proteins and Neurotransmitters 72
2.10.1 Evoked-Release Field Stimulation 72
2.10.2 High-Pressure Liquid Chromatography with Electrochemical Detection 73
2.10.3 Protein Extraction 74
2.10.4 Protein Concentrations and Enzyme Activity Measurements 74

2.10.5 Statistical Analysis of Assays 78

2.11 Reagents 78

Chapter Three: RNA Sequencing of Sympathetic Stellate Ganglia 79

3.1 Introduction 80

3.2 Chapter Aims 81

3.3 Methods 82

3.3.1 Animals 82

3.3.2 Neuronal Isolation 82

3.3.3 Förster Resonance Energy Transfer (FRET) Microscopy 82

3.3.4 RNA Extraction from Sympathetic Cardiac Ganglia 83

3.3.5 cDNA library preparation for RNA Sequencing 84

3.3.6 Quasi-mapping and Differential Expression Analysis 84

3.3.7 Gene Ontology Analysis 85

3.3.8 cDNA Library Preparation and Quantitative Real-Time PCR 85

3.3.9 Statistical Analysis and Data Availability 86

3.4 Results 87

3.4.1 Study Design 87

3.4.2 Differential Expression Analysis 87

3.4.3 Overview of the Transcriptome of Wistar and SHR Stellate Ganglia 89

3.4.5 Differential Expression in SHR Stellate Ganglia 90

3.4.6 Distinct Alterations in Gene Ontology in the SHR Stellate Ganglia 91

3.4.6.1 Cellular Component Gene Ontology 91

3.4.6.2 Biological Processes Gene Ontology 93

3.4.6.3 Molecular Function Gene Ontology 96

3.4.6.4 Extracellular Ligand-Gated Ion Channel Activity 98

3.4.6.5 Phosphoric Ester Hydrolase Activity 100

3.4.7 KEGG Functional Enrichment Pathways are Impaired in SHR 103

3.4.8 Cyclic Nucleotide Signalling in Cardiac-Stellate Ganglionic Neurons 105

3.4.9 Phosphodiesterase Signalling in Cardiac-Stellate Neurons 107

3.5 Discussion 109

3.5.1 RNA Sequencing Reveals Differences in the SHR Stellate Ganglia 110

3.5.2 Altered Transcripts Linked to Neurotransmission in the SHR 110

3.5.3 Impaired Regulatory Cardiovascular Genes in SHR Stellate Ganglia 111

3.5.4 Altered Extracellular Ligand-Gated Ion Channel Activity in SHR 112
3.5.5 Altered Phosphoric Ester Hydrolase Activity Impairs PDE Function 113

3.6 Limitations 115

3.7 Conclusion 117

Chapter Four: β-Adrenergic Signalling in Sympathetic Stellate Neurons 118

4.1 Introduction 119

4.2 Chapter Aims 120

4.3 Methods 121
4.3.1 Animals 121
4.3.2 Human Donor Stellates 121
4.3.3 Neuronal Isolation 121
4.3.4 RNA Extraction and RNA Sequencing 121
4.3.5 Quantitative Real-Time Polymerase Chain Reaction 121
4.3.6 Immunocytochemistry 122
4.3.7 Enzyme-linked Immunosorbent Assays 122
4.3.8 Live-Cell Förster Resonance Energy Transfer (FRET) Microscopy 123
4.3.9 Intracellular Calcium Measurements 124
4.3.10 Compounds 125
4.3.11 Statistical Analysis 125

4.4 Results 126
4.4.1 Stellate Ganglia Express mRNA Encoding β-Adrenergic Receptors 126
4.4.2 β-Adrenergic Receptors are Expressed on Human and Rat Stellate Ganglia 129
4.4.3 Enhanced βAR-evoked cAMP and PKA Activity in PreSHR Neurons 133
4.4.4 βAR Activation Elevates KCl-evoked Calcium in PreSHR Neurons 135
4.4.5 Contribution of β_1AR and β_2AR to Neuronal cAMP Generation 137
4.4.6 β_2AR Signalling Plays a Dominant Role in Neuronal cAMP 138

4.5 Discussion 141
4.5.1 Sympathetic Stellate Ganglia Express β-Adrenoceptors 142
4.5.2 Elevated β-Adrenergic Signalling in preSHR Sympathetic Neurons 143
4.5.3 β_2AR Plays a Dominant Role in Sympathetic cAMP Generation 144

4.6 Limitations 146

4.7 Conclusion 147

Chapter Five: Adrenaline Synthesis in the Sympathetic Stellate Ganglia 150

5.1 Introduction 151

5.2 Chapter Aims 152

5.3 Methods 153

5.3.1 Animals 153

5.3.2 Human Donor Stellates 153

5.3.3 RNA Extraction and RNA-seq 153

5.3.4 Quantitative Real-Time Polymerase Chain Reaction 153

5.3.5 Enzyme-linked Immunosorbent Assays 154

5.3.6 Whole Ganglia and Electrical Release of Catecholamines 154

5.3.7 High-Pressure Liquid Chromatography with Electrochemical Detection 155

5.3.8 Statistical Analysis 155

5.4 Results 156

5.4.1 RNA Sequencing Illustrates Catecholamine Synthesising Pathway 156

5.4.2 Stellate Ganglia Express Phenylethanolamine N-Methyltransferase 158

5.4.3 Total Catecholamine Concentration in Rat Stellate Ganglia 161

5.4.4 Evoked Catecholamine Release from Rat Stellate Ganglia. 162

5.5 Discussion 164

5.5.1 Stellate Ganglia Express Phenylethanolamine N-Methyltransferase 165

5.5.2 Adrenaline Synthesis and Release from Stellate Ganglia 167

5.6 Limitations 168

5.7 Conclusion 170

Chapter Six: Angiotensin Synthesis in the Sympathetic Stellate Ganglia 173

6.1 Introduction 174

6.2 Chapter Aims 175

6.3 Methods 176

6.3.1 Animals 176

6.3.2 Human Donor Stellates 176

6.3.3 Rat Sympathetic Stellate Ganglia Extraction 176

6.3.4 Neuronal Isolation 176

6.3.5 Immunocytochemistry 177

6.3.6 RNA Extraction and RNA Sequencing Analysis 177

6.3.7 Quantitative Real-Time Polymerase Chain Reaction 177
6.3.8 Protein Extraction 178
6.3.9 Evoked-Release of Angiotensin Peptides by Field Stimulation 178
6.3.10 Enzyme-Linked Immunosorbent Assay and Enzyme Immunoassay 179
6.3.11 Fluorometric Enzyme Activity Assays 179
6.3.12 Statistical Analysis 180

6.4 Results 181
6.4.1 Angiotensin II Synthesis Pathway in Sympathetic Stellate Ganglia 181
6.4.2 Angiotensin II Synthesising Enzyme Transcripts in Stellate Ganglia 181
6.4.3 Stellate Ganglia Express Angiotensin II Synthesising Enzymes 185
6.4.4 Angiotensin II is Synthesised in Human and Rat Stellate Ganglia 188
6.4.5 Angiotensin II Evoked-Release from Rat Stellate Ganglia 190
6.4.6 Angiotensin Converting Enzyme 2 Expression in Stellate Ganglia 191
6.4.7 ACE2 Activity is Elevated in the Hypertensive Rat Stellate Ganglia 193
6.4.8 Angiotensin 1-7 is Synthesised in Human and Rat Stellate Ganglia 195
6.4.9 AngII and Ang1-7 Receptors are Expressed on Stellate Ganglia 197

6.5 Discussion 201
6.5.1 The Angiotensin II Synthesis Pathway is Present in Stellate Ganglia 202
6.5.2 Angiotensin II is Present in Rat and Human Stellate Ganglia 203
6.5.3 Angiotensin 1-7 is Present in Rat and Human Stellate Ganglia 205

6.6 Limitations 207

6.7 Conclusion 209

Chapter Seven: Concluding Discussion 212

7.1 Introduction 213

7.2 The Main Findings of this Thesis 214

7.3 RNA Sequencing Highlights a Genetic Component for Sympathetic Over-activity in the Spontaneously Hypertensive Rat 215
7.3.1 RNA Sequencing Highlights a Genetic Component for Impaired Cardiovascular Regulation in the Spontaneously Hypertensive Rat 215
7.3.2 RNA Sequencing Highlights a Genetic Component for Elevated Neuronal Excitability in the Spontaneously Hypertensive Rat 216
7.3.3 RNA Sequencing Highlights a Genetic Component for Altered Phosphodiesterase Activity in the Spontaneously Hypertensive Rat 217

7.4 Elevated Presynaptic β-Adrenergic Signalling in the Stellate Ganglia of Prehypertensive Spontaneously Hypertensive Rat 217

7.5 The 'Adrenaline Hypothesis' of Essential Hypertension: Adrenaline Synthesis in Sympathetic Stellate Ganglia 218

7.6 Intracrine Angiotensin Synthesis in the Stellate Ganglia 220

7.7 Clinical Significance 222

7.8 Conclusion 223

References 226

Appendix 271

8.1 Differential Expression Analysis using DESeq2 271

8.2 Gene lists for Cellular Component Gene Ontology Group 272

8.3 Gene lists for Biological Processes Gene Ontology Group 273

8.4 Gene lists for Molecular Function Gene Ontology Group 275

8.5 Gene lists for KEGG Functional Enrichment Analysis 276

8.6 ΔC_T values for qRT-PCR in Rat Stellate Ganglia 276

1

Introduction

1.1 Hypertension: Prevalence and Cause

Primary (essential, idiopathic) hypertension is the most prevalent chronic disease in the Western world and affects over one billion adults worldwide[1-5]. Hypertension is clinically defined as a sustained increase in arterial blood pressure (>130/80 mmHg)[6,7] and is a primary risk factor for adverse cardiovascular events[8] including ischaemic heart disease[9], stroke and cerebrovascular disease[8,10,] heart failure [11-13], myocardial infarction[8,14,15], type 2 diabetes[8,16-18] and chronic kidney disease[8,19]. The significant increase in all-cause mortality that results[8] places a significant economic burden on global health-care systems[2]. The management of blood pressure is associated with beneficial outcomes and clinical prognosis in patients with cardiovascular co-morbidities[20]; however, due to the absence of obvious symptoms, the majority of adults are unaware of their blood pressure status[5,21,22]. Thus, there is a clear requirement for advancements in hypertension diagnostic technologies and prophylactic interventions that is illustrated by the increasing number of cardiovascular disease (CVD) publications. Indeed, a literature search on PubMed for 'hypertension' since 2008 produces 446,117 results.

1.2 Essential Hypertension: Origins and Risk Factors

Essential (idiopathic) hypertension has no clear cause and accounts for 90-95 % of all cases, whereas secondary hypertension (5-10 %) is caused by identifiable factors such as renal or adrenal disease or occurs as a side-effect of some therapeutics[4]. The origins of essential hypertension are multifactorial and involve the vasculature[23-25], kidneys[26] and autonomic nervous system[27-29], where a complex interplay between genetic and environmental factors influences an individual's susceptibility to developing hypertension[30,31] in a model sometimes described as the 'Mosaic Theory of Arterial Hypertension' [32,33]. Environmental risk factors include high salt intake[34], obesity[35-37], smoking[38,39], alcohol consumption, diet[31], aging[24], lack of physical activity[40,41], and stress[4,5]. Epidemiological studies have also highlighted a greater incidence of hypertension in certain ethnic groups[42], and in males[43] and substantial evidence

suggests that the susceptibility for hypertension may be heritable. Indeed, familial studies have identified an increased risk for the development of hypertension in progeny from hypertensive parents[36,44-47]. Moreover, Genome Wide Association Studies (GWAS) have identified numerous genetic mutations as risk factors for hypertension[48-50], myocardial infarction[48,51] coronary artery disease[48,50-52], stroke[50,53,54] and arrhythmia[53-55].

1.3 Arterial Blood Pressure Regulation and Hypertension

1.3.1 Acute Blood Pressure Regulation

The acute regulation of arterial blood pressure is critical for maintaining adequate perfusion of distal tissues in proportion to their metabolic requirements, where short-term fluctuations in blood pressure occur in response to changes in physical activity[56,57], emotional stressors[57,58], or environmental influences[59,60]. The first accurate description of the mechanisms of the circulatory system and the motion and function of the heart may be attributed to the English physician William Harvey (1578-1657)[61]. Harvey's account of a closed-loop one-way mammalian system for vascular blood flow was described as "…*blood passes from the right ventricle of the heart through the pulmonary artery to the lungs, from there through the pulmonary vein into the left auricle, and then into the left ventricle*". Moreover, Harvey also documented the notion of rhythmic contraction of the heart *"..from these points it is reasonable to conclude that the heart at the moment it acts, becomes constricted all over, thicker in its walls and smaller in its ventricles, in order to expel its content of blood…"*[62]. These observations were revolutionary for the field of physiology. Since the 1600's, many advancements have contributed towards our understanding of cardiovascular physiology and it is now clear that arterial blood pressure, a function of cardiac output (CO) and peripheral vascular resistance[63,64], is critically regulated by the autonomic nervous system (Fig 1.1). Several layers of integrated feedback regulation enable rapid physiological adaptations to behaviour[27,65], where acute increases in noradrenergic transmission facilitate vascular constriction and raise CO[66]. Two primary

mechanisms, namely the baroreceptor[67,68] and chemoreceptor[69,70] feedback systems play a critical role in autonomic reflex activity (Fig's. 1.2, 1.3), and as such, have a profound influence on blood pressure regulation[66,71-73].

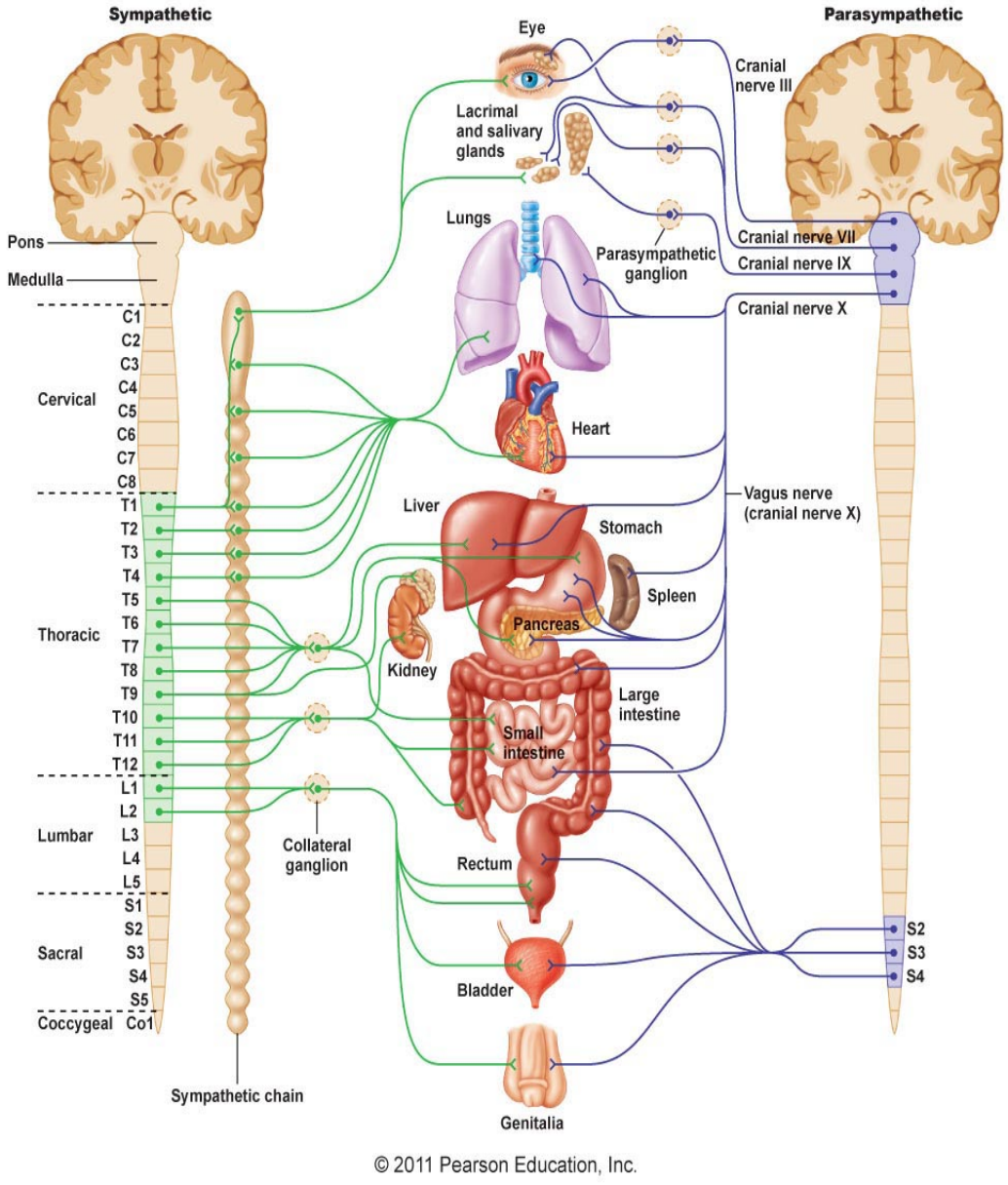


Figure 1.1. The Autonomic Nervous System and Peripheral Innervation
The parasympathetic and sympathetic branches of the Autonomic Nervous System (ANS) innervate a large number of organs to regulate and control functional processes. Parasympathetic and sympathetic divisions often work in a complementary manner to regulate and maintain homeostasis. The sympathetic stellate ganglia (cervicothoracic ganglia) are located alongside vertebrate T1 to T4. They are the primary sympathetic ganglia that innervate the heart and as such exert the greatest control over increases in heart rate and contractility. This figure was reproduced from: http://droualb.faculty.mjc.edu/

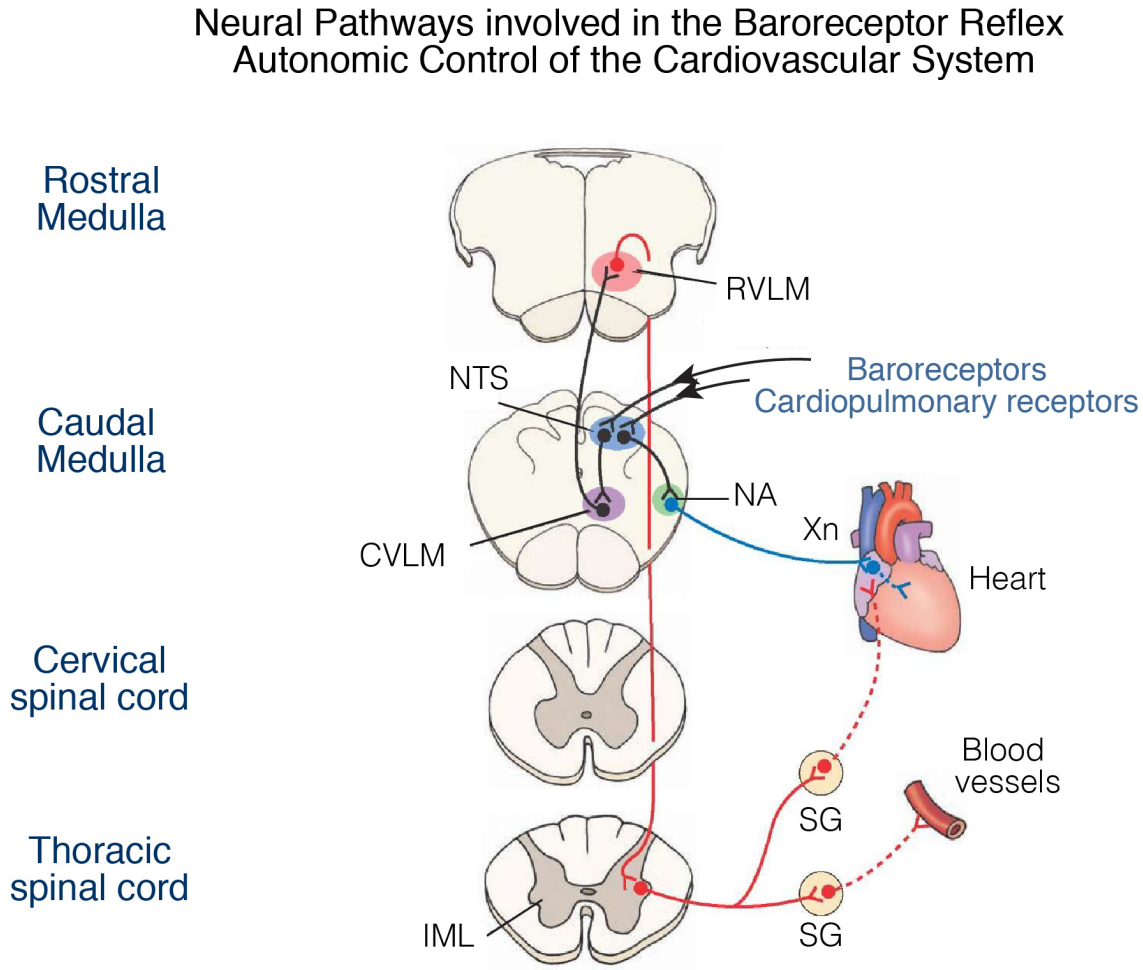


Figure 1.2. Baroreceptor Reflex Control of Autonomic Outflow
The baroreceptor reflex describes a regulatory process where mechanoreceptors in the carotid sinus and aortic arch are stimulated by stretch activation of the vascular walls. An acute elevation in blood pressure activates baroreceptor afferents that terminate in the NTS. excitation of the NTS facilitates activation of inhibitory interneurons in the CVLM, where the release of gamma-amino butyric acid (GABA) inhibits tonic RVLM activity. This in turn reduces sympathetic outflow from the IML, reducing activity of sympathetic efferents that regulate the myocardium and arterioles. In addition, excitation of the NTS also stimulates the NA that raises vagal tone to the heart. *NTS, nucleus tractus solitarius; RVLM, rostral ventrolateral medulla; CVLM, caudal ventrolateral medulla; IML, intermediolateral column of the spinal cord; NA nucleus ambiguus; Xn, vagus nerve.* This figure was adapted from: http://what-when-how.com/neuroscience/the-autonomic-nervous-system-integrative-systems-part-5/

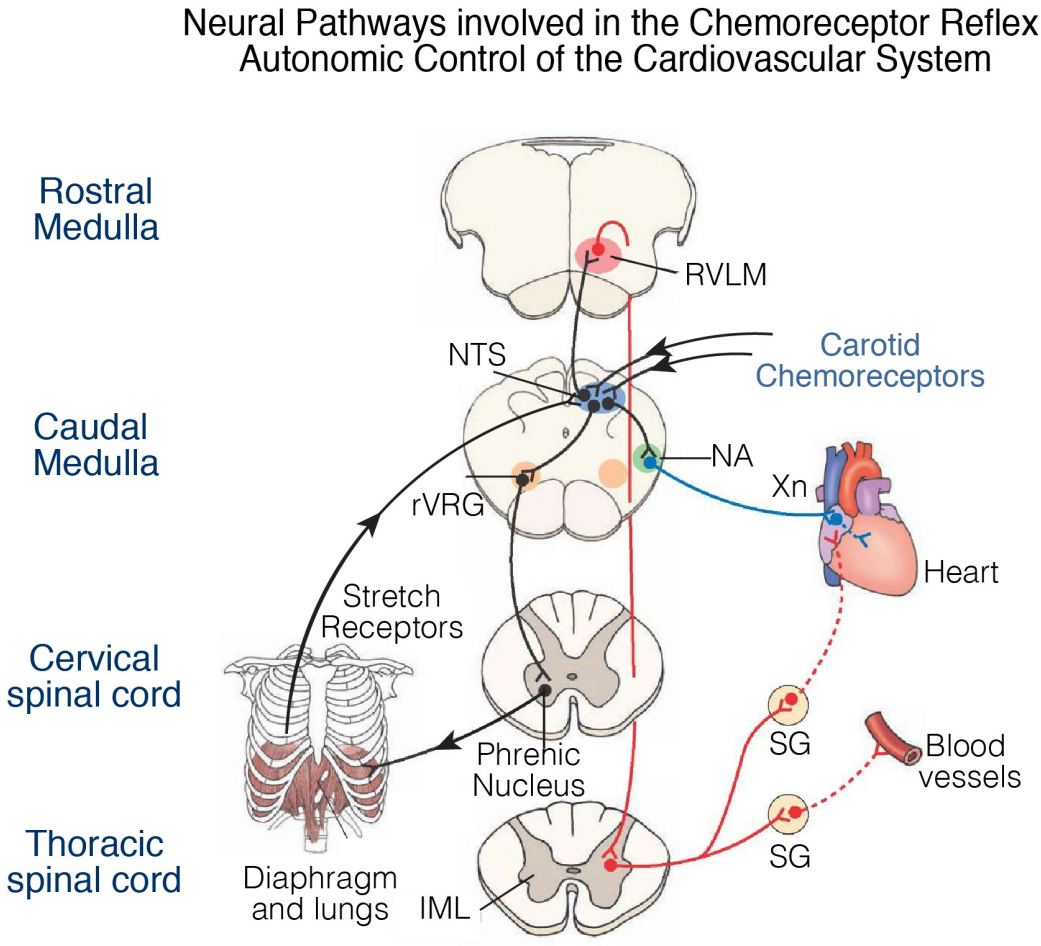


Figure 1.3. Chemoreceptor Reflex Control of Autonomic Outflow
The chemoreceptor reflex describes a feedback regulatory process where chemoreceptors in the carotid and aortic bodies are primarily stimulated by acidosis, hypoxia (low O_2), hypercapnia (high CO_2) and hyperkalaemia (high K^+), that change alongside physical activity. Depolarisation of the carotid bodies leads to increased afferent firing of the glossopharyngeal nerve that terminates in the NTS resulting in three primary effects. 1. Elevated sympathetic outflow via RVLM stimulation of the IML that increases arteriole constriction. 2. Respiratory activation via stimulation of rostral ventral respiratory neurons activates phrenic motor neurons that innervate the diaphragm, thus triggering inhalation. The activation of pulmonary stretch receptors provides negative feedback signals to the NTS that inhibits firing. 3. Cardiac response via NTS activation of the NA that elevates vagal cardiac tone and leads to bradycardia. The overall integrated cardiovascular outcome depends on the individual strength of the afferent reflexes. *NTS, nucleus tractus solitarius; RVLM, rostral ventrolateral medulla; rVRG, rostral ventral respiratory group; IML, intermediolateral column of the spinal cord; NA nucleus ambiguus; Xn, vagus nerve.* This figure was adapted from: http://what-when-how.com/neuroscience/the-autonomic-nervous-system-integrative-systems-part-6/

1.3.2 Long-term Blood Pressure Regulation

The long-term control of blood pressure is dependent on a number of processes that are involved directly or indirectly in fluid volume homeostasis. Reductions in arterial blood pressure facilitate the kidney pressure-natriuresis response[74,75], where decreased renal perfusion pressure, baroreflex-stimulated elevations in renal sympathetic nerve activity (RNSA) and reductions in in NaCl concentration stimulate juxtaglomerular renin secretion. This in turn initiates the classical Renin-Angiotensin-Aldosterone system (RAAS) signalling cascade[76,77]. RAAS signalling plays a critical role in blood pressure elevation where activation of the G_q-coupled angiotensin II (AngII) receptor (AT_1R)[78] facilitates vasoconstriction[79], augments sympathetic outflow and peripheral sympathetic nerve activity[80,81] and stimulates aldosterone secretion from the adrenal cortex[79,82], thus promoting Na^+ and H_2O retention and elevation in blood volume[82-84].

1.3.3 Clinical Anti-hypertensive Agents and Therapeutic Strategies

Reductions in arterial blood pressure may be achieved by reducing peripheral vascular resistance and / or CO, and compounds that reduce peripheral resistance may also improve vascular compliance. Due to the different mechanisms of action, drugs of this class differ structurally and pharmacologically, and thus confer different therapeutic advantages, side-effect profiles and contraindications. Anti-hypertensives may be classified into five main pharmacological classes including β-adrenergic receptor (βAR) inhibitors (β-blockers), diuretics, angiotensin converting enzyme inhibitors, angiotensin II receptor antagonists and calcium channel blockers. Other additional classes include alpha-1 adrenergic receptor (α_1AR) antagonists, renin inhibitors and less commonly centrally acting agents.

1.3.3.1 β-Adrenergic Receptor Blockers

β-blockers are a large class of antihypertensive therapeutics including a range of different compounds with varying pharmacokinetic and pharmacodynamic profiles. Various mechanisms of action are thought to contribute to the anti-hypertensive action of β-blockers. Initially, β-blockers reduce CO as a result of bradycardia and although this can lead to a reflex increase in peripheral resistance, the resetting of the baroreflex attenuates this effect. Indeed, β_1AR-blockers significantly reduce myocardial conduction velocity and cardiac automaticity, inducing a depressor effect on the heart that decreases inotropy and chronotropy[85]. β-blockers also reduce sympathetic activity though central actions and via inhibition of presynaptic βARs that reduces NA release, that inhibits vasoconstriction, renin secretion from kidneys, and decreases heart rate and contractility[85,86]. B_1AR selective inhibitors (atenolol) in particular are thought to lower blood pressure though preferential action on cardiac βARs and via unopposed β_2AR-mediated arterial vasodilation. Moreover, some βAR antagonists have been synthesised to confer partial agonism at β_2ARs, antagonist activity at α_1ARs in addition to NO potentiation, that enhances small artery. Conversely, in some studies β_1AR selective antagonists have not been found to reduce sympathetic tone and drugs of this class are often associated with a high side effect profile, including insomnia, hallucinations and depression. Moreover, contraindications include patients with asthma, atrioventricular block and glucose intolerance.

1.3.3.2 Diuretics

Thiazide diuretics and loop diuretics increase natriuresis and diuresis via different mechanisms. Thiazide diuretics (e.g. hydrochlorothiazide) act in the kidney within the early distal tubule to inhibit the Na^+ / Cl^- symporter, preventing the reabsorption of Na^+ and Cl^- and raising H_2O excretion thus lowering extracellular fluid volume reducing cardiac preload to reduce CO[87]. Conversely, loop diuretics (e.g. furosemide and bumetanide) inhibit the Na^+ / K^+ / $2Cl^-$ cotransporter by competing with Cl^- binding within the loop of Henle. Loop diuretics reduce blood

pressure by decreasing plasma volume that decreases venous return thus lowering cardiac preload and CO.

1.3.3.3 Angiotensin Converting Enzyme Inhibitors

Angiotensin Converting Enzyme Inhibitors (ACEIs, e.g. enalapril) inhibit the conversion of Angiotensin I to AngII peptide. By reducing concentrations of the vasoconstrictor peptide AngII, ACEIs facilitate vasodilation particularly within small resistance arteries. Consequently, peripheral resistance is decreased thus underpinning the blood pressure lowering properties of these drugs, although CO remains unchanged[88,89]. Nevertheless, ACEIs do not inhibit the synthesis of AngII via other alternate pathways that may upregulate with chronic suppression of AngII production.

1.3.3.4 Angiotensin II Receptor Blockers

Angiotensin II receptor blockers (ARBs, e.g. valsartan) inhibit the activation of the AngII type I Receptor (AT_1R) with a high level of affinity. In a similar manner to ACEIs, ARBs attenuate the vasoactive effects of AngII and also attenuate the effects of upregulation of AngII via alternative enzymatic pathways that is common following administration of ACEIs. The haemodynamic effects of ARBs include vasodilation of small resistance arteries, reduction in vascular resistance, and blood pressure lowering although CO and heart rate remain unchanged[88,89]. Moreover, in addition to blood pressure lowering, evidence now suggests that ARBs may play a role in reverse remodelling of arteries, decreased left ventricular hypertrophy and attenuated arterial stiffness compared with other anti-hypertensive therapies. AngII antagonists may also confer additional efficacy by reducing sympathetic transmission, inhibition of acute pro-inflammatory processes and oxidative stress[83].

1.3.3.5 Calcium Channel Blockers

Calcium channel blockers (CCBs) are a large class of drugs including dihydropyridines, phenylalkylamines and benzothiazepine that have different mechanisms and sites of action. Dihydropyridines (DHPs e.g. nifedipine) primarily act on voltage-gated L-type (long-lasting) Ca^{2+} channels; a group of calcium channels that open at less negative voltages, or at later stages of depolarisation[90,91]. They bind to a specific site on the α_1 subunit of the Ca^{2+} channel pore and reduce the rate at which Ca^{2+} ions enter the cell. DHPs have a greater vascular compared with cardiac selectivity and have little effect on nodal tissue (sinoatrial and atrioventricular) therefore are not negatively inotropic[92]. The vascular selectivity of DHPs is thought to be due to the depolarised resting membrane potential of smooth muscle cells compared to myocytes because DHPs bind with high affinity to inactivated states of the channel[93]. Conversely, non-DHPs such as phenylalkylamines (diltiazem) and benzothiazepines (verapamil) show greater selectivity for cardiomyocytes rather than vascular smooth muscle cells. This is due to the fact that non-DHP display high use-dependency i.e. bind with greater affinity to L-type Ca^{2+} channel with repeated opening of the channel that occurs upon cellular depolarisation[93]. As such, non-DHPs such as verapamil and diltiazem are known as negative inotropes and lower heart rate due to actions on nodal tissue.

1.3.3.6 α_1 Adrenergic Receptor antagonists

Three α_1AR antagonists are clinically available for the treatment of hypertension (prazosin, terazosin and doxazosin) where significant reductions in blood pressure are mediated via decreases in total peripheral resistance. Vasodilatation is mediated as a result of inhibition of G_q-phospholipase C (PLC) mediated increases in inositol triphosphate (IP_3) and $[Ca^{2+}]_i$ liberation in vascular smooth muscle cells[94]. Unfortunately, a major limitation to the use of α_1AR antagonists is sudden severe orthostatic hypertension that often occurs on first dose of the day.

A list of the common anti-hypertensive agents is included in Table 1.1 and the sites of actions are depicted in Figure 1.4.

Table 1.1 Common Anti-hypertensive Therapeutics Categorised by Class

Class	Compound
Decreased Vascular Resistance	
Calcium channel blockers (dihydropyridine)	Nifedipine
Alpha1 adrenergic receptor antagonists	Prazosin
Decreased Cardiac Output	
Loop diuretics	Furosemide
Thiazides	Hydrochlorothiazide
Potassium sparing diuretics	Amiloride
Aldosterone inhibitors	Spironolactone
Calcium channel blockers (non-dihydropyridine)	Verapamil, Diltiazem
Beta adrenergic receptor antagonists	Metoprolol
Combined Effects	
AngII receptor antagonists	Valsartan
ACE inhibitors	Captopril
Direct renin inhibitors	Aliskiren

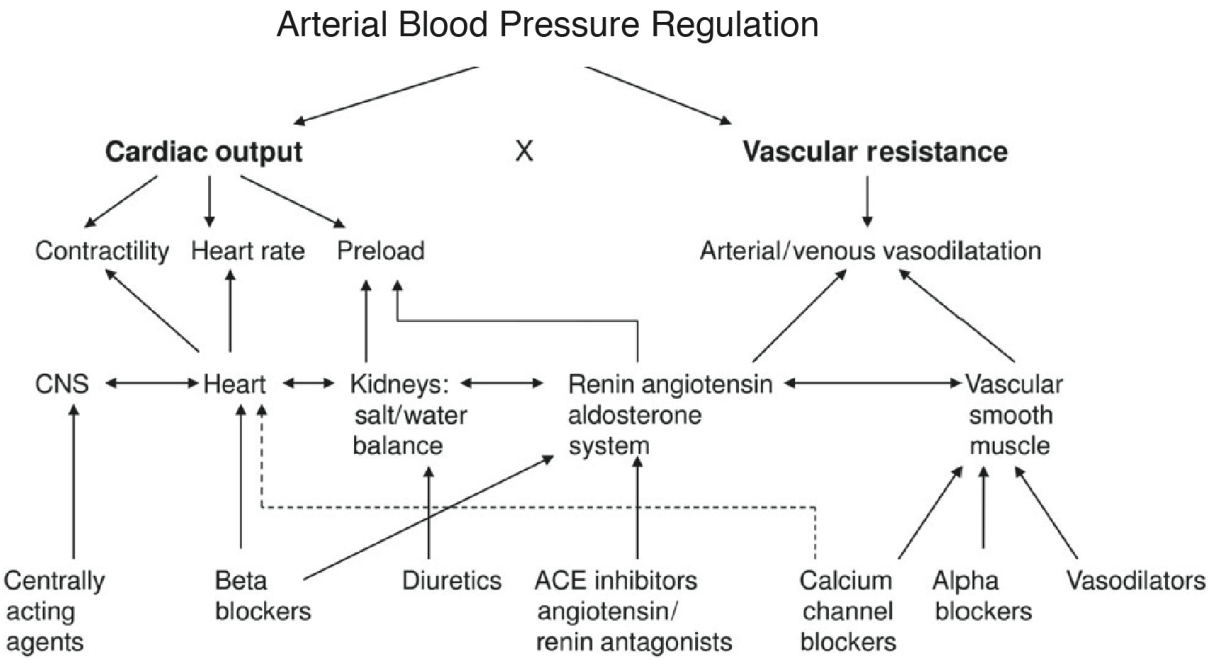


Figure 1.4. Primary sites of action for common anti-hypertensive therapeutics
This figure was reproduced from Zamponi et al.,[87].

Sustained impairments in one or several blood pressure regulatory processes may directly contribute to a chronic elevation in blood pressure, yet it is difficult to dissociate the primary causative events from secondary consequential factors as patients are usually diagnosed at various stages of established disease[95]. Sympathetic over-activity is a key feature of human hypertension measured by microneurography and NA spill techniques that is also observed in animal models of CVD[95,96]. In the Goldblatt two-kidney one-clip model (2K1C)[97], impaired baroreflex sensitivity and cardiac-sympathetic nerve over-activity occur prior to elevations in arterial blood pressure[97]. Moreover, elevated sympathetic nerve activity and vagal depression are also observed in the spontaneously hypertensive rat (SHR)[98-100] as well as in patients with hypertension[29,101], arrhythmia[102] and heart failure[103,104] demonstrating the importance of autonomic balance in cardiac regulation. Nevertheless, interventions that target this sympathetic phenotype are problematic to develop, due to the anatomical location of the cardiac-sympathetic ganglia[105] and the complex pathophysiological mechanisms involved in sympathetic over-activity. Surgical approaches such as renal or carotid chemoreceptor denervation, sympathectomy, and baroreceptor or vagal nerve stimulation provide symptomatic relief and lead to fewer cardiovascular co-morbidities in hypertension[106] as well as reducing the incidence of ventricular arrhythmia[107,108]. Success following the application of these techniques underpins the role of dysautonomia in the maintenance of high blood pressure. Nevertheless, surgical interventions are not without risk[107], and when introduced clinically have often failed to reach primary therapeutic endpoints due to heterogeneity in patient populations and patient-patient variations in responses. An example of this was seen in the SIMPLICITY HTN-1, HTN-2 and HTN-3 trials for renal denervation in the treatment of resistant hypertension[109]. Outcomes of the trial suggested that when carried out correctly renal denervation may be beneficial in the appropriate patient population, although the precise mechanisms that underpin the sustained reductions in blood pressure remain unclear[109,110]. Currently, the National Health Service (NHS) cannot routinely recommend surgical interventions such as renal denervation for hypertension due to the lack of conclusive evidence, although research in this field is ongoing [111]. Approaches

that aim to modulate sympathetic over-activity may have both a therapeutic and physiological advantage to high risk surgical interventions. Neuromodulation of sympathetic tone will counteract hypertension-induced cardiovascular damage, whilst retaining sympathetic reserve to enable cardiac performance during physical exertion. Genetic manipulations that alter cyclic nucleotide (cN) activity have had some success in attenuating sympathetic over-activity in hypertensive models, and advances in the field of genetic interventions can only be advantageous for enabling precise therapeutic targeting[112,113]. Moreover, the application of bioinformatics techniques to primary research observations may help to clarify some the complex interactions between pathways and their associated cellular and molecular processes[114-119], to enhance our understanding of the underlying pathophysiological processes that underpin disease initiation and progression[120-123]. However, the question that remains unanswered; does sympathetic impairment follow the disease itself, or does it actively contribute to the aetiology and progression of hypertension?

1.4 Animal Models of Hypertension

Throughout history, the application of animals for research purposes has provided anatomical insight and underpins our current knowledge and understanding of fundamental physiological concepts[124]. Alongside the expansion of an aging population, societies are now encountering the emergence of a wide number of problematic and debilitating illnesses. The primary use of animals in research is to provide physiological context to human pathological observations and to develop efficacious therapeutics for tackling and preventing disease. In order to develop relevant models for accurate experimental outcomes, animal models should mimic human disease pathology and progression with quantifiable characteristics, develop predictable symptomatic phenotypes that are sensitive to relevant therapeutic interventions and fulfil economic and animal welfare parameters[125]. However, modelling human disease phenotypes is often complicated by the multi-factorial nature of disease as well as species-related

physiological characteristics, comorbidities and differential life-spans. Hypertension is thought to be both polygenic and multifactorial, thus, a wide-range of animal models have been developed to study hypertension and the related pathophysiological phenotypes (Fig. 1.5). These models may be broadly classified as genetic or non-genetic models, and subsequently categorised by the root mechanism of hypertension inducibility. Of the non-genetic models, the Goldblatt two-kidney one-clip (2K1C) model of hypertension developed by Harry Goldblatt in 1934 is perhaps the most commonly used model for studying secondary hypertension[126]. The development of renal ischaemia leads to elevations in RAAS production and decreased diuresis causing vasoconstriction and increased blood pressure[127-129]. Elevations in renal and cardiac sympathetic nerve activity[130-132] and increased chemoreflex sensitivity[133] are also observed. Yet, the variation in kidney collateral vasculature between species, leads to vast differences in the duration of blood pressure elevation[129]. Transgenic animal experiments are most commonly conducted in mice due to the wide number of readily available models, however, these models display a wide range of characteristics and phenotypes depending on the specific mutation[134]. Although transgenic models are considered a model of primary hypertension and commonly display clinical CVD phenotypes, there are very few clinical cases of hypertension caused by single gene mutations, therefore the translational relevance for monogenic mutations in mice and human hypertension may be limited.

The SHR[135] is a genetic model of hypertension that was derived from the normotensive Wistar colony[135]. The SHR is one of the most widely utilised models for experimental hypertension[126,136] as the disease progression reflects a typical clinical hypertensive phenotype[129] and is also attenuated by clinical therapeutics. Both Wistar and the inbred Wistar-Kyoto (WKY) are deemed relevant controls for the SHR since both strains display similar hemodynamic profiles at all ages as measured using multiple methods including tail cuff and telemetric measurements [97,100,133,137-141]. The SHR displays normal blood pressure at four-weeks of age[23,100,125,139,142-147] with the early development of hypertension occurring from five- to six-weeks of age[125,139,143,144,147-150]. This

prehypertensive phase enables investigation of the pathophysiological phenotypes prior to the development of arterial hypertension. Moreover, an autonomic phenotype progressively develops, mirroring the early clinical phenotype[36,44-47]. Established hypertension develops after 12-weeks in almost 100 % of rats[125,139,143,145,147-149,151,152] and coincides with the development of secondary pathologies including impaired baroreflex sensitivity and control of heart rate[153,154], elevated chemoreceptor sensitivity[155], ventricular hypertrophy[126,142], cardiac arrhythmia[156] and vascular dysfunction[23,142,146,148,149,151]. These phenotypes are also sensitive to clinical blood pressure lowering interventions[126], making the SHR a highly relevant model for the study of hypertension (Fig. 1.5).

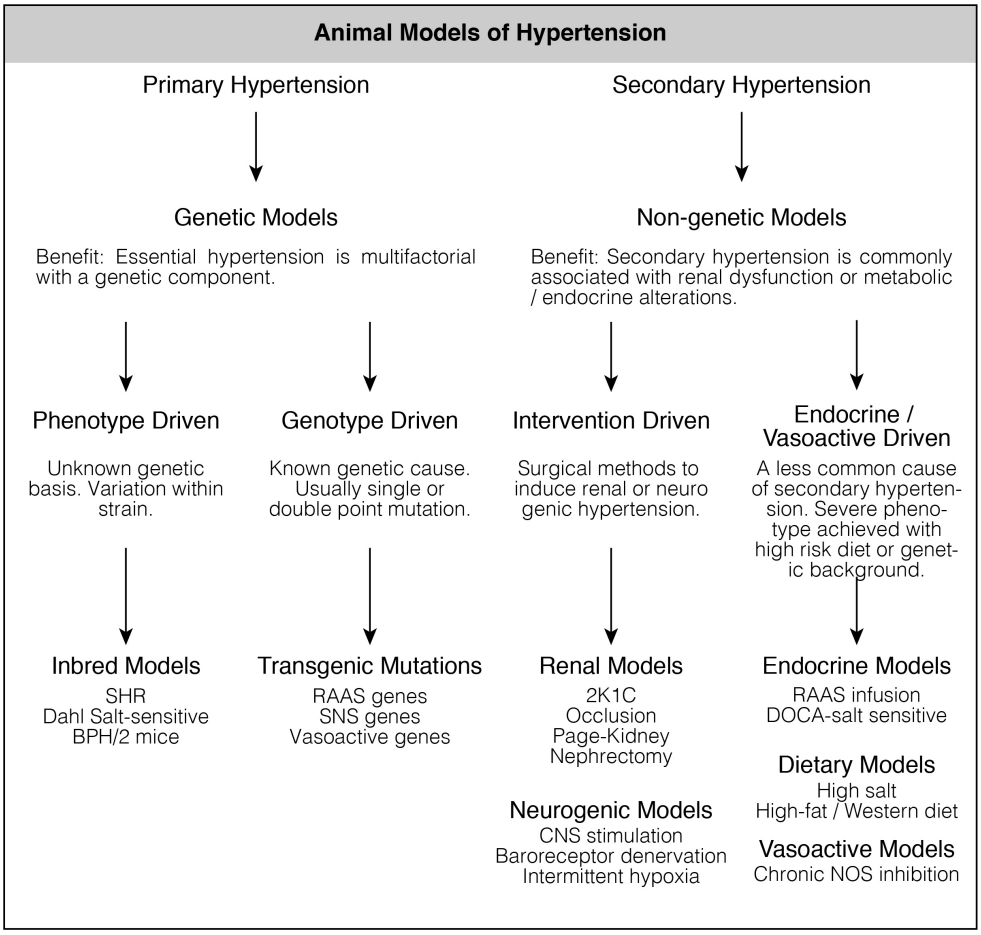


Figure 1.5. Animal Models of Hypertension
Animal models of hypertension can be broadly classified into genetic and non-genetic models. Genetic models may be used as surrogates for modelling primary hypertension and may be subclassified into phenotype driven or genotype driven models. Alternatively, non-genetic models provide a surrogate for investigating secondary hypertension and may be subclassified as surgical (intervention) or endocrine driven. This schematic was modified from Lerman et al., [129].

1.5 The Autonomic Nervous System

1.5.1 Overview of Autonomic Regulation

The 'autonomic nervous system' coined by Langley in 1898[157], comprises parasympathetic and sympathetic branches that provide a reciprocal regulatory link between the central nervous system (CNS), myocardium, and other peripheral organs[66] (Fig. 1.1). The regulation of autonomic tone is dependent on the integration of peripheral afferent signals with higher cortical inputs that determines the dominance of sympathetic or parasympathetic outflow. Increases in pressure (baroreflex) or changes in the chemical composition of blood (O_2, CO_2, pH, K^+, ions; chemoreflex) activate peripheral afferents that project to the nucleus tractus solitarius (NTS). Increased transmission from the NTS raises rostral ventrolateral medulla (RVLM) activity, that elevates sympathetic outflow from the intermediolateral column (IML)[158,159]. Autonomic outflow is also influenced by supramedullary nuclei inputs including the paraventricular nucleus (PVN), periaqueductal gray (PAG) and hypothalamus[160], where the integration of these signals underpins acute regulation of sympathetic and parasympathetic balance (Fig. 1.6).

1.5.2 Key Milestones in Neuroscience Research: A Brief Historical Perspective

During the last 10 years, the development of progressive technologies has led to exponential advancements in the field of neuroscience, yet our understanding of the fundamentals and principles of modern-day neuroscience are underpinned and shaped by two millennia of discoveries and observations. The Greek physician Herophilus of Chalcedon may be championed with the first anatomical identification of the nervous system in 335-280 BC[163]. By dissecting the spinal cord, Herophilus observed a physical and communicatory connection between the brain and peripheral organs. Two types of nerves were correctly described as motor neurons that could induce "*voluntary motion*" and sensory nerves "*capable of sensation*"[164,165]. This work was subsequently supported by Galen and others, but the discovery

was not appreciated until 1822, when Sir Charles Bell reported the differentiation between motor and sensory neurons[166].

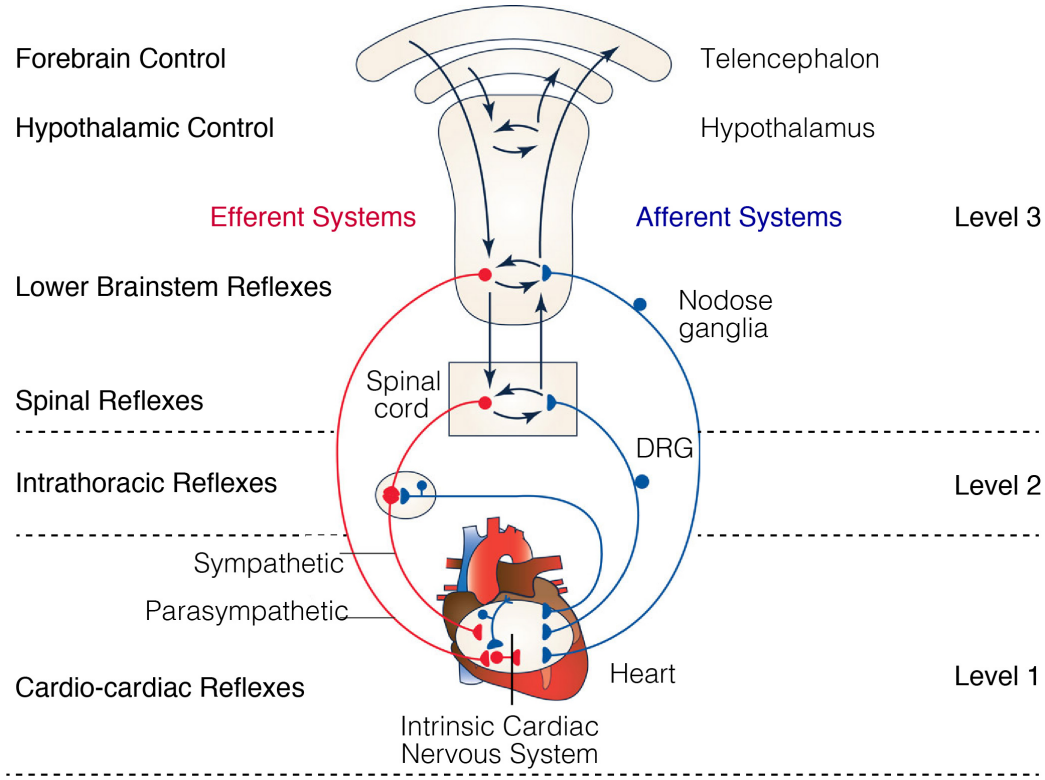


Figure 1.6. The Neuro-Cardiac Axis
Multiple levels of the neural-axis are involved in cardiac regulation. Autonomic control of the heart is comprised of several feedback loops including intracardiac neural feedback (level 1), intrathoracic extracardiac ganglia integration (level 2) and CNS feedback regulation (level 3)[161]. *DRG, dorsal root ganglia.* This figure was adapted from Hanna et al.,[161] and Shivkumar et al.,[162].

The birth of modern-day electrophysiology was defined by the observation of electrical signalling in tissues by Julian Bernstein and Emil du Bois-Reymond's. In 1865, the first recordings for the duration and nature of an electrical nerve impulse demonstrated that "*an action potential is a wave that travels along the nerve in both directions away from the stimulus*" [167,168]. Two decades later, in 1888, Sydney Ringer inadvertently recognised the fundamental importance of solutions containing Ca^{2+} ions for maintaining frog heart contractility[169] and identified the close relationship between Ca^{2+} and the electrical excitability of cells[170]. These discoveries proved

critical, and paved the way for the physiologist John Scott Burdon Sanderson who characterised and recorded the rate of electrical conduction and propagation throughout the heart[171]. In the closing decades of the 19th Century, Emil du Bois-Reymond proposed the notion of chemical transmission, stating "*Of known natural processes that might pass on excitation…either there exists at the boundary of the contractile substance a simulative secretion… or some other powerful stimulatory substance, or the phenomenon is electrical in nature*"[172]. Subsequently, in 1935 the Nobel Prize in Physiology or Medicine was awarded to Henry Dale and Otto Loewi for their discoveries relating to neurotransmission, where seminal experiments demonstrated the role of neurotransmitters in synaptic communication[172]. The field of chemical neurotransmission was advanced by Ulf von Euler who reported the discovery of noradrenaline (NA) in 1946, for which he was awarded the Nobel Prize in Physiology or Medicine with Bernard Katz and Julius Axelrod in 1970.

The field of neuroscience advanced rapidly throughout the 20th Century. In 1952, Alan Hodgkin and Andrew Huxley[173] discovered that the initiation and propagation of neuronal action potentials are facilitated by the transition in membrane permeability from potassium ions at rest, to sodium ions during depolarisation[174-177]. This breakthrough led to the realisation that changes in neuronal voltage underpin ionic changes that facilitate Ca^{2+}-dependent synaptic transmission and in 1963, Hodgkin and Huxley along with J. C. Eccles were awarded the Nobel Prize in Physiology or Medicine for their discoveries. The precise mechanisms responsible for presynaptic neurotransmitter release, however, remained unclear until 1993 where Thomas Südhof demonstrated that the fusion of transmitter-containing synaptic vesicles with the presynaptic membrane depended on the association of a multi-protein complex triggered by Ca^{2+}. In 2013, Südhof, J.E Rothman and R.W Schekman were awarded the Nobel Prize in Physiology or Medicine for their discovery of the molecular machinery and mechanisms involved in neurotransmitter release, which define our understanding of synaptic transmission today[178,179].

1.5.3 Autonomic Dysfunction in Hypertension

The regulation of sympatho-vagal balance plays an integral role in cardiovascular homeostasis and cardiac responses to physical or emotional disturbances[66,180-182]. The relationship between the brain and the heart has been observed by many scientists throughout history, but it was perhaps first recorded in 30 AD by the Roman physician Aulus Cornelius Celsus, who wrote "*fear and anger and any other state of mind may often be apt to excite the pulse"* [183]. Yet, the physiological mechanisms responsible for the mind-body connection remained elusive until the 19th Century, whereupon it was discovered that heart rate could be accelerated or decelerated by stimulation of two antagonistic systems: sympathetic or parasympathetic nerve fibres[157,184-187]. A chronic alteration in sympathetic / parasympathetic balance (dysautonomia) is a well-established contributor to many CVDs and is strongly linked to clinical outcome and prognosis[28,101,188-190]. Clinical techniques including microneurographic measurements of human muscle sympathetic nerve activity[28,191-193] and radiolabelled NA spill-over measurements within coronary arteries and arterial blood[28,101,130,131,193] consistently support preclinical observations that sympathetic activity is elevated in hypertension[130,131,190,192,194] and other CVDs[191,195].

What underpins elevated neurotransmission from sympathetic nerves in hypertension? The precise mechanisms that initiate and sustain sympathetic over-activity are not clear. Evidence suggests a potential role for reduced baroreflex sensitivity[27,28], elevated chemoreceptor sensitivity[18,70,133,196-199] as well as impaired afferent reflex sensitivity[200,201]. Moreover, elevated sympathetic activity is repeatedly observed using non-invasive microneurography techniques in young normotensive offspring of hypertensive patients[36,44-46,137,202-208] highlighting a potential causative role and genetic basis[142,209,210] for autonomic dysfunction in the aetiology of hypertension. Nevertheless, it is well-established that SNA is not uniformly altered within each ganglionic site, where differential sympathetic outflow from regional sympathetic ganglia is observed[29,95,144,193,211-213]. In primary human hypertension, it has been estimated that 50 % of

the increase in whole body NA spill-over may be attributed to increased overflow of NA from the kidneys and heart, where no increase in sympathetic nerve activity has been observed from ganglia innervating lungs, skeletal muscle or hepatomesenteric arteries[211]. Increased cardiac-sympathetic nerve activity (cSNA) specifically, is significantly elevated in younger patients that underpins early elevations in heart rate and CO[211] leading to the development of secondary pathologies such as hypertrophy[214] cardiac arrhythmia[102] and heart failure[104,194,195,215,216]. Moreover, in a recent sheep model of surgical renovascular hypertension, cSNA was shown to actively increase during the development of hypertension, where no increase in renal sympathetic nerve activity (rSNA) was observed[132]. Together, preclinical and clinical reports highlight a critical role for elevated cSNA, specifically, in the initiation and maintenance of hypertension[96,100,130,132,155,217] . Whether sympathetic over-activity is underpinned by a combination of impaired reflex pathways that are inappropriately regulated by altered higher centres inputs or, alternatively, whether pathology arises within peripheral sympathetic ganglia themselves is not known[28].

1.5.4 Cardiac-Sympathetic Over-Activity in Hypertension

The cervicothoracic sympathetic stellate ganglion located adjacently to T1-T4 of the spinal cord (Fig. 1.1) preferentially innervates the heart[184,218] and as such, exerts the greatest control over heart rate acceleration, contractility and conduction velocity at the atrio-ventricular node (AVN)[162]. Within the cardiac-sympathetic axis, intrinsic electrical pacemaker activity dictates resting heart rate and contractility that is increased via sympathetic NA and activation of myocardial $G\alpha_s$-coupled βARs. Within the sinoatrial node (SAN) the I_f or pacemaker current flows through the hyperpolarisation-activated cyclic nucleotide-gated (HCN) channel. HCN channels are often described as pacemaker channels as they generate rhythmic activity within the cells that they are expressed and are highly regulated by cNs[219]. The binding of cAMP to HCN channels expressed within the SAN lowers the threshold potential of these channels

required for activation and leads to cellular depolarisation; therefore, elevated levels of NA that increase myocardial cAMP, lead to increased rates of depolarisation of the SAN subsequently raising heart rate [220]. Conversely within the myocardium, PKA primarily mediates the effects caused by increased concentrations of βAR-evoked cAMP, and in particular plays a key role in regulating $[Ca^{2+}]_i$ concentrations. A sustained elevation in ventricular myocyte cAMP-PKA activity when measured by Förster Resonance Energy Transfer (FRET) microscopy[221] and / or reductions in cardiac NO-cGMP signalling[222-224] have been shown to enhance Ca^{2+} influx through L-type Ca^{2+} channels[225-227] and augment Ca^{2+}-induced Ca^{2+} release from sarcoplasmic reticulum (SR) stores[228]. Greater increases in $[Ca^{2+}]_i$ leads to larger ventricular contractions, however sustained elevations in $[Ca^{2+}]_i$ can also delay repolarisation leading to early after depolarisations and arrhythmia. Increases in cAMP or decreases in cGMP signalling are now though to play a key role in the aetiology of hypertension[100,130,132,155,217,229], cardiac remodelling and hypertrophy[221,230], cardiac arrhythmia[102 231] and heart failure[103,104,232 104,194,195,215,216].

1.5.5 Intrinsic Excitability: Regulators of Cardiac-Sympathetic Activity

The *N*-type Ca^{2+} channel is the primary neuronal voltage gated Ca^{2+} conductance [233,234] and as such, plays a key role in determining cytosolic Ca^{2+} concentrations during an action potential in sympathetic neurons[96,216,235-238]. Emerging evidence suggests that *N*-type Ca^{2+} channel activity is elevated in cardiac sympathetic ganglia of the preSHR (Fig. 1.7)[96] and in heart failure[216], augmenting $[Ca^{2+}]_i$ and raising the intrinsic excitability of these nerves[239]. Voltage-gated Ca^{2+} channel conductance is differentially regulated by kinase phosphorylation[96,240,241], where processes that decrease cGMP-PKG signalling or elevate cAMP-PKA signalling result in a net increase in Ca^{2+} channel conductance, when measured by voltage clamp in single cell experiments[227,240-245]. Thus, processes that selectively modulate the strength of cAMP or cGMP signals effectively regulate neuronal transmission[227,236-238,246-248].

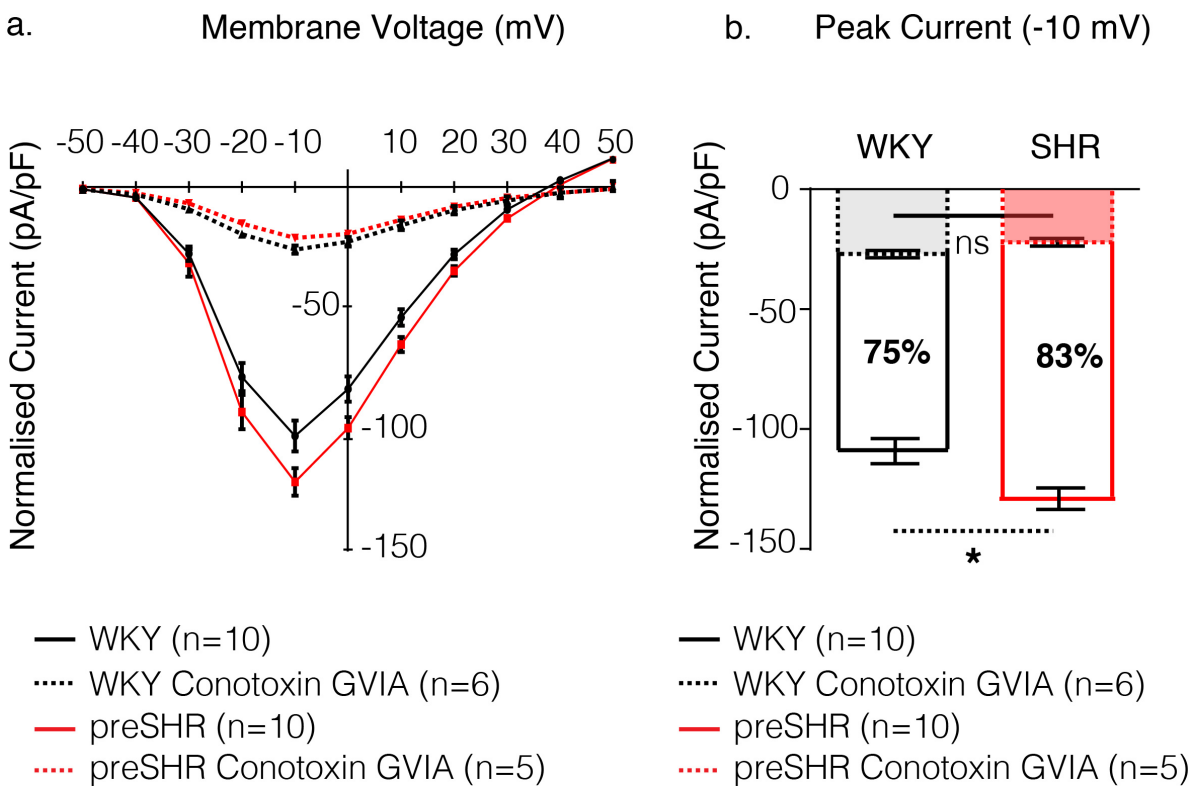


Figure 1.7. Elevated Calcium Conductance in preSHR Sympathetic Neurons
Whole cell voltage clamp was performed on cardiac sympathetic stellate neurons to investigate whole cell calcium properties (a). The whole cell Ca^{2+} current is larger in young preSHR sympathetic nerves compared to age-matched WKY cells (b). ω-Conotoxin GVIA (1 µM) that selectively blocks N-Type Ca^{2+} Channels (IC_{50} = 0.15 nM)[249], significantly reduced the current *N*-type Ca^{2+} current to similar levels in both strains. A 75 % reduction was observed in cells cultured from WKY stellate ganglia and an 83 % reduction was measured in neurons cultured from preSHR ganglia (b). Solid lines represent the mean of the WKY (black) and preSHR (red) control data. Dashed lines represent the mean of WKY (black) and preSHR (red) in the presence of ω-Conotoxin GVIA. Data are represented as mean ± SEM. This figure is adapted from Larsen et al.,[96].

Nitric oxide (NO) plays a critical role in regulating cardiovascular haemodynamics, however, the discovery of an endogenous role for NO has a long history. In 1859, Fredrick Guthrie found that the inhalation of amyl nitrite had significant cardiovascular modulating properties *"…one of the most prominent of its properties is the singular effect of its vapour, when inhaled, upon the action of the heart… after about 50 seconds, a sudden throbbing of the arteries of the neck is felt…"*[250]. Subsequently, in the late 1860's, the haemodynamic effects produced by amyl nitrite were explored and described by Thomas Lauder Brunton *"The diminished blood-pressure might*

be due to either a lessened power of the heart, or a dilatation of the arteries and a consequently diminished resistance" [251,252]. It took almost a whole century, however, until a physiological role for NO was described. Indeed, NO was found to induce significant vasorelaxation when applied to cultured cells that was shown to be dependent on the activation of soluble guanylyl cyclase (sGC) and 3',5'-cyclic guanosine monophosphate (cGMP)[253]. This discovery by Ferid Murad raised the question as to whether NO might serve as an endogenous signalling molecule. Concurrently, during the 1980's Robert Furchgott and John Zawadski made the serendipitous observation that only blood vessels with an intact endothelium would relax in response to acetylcholine, leading to the proposition of an endogenous 'Endothelial-derived Relaxing Factor' (EDRF) released from endothelial cells onto the underlying smooth muscle layer[254,255]. In 1988, Salvador Moncada[256] and Louis Ignarro[257] united these ideas independently, and each reported that EDRF was in fact NO, and that NO was released endogenously from endothelial cells onto smooth muscle cells of blood vessels, facilitating vasodilation[256 257]. Subsequently, the Nobel Prize in Physiology or Medicine was awarded to Murad, Furchgott and Ignarro in 1998 for their contributions towards the discovery of NO as an endogenous signalling molecule[258]. It is now well established that NO is synthesised constitutively in a wide range of tissues by the action of NO synthase enzymes (NOS) for which three isoforms have been identified: neuronal (nNOS, NOS1), endothelial (eNOS, NOS3) and inducible (iNOS, NOS2)[66]. The NOS enzymes are preferentially expressed in a distributed number of organs and tissues and NO plays a key role in cardiovascular regulation, relaxing vascular tone and modulating sympatho-vagal activity[259,260].

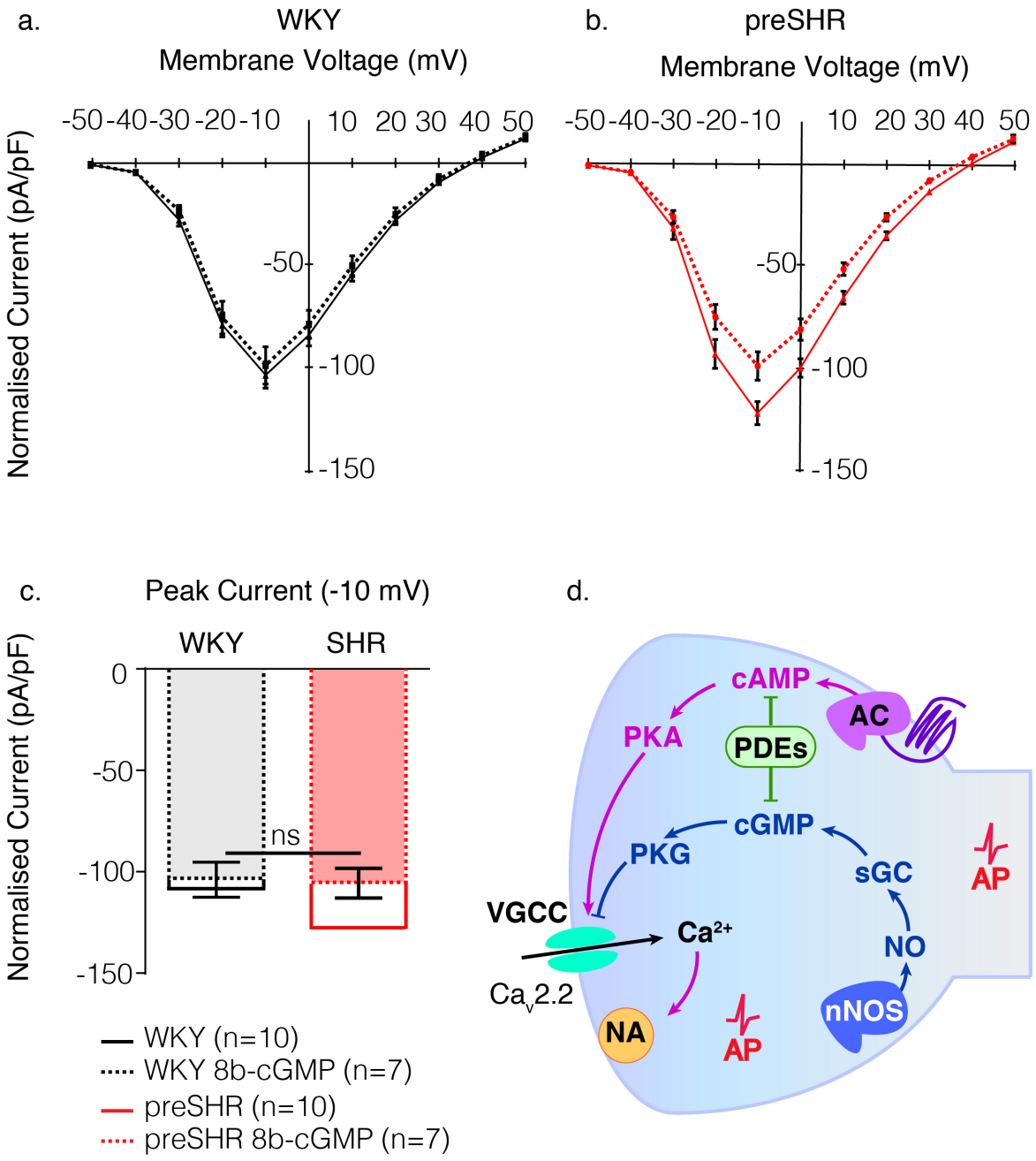


Figure 1.8. cGMP Reduces Calcium Conductance in preSHR Neurons
To ascertain whether cGMP signalling inhibits Ca^{2+} currents, whole cell voltage clamp was performed on WKY (a) and SHR (b) sympathetic neurons in the presence of a cGMP analogue 8-bromo-cGMP (8b-cGMP, 100 µM). 8bcGMP significantly reduced the elevated preSHR calcium currents to levels that were no longer greater than WKY calcium currents. Moreover, 8b-cGMP had no significant effect on the WKY calcium current (c). Solid lines represent the mean of the WKY (black) and preSHR (red) control data. Dashed lines represent the mean of WKY (black) and preSHR (red) in the presence of 8b-cGMP. Data are represented as mean ± SEM. Panels a-c are adapted from[96]. Model diagram represents *N*-type Ca^{2+} channel control by PKA and PKG; where PKA augments and PKG inhibits channel conductance. A model figure is depicted in (d) where NO-cGMP signalling pathways are decreased (blue) and cAMP-PKA signalling pathways are increased (pink) in disease. *VGCC, voltage-gated calcium channel.*

Within the vasculature NO is known to play a key role in regulating vascular blood flow, where NO released from endothelial cells acts on neighbouring vascular smooth muscle cells leading to vasorelaxation of large arteries. Unsurprisingly, impaired NO bioavailability is now known to be a key feature of endothelial dysfunction and also plays a key role in hypertension. The role of eNOS in regulating endothelial-dependent vasodilation is well known, however, more recently the importance of nNOS in the regulation of blood pressure maintenance has been recognised and. Preclinical studies have demonstrated that nNOS-dependent NO plays a key role in blood pressure regulation via reductions in sympathetic outflow from the CNS, alterations in baroreflex responses and attenuated βAR-evoked responses within the myocardium. Recently these findings have been confirmed in humans thus supporting preclinical evidence for the importance of nNOS in the regulation of blood pressure and peripheral resistance.

NO generated from nNOS is also a key player in sympathetic nerve activity regulation. In the SHR, impaired NO generation via nNOS[99,113,260-263] and downregulation of sGC[113] leads to significant reductions in cGMP production and PKG activity[96,113,262] that is critically linked to elevations Ca^{2+} conductance (Fig. 1.8)[96] contributes to the increased firing rate and spike amplitude observed in models of hypertension[216,239,264]. Consequently, it appears that processes coupled to NO-cGMP are critically impaired in cardiac sympathetic nerves early in disease, thus exacerbating or underpinning the observed Ca^{2+} phenotype in models of hypertension [96,113,262]. Whether adaptations in up-stream mediator reactivity (e.g. changes in GPCR membrane expression or alternate AC isoform activity) play a significant role in impaired cAMP and/or cGMP signalling in sympathetic neurons in hypertension remains to be established.

1.5.6 Phosphodiesterase Enzymes: Regulation of Cyclic Nucleotides

Phosphodiesterase enzymes (PDEs) regulate ion channel activity through selective termination of either cAMP and/or cGMP signals[225,226,248]; therefore, the acute spatial and temporal regulation of cN levels by PDEs is critical for maintaining a fine-balance between PKA- and/or PKG-mediated effects [265,266]. PDEs are a superfamily of enzymes (PDE1-11) that may be categorised by their specificity for either cAMP, cGMP or both cNs[267,268]. Five PDE isoforms (PDEs: 1, 2, 3, 10, 11) possess affinity for both cAMP and cGMP[266,269] (Table 1.2) acting as a point of convergence for cAMP/cGMP signalling cascades[270,271] (Fig. 1.9). As such, impairment of one of the cN signalling arms may correlate with defective signals in the alternative cascade[272]. Mutations in genes encoding PDEs have been observed in preclinical models and several human CVDs [224,230,266,270,273-279] and these data provide compelling evidence for a significant role of impaired PDE activity in the pathophysiology of hypertension[266]. In human and rat stellate sympathetic ganglia, PDE2A activity is reportedly elevated in hypertension[262,280] and previous reports indicate that this elevation results in preferentially diminished cGMP-PKG signalling[96,262]. Moreover, genetic over-expression of PDE2A in neuronal stellates has been shown to recapitulate the sympathetic Ca^{2+} phenotype seen in disease[262]. Which specific PDE isoforms are present in the sympathetic stellate ganglia and the relationship between the PDE superfamily and sympathetic over-activity remains to be established.

Table 1.2. Phosphodiesterase Isoforms and Cyclic Nucleotide Substrates

Substrate Specificity	PDE Subtype
cAMP	4, 7, 8
cGMP	5, 6, 9
Dual Specificity (cAMP / cGMP)	1, 2, 3, 10, 11

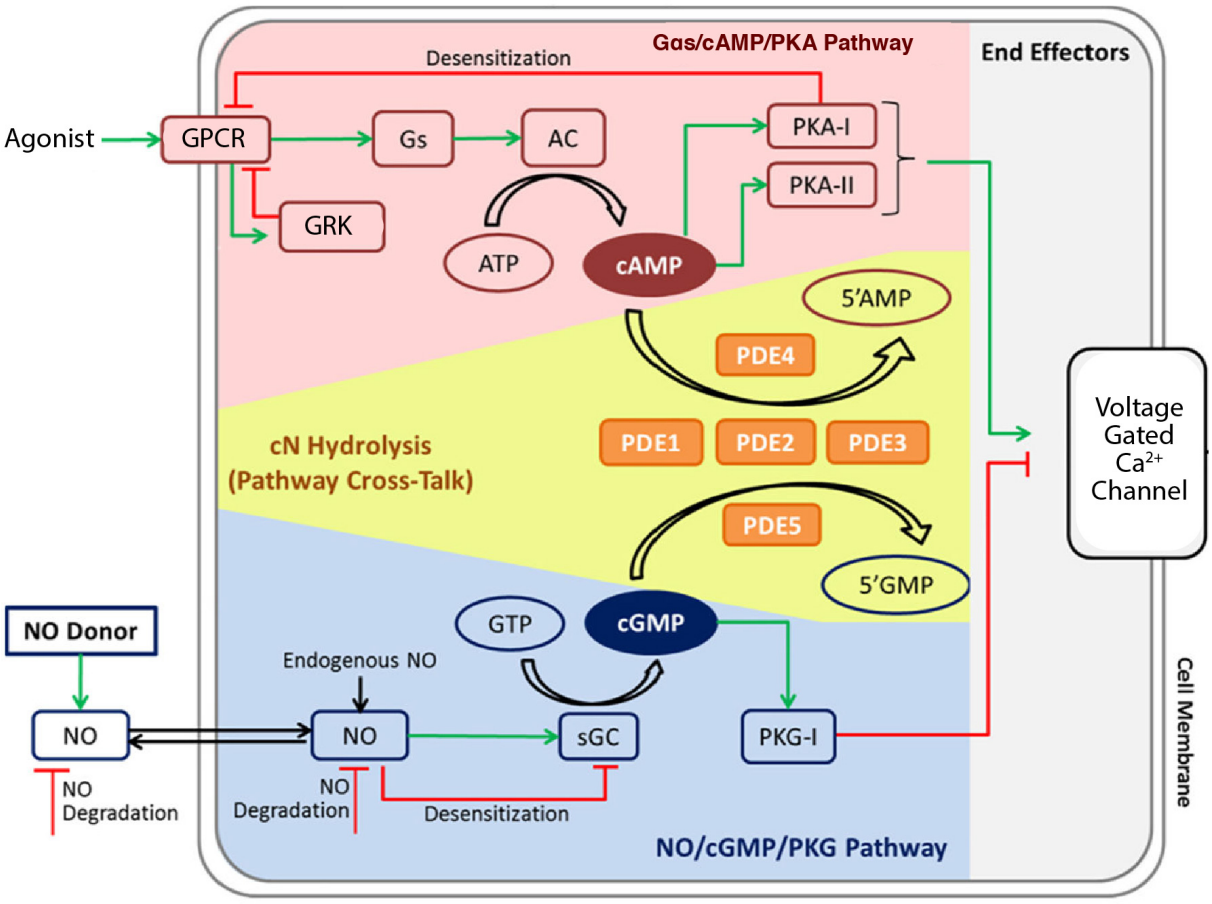


Figure 1.9. Voltage-gated Calcium Channel Regulation by Cyclic Nucleotides
PDEs reduce cN activity, and are also regulated by cNs themselves, forming a point of convergence between the two cN signalling pathways. Signalling via cAMP and cGMP leads to activation of the protein kinases, PKA (isoforms PKA-I and PKA-II) and PKG (PKG-I) respectively. cAMP-PKA signalling has a stimulatory effect on voltage-gated calcium channels, where PKG has an inhibitory effect on calcium conductance. *GPCR, G-Protein Coupled Receptor; GRK, GPCR Kinase; AC, adenylyl cyclase; NO, nitric oxide; sGC, soluble guanylyl cyclase.* This figure was adapted from Zhao et al., [226]

1.6 Conclusion

Several key sympathetic adaptations are reported in models of neurogenic hypertension, including increased neuronal firing rate and burst frequency[239,281], elevated and aberrant regulation of $[Ca^{2+}]_i$ that facilitates exocytosis[113,282], decreased transmitter reuptake[283-287], and alterations in inhibitory feedback systems coupled to intracellular signalling cascades[100,288]. Establishing which molecular and biochemical alterations occur in rat and human sympathetic ganglia prior to elevations in blood pressure may be considered critically important for advancing our understanding of the pathophysiology of hypertension and the development of new diagnostic technologies as a way to facilitate precise therapeutic targeting. The overall objective of this thesis was to establish which gene transcripts are altered in hypertensive rat stellate ganglia and to confirm the presence of these genes in stellate ganglia from human donors to give this work translational relevance. Using this transcriptomic dataset, I have aimed to identify targets that may be functionally impaired in the hypertensive model and to test these hypotheses using a combination of fluorescence microscopy and cellular and molecular biochemistry techniques.

1.7 Thesis Aims

My specific aims were:

1. To establish whether the observed Ca^{2+} phenotype in the stellate ganglia may be underpinned by changes in gene transcription in rat models of hypertension.
2. To assess whether changes in gene transcription correlate with physiological alterations in protein expression and / or the activity of intracellular signalling pathways.
3. To determine whether receptor pathways coupled to cN generation are altered in the SHR stellate ganglia and to ascertain whether these pathways influence exocytosis.
4. To quantify catecholamine release and to gain an overview of neurotransmitter/co-transmitter profiles from healthy and diseased sympathetic stellate ganglia.
5. To confirm key observations in human donor stellates for contextual relevance i.e. are our *a priori* transcripts conserved?

2

General Methods

2.1 Introduction

This chapter examines the methods used to investigate the sympathetic stellate ganglia phenotypes in adult hypertensive SHR, young prehypertensive SHR (preSHR) and age matched normotensive Wistar control rats. First, I present an overview of the surgery required for sympathetic stellate ganglia dissection and describe the techniques required for culturing sympathetic stellate neurons. Secondly, I describe a protocol for immunocytochemistry and confocal imaging. Thirdly, I describe the optimisation and experimental techniques employed to measure intracellular cAMP, PKA using FRET microscopy and $[Ca^{2+}]_i$ using live Ca^{2+} imaging. Fourthly, I describe the techniques and optimisation parameters for RNA extraction. Fifthly, I describe the differential expression, gene ontology and pathway analyses for RNA sequencing (RNA-seq) data between hypertensive and normotensive rats. Finally, I explain the methods for quantitative real-time polymerase chain reaction (qRT-PCR), in addition to the biochemical approaches for measuring protein levels and enzyme activity.

2.2 Animals

Three- to five-week-old male young SHR (preSHR; 70-120 g), 12- to 14-week-old (300-340g), and 16- to 20-week-old male SHRs (340-380 g) with established hypertension, and age-matched normotensive Wistar control rats were obtained from Envigo, UK. At this age, the SHR are classified as prehypertensive as blood pressure is not elevated relative to control rats until six-weeks of age[150], but sympathetic activity is already increased[100]. All rats were housed in standard plastic cages and artificial lighting was fixed to a natural 12-hour light/dark cycle. Food and water were available ad libitum. All experiments were performed in accordance with the UK Home Office Animal Scientific Procedures Act 1986 (ASPA) and approved by the University of Oxford (PPL 30/3131; David J. Paterson). Rats were anaesthetized in an induction chamber (3-5 % isoflurane) and humanely killed by a Home Office approved Schedule 1 method: overdose of pentobarbital (Euthatal, 200 mg/ml) and exsanguination.

2.3 Isolation of Rat Sympathetic Stellate Neurons

Cardiac-sympathetic stellate ganglia were cultured into a single cell preparation to investigate the cellular and molecular properties of stellate neurons from hypertensive and prehypertensive rats compared with stellate neurons from healthy control rats.

2.3.1 Cardiac-Sympathetic Stellate Ganglia Dissection

The sympathetic stellate ganglia (cervicothoracic ganglia) are located alongside vertebrate T1 to T4 (Fig. 2.1,a). The stellate ganglia are the primary sympathetic ganglia that innervate the heart[162], and as such exert the greatest control over increases in heart rate and contractility. Cardiac stellate ganglia were identified by their anatomical location and distinct morphology (Fig. 2.1,b). Ganglia were removed and dissected from the right and left sides of the spinal column, and combined for culturing to increase cell yield. The dissected were ganglia were placed in ice-cold Hank's Balanced Salt Solution (HBSS).

2.3.2 Neuronal Isolation from Rat Sympathetic Cardiac-Stellate Ganglia

Stellate ganglia dissociated into single cell neurons using a previously described method [289]. Stellate ganglia were de-sheathed from surrounding connective tissue and sub-dissected into small (1 mm^3) pieces. Stellates were enzymatically digested with collagenase (Type IV, 1 mg/ml, Worthington) in Ca^{2+} and Mg^{2+}-free Dulbecco's phosphate-buffered saline (dPBS) in a shaking water bath (37 °C , 18-30 mins) with the duration of digestion determined by the age of the animal and size of the ganglia. Collagenase was removed and replaced with trypsin (TRL3, 1 mg/ml) in dPBS without Ca^{2+} and Mg^{2+} (37 °C , 18-30 mins). Following trypsin incubation, the stellates were washed with neuronal blocking medium (Table 2.1) that was temperature-equilibrated prior to use (37 °C), to inhibit enzyme activity. The ganglia were dissociated into a single-cell suspension in a 15 ml falcon tube via manual trituration using fire-polished Pasteur pipettes in a temperature equilibrated (37 °C) neuronal plating medium (Table 2.1). The cell

suspension was left for 2-3 minutes for large debris to settle at the base of the tube, and the top 0.5 ml of solution removed and placed in a plastic petri dish (6 cm diameter). Fresh temperature-equilibrated (37 °C) neuronal plating medium (0.5 ml) was added to the tube and this process was repeated five to six times until an appropriate number of cells were collected in the petri dish. The cell suspension was added to 4-well plates (10 mm diameter) containing poly-D-lysine / laminin-coated glass coverslips (6 mm, VWR International) and the cells were incubated in neuronal plating medium (37 °C , 95 % O_2 / 5 % CO_2) for 2-3 days until required for use.

2.3.3 Preparation of Culturing Media

The media used for the isolation and culturing of isolated sympathetic neurons was based on methods previously described[290]. Modified Leibovitz's L-15 neuronal blocking medium contained: 96.8 % L-15 medium supplemented with 0.6 % D-(+)-glucose solution, 2 mM L-glutamine, 100 units/ml penicillin, 100 µg/ml streptomycin, 10 % foetal bovine serum (FBS). Modified Leibovitz's L-15 plating medium contained: L-15 medium (90 %) supplemented with 24 mM $NaHCO_3$, 38 mM glucose, 50 units/ml penicillin and 50 µg/ml streptomycin, 50 ng/ml Nerve Growth Factor (NGF), 10 % FBS. The solution was adjusted to pH 7.6 and all media were filter sterilised (0.2 µm filter) before storage at -20 °C. A list of the media constituents are included (Table 2.1).

Table 2.1. Neuronal Blocking and Plating Media

Neuronal Blocking Medium	Neuronal Plating Medium
96.8 % L-15 Medium	90 % L-15 Medium
2 mM L-glutamine	24 mM $NaHCO_3$
0.6 %D-(+)- Glucose solution	38 mM Glucose
0.5 % penicillin/streptomycin	1 % penicillin/streptomycin
10 % FBS	50 ng/ml NGF
	10 % FBS

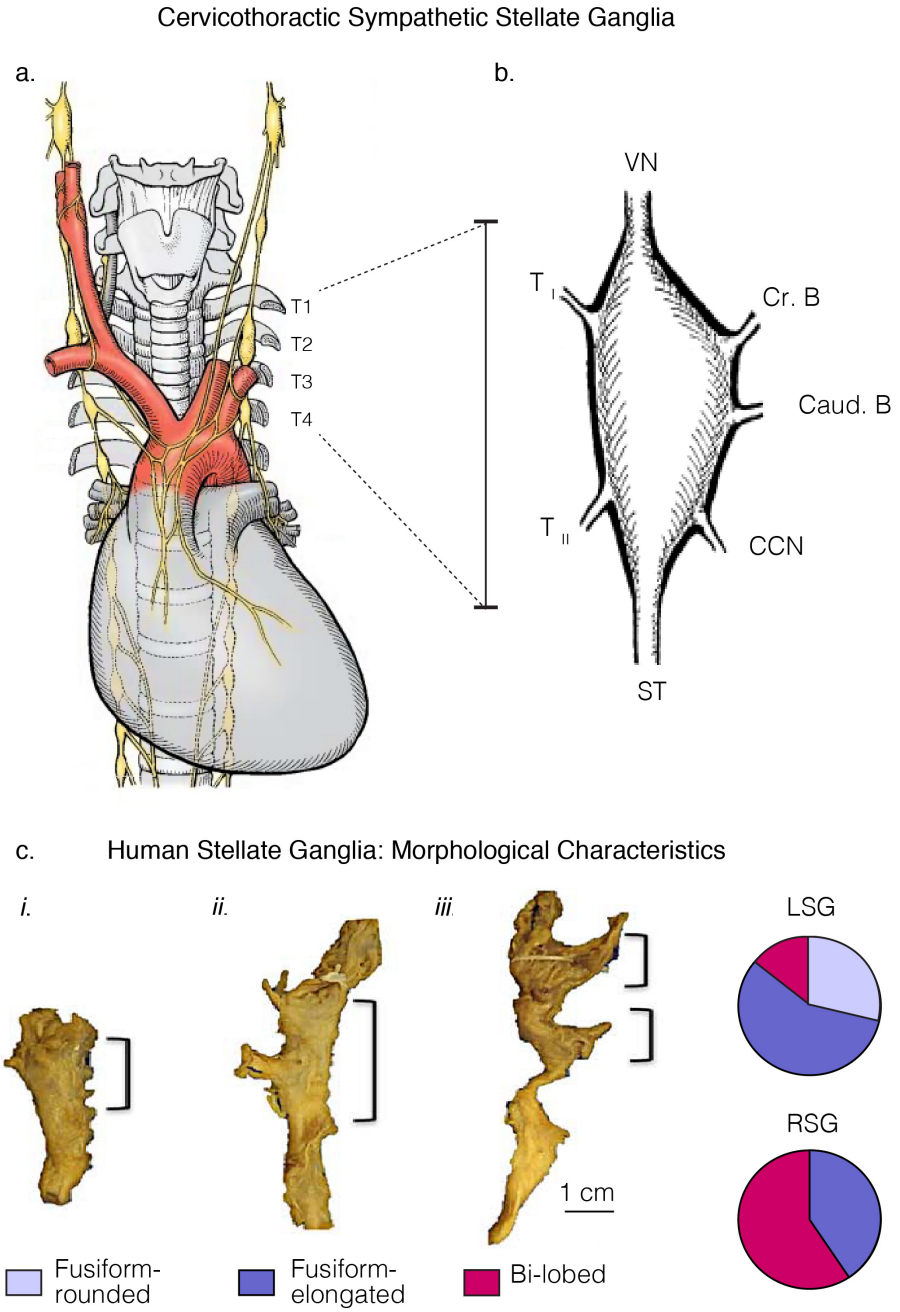


Figure 2.1. Anatomical and Morphological Characteristics of Stellate Ganglia
The cervicothoracic stellate ganglia are located bilaterally, and are localised adjacently to the spinal cord vertebrate T1-T4 (a). The stellate ganglia project to different anatomical sites via distinct ganglionic projections (b). These include Cr.B that represents the cranial branch of the subclavian loop, Caud. B that projects to the caudal branch of the subclavian loop. CCN corresponds to the caudal cardiac nerve. T_I and T_{II} are connecting branches to the spinal nerves. VN represents the vertebral nerve and ST is the inter-ganglionic branch of the sympathetic trunk. The size of the stellate ganglion increases during the first 2 months from birth. Based on the observations in this thesis and previously reported observations[218], the size of the rat stellate ganglia ranges from ~2-3 mm in young 3- to 6-week-old rats, to ~4-6 mm in adult 12- to 20-week-old rats. Human stellate ganglia are characterised by three major morphological groups including fusiform-rounded (c.*i*), fusiform elongated (c.*ii*) and bi-lobed (c.*iii*). No fusiform-rounded ganglia were observed on the right-side in human. Scale bar 1 cm. Panels are adapted from http://www.brainkart.com/article/Sympathetic-Trunk_14914/ (a), Korzina et al., (b) [218] and Kwon et al., (c) [105].

2.3.4 Preparation of Poly-D-Lysine / Laminin Coated Coverslips

Poly-D-lysine was prepared to a stock solution (1 mg/ml) in double distilled H_2O (ddH_2O) with borate buffer (borax, 4.75 mg/ml) and boric acid (3.1 mg/ml) and stored at -20 °C. Glass coverslips (6 mm, VWR International) were coated in poly-D-lysine solution (0.1 mg/ml) over-night at room temperature before washing with ddH_2O. Coverslips were dried and kept in the refrigerator (4 °C) for one month. On the day of use, poly-D-lysine-coated coverslips were placed in a laminin solution (30 µl laminin with 720 µl Leibovitz's L-15 solution) and incubated for three to four hours, before removal of the solution prior to cell plating.

2.4 Immunocytochemistry

Immunofluorescence was carried out to identify the expression of receptors of interest on tyrosine hydroxylase (TH) positive sympathetic neurons. Sympathetic stellate neurons were cultured from three- to five-week preSHR and age-matched Wistar control rats as described, and cells were plated on poly-D-lysine / laminin pre-coated coverslips (12 mm; BD Bioscience). Stellate neurons were fixed with paraformaldehyde (2 %, 5 mins) before blocking and permeabilising with a solution containing goat serum (10 %), bovine serum albumin (0.3 %) and Triton X-100 (0.1 %) in dPBS without Ca^{2+} and Mg^{2+} (1-hour, room temperature). Cells were washed thoroughly with dPBS (3 x 10 min) and incubated in primary antibodies (1-hour, 37 °C). The antibodies used in this thesis and their concentrations are listed in Table 2.2. Cells were incubated with the appropriate secondary antibodies (Table 2.2) for 2 hours (37 °C) before they were mounted on microscope slides using DAPI-containing medium to label nucleii (Vectashield, Vector Laboratories). The slides were sealed with nail polish and kept refrigerated in the dark (4 °C) until required. For negative control experiments, no primary antibodies were used. Cells were imaged using 40X or 60X objectives on a confocal microscope (Zeiss LSM 880 Airy Scan Upright Confocal) and data were captured using Zen Black software. Z-stack images were combined into stacks and cell sizes measured using Fiji software (ImageJ)[291,292].

Table 2.2. List of Primary and Secondary Antibodies and Optimal Dilutions

Reactivity	Antibody	Derivation	Catalogue	Dilution
TH	Anti-Tyrosine Hydroxylase	Monoclonal Mouse IgG1	T1299, Sigma	1:250
β_1AR	Anti-beta 1 Adrenergic Receptor	Rabbit polyclonal IgG	Ab3442, Abcam	1:100
β_2AR	Anti-beta 2 Adrenergic Receptor	Rabbit monoclonal IgG [EPR707(N)]	Ab182136, Abcam	1:200
α_{2A}AR	Anti-alpha 2a Adrenergic Receptor	Rabbit polyclonal IgG	Ab92650, Abcam	1:100
AT_1R	Anti-Angiotensin Type 1 Receptor	Goat polyclonal IgG	sc-31181, Santa Cruz	1:100
Mouse	Secondary AlexaFluor A488	Goat	Invitrogen general	1:1000
Rabbit	Secondary AlexaFluor A647	Goat	Invitrogen general	1:1000
Goat	Secondary AlexaFluor A647	Donkey	Invitrogen general	1:1000

2.5 Förster Resonance Energy Transfer (FRET)

2.5.1 FRET Overview

Cyclic nucleotide signalling is a rapidly expanding field of research. With the development of improved methods for detecting cAMP and cGMP signalling, cNs are now known to be involved in the amplification and regulation of a wide-range of cellular effects, where impaired signalling plays a key role in the pathophysiology of several diseases [266,278,293]. As mentioned in Chapter One, cNs play a critical role in regulating $[Ca^{2+}]_i$ through activation of protein kinases that modulate voltage-gated ion channel activity[226,234]. Emerging evidence suggests that cN cascades may play a role in sympathetic over-activity through altered phosphorylation of voltage gated *N*-type Ca^{2+} Channels that results in elevated Ca^{2+} conductance[96]. In this thesis, FRET microscopy was utilised to measure real-time cAMP generation and PKA activity in sympathetic stellate neurons in response to pharmacological stimuli. FRET microscopy is a reliable and sensitive method that has been developed for the investigation of real-time intracellular signalling dynamics, and is most commonly used for the measurement of cNs and their effectors (protein kinases)[265,266,294]. Prior to the development of FRET sensors and advancements in fluorescence microscopy techniques, radioimmunoassays[295] or protein-binding assays[296] were the primary techniques for measuring cN activity within tissues, yet these assays were limited by their lack of sensitivity (i.e. measurements were conducted in tissues rather than single cells)

and their inability to measure fast, dynamic changes in cN generation and inhibition. In the last 20 years, significant advances in technology have led to the development of genetically-encoded FRET probes that are able to successfully measure rapid changes in cN signalling with high spatiotemporal resolution in single cells [297,298].

2.5.2 cAMP FRET Sensors

cAMP is a ubiquitous second messenger protein that regulates physiological processes on a millisecond scale, via acute targeting of several downstream proteins[298]. These include PKA that phosphorylates a plethora of intracellular targets, cN-gated ion channels (CNCG) [299], two isoforms of Exchange Protein directly activated by cAMP (Epac1, Epac2) [300] and the Popeye domain-containing (POPDC) family of proteins[301]. The first FRET sensors designed to measure cAMP were developed in the early 2000's [297,302] and were based on the structure of PKA. FRET describes an energy transfer process, where electrons are transferred from a donor to an acceptor fluorophore when the fluorophores are in close proximity (<10 nm). This transfer of energy changes the emission wavelengths of the sensor fluorophores, which can be used as a surrogate for the molecule of interest. The first improvements in the development of cAMP indicators were achieved by modifying the structure of the FRET backbone to mimic the high affinity, cAMP-binding domain of Epac1 [303-305]. This new generation of Epac1-based cAMP FRET sensors [25,26] exhibited several advantages over the initial PKA-based FRET sensors by the incorporation of a single cAMP-binding domain and backbone mutations that prevented catalytic activity [303-305]. The cAMP FRET sensors Epac1-H30 and Epac1-H187 cAMP were used in this thesis. Epac1-based FRET sensors are described as loss-of-FRET sensors because in its native structure (i.e. low cAMP) the donor and acceptor fluorophores are in close proximity (~10 nm), whereas the binding of cAMP relieves Epac1 from its closed conformation driving the fluorophores further apart [303]. Secondary improvements to the Epac1 sensor construct were made by the development of a cytosolic-localised, catalytically inactive sensor with a greater

dynamic range than previous sensors[305]. This was achieved through the mutation of the catalytic sequence Dishevelled-Egl-10-Pleckstrin (DEP) into a catalytically dead variant, to generate the cyan fluorescent protein (CFP) and yellow fluorescent protein (YFP) labelled FRET sensor (CFP-Epac1-(δDEP-CD)-YFP), known as Epac1-H30 (Fig. 2.2).

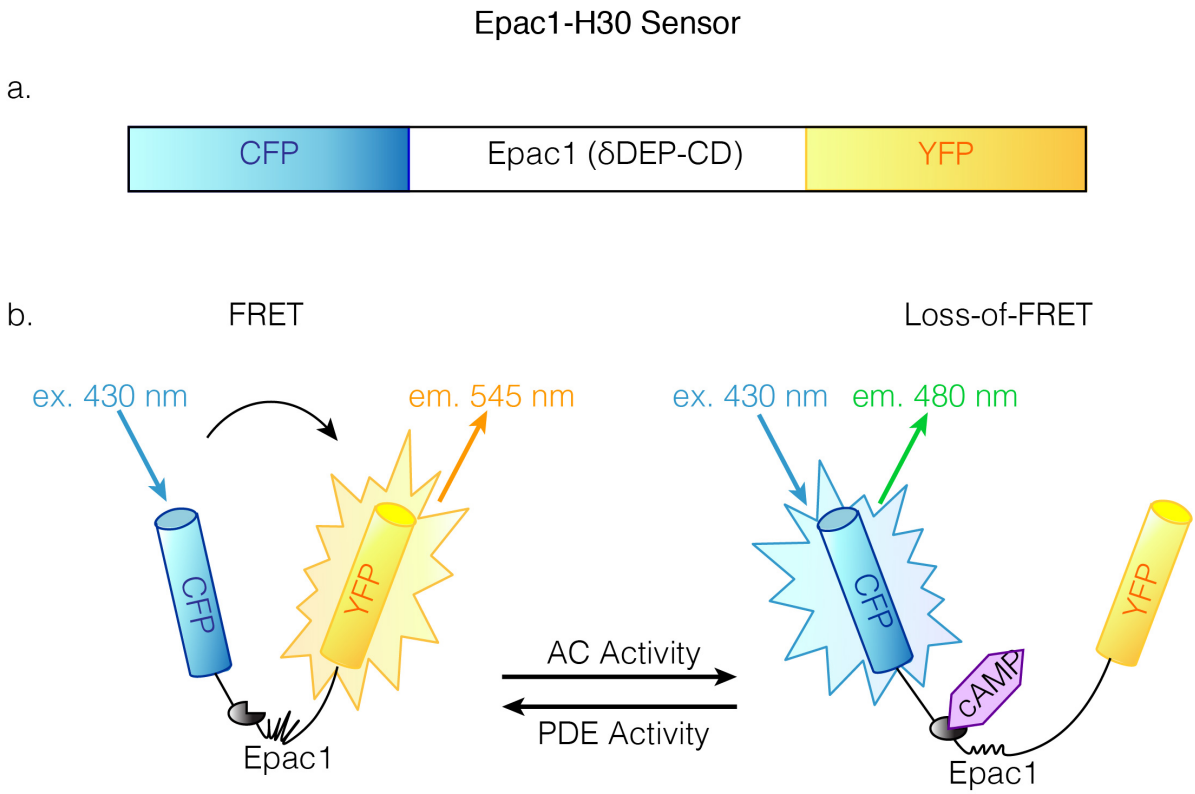


Figure 2.2. Epac1-H30 FRET Biosensor Construct and Mechanism
The Epac1-H30 FRET sensor construct is based on the native Epac1 structure. Mutations were made in the Dishevelled-Egl-10-Pleckstrin (DEP) to obtain a catalytically dead variant (δDEP-CD). Two fluorophores cyan fluorescent protein (CFP) and yellow fluorescent protein (YFP) are attached to the Epac1 backbone[305] (a). At low cAMP concentrations, Epac1-H30 resides in a closed conformation, enabling electron transfer (i.e. FRET) between the fluorophores. When concentrations of cAMP increase, a cAMP molecule binds Epac1, relieving the sensor of its closed structure driving the fluorophores further apart preventing electron transfer (i.e. loss-of-FRET) shifting the emission wavelength preferentially from a yellow towards the blue spectra. *AC, adenylyl cyclase; PDE, phosphodiesterase.* Panel b was adapted from Zaccolo, 2015 [306].

Epac1-H187 (classified Epac-S^{H187} by the developers[307]) is a modified 4th generation loss-of-FRET sensor generated by Jalink et al., [307] that was incorporated into a viral vector by Dr. Lefkimmiatis for improved transduction into mammalian cells[96]. The development of Epac1-H187 FRET biosensor incorporated a superior donor fluorophore (mTurquoise2) and two copies of an optimised acceptor fluorophore, the circular permutated Venus (cp^{173}Venus) which is pH and UV insensitive and more efficient in energy absorption than YFP (Fig. 2.3) [308]. A point mutation introduced into Epac1 (Q270E) also increased the affinity for of the cAMP-binding domain by more than 2.5-fold[307]. Accordingly, Epac1-H187 has a vastly improved dynamic range, increased brightness and photostability compared with Epac1-H30 [307].

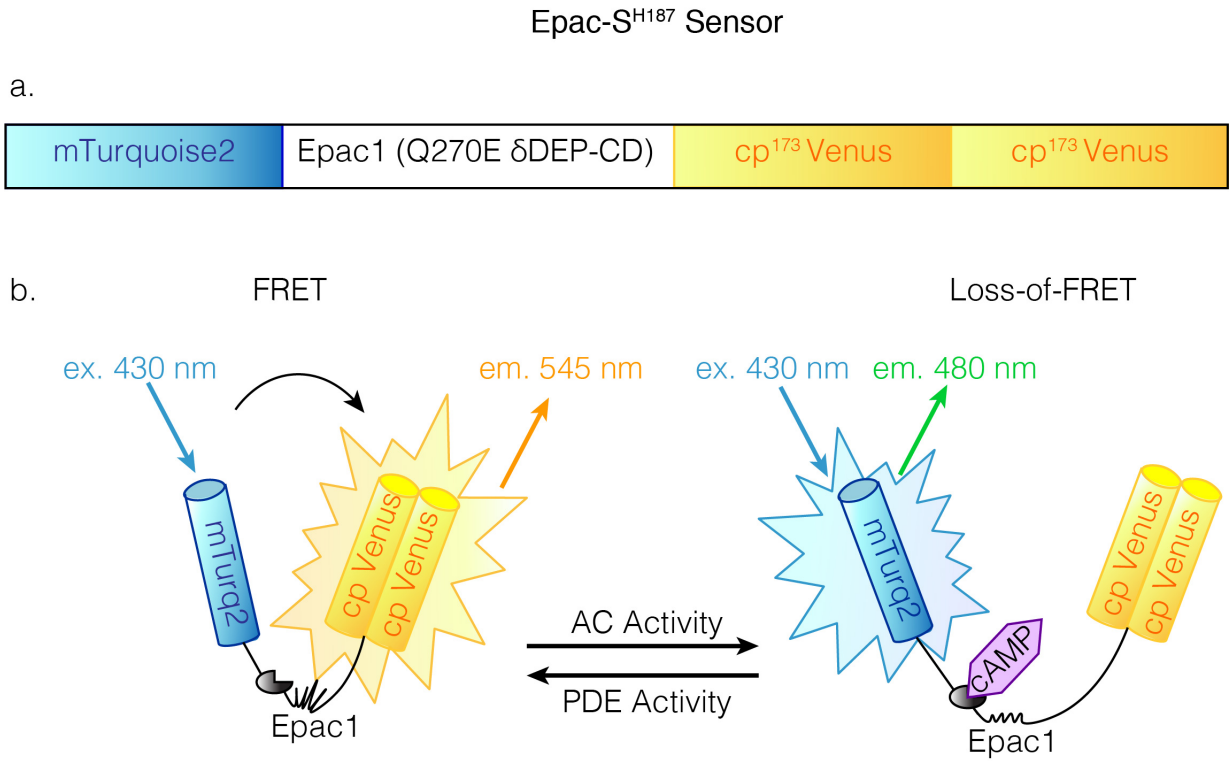


Figure 2.3. Epac1-H187 FRET Biosensor Construct and Mechanism
The Epac1-H187 FRET sensor construct is based on the native Epac1 structure. Mutations were made in the Dishevelled-Egl-10-Pleckstrin (DEP) to obtain a catalytically dead variant (δDEP-CD). The point mutation in Epac1 (Q270E) to increase the affinity of the cAMP-binding domain. The addition of an improved donor fluorophores mTurquoise2 (mTurq2) and two copies of the circular permutated Venus (cp^{173}Venus) increased the dynamic range and stability of the Epac1-H187 FRET sensor compared to previous variants [307] (a). At low cAMP concentrations, Epac1-H187 resides in a closed conformation, enabling electron transfer (i.e. FRET) between the fluorophores. Increasing concentrations of cAMP prevent electron transfer between the fluorophores (i.e. loss-of-FRET) shifting the emission wavelength preferentially from yellow towards the blue spectra. *AC, adenylyl cyclase; PDE, phosphodiesterase.* Panel b was adapted from Zaccolo, 2015 [306].

2.5.3 PKA FRET Sensor

To detect subtle changes in PKA activity, sympathetic neurons were transduced with the cytosolic A kinase Activity Reporter 4 (AKAR4) FRET sensor. The AKAR4 construct was generated by Depry et al.,[309] by placing a substrate for PKA (phosphorylation sensing domain, PSD) and a 'molecular switch' between the donor (Cerulean) and acceptor (cp^{173}Venus) fluorophores[309].

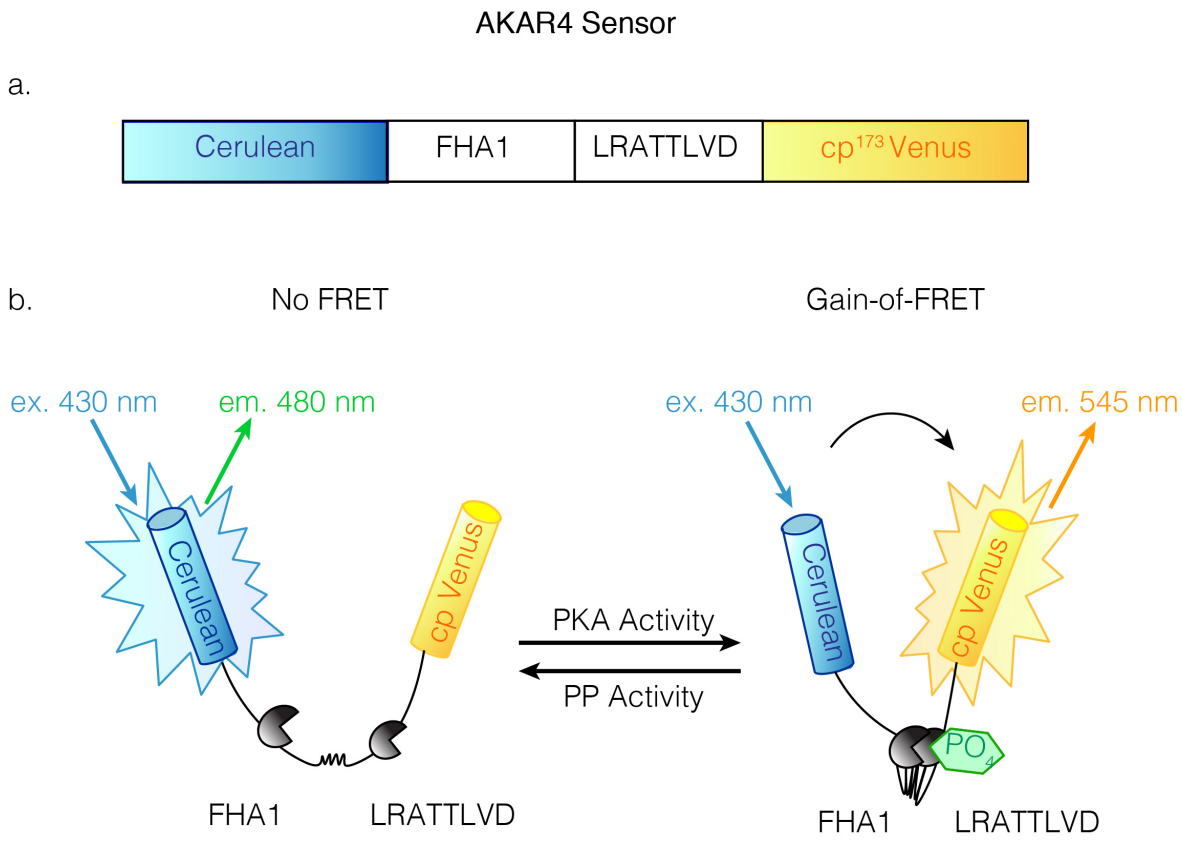


Figure 2.4. AKAR4 FRET Biosensor Construct and Mechanism
The cytosolic A kinase Activity Reporter 4 (AKAR4) [309] was generated by placing a substrate for PKA (phosphorylation sensor, LRATTLVD) and a high affinity 'molecular switch' (FHA1) between the donor (Cerulean) and acceptor (cp^{173}Venus) fluorophores. with low PKA activity, the FRET sensor resides in an open conformation preventing electron transfer between the fluorophores (i.e. no FRET). When PKA activity increases, the phosphorylation of the phosphorylation sensor (LRATTLVD) enables its binding to FHA1 resulting in a conformational change in the FRET sensor that brings the fluorphores in close proximity enabling electron transfer (i.e. gain-of-FRET). This shifts the emission wavelength preferentially from a blue towards the yellow spectra. P*KA, protein kinase A; PP, phosphatase.* Panel b was adapted from Zaccolo, 2015 [306].

Phosphorylation of the phosphorylation-sensing domain (LRATTLVD) by PKA, enables the PSD to bind a phospho-amino acid binding sequence, initiating a conformational change that facilitates close proximity of the two fluorophores (Fig. 2.4). The phospho-amino acid binding domain selected for AKAR4 was a phospho-threonine binding Forkhead Associated Domain I (FHA1) due to its high affinity to the PSD sequence[309]. As AKAR4 is a surrogate substrate for PKA, activation of the sensor reflects the activity of PKA, therefore, when pharmacological agents activate targets upstream of PKA (e.g. $G\alpha_s$-coupled G-protein Coupled Receptor (GPCR) agonists or AC activators) the FRET change observed reflects the amplification of the cAMP second messenger signalling system[310]

2.5.4 Generation and Amplification of FRET Sensors

2.5.4.1 Epac1-H187

The Epac1-H187 vector was made by Dr. Lefkimmiatis. The mammalian expression vector pcDNA3 encoding Epac-S^{H187} developed by Klarenbeek J et al.,[307] was digested with the restriction enzymes EcoRI and HindIII yielding the complete Epac-S^{H187} open reading frame and introduced in the pDual vector. Ad-CMV-Epac1-H187 was generated, amplified, purified and titrated to stock containing 3.2 $x10^{10}$ viral particles/ml (PFU / ml) by Vector Biolabs.

2.5.4.2 AKAR4

Ad-CMV-AKAR4 was amplified, purified and titrated to stock containing 8.4 x 10^{10} viral particles (PFU/ml) by Vector Biolabs.

2.5.4.3 Epac1-H30

Ad-CMV-Epac1-H30 stock (sourced from Vector Biolabs) was amplified in HEK293T cells. The Ad-CMV-Epac1-H30 virus was purified and titrated to a final concentration 7.9 x 10^{11} PFU / ml using an adenovirus purification kit (Puresyn, Inc., US).

2.5.4.4 HEK293T Cell Culture

Human Embryonic Kidney (HEK293T) cells were placed in a pre-heated water-bath for two minutes (37 °C) to defrost from storage (-80 °C). Cells were added to a 15 ml falcon tube containing pre-warmed growth medium (10 ml, 37 °C) and centrifuged for three minutes (1000 xg). The supernatant was removed and the cell pellet was resuspended in 14 ml fresh growth medium (Table 2.5). Cells were transferred to a 25 cm^3 culture flask (T25) and incubated for two- to three-days (37 °C, 5 % CO_2) before expansion into 175 cm^3 culture flasks (T175). HEK293T cells were passaged at 70% to 80 % confluency. The medium was replaced every two- to three-days days as required. During passage, growth medium was carefully aspirated from the cells before rinsing with dPBS. Trypsin-EDTA (0.05 %, 3 ml T25 Gibco) was added for three- to five-minutes to release the cells from the flask and the HEK293T cells (10 ml) were resuspended in growth medium (40 ml, T175) before mixing carefully. The cell suspension was divided equally between 175 cm^3 sterile flasks and additional growth medium was added to each T175 flask to make a final volume of 50 ml.

2.5.4.5 Ad-CMV-Epac1-H30 Amplification

To amplify the Epac1-H30 adenovirus, five 175cm^3 culture flasks containing confluent HEK293T cells (70 % to 80 %) were transfected with Epac1-H30 viral stock (3 μL / flask) diluted in fresh (40 ml) infection medium (Table 2.3). Cells were incubated (37 °C , 5 % CO_2) for three- to five-days days until a complete cytopathic effect was evident in 70% to 80 % of HEK293T cells.

2.5.4.6 Ad-CMV- Epac1-H30 Harvest and Purification

The cell fragments and lysate were harvested from T175 flasks and centrifuged for 10 minutes (500 xg, 4 °C). The pellet was resuspended in infection medium (5 ml) and lysed by three rapid freeze-thaw cycles in liquid nitrogen. The lysate was centrifuged (10 minutes, 500 xg, 4 °C) and the cell debris in the pellet was discarded. The supernatant was collected and filter sterilised

(0.2 μm). An adenovirus purification kit (Puresyn) was used to elute the viral stock as per the manufacturer's instructions. Benzonase (25 U / μl) was added to the virus lysate, incubated for 30 minutes (37 °C) and the solution was diluted with 10X Dilution Buffer. An 'Adenopump' (Puresyn) was equilibrated using equilibration buffer and the diluted lysate was loaded onto a virus-binding module. The virus-loaded module was washed with equilibration buffer before the virus was eluted with elution buffer and filter sterilised with a vacuum pump (0.2 μm).

2.5.4.7 Ad-CMV-Epac1-H30 Titration and Quantification

Spectrophotometer measurements were used to quantify the virus RNA in the samples. A blank sample of elution buffer was used to calibrate the spectrophotometer. The absorbance in the adenovirus stocks (10 %, 20 % in elution buffer) were measured (two repeats). A 260/280 nm ratio was obtained and the background (blank sample) was subtracted from these values. For RNA, a ratio between the range 1.17-1.35 was required. Equation 1 was used to calculate the concentration of the number of virus particles capable of forming plaques (plaque forming units; PFU) per unit volume. The final Epac1-H30 concentration was calculated as 7.9 x 10^{11} PFU/ml.

Equation 1.

$$\text{Viral Stock (PFU/ml)} = \text{Value at 260 nm x 10 x dilution factor x 1.1 x } 10^{12}$$

2.5.4.8 HE293T Cell Media

The media used for HEK293T cell culture and infection are included in Table 2.3. Growth Medium for HEK293T cells contained: 89 % Dulbecco's Modified Eagle Media (DMEM, Gibco) supplemented with 2 mM L-glutamine, 10 % heat inactivated FBS, 1 % Penicillin-Streptomycin. Infection Medium for HEK293T cells: 97 % DMEM with 2 mM L-glutamine, 2 % heat inactivated FBS, 1 % Penicillin-Streptomycin. Cell media were filter sterilised (0.2 μm) and stored at -20°C.

.

Table 2.3. HEK293T Growth and Infection Media

HEK293T Growth Medium	HEK293T Infection Medium
89 % DMEM 2 mM L-glutamine 1 % penicillin/streptomycin 10 % Heat Inactivated FBS	97 % DMEM 2 mM L-glutamine 1 % penicillin/streptomycin 2 % Heat Inactivated FBS

2.5.5 FRET Experimental Setup

2.5.5.1 FRET Sensor Expression

For FRET measurements of cytosolic cAMP generation and PKA activity, sympathetic stellate neurons were transduced with the relevant FRET biosensor in neuronal plating media at the following concentrations Epac1-H30: 6.3 x 10^9 PFU/ml, Epac1-H187: 5.1 x 10^8 PFU/ml, AKAR4: 1.3 x 10^9 PFU/ml. After 24-hours, the media was replaced with virus-free neuronal plating media and the neurons were incubated for a further 24-36 hours (37 °C , 5 % CO_2) to obtain an appropriate level of biosensor expression for FRET imaging as previously described[96,311].

2.5.5.2 Microscope Setup for FRET Imaging

FRET biosensor-expressing neurons were imaged on an inverted Nikon microscope connected to an OptoLED fluorescence imaging system (Cairn Research Ltd., UK). Cells were imaged on a 40X or 60X oil-immersion objective and images were captured with a CoolSNAP HQ2 digital CCD camera (Photometrics). A dual-view beam splitter (DV2 multichannel imaging system, Photometrics) with a dichroic mirror at 505 nm (505DCXR) was used to split the fluoresce emission into two channels with 480/30 nm and 535/40 nm band pass filters for CFP and YFP respectively (Et480/30M, ET535/40M). Accurate alignment of the DV2 beam splitter was ensured prior to imaging to prevent emission cross-over and to ensure parallel apertures. When alignments were required, OptoFluor software adjustments (Cairn Research Ltd., UK) or manual DV2 manipulations were made as per the Photometrics DV2 alignment guidelines.

2.5.5.3 FRET Imaging Protocol

During imaging, cells were excited at 430 nm for 100 ms every 15 s. The emission intensities for CFP and YFP were measured at 480 nm and 535 nm and were acquired using OptoFluor software (Cairn Research Ltd., UK). For Epac1-H30 and Epac1-H187 loss-of-FRET sensors, CFP / YFP ratios were calculated. For AKAR4, a gain-of-FRET sensor, YFP / CFP emission intensity ratios were calculated. Background fluorescence was subtracted from all emission intensity ratios and the data were expressed as intensity per unit time. For all experiments, the baseline emission intensity was recorded and averaged over a 30 second period. Emission intensities were converted to FRET ratios (R) and expressed as a percentage FRET change (%) from baseline using Equation 2.

Equation 2.

$$\text{FRET Change} = \frac{\Delta R}{R_0}$$

Where:

$\Delta R = R - R_0$

R_0 = The CFP/YFP* intensity ratio recorded at baseline (T = 0-30 seconds)

R = CFP/YFP* intensity recorded at any time-point in the experiment (T = seconds)

*A CFP/YFP ratio was calculated for Epac1-based FRET sensors. A YFP/CFP ratio was calculated for the AKAR4 FRET sensor.

2.5.6 Establishing the Dynamic Range of the FRET Sensors

2.5.6.1 Dynamic Range of Epac1-H30

To determine the dynamic range of Epac1-H30 in sympathetic stellate neurons, cells expressing the FRET sensor were stimulated with increasing concentrations of an adenylyl cyclase (AC) activator forskolin (0.1-75 µM) to generate cAMP. Maximal FRET changes of 30 % ± 3 % have been previously demonstrated in HEK293 cells during stimulation with forskolin (25 µM) and a non-specific PDE inhibitor 3-isobutyl-1-methylxanthine (IBMX,100 µM)[305], where the Epac1-H30 sensor itself has a reported Kd of 50 µM for cAMP [305]. As can be seen in Figure 1, there was a slight but non-significant increase in FRET change following the application of 20-75 µM forskolin (Fig. 2.6). Near-complete Epac1-H30 saturation (30.4 % ± 5.7 %) was achieved with 25 µM forskolin and 100 µM IBMX, similar to values reported previously [305]. This combination of forskolin (25 µM) and IBMX (100 µM) was selected to maximally stimulate cells at the end of each subsequent experiment for internal standardisation of Epac1-H30 sensor activity and as a marker of cell viability.

2.5.6.2 Dynamic Range of Epac1-H187

Maximal FRET changes of 163.9 % ± 10 have been demonstrated previously in Epac1-H187 expressing HEK293 cells exposed to forskolin (25 µM) and IBMX (100 µM) [307].To validate the dynamic range of Epac1-H187, a Chinese Hamster Ovary (CHO) cell line and sympathetic stellate neurons were transduced with the Epac1-H187 virus. The percentage FRET changes to forskolin (25 µM) and IBMX (100 µM) were measured as 245.2 % ± 7.0 % in the CHO cell line, whereas in sympathetic stellate neurons the maximal FRET response was recorded as 153.7 % ± 17.0 % (Fig. 2.6).

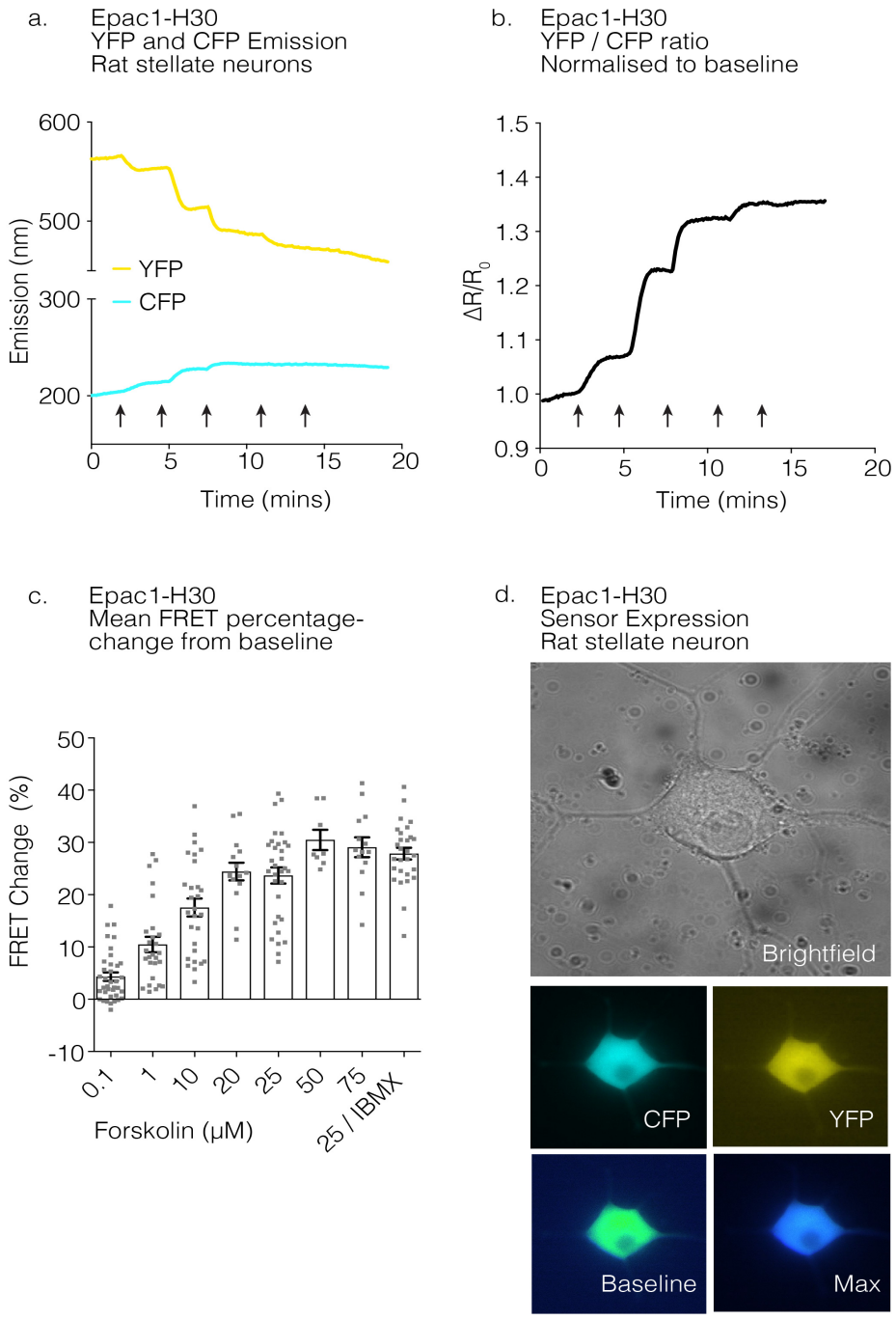


Figure 2.5. Epac1-H30 FRET Sensor Dynamic Range
Stellate neurons from healthy rats were transduced with Epac1-H30 and the emission wavelengths for CFP and YFP were recorded in response to increasing concentrations of forskolin (0.1, 1, 10, 25 μM) and forskolin (25 μM) with IBMX (100 μM). The administration of forskolin is represented by arrows (a, b). The ratio (CFP/YFP) normalised to baseline was calculated (R/R_0; b). Percentage FRET changes in response to increasing concentrations of forskolin are depicted (n=8-37) (c). There was no difference in the peak cAMP generated by top concentrations of forskolin (50-75 μM) or a combination of forskolin (25 μM) and IBMX (100 μM) where Epac1-H30 saturation lead to a maximal FRET change of 30.4 % ± 5.7 %. An example stellate neuron is shown in phase contrast and the emission channels for CFP and YFP. A ratio of the CFP/YFP emission wavelengths is shown at baseline and with maximal forskolin/IBMX stimulation, where loss-of-FRET is observed (d).

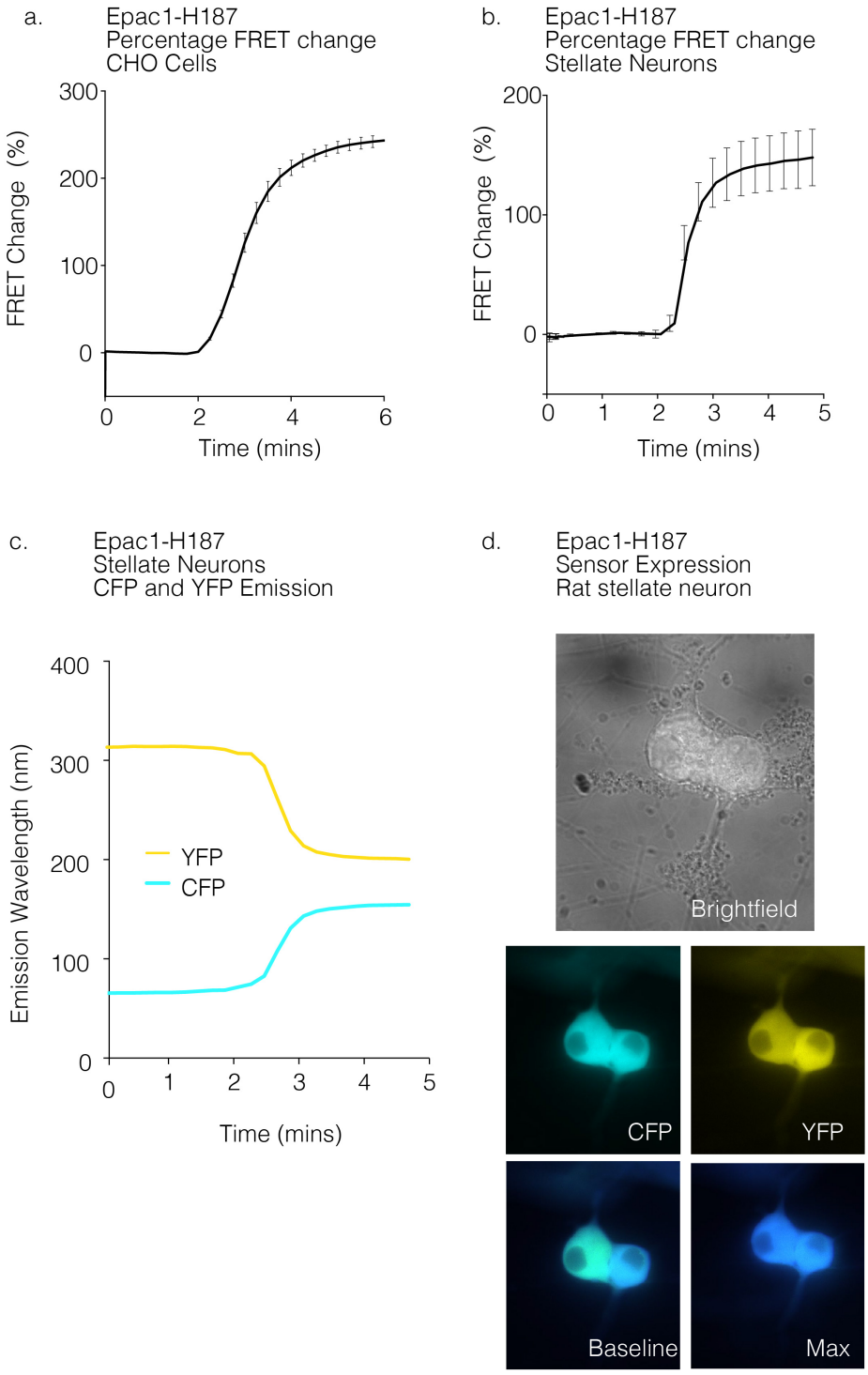


Figure 2.6. Epac1-H187 FRET Sensor Dynamic Range
To validate the dynamic range of Epac1-H187, Chinese Hamster Ovary (CHO) cells (n=17) transduced with the Epac1-H187 virus and FRET changes to forskolin (25 μM) and IBMX (100 μM) were measured as 245.2 % ± 7 (a). In sympathetic stellate neurons (n=5), the maximal FRET response was measured as 153.7 % ± 17.0 (b). Example traces are shown depicting the emission wavelengths of CFP and YFP (c). A brightfield image of two stellate neurons and the emission channels for CFP and YFP are shown. A ratio of the CFP/YFP emission wavelengths is shown at baseline and with maximal forskolin/IBMX stimulation, where loss-of-FRET is observed (d).

2.5.6.3 Dynamic Range of AKAR4

PKA is a promiscuous heterotetrametric enzyme that comprises a catalytic and a regulatory domain each formed of two subunits[312]. The binding of cAMP to the PKA regulatory subunits releases the PKA catalytic subunits into the cytosol that catalyse the transfer of a phosphate from ATP to substrate proteins, leading to changes in protein and cellular function. The cAMP signal is acutely maintained by PDEs that regulate the localisation, duration and amplitude of cAMP signals within subcellular compartments to acutely regulate effector responses[294]. Moreover, cAMP is localised in close proximity of its effectors and regulators where PKA, PDEs and phosphatases (PPs) are tethered to A Kinase Anchoring Proteins (AKAPs) forming signalosomes that restrict the duration and magnitude of the cAMP-PKA signal within specific subcellular domains[298]. Sustained elevations in cAMP generation or alterations in PDE activity, underpin several cardiovascular pathologies including cardiac hypertrophy[221,230,266] and sympathetic over-activity in hypertension [96,280] where it is thought that cAMP signals saturate the available PDEs and diffuse into neighbouring subcellular compartments leading to aberrant effector activity[96,226].

In this thesis, the AKAR4 FRET sensor was used to identify whether global cytosolic PKA activity is altered in stellate neurons from prehypertensive or hypertensive rats. Previous reports have demonstrated a dynamic range of 58 % ± 2 % in AKAR4-expressing HEK293 cells in response to isoprenaline (ISO, 1 μM) [309], therefore, to test the dynamic range of AKAR4 in sympathetic post-ganglionic neurons, cells expressing the FRET sensor were stimulated with forskolin (25μM) and IBMX (100 μM). Complete AKAR4 saturation was measured as 37.5 % ± 7.6 % (Fig. 2.7). There was no further increase with administration of 25 μM forskolin and 500 μM IBMX, therefore the former was selected to maximally stimulate cells in subsequent experiments.

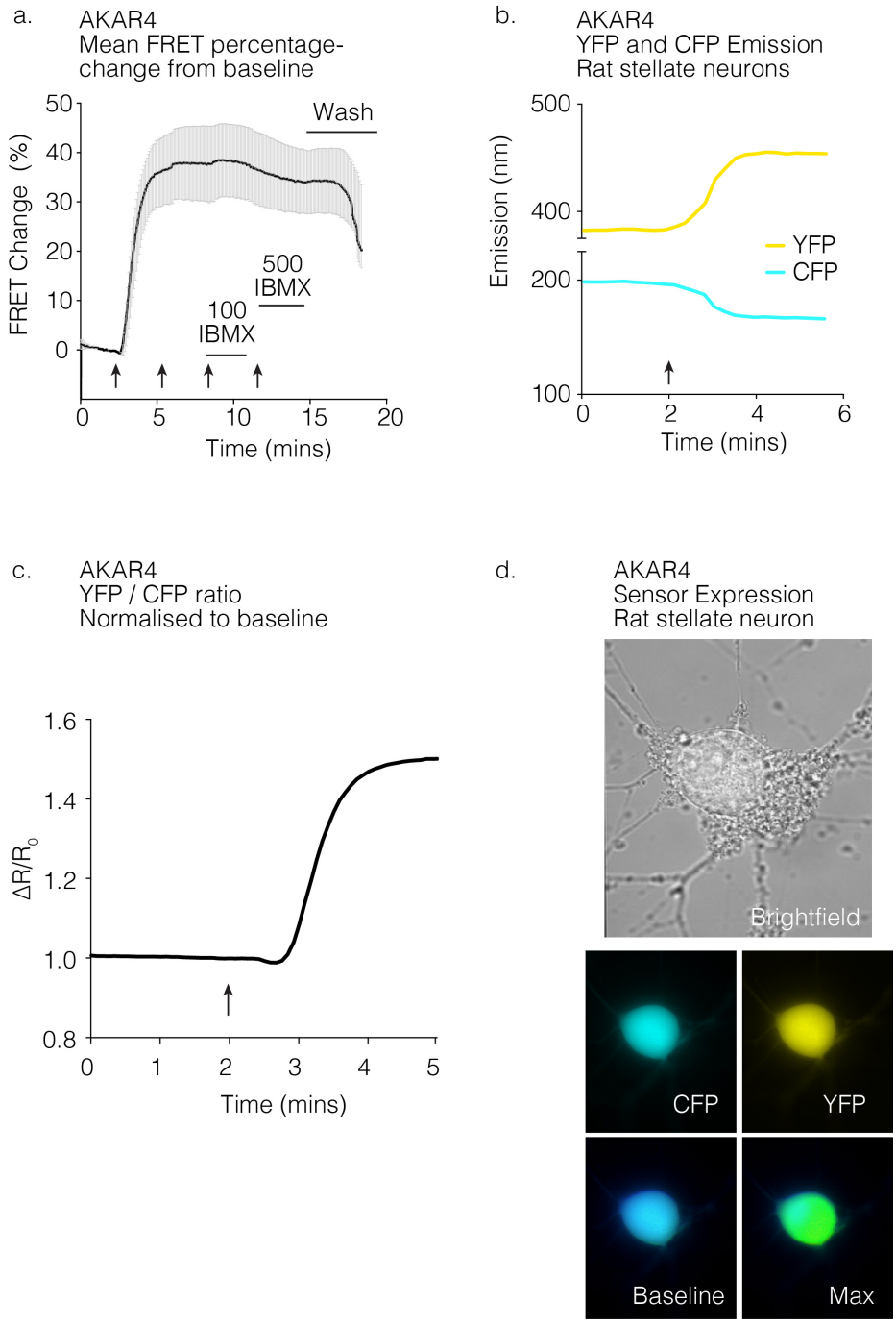


Figure 2.7. AKAR4 FRET Sensor Dynamic Range
To validate the dynamic range of AKAR4, sympathetic neurons (n=4) from healthy rats were transduced with the AKAR4 virus and percentage FRET changes were measured in response to two concentrations of forskolin (10 μM, 25 μM) as well as forskolin (25 μM) in the presence of IBMX (100 μM, 500 μM). The maximal FRET change was determined as as 37.5 % ± 7.6 % (a). Example traces are shown depicting the emission wavelengths of CFP and YFP in response to forskolin (25 μM) and IBMX (100 μM) are shown (b). The administration of forskolin is represented by arrows (a-c). An example trace representing the emission ratio (YFP/CFP) normalised to baseline is depicted (R/R_0; c). A brightfield image of two stellate neurons and the emission channels for CFP and YFP are shown. A ratio of the YFP/CFP emission wavelengths is shown at baseline and with maximal forskolin/IBMX stimulation, where gain-of-FRET is observed (d).

2.5.7 FRET Experimental Protocol

During FRET experiments, cells were perfused continuously with HEPES-buffered Tyrode's solution at room temperature via a gravity-fed perfusion system and the flow rate was controlled at 2-3 ml/min. A list of the buffer constituents is included in Table 2.4. A stable baseline was recorded at the start of each experiment for at least two minutes. Pharmacological agents were diluted in Tyrode solution and the duration of administration was optimised for each compound until cAMP signals reached an equilibrium. In all experiments, the maximal FRET change of each cell was recorded by exposing the cells to saturating concentrations of the AC activator forskolin (25 µM) and the non-specific PDE inhibitor IBMX (100 µM) to ensure that the cells responded similarly to the sensor.

2.5.8 FRET Statistical Analysis

Data were analysed using GraphPad Prism software (v6/7). When the data passed normality tests (D'Agostino-Pearson omnibus test or Shapiro-Wilk[313]) unpaired two-tailed Student's t-tests were used to compare the peak FRET change (%) in response to a stimulus. A one or two-way analysis of variance (ANOVA) was used if there were multiple groups or a time comparison was desired. When the data were not normally distributed, the appropriate nonparametric tests were used with the specific statistical test reported in the figure legend. All data are expressed as the mean ± SEM. Statistical significance was accepted at $p<0.05$ unless otherwise described.

2.6 Intracellular Calcium Imaging

2.6.1 Calcium Imaging Protocol

Intracellular Ca^{2+} measurements were acquired in cells loaded with the membrane-permeable, leakage-resistant Ca^{2+} binding dye Indo-1 acetoxymethyl (AM) ester. Cells were imaged on an inverted Nikon Diaphot 200 microscope (Nikon, Tokyo, Japan) and Indo-1AM was excited at 340 nm with a 100 W Xenon bulb (Nikon, Tokyo, Japan). The emission was split by a dichroic mirror (450 nm) and fluorescence was detected at 405 nm (Ca^{2+}-bound) and 495 nm (Ca^{2+}-free) by two tri-alkali photomultiplier tubes (PMTs, ET Enterprises Ltd., UK) each housed in air cooled enclosures (FACT50, ET Enterprises Ltd., UK) to maintain PMT temperatures at -20 °C. The output from each PMT was integrated in a current-to-voltage converter and digitized at a sampling frequency of 250 Hz (CED 1401). The emission signals at 405 nm and 495 nm were acquired with Spike2 software and automatically converted into a ratio (405/495 nm). The emission ratio is calculated by Equation 3. The recorded values were averaged at 0.5 s intervals providing a sampling rate of 2 Hz. Ratiometric data were obtained by the conversion of raw data into text files. Indo-1AM is a ratiometric indicator where the Ca^{2+}-bound (405 nm) and Ca^{2+}-free (495 nm) forms of the dye display peaks at different emission wavelengths.

Equation 3.

$$\text{Emission Ratio} = \frac{\text{Emission at 405 nm}}{\text{Emission at 495 nm}}$$

Where:

Maximum fluorescence obtained at 405 nm is yielded with high intracellular Ca^{2+}.

Maximum fluorescence obtained at 495 nm is yielded with low intracellular Ca^{2+}.

2.6.2 Calcium Imaging Experimental Protocol

Sympathetic stellate ganglia from three- to four-week-old preSHR and age matched Wistar rats were dissociated into single cells and incubated for four- to six-hours on the day of culture (37 °C , 5 % CO_2). When neurons were fully adhered to poly-D-lysine / laminin-coated coverslips, cells were incubated in plating media with the Ca^{2+} dye Indo-1 acetoxymethyl ester (Indo-1AM, ThermoFisher; 2 mM, 45 mins, room temperature). During Ca^{2+} imaging experiments, cells were perfused continuously via a gravity-fed perfusion system with bicarbonate-buffered Tyrode's solution that was buffered with 95 % Oxygen and 5 % CO_2. The flow rate was controlled at 2-3 ml/min. A stable baseline was recorded at the start of each experiment for at least 30 seconds. Pharmacological agents were diluted in Tyrode's solution. All Ca^{2+} experiments were conducted at 37 °C. Cells were challenged with 50 mM KCl (with an equimolar reduction in NaCl at the end of each experiment. In the absence of a KCl response, cells were excluded from analysis. A list of the buffer constituents is included in Table 2.4.

2.6.3 Ionomycin Calibration of Indo-1AM

Ionomycin calibrations were carried out to transform fluorescence values to $[Ca^{2+}]_i$ concentrations using Equation 4 derived by Grynkiewicz et al.,[314]: Cells were pre-incubated with Indo-1AM (2 μM, 1 hr, 37 °C , 95 % air / 5 % CO_2). When the cells were fully loaded with the Ca^{2+} dye, the cells were incubated in ionomycin (10 μM) to perforate the cells with ethylene glycol-bis(β-aminoethyl ether)-N,N,N′,N′-tetraacetic acid (EGTA) to chelate $[Ca^{2+}]_i$ (2 mM, 1hr, room temperature). To obtain a value for R_{min} cells were placed onto the microscope chamber and perfused with a modified zero Ca^{2+} HEPES-buffered Tyrode solution containing ionomycin (1 μM), and EGTA (2 mM) until a stable baseline was recorded. To obtain a value for R_{max} cells were perfused with a modified high Ca^{2+} HEPES-buffered Tyrode solution containing ionomycin (1 μM) and $CaCl_2$ (2 mM) until equilibrium (i.e. plateau) was reached (Fig. 2.8). A list of the

buffer constituents is included in Table 2.4. The constants R_{min} and R_{max} were determined as 1.081 and 5.222, respectively.

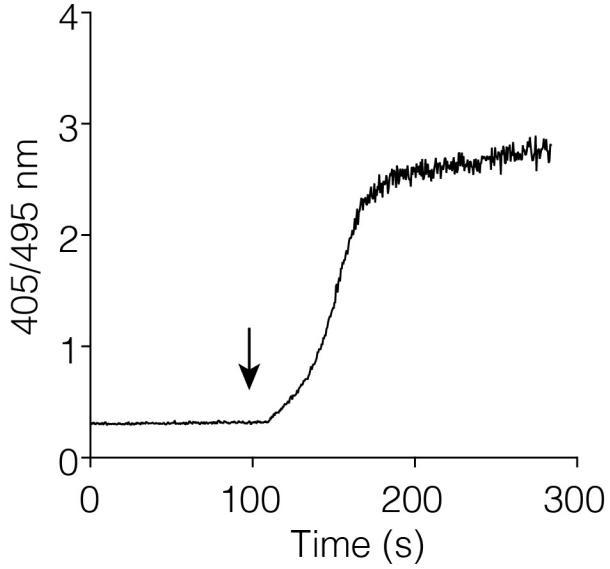


Figure 2.8. Emission Ratio from Cells Loaded with Indo-1AM
Cells were pre-incubated with Indo-1AM (2 μM, 1 hr, 37 °C , 95 % air / 5 % CO_2). To obtain a value for R_{min} (minimal Ca^{2+}), cells were incubated in ionomycin (10 μM) to perforate the cells and EGTA to chelate intracellular Ca^{2+} (2 mM, 1hr, room temperature). Cells were perfused with a modified zero Ca^{2+} HEPES-buffered Tyrode solution (t=0-100 s). To obtain a value for R_{max} (maximal Ca^{2+}), cells were perfused with a modified high Ca^{2+} HEPES-buffered Tyrode solution (black arrow) containing ionomycin (1 μM) and $CaCl_2$ (2 mM) until equilibrium (i.e. plateau) was reached. Figure depicts a raw emission ratiometric signal (405/495 nm).

Equation 4.

$$[Ca^{2+}]_i = Kd \times \{\frac{sf}{sb}\} \times \{\frac{(R - Rmin)}{(Rmax - R)}\}$$

Where:

Kd is the dissociation constant for Indo-1AM (Kd: 224 nM under standard conditions)

Sf is the emission intensity at 495 nm in Ca^{2+}-free media (i.e. unbound)

Sb is the emission intensity at 495 nm in high Ca^{2+} solution (i.e. bound)

R is the measured Indo-1AM emission ratio (405 nm / 495 nm) at baseline

R_{min} is the Indo-1AM emission ratio in Ca^{2+}-free media

R_{max} is Indo-1AM emission ratio obtained at saturating Ca^{2+} conditions

2.7 Buffers and Solutions

2.7.1 HEPES-buffered Tyrode's Solution

In millimolar (mM): 135 NaCl, 4.5 KCl, 11 glucose, 1 $MgCl_2$, 2 $CaCl_2$, 20 HEPES, adjusted to pH 7.4.

2.7.2 Carbon Dioxide / Bicarbonate-buffered Tyrode's Solution

In millimolar (mM): 117 NaCl, 4.5 KCl, 11 glucose, 1 $MgCl_2$, 2.5 $CaCl_2$, 23 $NaHCO_3$. Equilibrated to pH 7.4 with 95 % air / 5 % CO_2 at 37 °C.

2.5.3 High K^+ Carbon Dioxide / Bicarbonate-buffered Tyrode's Solution

In millimolar (mM): 71.5 NaCl, 50 KCl, 11 glucose, 1 $MgCl_2$, 2.5 $CaCl_2$, 23 $NaHCO_3$. Equilibrated to pH 7.4 with 95 % air / 5 % CO_2 at 37°C.

2.5.4 Zero Ca^{2+} HEPES-buffered Tyrode's Solution

In millimolar (mM): 150 KCl, 10 HEPES, 10 glucose, 2 EGTA. Adjusted to pH 7.55 at room temperature to reach a final pH 7.4 at 37 °C .

2.5.5 High Ca^{2+} HEPES-buffered Tyrode's Solution

In millimolar (mM): 150 KCl, 10 HEPES, 10 glucose, 2 $CaCl_2$. Adjusted to pH 7.55 at room temperature to reach a final pH 7.4 at 37 °C .

Table 2.4. Buffers and Solutions

HEPES-buffered Tyrode's (mM)	Bicarbonate-buffered Tyrode's (mM)	High K^+ bicarbonate-Tyrode's (mM)	Zero Ca^{2+} Tyrode's (mM)	High Ca^{2+} Tyrode's (mM)
135 NaCl	117 NaCl	71.5 NaCl		
4.5 KCl	4.5 KCl	50 KCl	150 KCl	150 KCl
11 glucose	11 glucose	11 glucose	10 glucose	10 glucose
1 $MgCl_2$	1 $MgCl_2$	1 $MgCl_2$	10 HEPES	10 HEPES
2 $CaCl_2$	2.5 $CaCl_2$	2.5 $CaCl_2$	2 EGTA	2 $CaCl_2$
20 HEPES	23 $NaHCO_3$	23 $NaHCO_3$		
Adjust to pH 7.4	95 % air / 5% CO_2	95 % air / 5% CO_2	Adjust to pH 7.4	Adjust to pH 7.4

2.8 RNA Sequencing

The development of high-throughput next-generation sequencing techniques and the expansion of bioinformatics tools have led to rapid progress in our understanding of transcriptomics and its potential applications in understanding genetic influences in health and disease. The transcriptome is defined as 'the array of RNA transcripts in a particular cell or tissue type', and in contrast to the genome, changes dynamically in response to cell signals derived from a complex interaction of environmental, behavioural and developmental influences[315]. The technology for transcriptome expression profiling includes RNA-seq and microarray. RNA-seq is now the preferred method of choice due to the rapid and regular improvements in the Illumina Sequencing platform that increase the depth and accuracy of the RNA-seq data. In this thesis, RNA-seq was carried out to profile the transcriptome of the sympathetic stellate ganglia from adult normotensive and hypertensive adult rats to identify changes in RNA that may be involved in sympathetic over-activity.

2.8.1 Stellate Ganglia Tissue Preparation for RNA Extraction

Left and right stellate ganglia were dissected from three- to five-week-old and 16-week Wistar and age-matched SHR rats. Stellates were placed immediately in a plastic petri dish (5 cm diameter) and de-sheathed from connective tissue in ice-cold HBSS without Ca^{2+} and Mg^{2+}. Human stellate ganglia (n=5 patients, left or right stellates) were extracted at UCLA. The human study was approved by an institutional committee, the UCLA Institutional review board, approval # 12-000701, and informed consent was obtained from all subjects. The characteristics of the human donor patients is outlined in Table 2.5. Human stellate ganglia were shipped on dry ice in RNA*later*® RNA Stabilization Solution (ThermoFisher) to preserve the integrity of the RNA and to prevent degradation of the tissue. Stellate ganglia were defrosted in a plastic petri dish (6 cm diameter) and submerged in ice-cold HBSS without Ca^{2+} and Mg^{2+}. Stellate ganglia were thoroughly cleaned and dissected from blood vessels, debris and connective tissue. Ice-cold

HBSS was replaced regularly during the preparation until the stellates were clean. Tissue was weighed (~80 mg) for the RNA extraction procedure and the remaining stellate was snap frozen for subsequent experiments.

Table 2.5. Human Stellate Donor Characteristics

Donor	Gender	Age	Complications
#19	Male	77	Non-ischaemic cardiomyopathy, ventricular fibrillation, LVEF 30-35%
#21	Female	34	Excessive tachycardia, normal heart, LVEF presumed normal
#22	Male	70	Ischaemic cardiomyopathy, ventricular tachycardia, coronary artery disease, LVEF 30%
#23	Male	19	Healthy, normal heart size, and chamber, LVEF 55-60%
#24	Male	62	Non-ischaemic cardiomyopathy, polymorphic ventricular tachycardia/fibrillation, LVEF 30- 50%

2.8.2 Rat and Human Stellate Ganglia RNA Extraction Protocol

Rat stellate RNA was extracted from single stellates using an RNeasy Mini RNA Extraction Kit (Qiagen). 10 µl β-mercaptoethanol (β-ME) was added to 990 µl buffer RLT (supplied) to make a working stock of RLT lysis buffer. Rat stellates were placed in a 1.5 ml Eppendorf tubes containing RLT lysis buffer (350 µl), chopped into small pieces (1 mm^3) under a dissection microscope and manually triturated using fire-blown Pasteur pipettes. Human RNA was extracted from approximately 150 mg tissue using an RNeasy Maxi RNA Extraction Kit (Qiagen). 10 µl β-ME was added to 990 µl buffer RLT (supplied) to make a working stock of RLT lysis buffer. The human stellate sections were chopped with scissors in ice-cold HBSS without Ca^{2+} and Mg^{2+} under a dissection microscope. The stellate pieces were transferred into a falcon tube (supplied) for homogenisation in RLT lysis buffer (5 ml) using a tissue disrupter. The human stellate lysate (5-6 ml) was centrifuged at room temperature (5000 xg, 10 min). For human and rat RNA extraction protocols, the stellate lysate was vortexed and transferred to an

RNA extraction spin column. An equal volume of 70 % ethanol was added to the homogenised lysate in each spin column to allow the RNA to bind the membrane. Human and rat RNA was extracted following a series of centrifugal spins at room temperature outlined in Tables 2.6a, b. When the RNA sample was eluted, the samples were divided for quality validation (3 µl) and for RNA-seq (27 µl) or qRT-PCR (27 µl) before snap freezing in liquid nitrogen and storage at -80 °C.

Table 2.6. RNA Extraction Protocols for Rat and Human Stellate Ganglia

a. RNEasy Mini
Rat RNA Extraction Protocol

Solution	Volume	Centrifuge	Time
RLT / EtOH	700	8800 G	30 s
RW1	700	8800 G	15 s
RPE	500	8800 G	15 s
RPE	500	8800 G	2 min
nuclease-free H_2O	30	8800 G	1 min

b. RNEasy Maxi
Human RNA Extraction Protocol

Solution	Volume	Centrifuge	Time
RLT / EtOH	5	5000 G	5 min
RW1	7.5	5000 G	5 min
RPE	5	5000 G	2 min
RPE	5	5000 G	10 min
nuclease-free H_2O	150	5000 G	1 min

2.8.3 RNA Integrity Validation

To assess the quantity and purity of the extracted stellate RNA, the samples were analysed by automated electrophoresis using an Agilent 2100 Bioanalyzer Instrument using an RNA 6000 Pico Assay (Agilent) as per the manufacturer's guidelines. In preparation for RNA sample analysis, the Bioanalyzer electrodes were cleaned to prevent sample contamination by inserting an electrode cleaning chip loaded with RNase-free water for 5 min (Ambion, Inc). The electrode cleaning chip was removed and the electrode pins left to dry (30 s). Reagents were equilibrated at room temperature for 30 minutes prior to use.

In preparation, an RNA 6000 Pico ladder (Agilent) was heat denatured (70 °C , 2 min) and diluted from stock in ice-cold RNase-free H_2O (90 µl). Ladder aliquots were stored at -80 °C until required for use. To prepare the electrophoresis gel, the RNA 6000 Pico gel matrix (550 µl) was added to a spin filter, centrifuged (1500 G, 10 min) and refrigerated at 4 °C for a month until required. On the day of analysis, all required reagents were brought to room temperature. A gel-dye mix was prepared for electrophoresis as per the manufacturer's instructions. Briefly, the RNA 6000 Pico dye concentrate (Agilent) was vortexed (10 s) spun down and the dye (1 µl) was added to the prepared Pico gel matrix (65 µl). The gel-dye mix was vortexed and centrifuged (13000 G, 10 min, room temperature) with care taken not to expose the dye to light. The gel-dye mix was loaded (9 µl) on an RNA 6000 Pico chip into an allocated well (gel, G). To prime the RNA Pico Chip, the chip was placed on a priming station and the plunger was positioned at the 1 ml position. The priming station was closed, the syringe plunged until it was clipped into place, and held for 30 s before release. After a further 5 s the plunger was repositioned slowly to the 1ml position. The gel-dye mix was loaded (9 µl) into two other allocated wells (g) on the chip.

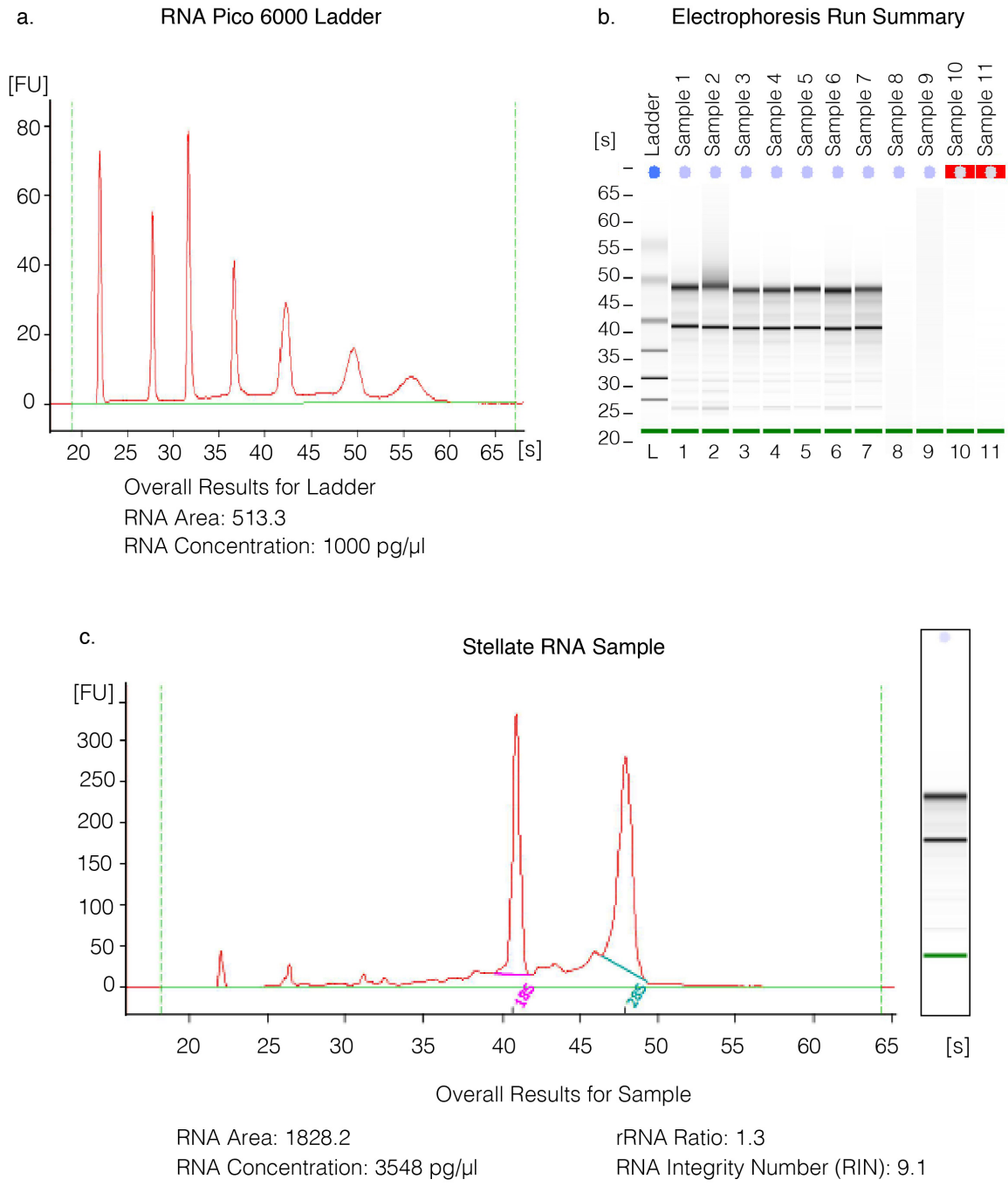


Figure 2.9. RNA Integrity and Quantity Validation
To assess the quantity and purity of the extracted stellate RNA, the samples were analysed by automated electrophoresis using an Agilent 2100 Bioanalyzer Instrument using an RNA 6000 Pico Assay (Agilent). The concentrations of each sample were quantified using an RNA 6000 Pico Ladder (a). An example of the automated electrophoresis run summary depicting the ladder (L) and samples in the lanes 1-7. No samples were run in lanes 8-9. The run was terminated prior to running lanes 10-11 (b). An example RNA sample run over a 65 second electrophoresis run. Two chromatogram peaks are seen at 40s-42s and 45s-50s, that correspond to the ribosomal RNA subunits (18S and 28S). The rRNA's are labelled with a fluorescent dye and are separated by electrophoresis passing the detector at different rates during the run. The software identifies the 18S/28S subunits by comparing against the ladder and calculates area under the curve for each of the peaks. The size of the peaks and contaminants in the sample influence the Bioanalyzer algorithm that determines RNA integrity (RIN). In this sample RNA integrity was determined as 9.1.

RNA conditioning solution (9 µl) was loaded into the well (CS) and RNA marker (5 µl) was distributed into all sample wells and the ladder well. The prepared heat-denatured ladder (1 µl) and the RNA samples (1 µl) were loaded into the sample wells and appropriate ladder well. RNA marker was added to the remaining wells in the absence of sample (1 µl). The chip was vortexed (IKA Vortexer, 2400 rpm, 1 min) and placed into the Agilent 2100 Bioanalyzer instrument within 5 minutes for the electrophoresis run. Rat samples with an RNA integrity number (RIN) less than 8.5 were discarded (Fig. 2.9). Due to difficulties with fast shipping of human samples human RNA samples with RINs above 5.7 were accepted. RNA concentrations were determined using a Qubit RNA High Sensitivity Assay Kit (Molecular Probes, Life Technologies) and a Qubit® 2.0 Fluorometer as per the manufacturer's instructions (Invitrogen, Life Technologies).

2.8.4 Optimisation of Stellate Tissue Preparation and RNA Extraction

To establish the optimal protocol and techniques required for good-quality RNA extraction, several parameters were tested. Firstly, the aim was to ascertain whether detectable differences were observed between RNA yield and RNA integrity (RIN) and between fresh and frozen stellate ganglia. Secondly, to determine whether de-sheathing and cleaning of stellates was required prior to freezing, and thirdly, to establish whether stabilisation reagents were required to improve the yield and quality of RNA in the samples. To test these parameters, RNA was extracted from (a) freshly dissected stellates; clean de-sheathed stellates that were frozen and stored at -80 °C in (b) RNA later stabilisation solution or (c) in dPBS without Ca^{2+} and Mg^{2+}. Alternatively, stellates were frozen and stored at -80 °C prior to cleaning in (d) RNA later stabilisation solution, or (e) in dPBS without Ca^{2+} and Mg^{2+}. The parameters for this optimisation are summarised in Table 2.7. The concentrations and RINs were ranked 1-5, where 5 represented the highest concentration and highest RIN, and 1 represented the lowest concentration and lowest RIN. Ranks were summed for both variables to establish the best

extraction parameters. It was concluded that RNA extracted from fresh tissue yields the highest concentrations and best RNA integrity as validated using the 2100 Bioanalyzer instrument (Agilent). RNA was also found to be better preserved if ganglia were cleaned before snap freezing, whereas storage in RNA later or dPBS appeared to have little effect on yield or quality of the RNA (Fig. 2.10). For all subsequent RNA extractions, fresh stellates were extracted and RNA was extracted immediately.

Table 2.7. Stellate RNA Extraction Optimisation Parameters.

Storage	Freezing Solution	Preparation	Concentration (pg/ml)	Rank concentration	RIN	Rank RIN	Sum rank
fresh	Fresh stellate	cleaned	20350	5	8.6	4	9
frozen	RNA later	cleaned	17100	4	8.5	3	7
frozen	RNA later	dirty	12350	3	7.6	1	4
frozen	dPBS, 0 Ca^{2+}, 0 Mg^{2+}	cleaned	10800	2	8.9	5	7
frozen	dPBS, 0 Ca^{2+}, 0 Mg^{2+}	dirty	9520	1	8.1	2	3

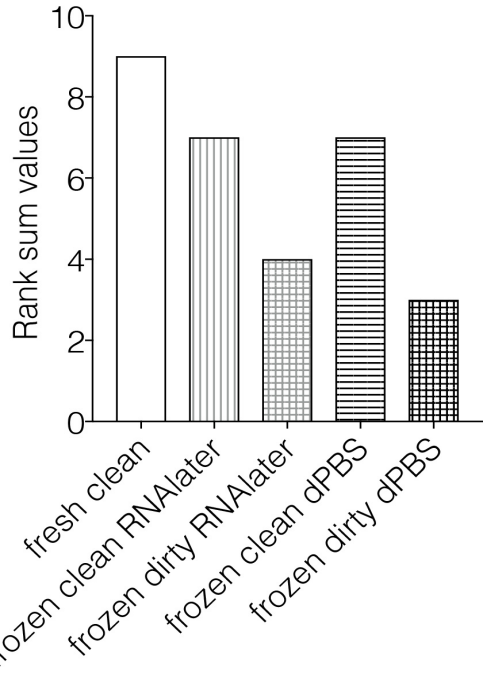


Figure 2.10. Stellate RNA Extraction Optimisation Parameters
RNA was extracted, and the integrity and concentration were calculated and ranked 1-5 (worst to best). The ranks were summed for both variables to establish the best extraction parameters. RNA extracted from fresh tissue yielded the highest concentrations and RNA integrity (RIN). RNA was better preserved if ganglia were cleaned before snap freezing. The storage solution (RNA*later*® or dBPS) appeared to have a minimal effect on RNA yield or quality.

2.8.5 RNA Extractions for RNA Sequencing and qRT-PCR

For RNA-seq library construction and sequencing, four replicate samples containing total RNA extracted from the right sympathetic stellate ganglion of 16-week-old male SHR (n=4) and age-matched Wistar (n=4) were sent to the High-Throughput Genomics Group at the Wellcome Trust Centre for Human Genetics (WTCHG). Left stellate ganglia were used for qRT-PCR experiments. The RNA-seq libraries were prepared by WTCHG using a SMARTer (Switching Mechanism at 5' End of RNA Template, Illumina) Low RNA Input Kit (Clontech Laboratories, Inc.) that was selected for its low starting RNA concentration requirements. The steps carried out to obtain double stranded cDNA with adapter sequences are highlighted in Figure 2.11. Briefly, a modified oligo(dT 30) primer (SMART CDS) was added to each RNA sample to initiate the first-strand cDNA synthesis and to incorporate a poly T-tail at the 5' end of the newly synthesised anti-sense strand. The addition of a modified reverse transcriptase (RT) enzyme (SMARTScribe) also facilitated the addition of a sequence of oligonucleotides (mostly deoxycytidine, CCCCC) to the 3' end of the newly synthesised anti-sense strand. These bases provided a complementary anchoring site (rGrGrG) for a modified oligonucleotide (SMARTer) to bind, enablling replication of the entire sequence including the full 5' end [316]. The SMARTer sequence (5') and the T-tail (3') act as universal priming sites for end-to-end cDNA amplification, where contaminating genomic DNA, or ribosomal RNAs that lack these sequences will not be amplified. Samples were prepared for 75 base pair, paired-end sequencing that enables higher and more accurate mapping than shorter sequences or single-end sequencing as the primers bind with higher accuracy to both ends of the cDNA fragment. Each sample was sequenced on two separate lanes to minimise technical error and to increase the sequencing depth (~15-25 million reads per lane) using an Illumina HiSeq 4000 platform (Illumina, Inc., San Diego, USA). The RNA-seq library preparation pipeline is outlined in Figure 2.11. The number of replicates and the sequencing parameters were based on recommendations from WTCHG and those published by Conesa et al., 2016[317].

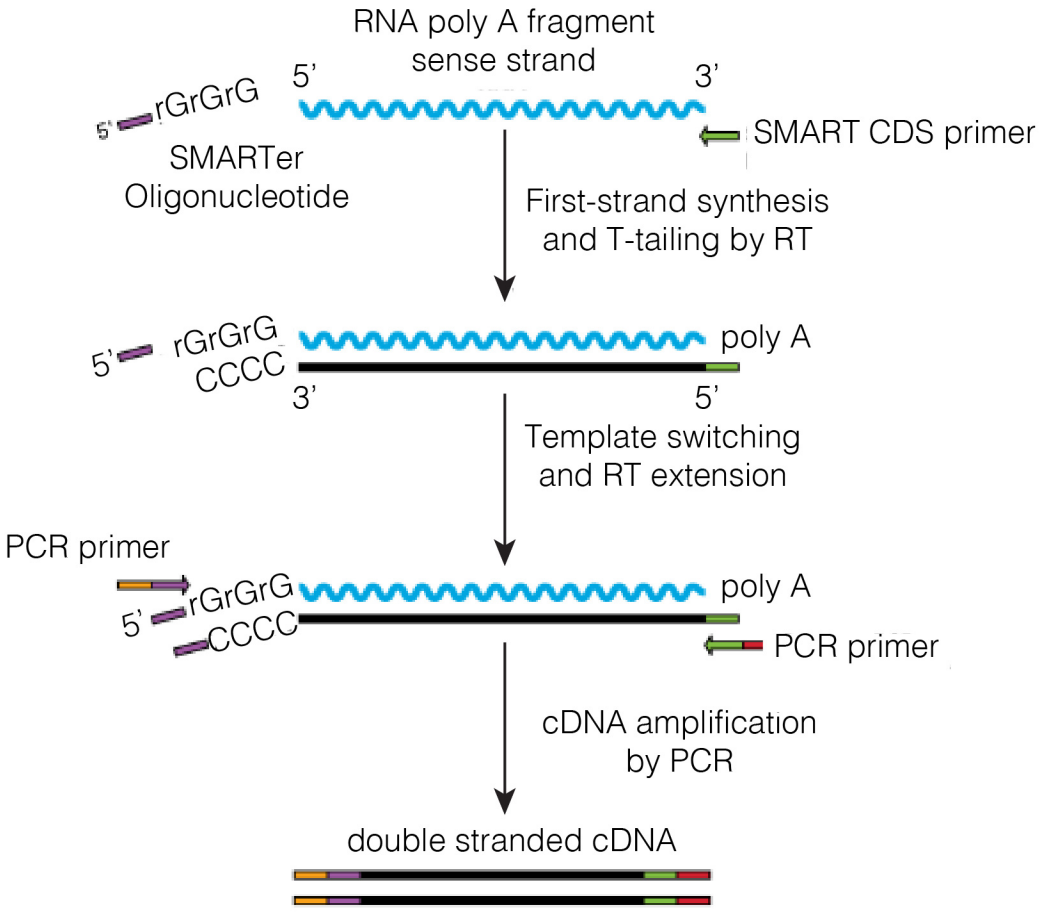


Figure 2.11. RNA-seq SMARTer cDNA Library Preparation
The fragmented RNA was converted to single-stranded cDNA using CDS randomized primers that anneal to the 3' end of the RNA sense strand. A second SMARTer oligonucleotide oligo containing a riboguanosine sequence (rGrGrG) adheres to the 5' end of the RNA sense strand. A modified reverse transcriptase (SMARTScribe RT) adds additional base pairs (mostly deoxycytidine, CCCCC) onto the 3' end of the newly transcribed anti-sense strand. PCR primers then copy from both strands of RNA and include full transcripts of RNA without losing bases that also includes. This figure was reproduced from the SMARTer Low Input RNA-seq Kit User Manual (Clontech Laboratories, Inc.)

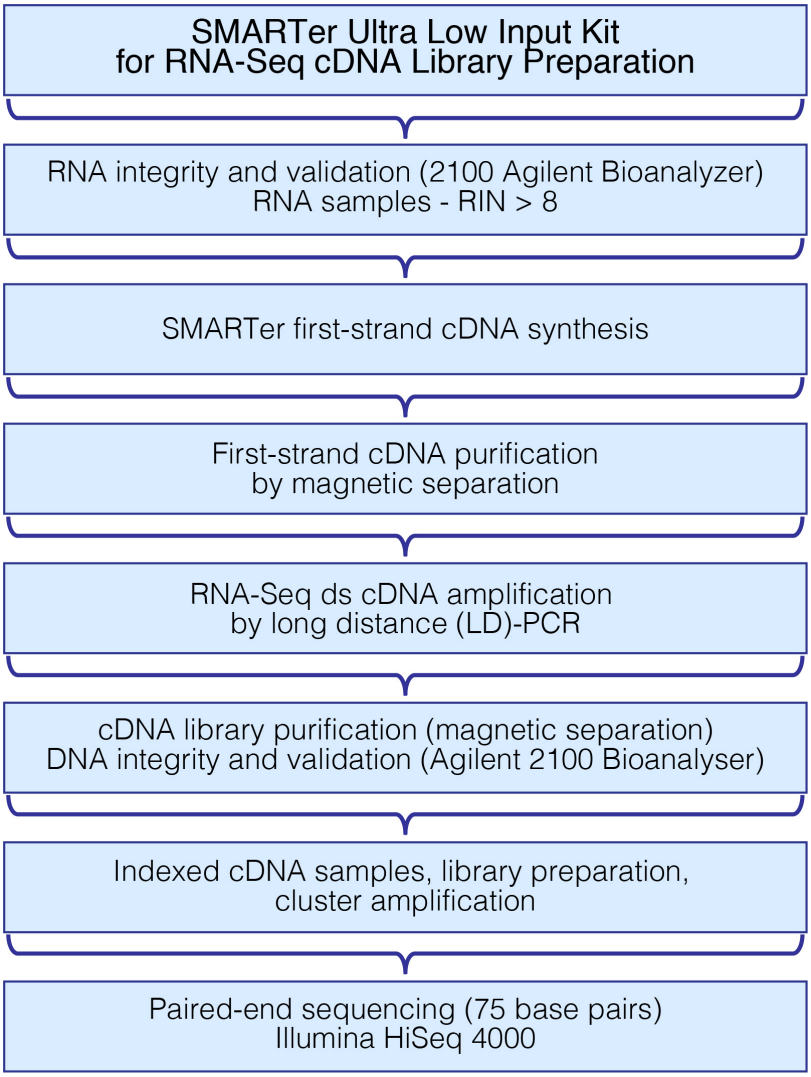


Figure 2.12. RNA to cDNA Library Preparation for RNA Sequencing
RNA samples were obtained from 16-week rat stellate ganglia. The RNA integrity was validated using an Agilent 2100 Bioanalyzer. Samples with an RNA integrity number (RIN) > 8 were sent to the Wellcome Trust Centre for Human Genomics (WTCHG), Oxford University for library preparation and RNA-seq. The SMARTer cDNA amplification protocol was chosen. The RNA was fragmented during first-strand cDNA synthesis. The cDNA libraries were purified and amplified by qRT-PCR. The DNA integrity was validated using an Agilent 2100 Bioanalyzer. Samples were sequenced (paired-end reads, 2 x 75 base pairs) on an Illumina HiSeq 4000 RNA Sequencer.

2.8.6 Transcript Mapping

A wide range of statistical analysis tools are available to accurately align sequencing data to a known transcriptome. Recent alignment tools such as HISAT2 [318] have made the rapid alignment of sequence reads possible and require only moderate computer processing power. However, alignment techniques become problematic when a single sequencing read aligns to multiple reference sequences, as it influences transcript abundance estimations and misalignment interferes with subsequent analysis[315,319]. Recent evidence suggests that the classical method of aligning reads to the reference transcriptome is not necessary to quantify the abundance of transcripts. Instead, rather than aligning base-to-base with the reference, a new method implementing 'quasi-mapping' has been developed, that reports the loci where the sequencing read originated and subsequently maps the reads to high probability positions on the reference transcriptome. The quasi-mapping method provides accurate estimates of transcript abundance and is much faster than base-by-base alignment tools [320].

In this study the Salmon package (version 0.8.2) was used in the quasi-mapping mode[321 322]. The transcript index used during quasi-mapping was derived from the UCSC refseq rn6.0 mRNA library available at the following URL: http://hgdownload.soe.ucsc.edu/goldenPath/rn6/bigZips/refMrna.fa.gz.

The transcriptome was indexed using the Salmon indexer:

salmon index -t/path_to/rattus6.fa.gz -i transcripts_index --type quasi -k 31

Where -k defined the minimum acceptable length for a valid match to the reference and was selected based on parameters in the Salmon guidelines.

Transcripts were quantified using the transcriptome-based (non-alignment) quasi-mapping mode that compares the paired-end reads against the indexed transcriptome using the Salmon 'quant' command. The following commands were used in accordance with the Salmon guidelines for paired-end reads:

salmon quant -i /path_to/transcripts_index -l ISR -1 /path_to/sampleX_lane1_mate1.fastq.gz /path_to/sampleX_lane2_mate1.fastq.gz -2 /path_to/sampleX_lane1_mate2.fastq.gz /path_to/sampleX_lane2_mate2.fastq.gz -o transcripts_quant/sampleX --dumpEq -- posBias --gcBias --WriteUnmappedNames

Where:

ISR (inward stranded reverse) dictated the library type[321] (Fig. 2.13).

--dumpEq flag was included to remove reads of equivalent classes[323].

--posBias and --gcBias flags correct for 3' 5' positional bias and GC biases[321].

–WriteUnmappedNames flag makes a file containing the names of reads that do not map to the transcriptome that can be retrospectively independently mapped[321].



Figure 2.13. Directional RNA Sequencing Library
Our library preparation was carried out with the SMARTer Low Input RNA Kit (Clontech Laboratories, Ltd.). During sequencing read 1 was derived from the anti-sense strand of the input RNA and read 2 corresponded to the sense strand [324,325]. This is defined as inward stranded reverse (ISR). An alternative example, inward stranded forward (ISF) is also illustrated. This image is reproduced from the Salmon documentation by Patro et al.,[321]

2.8.7 Differential Expression Analysis

Once each sample was quantified, the data were imported into R and summarised from transcriptome ID's to gene ID's using the 'tximport' function (v1.6.0) as per the vignette[326]. The differential expression analysis between Wistar and SHR samples was performed using the DESeq2 command in DESeq2 (v1.18.1)[327]. The full script used for the DESeq2 analysis is included in the Appendix Table 8.1. Significance for the differentially expressed transcripts was accepted at the Benjamini-Hochberg adjusted $p<0.05$ level. The 'LFCshrink' function was used to shrink log fold changes after analysis as per the DESeq2 vignette[327]. The mapping rates are shown in Figure 2.14.

Table 2.8. Salmon-Quasi Mapping Rates

Sample	Strain	Age	Stellate	Reads	Mapping Rate
1	Wistar	16wk	RS1	35509076	78.66%
2	Wistar	16wk	RS2	30112270	75.57%
3	Wistar	16wk	RS3	34634784	78.38%
4	Wistar	16wk	RS4	33764576	75.18%
5	SHR	16wk	RS1	31194868	70.63%
6	SHR	16wk	RS2	25820298	78.47%
7	SHR	16wk	RS3	32573670	68.50%
8	SHR	16wk	RS4	34026720	72.60%

Mapping rates indicates the number of assigned reads relative to the total number of reads. The total number of reads is also shown. *RS, right stellate.*

2.8.8 Gene ontology and KEGG Pathway Analysis

To assess the relevance of the observed differentially expressed genes, the significantly different transcripts at the Benjamini-Hochberg p. adjusted (p. adj)<0.05 level, were grouped into Gene Ontology (GO) families[328] using The Database for Annotation, Visualization and

Integrated Discovery (DAVID v6.8) tool suite [329,330]. The database functional annotation tool first identified the over-represented gene families in the three parent groups: biological processes (BP GO), cellular component (CC GO), and molecular function (MF GO). The filter GOTERM_FAT was applied to the gene-set to remove very broad GO groups from the dataset. A Kyoto Encyclopedia of Genes and Genomes (KEGG) [331] analysis was also performed using DAVID (v6.8) to provide information about pathway mapping. The over-represented GO and KEGG groups were filtered to exclude groups with <10 genes. An EASE score (a modified Fisher Exact statistical test) was implemented to determine the statistical probability of a differentially expressed group of genes belonging to a particular family or probability, rather than occurring by random chance. A conservative EASE score was applied ($p<0.01$) to both the GO and KEGG analyses as per the DAVID recommendations[329]. The final GO and KEGG families presented in this thesis were significant at the Benjamini-Hochberg p. adj<0.05.

2.9 Validation of the RNA-seq Dataset

2.9.1 cDNA Library Preparation

Rat and human stellate RNA were used to construct cDNA libraries. For rat stellate library synthesis, the SuperScript™ III VILO™ (ThermoFisher) protocol was followed, according to the manufacturer's instructions. Rat stellate RNA (50 ng, variable volume) was added to the SuperScript™ III VILO reaction mix (10 µl), enzyme mix (1 µl) and nuclease-free H_2O (up to a total of 20 µl). The samples were vortexed and incubated in a thermocycler (GStorm) at 25 °C (10 mins), 42 °C (60 mins), 80 °C (5 mins). For human stellate library synthesis, the SuperScript™ IV VILO™ (ThermoFisher) protocol was followed according to the manufacturer's instructions. Human stellate RNA (50 ng, variable volume) was added to ezDNAse buffer (1 µl), exDNAse enzyme (1 µl) and nuclease-free H_2O (up to a total of 20 µl).. The samples were mixed and incubated (37 °C , 2 min). SuperScript™ IV VILO™ master mix was added to each sample with nuclease-free H_2O. For controls, no reverse transcriptase was added to the RNA.

The samples were incubated in a thermocycler (GStorm, GS4822) at 25 °C (10 mins), 50 °C (10 mins), 85 °C (5 mins). The concentrations of cDNA in each sample were calculated (NanoDrop Lite) and 260/280 ratios were calculated to detect the presence of contaminants. Samples with an abnormal 260/280 ratio (<1.7 and >1.95) were discarded. Samples were aliquoted and frozen at -80 °C for long-term storage or refrigerated at 4 °C for immediate use.

2.9.2 Two-Step Quantitative Real-Time Polymerase Chain Reaction

The presence of the transcripts identified in the RNA-seq dataset were confirmed by qRT-PCR. The control genes beta-2-microglobulin (B2m) and glyceraldehyde-3-phosphate dehydrogenase (*Gapdh*) were selected from the RNA-seq dataset as appropriate control genes, as they were not differentially expressed between strains. The primers used in this thesis and the dilutions of samples and primers used are listed in Table 2.7. Data displayed in the results sections represents the genes normalised to *B2m*; however, each primer was analysed against the two housekeeping genes *B2m* and *Gapdh* for validation and accuracy of qRT-PCR data. TaqMan® Gene Expression Master Mix (ThermoFisher) was added to each cDNA sample in addition to the selected primer conjugated to a FAM dye and nuclease-free H_2O. cDNA samples or no reverse transcriptase controls were diluted for optimal PCR reactions. A 96-well plate with 20 µl samples (3 repeats) was run on a qRT-PCR thermocycler (ABI, PRISM). During PCR, temperatures were held at 50 °C (2 min) and 95 °C (10 min) before thermal cycling (40 cycles) under the following conditions 95 °C (15 s), 60 °C (1 min). The relative amount of each transcript was calculated using the comparative (C_T) method ($\Delta\Delta$ C_T, rat; Δ C_T, human) as described as Schmittgen et al.,[332].

Table 2.9. List of Primers and Dilutions for Optimal qRT-PCR Reactions

Gene	Rat primer	cDNA dilution	Primer diluton	Human primer	cDNA dilution	Primer diluton
B2m	Rn00560865_m1	Varies	Varies	Hs00187842_m1	Varies	Varies
Gapdh	Rn99999916_s1	Varies	Varies	Hs02786624_g1	Varies	Varies
Chrnb4	Rn00583822_m1	1:200	1:20	Hs00609523_m1	1:200	1:20
Gabra1	Rn00788315_m1	1:200	1:20	Hs00971228_m1	1:200	1:20
Gabra2	Rn01413643_m1	1:200	1:20	Hs00168069_m1	1:200	1:20
Glrb	Rn00583966_m1	1:200	1:20	Hs00923871_m1	1:200	1:20
Gria1	Rn00709588_m1	1:200	1:20	Hs00181348_m1	1:200	1:20
Gria2	Rn00568514_m1	1:200	1:20	Hs00181331_m1	1:200	1:20
Gria3	Rn00583547_m1	1:200	1:20	Hs01557466_m1	1:200	1:20
Grik1	Rn01458414_m1	1:200	1:20	Hs00543710_m1	1:200	1:20
Grik2	Rn00570853_m1	1:200	1:20	Hs00222637_m1	1:200	1:20
Grin2b	Rn00680474_m1	1:200	1:20	Hs01002012_m1	1:200	1:20
Htr3a	Rn00667026_m1	1:200	1:20	Hs00168375_m1	1:200	1:20
Htr3b	Rn00573408_m1	1:200	1:20	Hs01573423_m1	1:200	1:20
P2rx3	Rn00579301_m1	1:200	1:20	Hs01125554_m1	1:200	1:20
P2rx4	Rn00580949_m1	1:200	1:20	Hs00902156_g1	1:200	1:20
P2rx6	Rn00562354_m1	1:200	1:20	Hs01003997_m1	1:200	1:20
Adrb1	Rn00824536_s1	1:200	1:20	Hs02330048_s1	1:200	1:20
Adrb2	Rn00560650_s1	1:200	1:20	Hs00240532_s1	1:200	1:20
Adra2a	Rn00562488_s1	1:200	1:20	Hs01099503_s1	1:200	1:20
Pah	Rn00561708_m1	1:200	1:20	-	-	-
Th	Rn00562500_m1	1:200	1:20	Hs01002182_m1	1:200	1:20
Ddc	Rn01401189_m1	1:200	1:20	-	-	-
Dbh	Rn00565819_m1	1:200	1:20	-	-	-
Pnmt	Rn01495589_g1	1:200	1:20	Hs01557113_g1	1:200	1:20
Agt	Rn00593114_m1	1:100	1:20	Hs01586213_m1	1:200	1:20
Ren	Rn00561847_m1	1:5	1:5	Hs00982555_m1	1:4	1:10
Ace	Rn00561094_m1	1:200	1:20	Hs00174179_m1	1:200	1:20
Ace2	Rn01416293_m1	1:10	1:20	Hs01085333_m1	1:200	1:20
Agtr1a	Rn02132799_s1	1:100	1:20	-	-	-
Agtr1b	Rn02132799_s1	1:100	1:20	-	-	-
Agtr1	-	-	-	Hs00258938_m1	1:200	1:20
Agtr2	Rn01416293_m1	1:10	1:20	Hs02621316_s1	1:200	1:20
Mas1	Rn00562673_s1	1:50	1:20	Hs00267157_s1	1:200	1:20

2.9.3 qRT-PCR Statistical Analysis

Data were analysed using GraphPad Prism software (v6/7). When the data passed normality tests (D'Agostino-Pearson omnibus test or Shapiro-Wilk[313]) unpaired two-tailed Student t-tests or one-way ANOVA with Bonferroni post-hoc tests were used. To compare human stellate gene counts, paired t-tests were used to compare samples from the same patients, run on the same 96-well plate. When the data were not normally distributed, the appropriate nonparametric tests were used with the appropriate statistical test reported in the figure legend. Statistical significance was accepted at $p<0.05$.

2.10 Measurements of Proteins and Neurotransmitters

2.10.1 Evoked-Release Field Stimulation

Evoked-release field stimulation of rat stellate ganglia was conducted to investigate whether neurotransmitters or peptides released from the sympathetic stellate ganglia are altered in prehypertensive or hypertensive states. Whole fresh ganglia were dissected from three- to four-week-old preSHR and Wistar rats, and 14- to 15-week-old SHR and Wistar rats. In each experiment, a single ganglion was cleaned, de-sheathed and allowed to recover in pre-equilibrated bicarbonate-buffered Tyrode's solution (5 min, 37 °C , 95 % O_2 / 5 % CO_2). The buffer constituents are listed in Table 2.4.

For catecholamine measurements, perchloric acid (PCA, 0.1 M) was added at each step to prevent the oxidation of catecholamines. Desipramine, a norepinephrine transporter (NET) inhibitor (100 µM) was added for 10 minutes prior to electrical stimulation to prevent catecholamine reuptake. Stellate ganglia were electrically stimulated (5 Hz, 3mA, 5 minutes) using a DS3 constant current stimulator (Digitimer Ltd.) based on previous stimulation parameters[333]. The perfusate samples were kept on ice before freezing at -80 °C. At the end of each experiment, whole stellate ganglia were homogenised in bicarbonate-buffered Tyrode's

solution containing PCA (0.1 M). The homogenate was centrifuged (15,000 G, 15 min, 4 °C) and the supernatant stored at -80 °C for detection and quantification by high-pressure liquid chromatography coupled to electrochemical detection (HPLC-EC).

For AngII measurements, stellate ganglia were incubated in fresh bicarbonate-buffered Tyrode's containing an ACE2 inhibitor (DX600 100µM; BioVision) prior to stimulation to prevent degradation of AngII (5 min, 37 °C). Ganglia were electrically stimulated (3 mA, 5 Hz, 30 s pulse every 90 s, 7.5 minutes) using a DG2A train generator and DS3 constant current stimulator (Digitimer Ltd.) using parameters that were adapted from a previous electrical stimulation method[311] The perfusate was collected, snap frozen in liquid nitrogen and stored at -80 °C for analysis by Enzyme-linked Immunosorbent Assay (ELISA).

2.10.2 High-Pressure Liquid Chromatography with Electrochemical Detection

HPLC-EC was used to quantify concentrations of NA or adrenaline (Adr) in preSHR and Wistar stellate ganglia. Whole fresh ganglia were dissected from young four-week-old preSHR (n=4 rats) and age-matched Wistar (n=8 rats). For each experiment, a single ganglion was cleaned, de-sheathed and allowed to recover in bicarbonate-carbogen buffered Tyrode's solution (5 min, 37 °C , 95 % O_2 / 5 % CO_2). The ganglia were subsequently incubated in bicarbonate-buffered Tyrode's containing the NET-reuptake inhibitor, desipramine (1µM, 10 min, 37 °C). Ganglia were electrically stimulated (3 mA, 5 Hz, 5 mins), parameters that were adapted from previous electrical stimulation methods[262]. The perfusate was removed and perchloric acid (PCA, 0.1 M) was added at each step to prevent the oxidation of catecholamines. Samples were kept on ice before freezing at -80 °C. At the end of each experiment, whole stellate ganglia were homogenised in bicarbonate-buffered Tyrode's solution containing PCA (0.1 M), centrifuged (15,000 G, 15 min, 4 °C) and the supernatant was stored at -80 °C.

For detection and quantification of NA and Adr, the samples were loaded into an autosampler (JASCO, Model AS-2055/2057) and detected with an isocratic HPLC system. HPLC separation was performed at the flow rate 1 ml/min, using a C18 reverse-phase column (CP30710 Microsorb 100-5 C18 S250 x4.6mm, Agilent). The mobile phase (pH 4.7) comprised methanol (11.5 % v/v), NaH_2PO_4 (120 mM), EDTA (0.8 mM), and sodium octane sulfonate (OSA, 0.5 mM). Concentrations of NA and Adr were quantified using an LC-4B electrochemical detector and a carbon working electrode maintained at +0.7 V versus an Ag/AgCl reference electrode (Decade SDC, Antec). Chromatogram peaks were analysed (area under curve; CLARITY software) and the concentrations of NA were calculated against a 50 mg standard of NA and Adr dissolved in bicarbonate-buffered Tyrode's containing PCA (0.1 M).

2.10.3 Protein Extraction

Protein was extracted from stellate ganglia obtained from three- to four-week, 12- to 14-week-old or 16- to 20-week-old male SHR, as well as age-matched Wistar rats and human donors. Rat stellate tissue (~100 mg) was pooled and homogenized in ice-cold dPBS without Ca^{2+} or Mg^{2+}. In alternative experiments, tissue from human ganglia (~80 mg) was separately homogenized (n=5) in ice-cold dPBS without Ca^{2+} or Mg^{2+}. The protein concentration in each sample was quantified using a protein assay (BioRad DC) as per the manufacturer's instructions and the total protein concentration in each sample was normalised.

2.10.4 Protein Concentrations and Enzyme Activity Measurements

Sandwich ELISAs and Enzyme Immunoassays (EIA) were performed in 96-well plates to establish the concentrations of the proteins of interest in human and rat stellate ganglia. Details of each assay, the relevant protein dilutions and wavelengths for measurement are listed in Table 2.8. To quantify the protein content in the electrically-evoked perfusate, no dilutions were made. ELISA plates were purchased pre-coated with a capture antibody specific to the antigens

of interest. After incubation and removal of the samples, a biotin-conjugated antibody with high affinity for the antigen was added to each of the wells. Following a second incubation and a wash to remove unbound antibody-antigen conjugates, a solution containing streptavidin-conjugated Horseradish Peroxidase (HRP) was added to each well. Streptavidin has high affinity to biotin, and HRP reacts with TMB substrate inducing a colorimetric signal. A stop solution was added to each of the wells to terminate the reaction and absorbance values were read on a plate reader (Infinite F500, TECAN) within 5 minutes. Background absorbance was subtracted from the primary absorbance values. Concentrations of the relevant protein or activity were quantified using a standard curve generated from the supplied standards. A summary of the ELISA assay protocol is shown in Fig. 2.12.

Fluorometric assays were purchased to measure the activity of specific enzymes of interest in rat and human stellate ganglia (Table 2.8). Enzyme activity assays measure the rate of conversion of a substrate to a product, as an indicator of enzyme activity. For the enzyme activity assays (ACE, ACE2, Ren), a substrate conjugated to a fluorescent peptide was added to each sample well. Cleavage of the fluorescent peptide from the substrate peptide releases a free fluorophore leading to an increase in fluorescence. Measurements for ACE, ACE2 and Ren activity were made immediately after sample and substrate preparation, and the fluorescence in each sample was recorded for 30 minutes to two hours. (Infinite F500, TECAN). Background fluorescence was subtracted from the primary fluorescence values. Concentrations of the relevant protein or activity was quantified using a standard curve generated from the supplied standards. ELISAs, EIA and fluorometric assays are well-established protocols, therefore, in this thesis all experiments (timings and temperatures for incubation) were performed in accordance with the manufacturer's instructions and optimisation of these assays was not required.

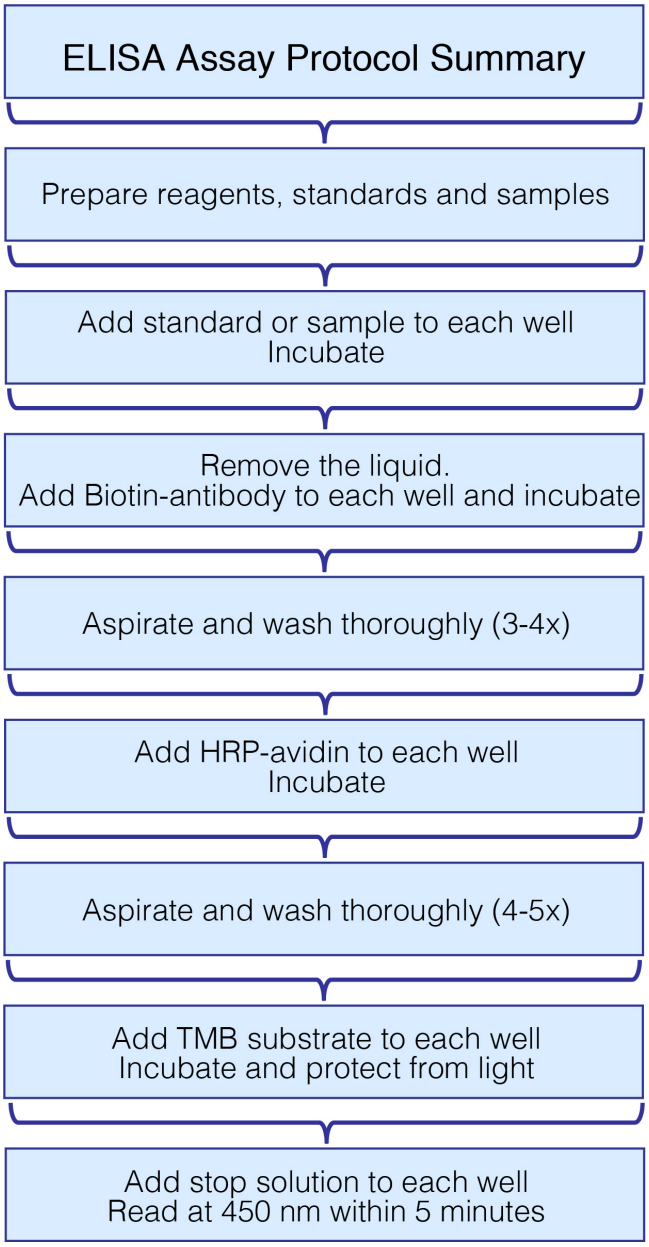


Figure 2.14. ELISA Protocol Summary
ELISAs were conducted using homogenised sympathetic stellate ganglia from human or rat with normalised protein concentrations. Standards and reagents were prepared as per manufacturer's instructions. Each sample was incubated with biotin antibody, washed, and re-incubated with horseradish peroxidase (HRP) conjugated streptavidin to bind to the antigen in the sample. After further washing to remove non-specific binding, a TMB substrate was added to induce a colorimetric signal. After the reactions were stopped, absorbance was read at 450 nm using a plate reader (Infinite F500, TECAN).

Table 2.10. List of Protein and Enzyme Assays and Optimal Sample Dilutions

Protein	Species	Assay	Protein diluton	Catalogue	Wavelength (nm)
β_1AR	Rat	ELISA	1:1	CSB-EL001391RA, CusaBio	450
β_1AR	Human	ELISA	1:1	CSB-EL001391HU, CusaBio	450
β_2AR	Rat	ELISA	1:1	CSB-EL001392RA, CusaBio	450
β_2AR	Human	ELISA	1:1	CSB-EL001392HU, CusaBio	450
TH	Rat	ELISA	1:1	CSB-E13102R, CusaBio	450
TH	Human	ELISA	1:1	CSB-E09661H, CusaBio	450
PNMT	Rat	ELISA	1:1	CSB-EL018274RA, CusaBio	450
PNMT	Human	ELISA	1:1	CSB-EL018274HU, CusaBio	450
AGT	Rat	ELISA	1:10	OKCD01237, Aviva	450
AGT	Human	ELISA	1:1	CSB-E08564H, CusaBio	450
Ang1-7	Rat	ELISA	1:10	CSB-E14241R, CusaBio	450
Ang1-7	Human	ELISA	1:10	CSB-E14242H, CusaBio	450
AngII	Rat / Human	EIA	1:10	RAB0010-1KT, Sigma	450
Ren	Rat	Fluorometric	1:1	Mak157-1KT, Sigma	Ex/Em: 540/590
Ren	Human	ELISA	1:3	Dren00, R&Dsystems	450
ACE	Rat / Human	Fluorometric	8:10	K227-100, BioVision	Ex/Em: 330/430
ACE	Human	ELISA	1:10	LS-F3949, LifeSpan BioSciences	450
ACE2	Rat	Fluorometric	1:10	K897-100, BioVision	Ex/Em: 320/420
ACE2	Human	ELISA	1:10	LS-F5886, LifeSpan BioSciences	450

2.10.5 Statistical Analysis of Assays

Data were analysed using GraphPad Prism software (v6/7). When the data passed normality tests, unpaired or paired two-tailed Student t-tests, or a one or two-way analysis of variance (ANOVA) were used. When the data were not normally distributed, the appropriate nonparametric tests were used with the specific statistical test reported in the figure legend. All data are expressed as the mean ± SEM. Statistical significance was accepted at $p<0.05$ unless otherwise described.

2.11 Reagents

All compounds were purchased from Sigma unless otherwise stated.HBSS, Leibovitz's L-15 medium, D-(+)-glucose solution (45 %), L-glutamine (200 mM), FBS, borax, and boric acid were purchased from Sigma. Dulbecco's Modified Eagle Medium (DMEM), Dulbecco's Phosphate-buffered Saline (dPBS), Nuclease-free water was purchased from Gibco by LifeTechnologies. Penicillin 10,000 units/ml; Streptomycin 10,000 µg/ml, Murine nerve growth factor 2.5S (NGF) was purchased from Millipore, Laminin from mouse Engebreth-Holm-Swarm (EHS) sarcoma (1 mg/ml) was purchased from ThermoFisher. Collagenase type IV and trypsin TRL3 were purchased from Worthington.

3

RNA Sequencing of Sympathetic Stellate Ganglia

3.1 Introduction

Sympathetic hyperactivity is a key feature of human hypertension[95] that is also seen in animal models of CVD[96]. Cardiac-sympathetic over-activity is commonly observed in young prehypertensive patients and correlates with elevated heart rate and CO, where chronic elevations in noradrenergic transmission has detrimental effects on myocardial function. Consequently, this neural phenotype is a powerful predictor of morbidity and mortality[29,188,189]. In the SHR, a genetic model of hypertension, sympathetic over-activity occurs prior to increases in arterial blood pressure[334,335] and arises within distinct neuroanatomical sites, and is commonly elevated within cardiac and renal sympathetic ganglia[211].

Within the cardiac-sympathetic stellate ganglia, neurons display increased $[Ca^{2+}]_i$ [113] as a result of elevated *N*-type voltage-gated Ca^{2+} (I_{CaN}, $Ca_v2.2$) channel conductance [96,216]. What causes increased neuronal excitability? Cyclic nucleotides and their effectors regulate Ca^{2+} conductance predominantly via phosphorylation of ion channels and endoplasmic reticulum (ER) proteins [228,282,336], yet the relationship between cN second messenger signalling pathways and abnormal $[Ca^{2+}]_i$ is still poorly understood in disease[96,334]. Previous work suggests that in young prehypertensive SHR, decreased bioavailability of NO leads to preferentially diminished cGMP-PKG signalling, resulting in disinhibition of *N*-type voltage-gated Ca^{2+} channel activity[96,334]. Whether there is a genetic basis for increased cardiac sympathetic over-activity is not known and evidence for genetic alterations linked to abnormal Ca^{2+} regulation in hypertension is lacking.

3.2 Chapter Aims

In this chapter, I aimed to carry out a non-biased hypothesis-neutral RNA-seq transcriptomic analysis to identify the differential expression of cell-specific RNA transcripts that are expressed in the sympathetic stellate ganglia from normotensive and hypertensive adult rats to provide a framework for future work and targeted investigation. I also aimed to validate the RNA-seq dataset by confirming the expression of key gene transcripts in stellate ganglia of human and rat using qRT-PCR. Additionally, I aimed to assess whether the observation of differentially expressed gene families leads to alterations in molecular function by applying fluorescence microscopy techniques to test the activity of key proteins in real-time. I am the first author on a manuscript describing this work that is published in Scientific Reports[337], and second author on a manuscript published in The Journal of Neuroscience, for which I planned and conducted all of the FRET experiments[96].

The specific aims of this Chapter were to:

1. Identify differential expression transcriptomic profiles in sympathetic stellate ganglia from adult normotensive and SHR with established hypertension.
2. Ascertain whether key gene transcripts identified in rat stellate ganglia are also expressed in human stellate ganglia to provide wider physiological context.
3. Establish whether changes in gene expression in sympathetic neurons have functional relevance and lead to impaired intracellular signalling.

3.3 Methods

3.3.1 Animals

Four-week-old male prehypertensive SHR, 16-week or 20-week-old male SHR with established hypertension and age-matched normotensive Wistar control rats were obtained from Envigo, UK. All experiments were performed in accordance with the UK Home Office Animal Scientific Procedures Act 1986 (ASPA) and approved by the University of Oxford (PPL 30/3131; David J. Paterson).

3.3.2 Neuronal Isolation

Sympathetic stellate ganglia were dissected and enzymatically digested with collagenase (type IV, 1 mg/ml, 37 °C) and trypsin (type I, 1 mg/ml, 37 °C). Stellates were washed with a modified L-15 blocking medium that was equilibrated prior to use (37 °C , 5 % CO_2) and the ganglia were dissociated into a single-cell suspension via manual trituration in pre-equilibrated plating medium (37 °C , 5 % CO_2). Neurons were plated on Poly-D-lysine/laminin-coated coverslips (6 mm, VWR International) and incubated in plating medium (37 °C , 5 % CO_2) until required.

3.3.3 Förster Resonance Energy Transfer (FRET) Microscopy

For live-imaging of cAMP or PKA measurements, cells were incubated with adenovirus' encoding the cAMP (Epacs-H30, Epac1-H187) or PKA (AKAR4) FRET sensors for 24-hours. The media containing virus was removed and cells were incubated (37 °C , 5 % CO_2) in plating medium for a further 24 hours for adequate viral load and FRET sensor expression. FRET biosensor-expressing neurons were imaged 3-4 days post-culture, on an inverted microscope (Nikon) connected to an OptoLED fluorescence imaging system (Cairn Research Ltd., UK). During FRET experiments, cells were perfused continuously with Tyrode's solution via a gravity-fed perfusion system and the flow rate was controlled at 2-3 ml/min. A stable baseline of at least

2 minutes was required at the start of each experiment. Forskolin, IBMX, and all other compounds were diluted to relevant concentrations in HEPES-buffered Tyrode's solution. To measure cAMP or PKA activity and to assess PDE activity in the respective experiments, forskolin (0.1-25 µM) or IBMX (1-100 µM) was administered in incremental concentrations over-time. The maximal FRET change of each cell was recorded by exposing the cells to saturating concentrations of forskolin 25 µM and IBMX 100 µM, to ensure that the cells responded similarly to the FRET biosensors.

3.3.4 RNA Extraction from Sympathetic Cardiac Ganglia

Right and left post-ganglionic sympathetic stellate neurons were dissected from 16-week-old male SHR and age-matched male Wistar rats. Right stellate ganglia were removed for RNA-seq and the left stellate ganglia were used for matched qRT-PCR experiments. Rats were anaesthetised in an induction chamber (3-5 % isoflurane) and humanely killed by a Home Office approved Schedule 1 method: overdose of pentobarbital (Euthatal, 200 mg/ml) and exsanguination. For clinical samples, human ganglia were extracted at UCLA and shipped on dry ice in RNA*later*® RNA Stabilization Solution (ThermoFisher). Human donor characteristics are included in the general methods section. Rat and human stellate ganglia were cleaned and de-sheathed and each sample contained RNA from one stellate. Rat RNA was extracted using the RNeasy Mini RNA Extraction Kit (Qiagen) and human RNA was extracted using an RNeasy Maxi RNA Extraction Kit (Qiagen) in accordance with the manufacturer's instructions. RNA samples were divided and aliquoted for qRT-PCR and quality control experiments before snap freezing in liquid nitrogen and storage at -80 °C. The RNA quality and integrity from each sample, was confirmed using automated electrophoresis on a 2100 Bioanalyzer Instrument with an RNA 6000 Pico Kit (Agilent), as described in Chapter Two. Rat samples with an RNA integrity number (RIN) less than 8.5 were discarded. Due to difficulties with fast shipping of human samples human RNA samples were accepted with RINs above 5.7. RNA concentrations were

determined using a Qubit RNA High Sensitivity Assay Kit (Molecular Probes, Life Technologies) and a Qubit® 2.0 Fluorometer (Invitrogen, Life Technologies). Regarding the removal of human ganglia, all methods were carried out in accordance with relevant guidelines and regulations. The human study was approved by an institutional committee, the UCLA Institutional review board, approval # 12-000701, and informed consent was obtained from all subjects.

3.3.5 cDNA library preparation for RNA Sequencing

Four RNA samples extracted from the right sympathetic stellate ganglion of 16-week-old male SHR (n=4) and age-matched Wistar (n=4) were sent to the High-Throughput Genomics Group at the Wellcome Trust Centre for Human Genetics (WTCHG) for RNA-seq library construction and sequencing using an Illumina HiSeq 4000 (Illumina, Inc., San Diego, USA). The sequencing libraries were constructed using a SMARTer Low Input RNA Kit (Clontech Laboratories, Ltd.) due to the low RNA concentrations obtained from a single stellate, and prepared for paired-end sequencing (2 x 75 base pairs). Each sample was sequenced on two separate lanes to minimise technical error and to increase the sequencing depth (~15-25 million reads per lane). Samples were randomized and blinded to the experimenter. The sequencing parameters established, were based on recommendations from WTCHG and those published by Conesa et al., 2016[317].

3.3.6 Quasi-mapping and Differential Expression Analysis

The transcripts were quantified via the Salmon (v0.8.2) package using the transcriptome-based quasi-mapping mode[322]. The commands are summarised in chapter two. Data files were assigned alternative names to blind the experimenter during the relevant stages of the quasi-mapping analysis. Once each sample was quantified, the data were imported into R statistical analysis program and summarised to a gene-level using the 'tximport' function (v1.6.0) [326]. Gene level differential expression analysis between Wistar and SHR samples was performed using

the DESeq2 command in DESeq2 (v1.18.1)[327]. Significance for differential expression was accepted at the Benjamini-Hochberg adjusted p (p.adj)<0.05 level.

3.3.7 Gene Ontology Analysis

To assess the relevance of the observed differentially expressed genes, the differentially expressed genes were grouped into GO families[328] using The Database for Annotation, Visualization and Integrated Discovery (DAVID, v6.8)[329]. The differentially expressed gene input was taken at the Benjamini-Hochberg p.adj<0.05 level. Significant GO groups were subsequently determined using Benjamini-Hochberg correction p.adj<0.05. GO groups were filtered to exclude groups with <10 genes. Very broad GO groups were subsequently filtered out based on the measured specificity of each term identified, using the GO_FAT filter. The parameters selected for DAVID were based on online recommendations and are described in the general methods section[329,330].

3.3.8 cDNA Library Preparation and Quantitative Real-Time PCR

Stellate RNA (50 ng) was used for constructing the qRT-PCR cDNA libraries to confirm the presence of the selected mRNA transcripts. For rat stellate samples, the SuperScript™ III VILO™ cDNA synthesis protocol was followed according to manufacturer's instructions (ThermoFisher). For human stellate samples, the SuperScript™ IV VILO™ cDNA synthesis protocol was followed according to manufacturer's instructions (ThermoFisher). The concentrations of cDNA in each sample and 260/280 ratios were calculated (NanoDrop Lite) to detect the presence of contaminants. Samples with an abnormal 260/280 ratio (<1.7 and >1.95) were discarded. Samples were aliquoted and frozen at -80 °C for long-term storage or kept at 4 °C for immediate use. TaqMan® Gene Expression Master Mix (ThermoFisher) was added to each cDNA sample in addition to the selected primer conjugated to a FAM dye and diluted for optimal PCR reactions. Primer information is included in the general methods section. Samples

(three technical repeats, three to four biological repeats) were run on a real-time quantitative PCR thermocycler (ABI, PRISM) using optimal qRT-PCR thermocycling parameters described in the General Methods. Data displayed in the results section depicts gene counts normalised to *B2m;* however, each primer was analysed against two housekeeping genes, *B2m* and *Gapdh* for validation and accuracy of qRT-PCR data. The relative amount of each transcript was calculated using the comparative (C_T) method ($\Delta\Delta C_T$, rat; ΔC_T, human)[332].

3.3.9 Statistical Analysis and Data Availability

qRT-PCR data were analysed using GraphPad Prism software (v7). When the data passed normality tests, an unpaired Student's *t*-test was used. When the data were not normally distributed, nonparametric tests were used with the specific statistical test reported in the figure legend. All qRT-PCR data are expressed as Log_2(fold change) ± SEM. Statistical significance was accepted at $p<0.05$, unless otherwise described. RNA-seq raw FastQ files were deposited in the NCBI short reads archive under SRA number SRP132271 (NCBI Short Read Archive) and the quasi-mapped data is available under Gene Expression Omnibus (GEO) accession number (GSE110197).

3.4 Results

3.4.1 Study Design

To study the rat stellate ganglia transcriptome, RNA was obtained from four 16-week-old male SHR with established hypertension and four age-matched male Wistar control rats. Using the HiSeq 4000 sequencing platform, ~345 million reads were generated from 75-bp paired-end RNA-seq data. A comparative analysis of the stellate ganglia transcriptome was performed between Wistar and SHR using a Salmon-DESeq2 analysis pipeline based on the protocol and parameters described previously[322] and in Chapter Two. The number of replicates (n=4 animals/group) and the sequencing parameters established were based on the recommendations of the Wellcome Trust Centre for Human Genomics (WTCHG), in addition to those published by Conesa et al., 2016[317]. The limitations of this study are discussed in section 3.6.

3.4.2 Differential Expression Analysis

Transcript level quantification was performed using the quasi-mapping function of the Salmon package, where inbuilt functions corrected for GC nucleotide and positional bias[322]. These data were converted into quantitative gene level expression values, and the differential gene expression between the strains was calculated and normalised using DESeq2[327]. An MA plot was constructed for visual representation of the genomic data and a Principal Component Analysis (PCA) plot with log normalisation demonstrates the variation within the samples (Fig. 3.1)[327].

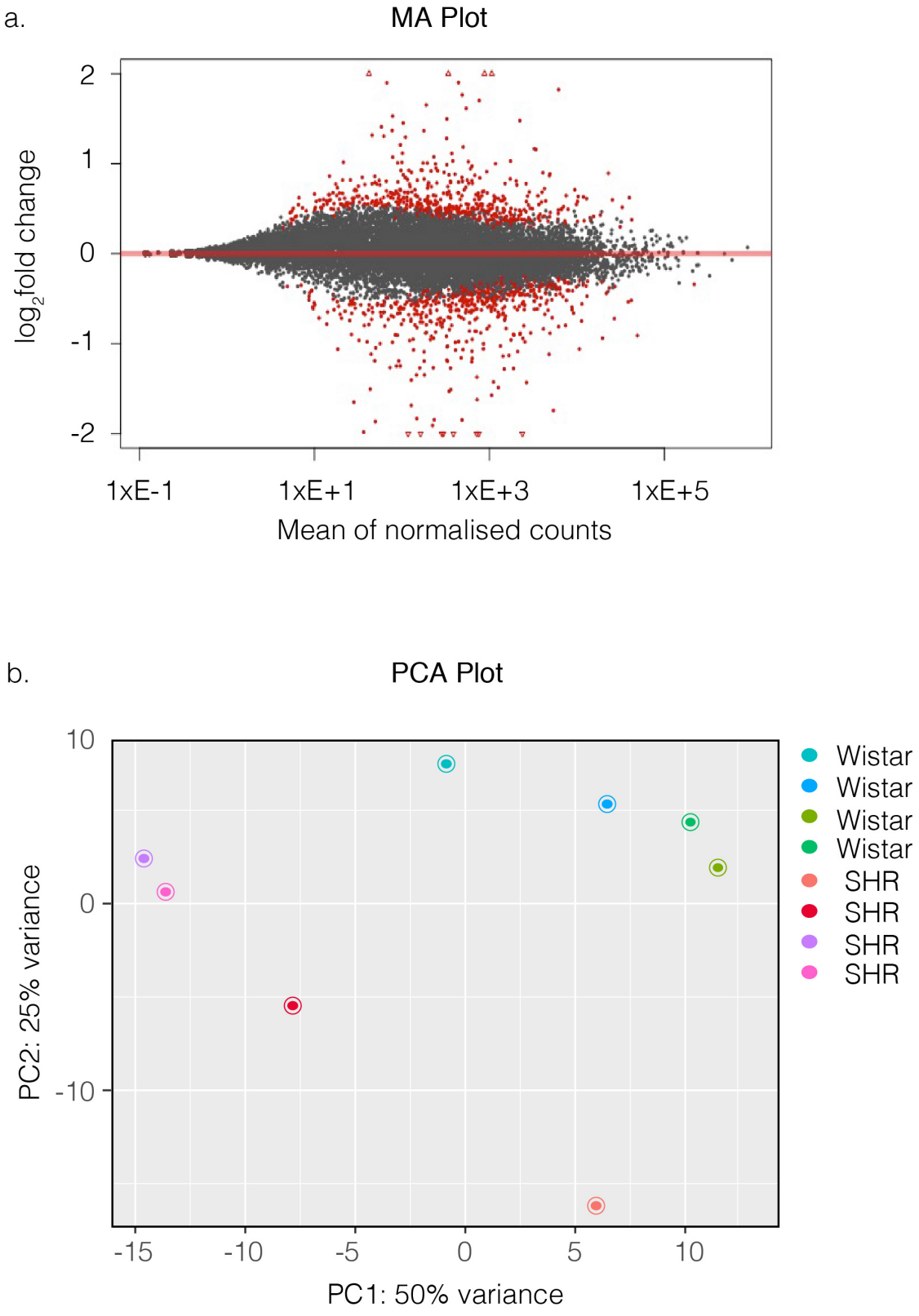


Figure 3.1. MA plot and PCA plot confirm validity of RNA-seq analysis.
The MA plot depicts the relationship between the number of counts per gene, the size of the fold change and the significance of fold changes. Significance is indicated by red spheres on a gene by gene basis. Non-significant transcripts are shown as grey spheres (a). A Principal Component (PCA) plot demonstrates the variation of the stellate ganglia transcriptome between strains (b).

3.4.3 Overview of the Transcriptome of Wistar and SHR Stellate Ganglia

In confirmation of the expected neuronal phenotype, genetic markers consistent with sympathetic neurons were among the most highly expressed genes in both strains (e.g. Dopamine-β hydroxylase, *Dbh;* and Neuropeptide Y, *Npy*). The most highly expressed genes are displayed in Table 3.1.

Table 3.1. Highest Abundance Gene Transcripts in Wistar and SHR Ganglia

Wistar		SHR	
Gene	Counts	Gene	Counts
Tuba1a	902254.5	*Tuba1a*	903662.8
Ubb	634608.5	*Ubb*	566905.8
Tubb3	505765.0	*Tubb3*	475576.0
Dbh	376310.5	***Dbh***	292282.0
Aldoa	268873.4	*Hspa8*	239735.8
Thy1	258729.0	*Actg1*	234697.0
Ndrg4	255907.9	*Aldoa*	229129.0
Hspa8	252383.8	*Ndrg4*	218274.5
Actg1	248451.5	*Actb*	188417.0
Actb	235332.0	*Thy1*	187021.3
Ubc	172035.0	***Npy***	185153.3
Npy	171911.5	*Hsp90ab1*	164202.3
Fth1	171831.0	*Gapdh*	162569.0
Tuba1b	170766.3	*Tuba1b*	162325.8
Gapdh	169646.5	*LOC310926*	160423.9
Uchl1	158139.3	*Uchl1*	132592.8
Hsp90ab1	155680.3	*Stmn2*	130962.3
Stmn2	143877.8	*Pkm*	126418.0
LOC310926	142530.5	*Ubc*	125959.8
Zwint	129453.3	*Fth1*	123169.5
Pkm	125560.5	*Cyb561*	121759.0
Cyb561	118581.3	*Eno1*	118345.0
Eno1	117333.7	*Fxyd6*	116652.5
Snap25	115665.7	*Ppia*	110293.8
Eef1a1	115008.8	*Tubb5*	109262.5
Tubb5	114583.8	*Zwint*	107398.5
Sncg	113412.0	*Sncg*	107054.5
Th	109402.0	*Eef1a1*	105872.3
Ppia	108746.8	*Tubb4a*	98589.5
Ap2m1	108245.3	*Ap2m1*	98564.3
Fxyd6	107218.1	*Calm1*	98132.8
Calm1	101187.8	***Snap25***	96320.1
Tubb4a	100285.5	***Th***	93452.0
Bcat1	95862.3	*Sepw1*	92354.0
Atp6v0c	89869.3	*Atp6v0c*	85477.0
Psap	89826.3	*LOC257642*	85169.0
Tubb2a	88907.6	*Gpi*	84403.5
Sepw1	86428.0	*Bcat1*	80402.4
Gpi	80323.8	*Map1b*	79939.0
LOC257642	77655.1	*Tubb2a*	79627.8

Table 3.1 includes a list of the top 40 genes and their mean counts in stellate ganglia obtained from Wistar and SHR. Genetic markers of neurons with a sympathetic phenotype are highlighted in bold. No significant difference was found in sympathetic or neuronal markers.

3.4.5 Differential Expression in SHR Stellate Ganglia

The differential expression analysis identified 744 differentially expressed genes in the stellate ganglia, where approximately 45 % of genes were upregulated and 55 % downregulated in the SHR. The top 20 differentially expressed genes are displayed in Table 3.2 and Figure. 3.2.

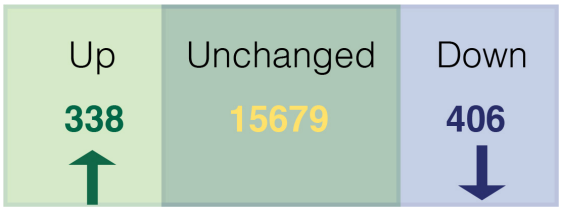


Figure 3.2. Differentially Expressed Genes in SHR Stellate Ganglia.
Venn diagram represents the total number of upregulated gene transcripts (338) and downregulated transcripts (406) in the SHR stellate ganglia, identified by DESeq2[327] where green and blue represent up- and downregulated genes respectively.

Table 3.2. Differentially Expressed Gene Transcripts in Stellate Ganglia

Gene Name	Description	RNAseq	
		Log_2 Fold Change	p. adjusted
Synpr	synaptoporin	-5.00	6.57E-81
Nudt17	nudix hydrolase 17	-4.21	7.95E-79
Pxmp4	peroxisomal membrane protein 4	2.98	8.39E-68
Gsta4	glutathione S-transferase alpha 4	2.78	8.12E-64
Nudt3	nudix hydrolase 3	2.02	4.76E-49
Lrsam1	leucine rich repeat and sterile alpha motif containing 1	-3.77	1.86E-46
LOC363337	similar to RIKEN cDNA 1700081O22	-1.94	2.52E-43
Hiatl1	hippocampus abundant transcript-like 1	2.04	1.87E-34
Perp	PERP, TP53 apoptosis effector	-2.64	1.27E-31
Camk2d	calcium/calmodulin-dependent protein kinase II delta	-2.59	3.83E-31
Tnni1	troponin I1, slow skeletal type	-4.49	4.70E-31
Ptgr1	prostaglandin reductase 1	1.97	4.70E-31
LOC287167	hemoglobin alpha, adult chain 3	-8.81	5.63E-30
Fbxw8	F-box and WD repeat domain containing 8	-1.79	3.12E-29
Fxyd7	FXYD domain-containing ion transport regulator 7	-1.88	1.79E-28
Cela1	chymotrypsin-like elastase family, member 1	-3.39	7.58E-27
Selenbp1	selenium binding protein 1	11.90	1.51E-26
Bdkrb2	bradykinin receptor B2	2.47	3.79E-26
Elk3	ELK3, ETS-domain protein	-1.74	1.79E-25

Table 3.2 depicts the top 20 differentially expressed transcriptomic changes in the stellate ganglia between Wistar and SHR in order of Benjamini-Hochburg significance. The table includes log_2 fold change values relative to Wistar and the associated Benjamini-Hochburg p. adjusted value.

3.4.6 Distinct Alterations in Gene Ontology in the SHR Stellate Ganglia

To assess the relevance of the observed differentially expressed genes, the differentially expressed genes were grouped into GO families[328] using The Database for Annotation, Visualization and Integrated Discovery (DAVID, v6.8) [329]. Significant differences between the SHR and Wistar transcriptome were identified within in the three broad GO categories: Biological Processes (GO BP) Molecular Function (GO MF) and Cellular Component (GO CC). The significantly over-represented GO CC (Fig. 3.3), GO BP (Fig. 3.4) and GO MF (Fig. 3.5) families and their hierarchical structures are illustrated. Significant overlap was found in genes in subcategories from parent groups, weighting the importance of these families.

3.4.6.1 Cellular Component Gene Ontology

The CC GO category indicated 4 main differential themes between Wistar and SHR stellate ganglia (Fig. 3.3). Significant over-representation was observed in gene families corresponding to: neuron projections and the synapse (highlighted in blue), cell junctions (pink), vesicles (orange), neuronal cell bodies (green), and perinuclear region of cytoplasm (purple). The most over-represented branch within this CC GO category was neuronal projections, suggesting that genes involved in axonal projections and synapse formation are altered in disease. The number of genes in each CC GO family, fold enrichment and Benjamini-Hochburg significance values are shown in Table 3.3. A list of CC GO genes corresponding to each group are included in the appendix (Table 8.1).

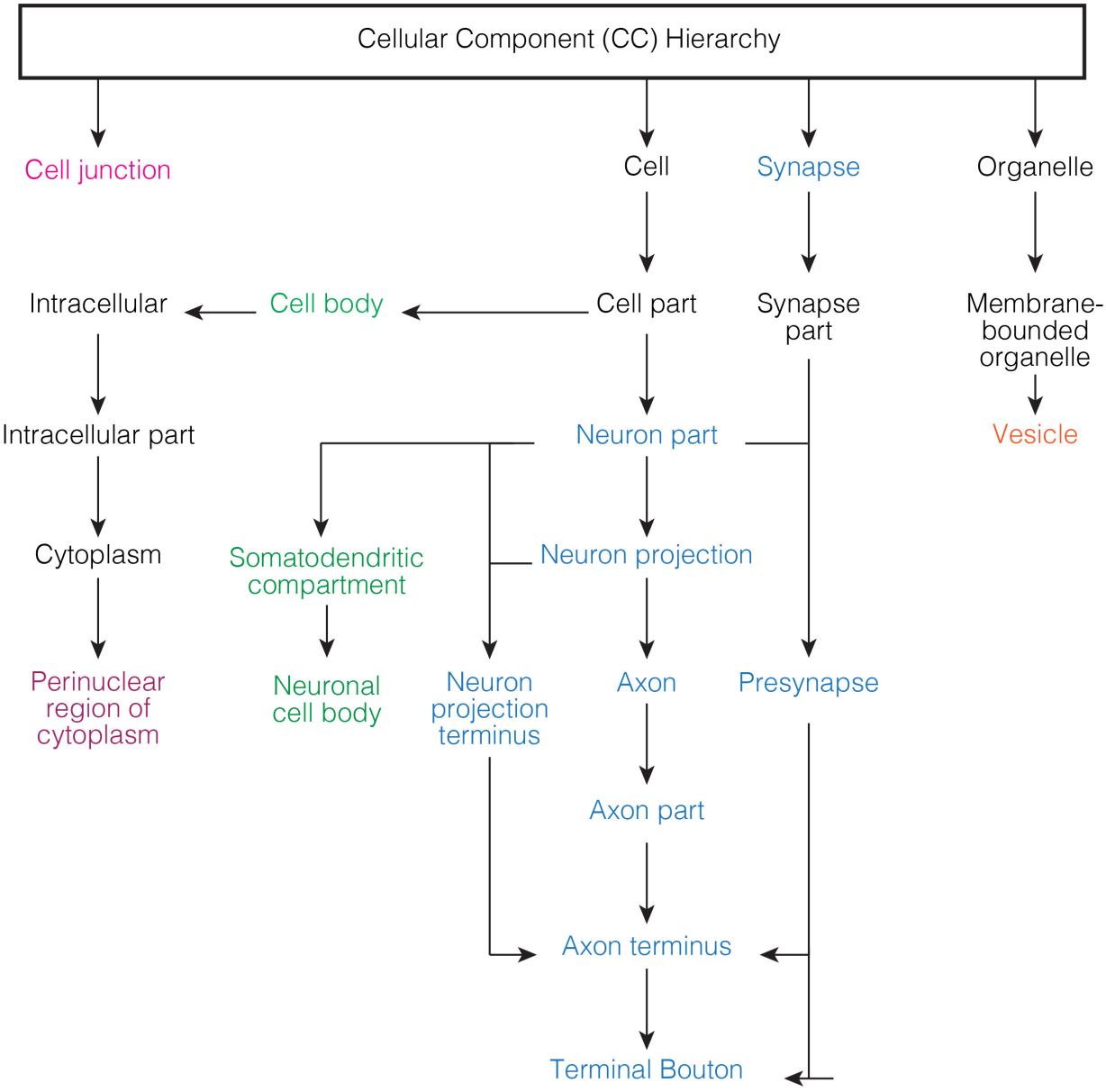


Figure 3.3. Over-represented Cellular Component Gene Ontology Group Hierarchy
Parent groups are represented at the top of the tree-diagram with branching child groups below. Significant CC GO groups are coloured, non-significant groups are black. Distinct categories are represented by colour.

Table 3.3. Over-represented Cellular Component Gene Ontology Groups

Gene Ontology ID	Cellular Component GO Description	Count	Fold Enrichment	p. adjusted
GO:0097458	Neuron Part	108	1.61	1.39E-04
GO:0043005	Neuron Projection	90	1.74	1.51E-04
GO:0030424	Axon	50	2.07	4.24E-04
GO:0033267	Axon Part	34	2.49	4.38E-04
GO:0043195	Terminal Bouton	19	3.69	4.74E-04
GO:0043679	Axon Terminus	24	2.87	1.02E-03
GO:0043025	Neuronal Cell Body	52	1.92	1.12E-03
GO:0036477	Somatodendritic Compartment	67	1.73	1.14E-03
GO:0048471	Perinuclear Region of Cytoplasm	52	1.87	1.45E-03
GO:0044306	Neuron Projection Terminus	24	2.68	2.17E-03
GO:0044297	Cell Body	54	1.77	3.60E-03
GO:0045202	Synapse	60	1.64	9.47E-03
GO:0031988	Membrane-Bounded Vesicle	176	1.26	2.03E-02

The over-represented Cellular Component Gene Ontology groups are listed by order of significance. The number of significant genes, the GO group enrichment and Benjamini-Hochburg p. adjusted values are included. For a full list of genes see Appendix Table 8.2.

3.4.6.2 Biological Processes Gene Ontology

The BP GO category highlighted 13 differentially expressed themes between Wistar and SHR stellate ganglia (Fig. 3.4). Over-representation was observed in gene families corresponding to regulation of heart contraction and blood pressure (red), renal system processes (dark orange), regulation of ion transport (orange), leukocyte chemotaxis (chartreuse), response to stress (green), response to chemical (teal), cell communication and synaptic transmission (light blue), signal transduction including receptor signalling pathways (dark blue), positive regulation of developmental process (highlighted in dark purple), metabolic process including catabolic processes and lipid metabolism (crimson), growth (light purple) and regulation of organismal processes (pink). The most highly over-represented groups weighted by the number of gene families was observed in the branches corresponding to circulatory system processes and cell-cell communication, highlighting the relevance of cardiac-sympathetic neurons in regulating myocardial function and their impairment in hypertension. The number of genes in each BP GO family and their significance values are shown in Table 3.4. A list of BP GO genes corresponding to each group are included in the appendix (Table 8.2).

Table 3.4. Over-represented Biological Processes Gene Ontology Groups

Gene Ontology ID	Biological Processes GO Description	Count	Fold Enrichment	p. adjusted
GO:0006629	lipid metabolic process	75	1.70	9.04E-03
GO:0010033	response to organic substance	160	1.39	9.58E-03
GO:0008217	regulation of blood pressure	22	3.05	1.17E-02
GO:0003013	circulatory system process	39	2.23	1.26E-02
GO:0042060	wound healing	36	2.23	1.30E-02
GO:0051051	negative regulation of transport	40	2.10	1.49E-02
GO:0008015	blood circulation	39	2.25	1.54E-02
GO:0060047	heart contraction	21	2.97	1.54E-02
GO:0007267	cell-cell signaling	78	1.62	1.66E-02
GO:0070887	cellular response to chemical stimulus	136	1.39	1.67E-02
GO:0044255	cellular lipid metabolic process	59	1.75	1.67E-02
GO:0009611	response to wounding	43	2.01	1.71E-02
GO:0006952	defense response	80	1.58	1.75E-02
GO:0099537	trans-synaptic signaling	44	1.94	1.77E-02
GO:0098916	anterograde trans-synaptic signaling	44	1.94	1.77E-02
GO:0007268	chemical synaptic transmission	44	1.94	1.77E-02
GO:0099536	synaptic signaling	44	1.94	1.77E-02
GO:0003015	heart process	21	2.93	1.77E-02
GO:0044282	small molecule catabolic process	25	2.46	2.94E-02
GO:0044712	single-organism catabolic process	52	1.97	2.97E-02
GO:0010038	response to metal ion	35	2.08	2.97E-02
GO:0043269	regulation of ion transport	43	1.87	4.14E-02
GO:0044057	regulation of system process	38	1.95	4.29E-02
GO:0006811	ion transport	81	1.52	4.40E-02
GO:0051094	positive regulation of developmental process	73	1.56	4.52E-02
GO:0030595	leukocyte chemotaxis	19	2.76	4.54E-02
GO:0040007	growth	63	1.62	4.58E-02
GO:0050900	leukocyte migration	25	2.32	4.59E-02
GO:0007166	cell surface receptor signaling pathway	114	1.38	4.63E-02
GO:0051049	regulation of transport	100	1.43	4.64E-02
GO:0008016	regulation of heart contraction	18	2.85	4.64E-02
GO:0003014	renal system process	14	3.48	4.65E-02
GO:0051240	positive regulation of multicellular organismal process	88	1.47	4.66E-02
GO:0042330	taxis	37	1.93	4.68E-02
GO:0097529	myeloid leukocyte migration	17	2.92	4.73E-02

The over-represented Biological Processes Gene Ontology groups are listed by order of significance. The number of significant genes, the GO group enrichment and Benjamini-Hochburg p. adjusted values are included. For a full list of genes see Appendix Table 8.2.

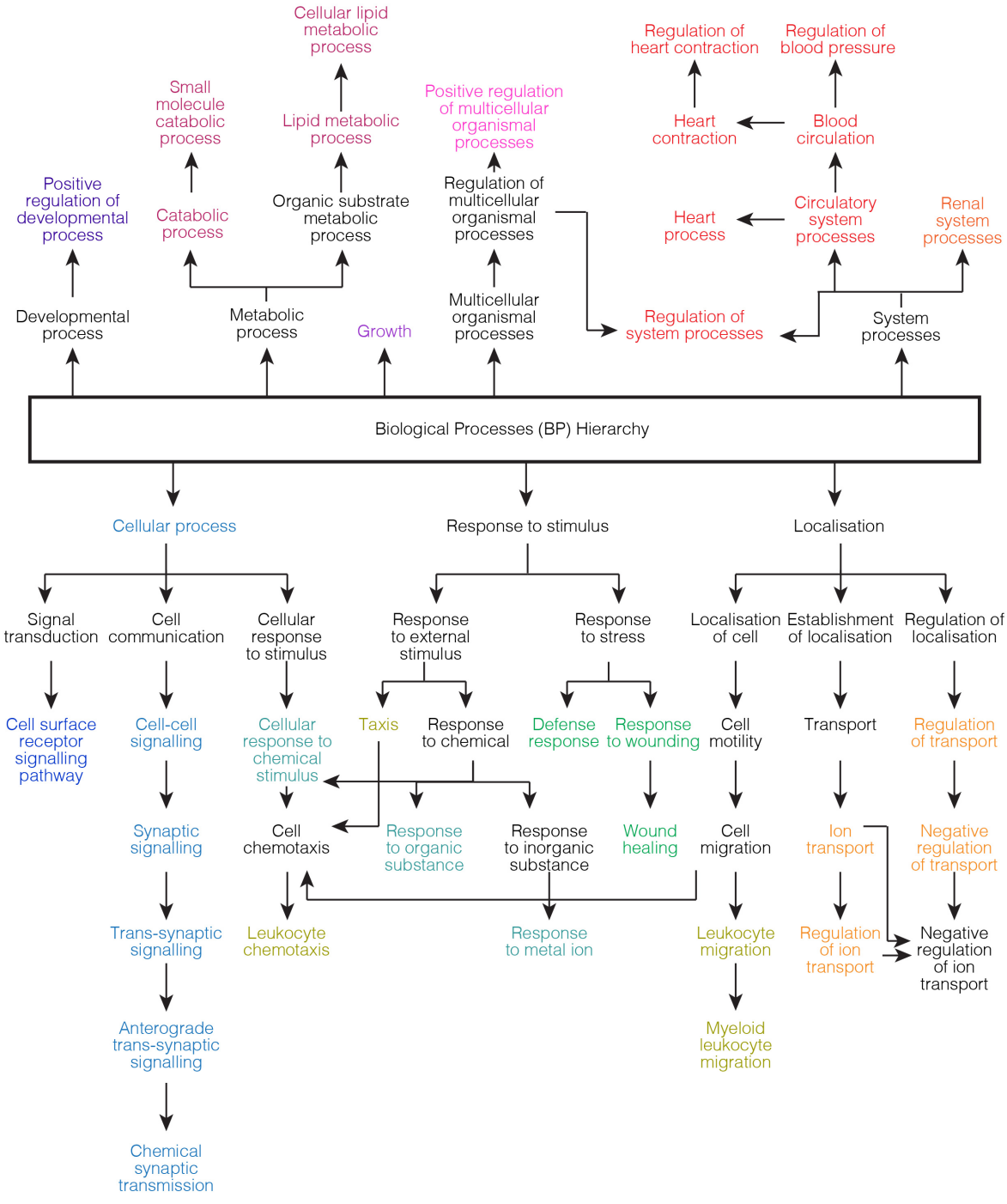


Figure 3.4. Over-represented Biological Processes Gene Ontology Group Hierarchy. Parent groups are represented at the centre of the tree-diagram with branching child groups. Significant BP GO groups are coloured, non-significant groups are black. Distinct categories are represented by colour.

3.4.6.3 Molecular Function Gene Ontology

The Molecular Function (MF) GO category revealed 3 differentially expressed themes between Wistar and SHR stellate ganglia (Fig. 3.5). Significant over-representation was observed in gene families corresponding to excitatory extracellular ligand-gated ion channel activity (blue), protein, anion and carboxylic acid binding (green), and phosphoric ester hydrolase activity (purple). Strong enrichment was seen in the groups corresponding to ligand-gated ion channel activity, suggesting a potential genetic basis for elevated sympathetic excitability in this model. The number of genes in each BP GO family and their significance values are shown in Table 3.5 A list of MF genes corresponding to each group are included in the appendix (Table 8.3). As the aim of this chapter was to assess the differences in the SHR stellate transcriptome that may be linked to sympathetic over-activity, the subsequent work in this chapter will focus on the over-represented MF GO groups.

Table 3.5. Over-represented Molecular Function Gene Ontology Groups

Gene Ontology ID	Molecular Function GO Description	Count	Fold Enrichment	p. adjusted
GO:0005231	excitatory extracellular ligand-gated ion channel activity	13	6.89	1.58E-04
GO:0005230	extracellular ligand-gated ion channel activity	15	5.79	2.79E-04
GO:0042578	phosphoric ester hydrolase activity	33	2.49	1.74E-03
GO:0015276	ligand-gated ion channel activity	17	3.65	5.21E-03
GO:0022834	ligand-gated channel activity	17	3.65	5.21E-03
GO:0042802	identical protein binding	78	1.59	1.09E-02
GO:0043168	anion binding	26	2.48	1.13E-02
GO:0022836	gated channel activity	27	2.35	1.63E-02
GO:0022838	substrate-specific channel activity	32	2.06	3.34E-02
GO:0031406	carboxylic acid binding	18	2.77	4.02E-02

The over-represented Molecular Function Gene Ontology groups are listed by order of significance. The number of significant genes, the MF GO group enrichment and Benjamini-Hochburg p. adjusted values are included. For a full list of genes see Appendix Table 8.3.

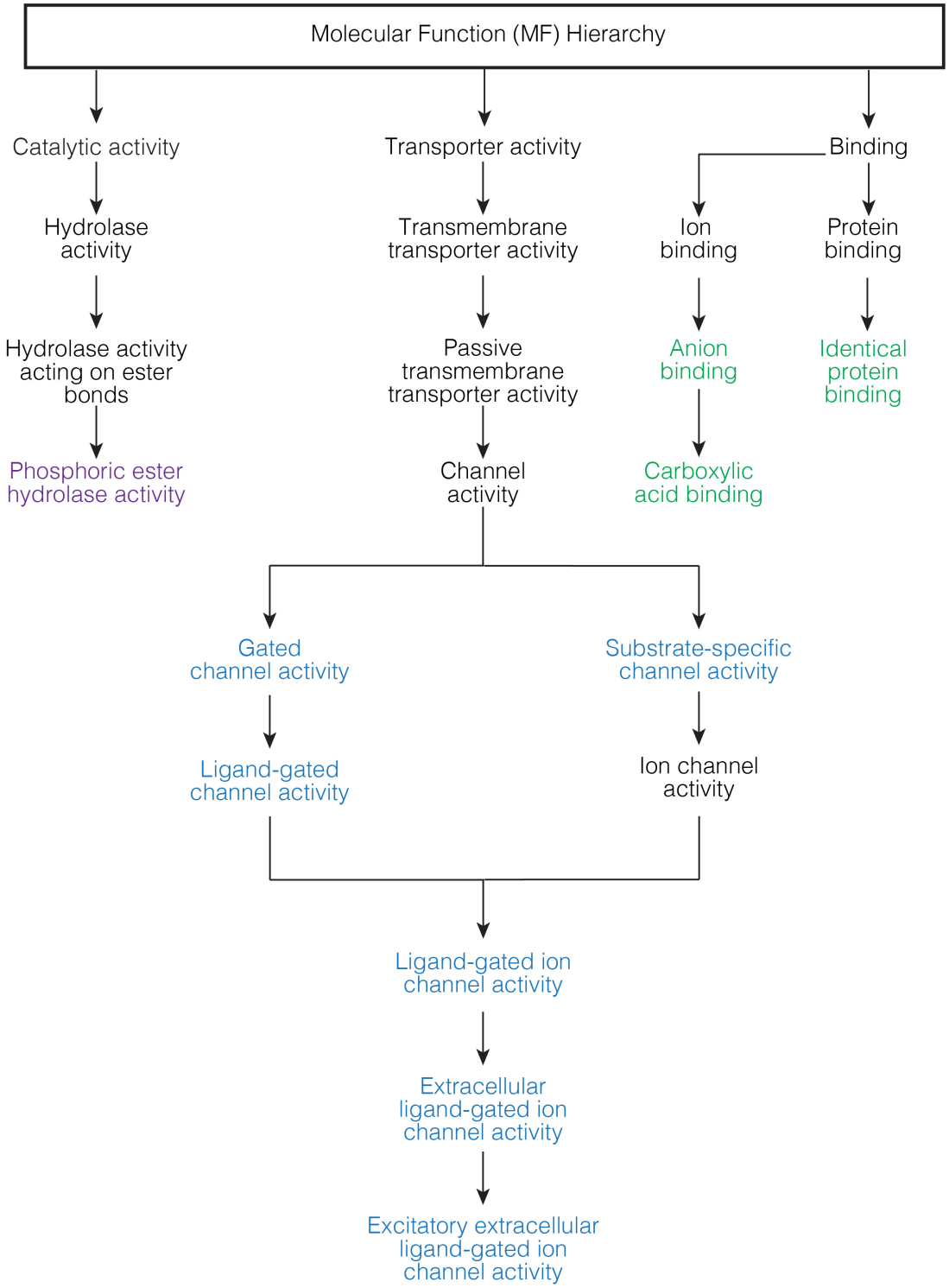


Figure 3.5. Over-represented Molecular Function Gene Ontology Group Hierarchy
Parent groups are represented at the top of the tree-diagram with branching child groups below. Significant MF GO groups are coloured, non-significant groups are black. Distinct categories are represented by colour.

3.4.6.4 Extracellular Ligand-Gated Ion Channel Activity

The transcripts that were found to be differentially expressed in the RNA-seq dataset within the extracellular ligand-gated ion channel activity (GO:0005230) included transcripts encoding the gamma-aminobutyric acid type A receptor ($GABA_AR$) alpha1 and alpha 2 subunits (*Gabra1, Gabra2*), the ionotropic glutamate receptors N-methyl-D-aspartate receptor (NMDA R) subunit 2B (*Grin2b*), α-amino-3-hydroxy-5-methyl-4-isoxazolepropionic acid receptor (AMPA-R) subunits 1, 2, 3 (*Gria1, Gria2, Gria3*), Kainate receptor subunits 1, 2 (*Grik1, Grik2*), the ionotropic 5-Hydroxytryptamine (5-HT) serotonin receptor subunits 3A, 3B (*Htr3a, Htr3b*), the ligand-gated purinergic receptors (P2XR) type 3, 4, 6 (*P2rx3, P2rx4, P2rx6*) the glycinergic receptor beta subunit (*Glrb*) and the Nicotinic Acetylcholine Receptor (nAchR) Beta 4 Subunit *(Chrnb4*) as depicted in Fig. 3.6 and Tables 3.6, 3.13. The expression of the 15 transcripts within this GO group was confirmed in rat stellate ganglia using qRT-PCR and revealed similar trends as that observed in the RNA-seq dataset; although only 4:15 genes reached significance in rat by qRT_PCR ($\Delta\Delta C_T$ comparative method)[332] including *Chrnb4*, *Gria1*, *Grik1* and *Grin2b* (Fig. 3.6). Furthermore, to assess whether these genes are conserved, expression was validated in stellate ganglia obtained from human donors (Fig. 3.6). Given the limited availability of human tissue from patients, it was not possible to assess the role of these genes in human disease itself. Importantly, however, the presence of glutamate (AMPA R, NMDA R, Kainate R) and $GABA_AR$ subunits were detected within the human sympathetic stellate ganglia, supporting previous evidence for the role of amino acids in regulating cardiac-sympathetic activity[338-341]. The presence of purinergic, glycinergic and serotonergic receptors was also confirmed.

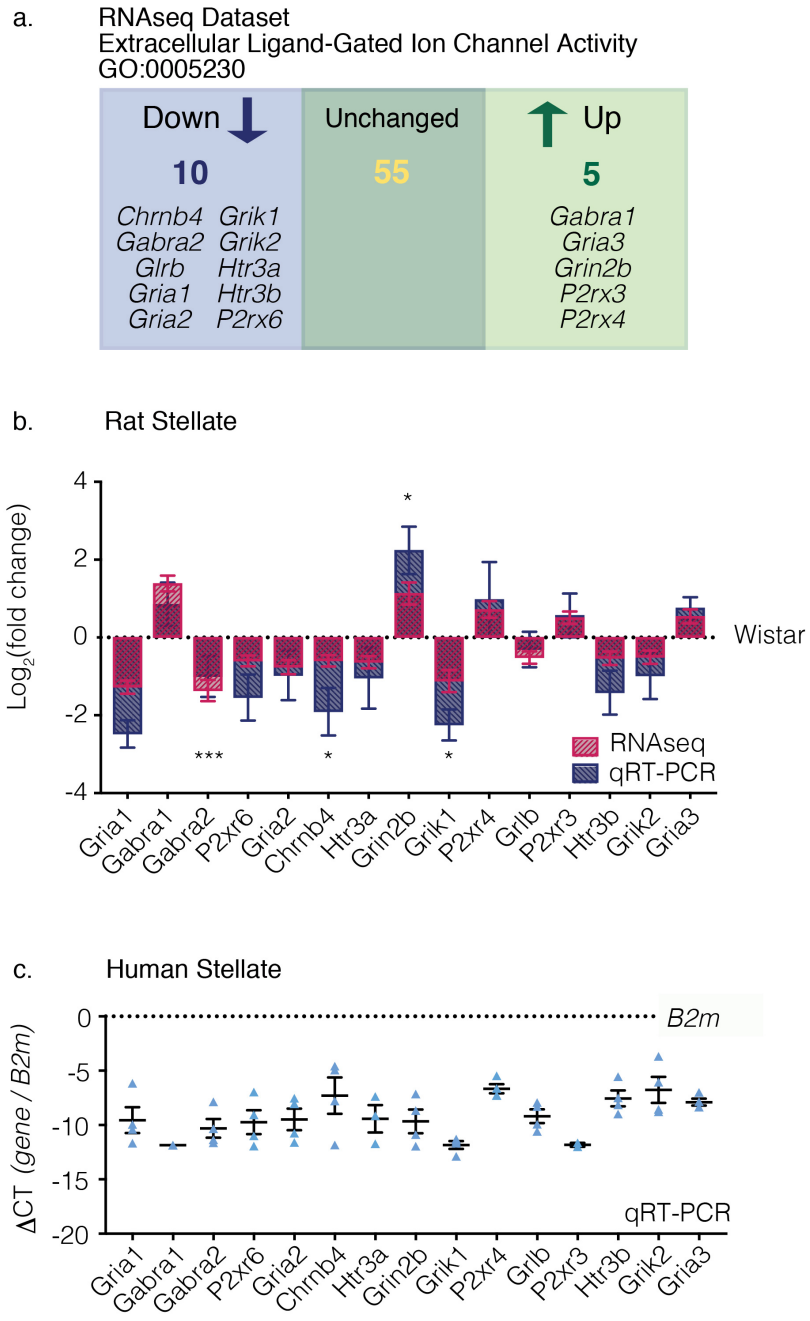


Figure 3.6. Extracellular Ligand-Gated Ion Channel Activity (GO:0005230)
The differentially expressed genes in the MF GO group 'extracellular ligand-gated ion channel activity' (GO:0005230) are listed, where green and blue represent up- and downregulated genes respectively (a). The presence of these genes was validated using qRT-PCR and the $\Delta\Delta C_T$ comparative method was applied for analysis (SHR/Wistar); with β2 microglobulin *(B2m)* selected as the housekeeping gene for comparison as there was no difference in *B2m* expression between strains in the RNA-seq dataset. Log_2 fold change of the differentially expressed genes in SHR stellates as identified by RNA-seq are represented in red (b). Log_2 fold change ± SEM of qRT-PCR SHR data are also depicted (blue; b) relative to Wistar. Significance is indicated above the relevant bars. The RNA-seq trends for up- or downregulation of each gene was confirmed with qRT-PCR; however, only *Chrnb4* ($p<0.05$), *Gria1* ($p<0.001$), *Grik1* ($p<0.05$) and *Grin2b* ($p<0.05$) were significantly different than expression levels measured in Wistar samples. The presence of these genes was confirmed in human stellate ganglia samples; with *Gabra1, Grik1* and *P2xr3* falling below the limit of detection (c). To quantify mRNA expression in human stellate samples, data were normalised to the housekeeping gene *B2m* and the ΔCT method was applied for analysis.

Table 3.6. Extracellular Ligand-gated Ion Channel GO Group (GO:0005230)

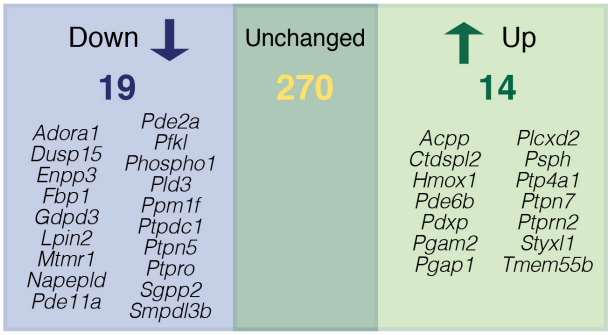
Gene Name	Description	RNAseq	
		Log_2 Fold Change	p. adjusted
Gria1	glutamate ionotropic receptor AMPA type subunit 1	-1.278	4.58E-12
Gabra1	gamma-aminobutyric acid type A receptor alpha1 subunit	1.386	1.51E-09
Gabra2	gamma-aminobutyric acid type A receptor alpha2 subunit	-1.366	3.47E-05
P2rx6	purinergic receptor P2X 6	-0.603	7.62E-04
Gria2	glutamate ionotropic receptor AMPA type subunit 2	-0.764	1.17E-03
Chrnb4	cholinergic receptor nicotinic beta 4 subunit	-0.601	1.31E-03
Htr3a	5-hydroxytryptamine receptor 3A	-0.635	2.28E-03
Grin2b	glutamate ionotropic receptor NMDA type subunit 2B	1.132	2.82E-03
Grik1	glutamate ionotropic receptor kainate type subunit 1	-1.121	3.06E-03
P2rx4	purinergic receptor P2X 4	0.72	1.94E-02
Glrb	glycine receptor, beta	-0.518	2.63E-02
P2rx3	purinergic receptor P2X 3	0.51	3.02E-02
Htr3b	5-hydroxytryptamine receptor 3B	-0.536	3.84E-02
Grik2	glutamate ionotropic receptor kainate type subunit 2	-0.509	4.78E-02
Gria3	glutamate ionotropic receptor AMPA type subunit 3	0.542	4.91E-02

The differentially expressed genes in the MF GO group 'extracellular ligand-gated ion channel activity' (GO:0005230) are listed by order of significance (Benjamini-Hochburg p. adjusted). Log_2(fold change) are represented as SHR relative to Wistar.

3.4.6.5 Phosphoric Ester Hydrolase Activity

Within the MF category, 33 differentially expressed transcripts were identified within the phosphoric ester hydrolase activity (GO:0042578) where 13 transcripts were upregulated and 20 were downregulated (Table 3.7, Fig. 3.7). The expression of 270 genes in this group was unchanged. Within this family, most of the affected transcripts were found to encode phosphatase related subunits that inhibit kinase activity, thus altering feedback inhibition of PDE activity[342].

a. RNAseq Dataset
Phosphoric Ester Hydrolase Activity
GO:0042578



b. Rat Stellate
Phosphoric Ester Hydrolase Activity
RNAseq Transcript fold change relative to Wistar

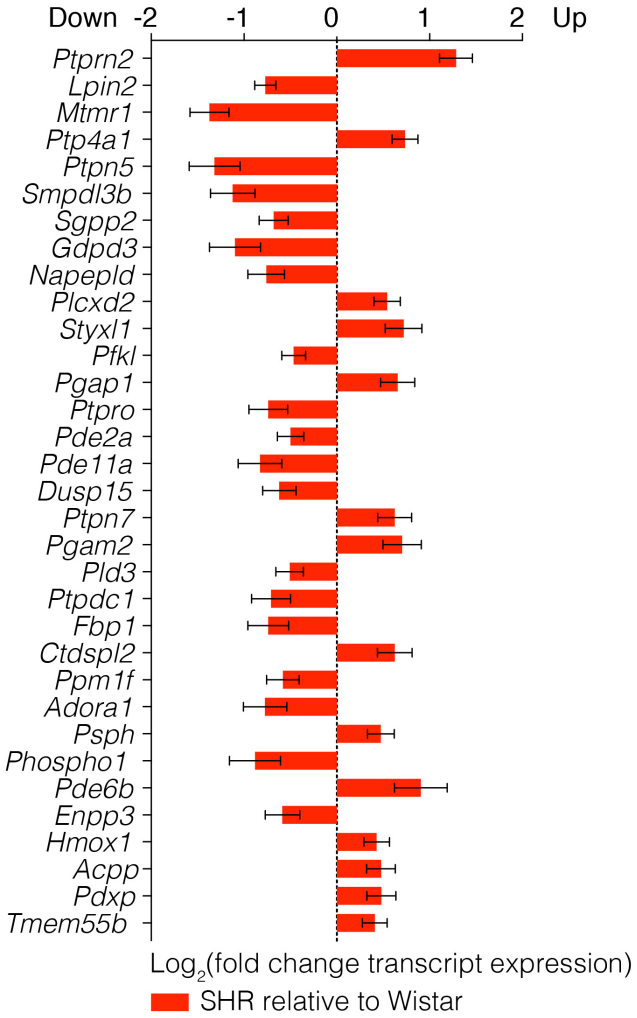


Figure 3.7. Phosphoric Ester Hydrolase Activity (GO:0042578)
The differentially expressed genes in the MF GO group 'phosphoric ester hydrolase activity' (GO:0042578) are listed, where green and blue represent up- and downregulated genes respectively (a). Log_2 fold change of the differentially expressed genes of interest in SHR relative to Wistar as identified by RNA-seq (b).

Table 3.7. Phosphoric Ester Hydrolase Activity GO Group (GO:0042578).

Gene Name	Description	RNAseq	
		Log_2 Fold Change	p. adjusted
Ptprn2	protein tyrosine phosphatase, receptor type N2	1.286	7.32E-11
Lpin2	lipin 2	-0.771	1.94E-09
Mtmr1	myotubularin related protein 1	-1.372	8.57E-09
Ptp4a1	protein tyrosine phosphatase type IVA, member 1	0.736	9.41E-06
Ptpn5	protein tyrosine phosphatase, non-receptor type 5	-1.317	9.63E-05
Smpdl3b	sphingomyelin phosphodiesterase, acid-like 3B	-1.121	1.76E-04
Sgpp2	sphingosine-1-phosphate phosphatase 2	-0.68	7.21E-04
Gdpd3	glycerophosphodiester phosphodiesterase domain containing 3	-1.097	2.78E-03
Napepld	N-acyl phosphatidylethanolamine phospholipase D	-0.76	4.46E-03
Plcxd2	phosphatidylinositol-specific phospholipase C, X domain containing 2	0.543	5.16E-03
Styxl1	serine/threonine/tyrosine interacting-like 1	0.721	8.38E-03
Pfkl	phosphofructokinase, liver type	-0.464	9.83E-03
Pgap1	post-GPI attachment to proteins 1	0.658	1.07E-02
Ptpro	protein tyrosine phosphatase, receptor type, O	-0.738	1.14E-02
Pde2a	phosphodiesterase 2A	-0.497	1.34E-02
Pde11a	phosphodiesterase 11A	-0.827	1.35E-02
Dusp15	dual specificity phosphatase 15	-0.619	1.57E-02
Ptpn7	protein tyrosine phosphatase, non-receptor type 7	0.624	1.61E-02
Pgam2	phosphoglycerate mutase 2	0.704	1.74E-02
Pld3	phospholipase D family, member 3	-0.507	1.83E-02
Ptpdc1	protein tyrosine phosphatase domain containing 1	-0.707	1.92E-02
Fbp1	fructose-bisphosphatase 1	-0.738	2.06E-02
Ctdspl2	CTD small phosphatase like 2	0.624	2.16E-02
Ppm1f	protein phosphatase, Mg^{2+}/Mn^{2+} dependent, 1F	-0.58	2.27E-02
Adora1	adenosine A1 receptor	-0.773	2.34E-02
Psph	phosphoserine phosphatase	0.476	2.34E-02
Phospho1	phosphoethanolamine/phosphocholine phosphatase 1	-0.882	3.04E-02
Pde6b	phosphodiesterase 6B	0.906	3.09E-02
Enpp3	ectonucleotide pyrophosphatase/phosphodiesterase 3	-0.585	3.43E-02
Hmox1	heme oxygenase 1	0.431	3.80E-02
Acpp	acid phosphatase, prostate	0.477	4.06E-02
Pdxp	pyridoxal phosphatase	0.481	4.11E-02
Tmem55b	transmembrane protein 55B	0.41	4.48E-02

The differentially expressed genes in the MF GO group 'phosphoric ester hydrolase activity' (GO:0042578) are listed are listed by order of significance (Benjamini-Hochburg p. adjusted). Log_2(fold change) are represented as SHR relative to Wistar.

3.4.7 KEGG Functional Enrichment Pathways are Impaired in SHR

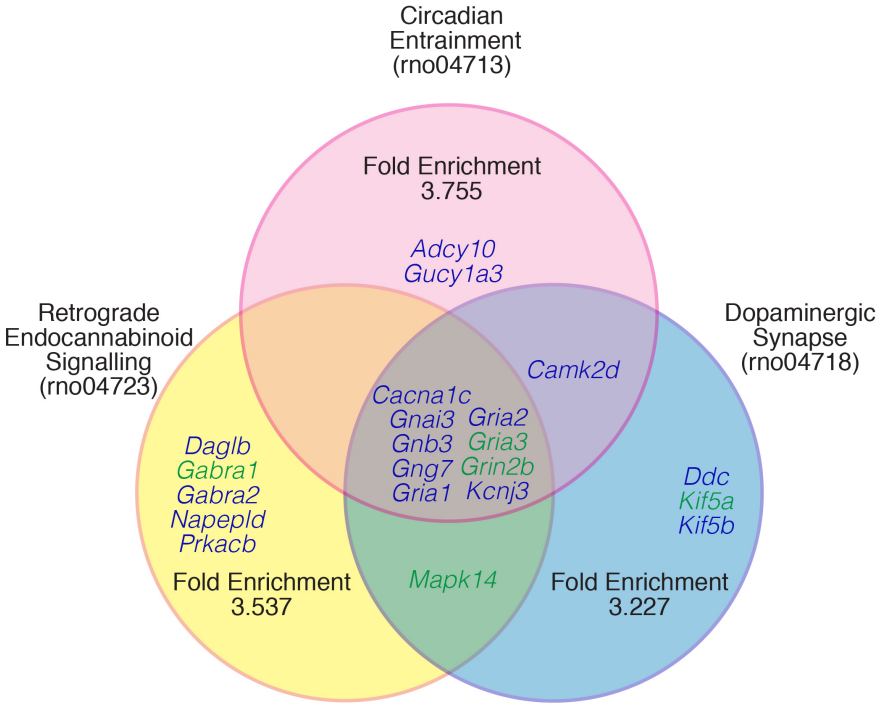
A Kyoto Encyclopedia of Genes and Genome (KEGG) enrichment pathway analysis was performed using DAVID (v6.8) to extend the GO analysis to functional enrichment pathways as described in Chapter Two[329]. The KEGG functional enrichment analysis links the observed differences within the SHR stellate transcriptome to relevant intracellular signalling pathways. The KEGG analysis identified 'Circadian Entrainment' (rno04713; p.adj=0.019), 'Dopaminergic Synapse' (rno04728; p.adj=0.0150), 'Retrograde Endocannabinoid Signalling' rno04723; p.adj=0.0124) and 'Metabolic Pathways' (rno04724; p.adj=0.0164) as the most over-represented pathways in the SHR stellate ganglia (Table 3.8). Many of the same genes were represented in each of these groups (Fig. 3.8), therefore the KEGG signalling pathways (Circadian Entrainment, Dopaminergic Synapse and Retrograde Endocannabinoid Signalling) were combined in a model diagram to identify the possible involvement of these transcriptomic changes on intracellular signalling (Fig. 3.8).

Table 3.8. Over-represented KEGG groups

KEGG ID	KEGG Description	Count	Fold Enrichment	p. adjusted
rno04723	Retrograde endocannabinoid signaling	14	3.54	1.24E-02
rno04728	Dopaminergic synapse	16	3.23	1.50E-02
rno01100	Metabolic pathways	74	1.49	1.64E-02
rno04713	Circadian entrainment	14	3.76	1.99E-02

The over-represented KEGG functional enrichment pathways are listed are listed by order of significance. A list of genes corresponding to each KEGG group is included in the Appendix, Table 3.12

a. KEGG Groups



b. Model Figure

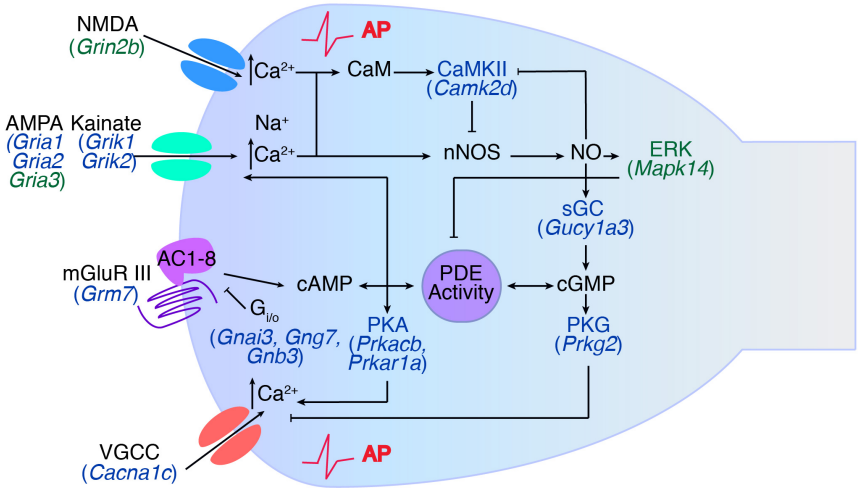


Figure 3.8. KEGG Differentially Expressed Functional Enrichment Pathways
Three KEGG functional enrichment pathways were identified as particularly relevant to post-synaptic post-ganglionic signalling (a). The KEGG analysis identified 'Circadian Entrainment' (rno04713; p.adj=0.019), 'Dopaminergic Synapse' (rno04728; p.adj=0.0150), 'Retrograde Endocannabinoid Signalling' rno04723; p.adj=0.0124) and 'Metabolic Pathways' (rno04724; p.adj=0.0164) as the most over-represented pathways in the hypertensive strain stellate ganglia. The Venn Diagram depicts the upregulated genes (green) and downregulated genes (blue) and highlights the overlap between each of the over-represented KEGG groups (b). A model figure depicts the integrated KEGG enrichment diagram, combining signalling pathways from the over-represented KEGG pathways 'Circadian entrainment', 'Dopaminergic synapse' and 'Retrograde Endocannabinoid Signalling'. The model figure highlights the involvement of these transcriptomic changes on intracellular signalling pathways. This figure is primarily based on the supplied rno04713 KEGG diagram.

In confirmation of the GO analysis, the KEGG enrichment analysis indicated that RNA transcripts associated with Ca^{2+} signalling are differentially expressed within SHR stellate ganglia. Glutamate receptor encoding genes are known to couple to $[Ca^{2+}]_i$ directly, where differences in subunit composition of glutamate-activated ion channels affect Ca^{2+} permeability. KEGG functional pathway analyses also highlighted significant alterations in cN signalling cascades; including downregulation of genes encoding sGC (*Gucy1a3*) and PKG II subunits (*Prkg2*), and upregulation of inhibitory $G_{i/o}$ G-proteins coupled to cAMP (*Gnai3, Gng7, Gnb3*) as well as the PKA type Iα regulatory subunit (*Prkar1a*) in SHR stellate ganglia. The generation of cNs and their effectors directly influence the activity of many voltage-gated Ca^{2+} channels[96,226,234].

3.4.8 Cyclic Nucleotide Signalling in Cardiac-Stellate Ganglionic Neurons

RNA-seq highlighted the differential expression of several transcripts involved in cN signalling, yet whether cN signalling and PKA activity are affected in sympathetic nerves is not known. To determine whether evoked cAMP generation or PKA activity is impaired in stellate neurons from SHR or in hypertension, FRET was used to measure the levels of intracellular cAMP generated by increasing concentrations of the AC activator forskolin (0.1-25 µM). Measurements for cAMP and PKA were recorded from stellate neurons obtained from prehypertensive four-week-old preSHR (n=16-33 cells), adult 16-week SHR with established hypertension (n=5-22 cells) and normotensive controls at four-week (n=18-32) and 16-weeks of age (n=8-16). At the concentrations tested, forskolin induced a dose-dependent increase in cAMP and PKA (Fig. 3.9).

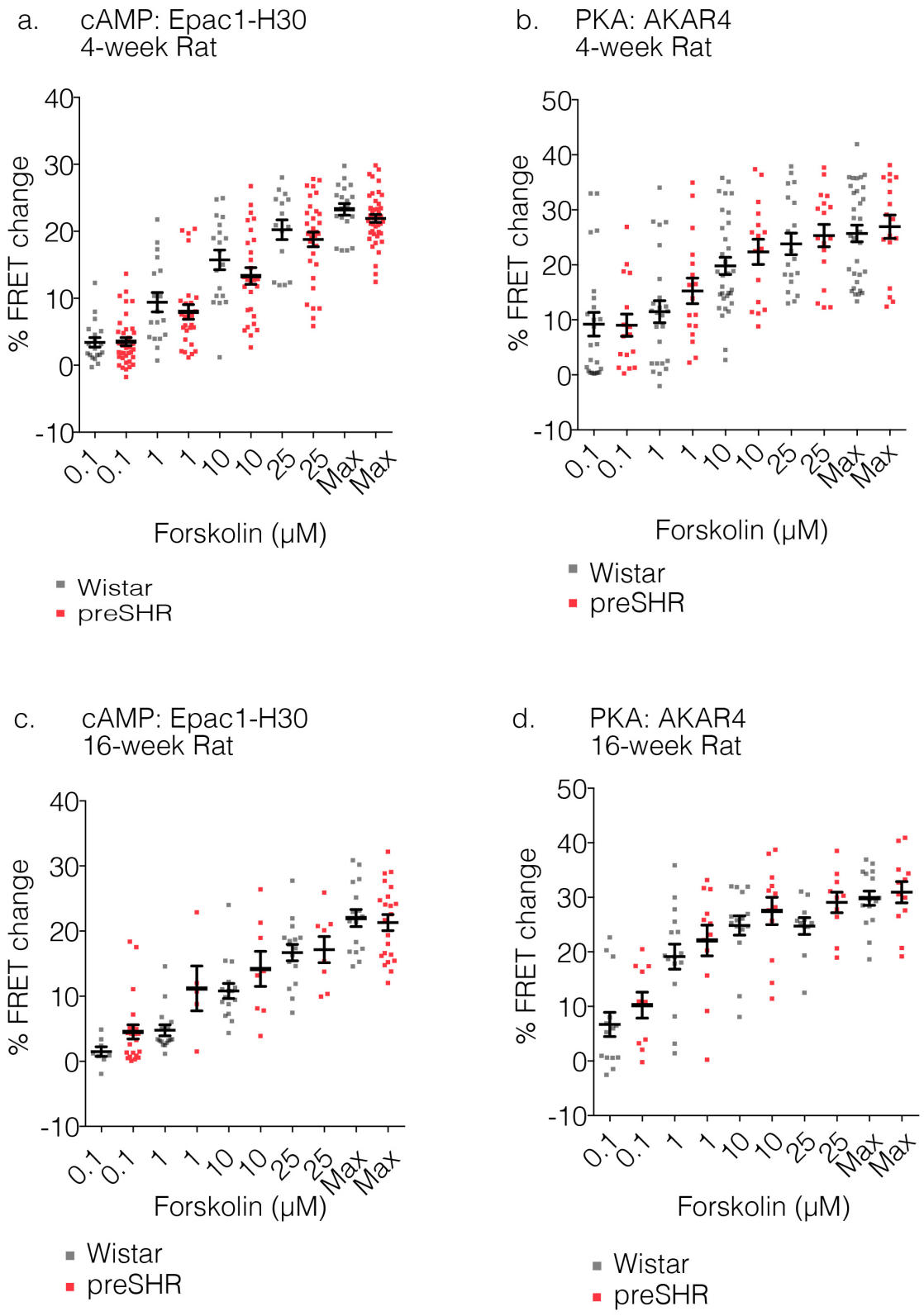


Figure 3.9. Cytosolic cAMP and PKA Activity are Not Altered in SHR Neurons
Sympathetic stellate nerves were obtained from 4-week Wistar (n=18-32) and preSHR (n=16-33 cells)as well as 16-week Wistar (n=8-16) and SHR (n=5-22 cells). Neurons were transduced with the Epac1-H30 or the AKAR4 FRET sensor to measure cAMP or PKA activity respectively and challenged with forskolin (0.1-25 μM). Max represents a combination of forskolin (25 μM) and IBMX (100 μM). There was no detectable difference in evoked cAMP or PKA activity between strains or age groups (Kruskal-Wallace, peak FRET responses). Data represents mean ± SEM.

There was no detectable difference in evoked cAMP or PKA activity between strains or age groups (Kruskal-Wallace, peak FRET responses), although the lack of sensitivity of these FRET sensors for detecting acute alterations in signalling cannot be ruled out, as perturbations would be likely to occur within distinct subcellular compartments rather than as a global cytosolic phenomenon[294].

3.4.9 Phosphodiesterase Signalling in Cardiac-Stellate Neurons

RNA-seq identified the differential expression of three PDE transcripts: *Pde2a, Pde6b* and *Pde11a*. PDE2A and PDE11A are dual-hydrolysing enzymes; i.e. capable of hydrolysing both cAMP and cGMP and PDE6 is cAMP specific. Whether PDE signalling is impaired in sympathetic stellate ganglia from preSHR is not known. To assess whether the differential expression of PDE-related transcripts has functional relevance for PDE activity, FRET was used to measure the levels of intracellular cAMP generated by increasing concentrations of the non-specific PDE inhibitor IBMX (1-100 μM). At all concentrations tested, IBMX administration led to significantly greater cAMP generation in Wistar (n=6) compared with preSHR ganglia (n=15, two-way ANOVA, $p<0.0001$). There was no detectable difference in forskolin evoked cytosolic cAMP or PKA between strains, implying that the observed response to IBMX does not lie with cAMP or PKA themselves but may reflect altered PDE activity in SHR stellate neurons (Fig. 3.10).

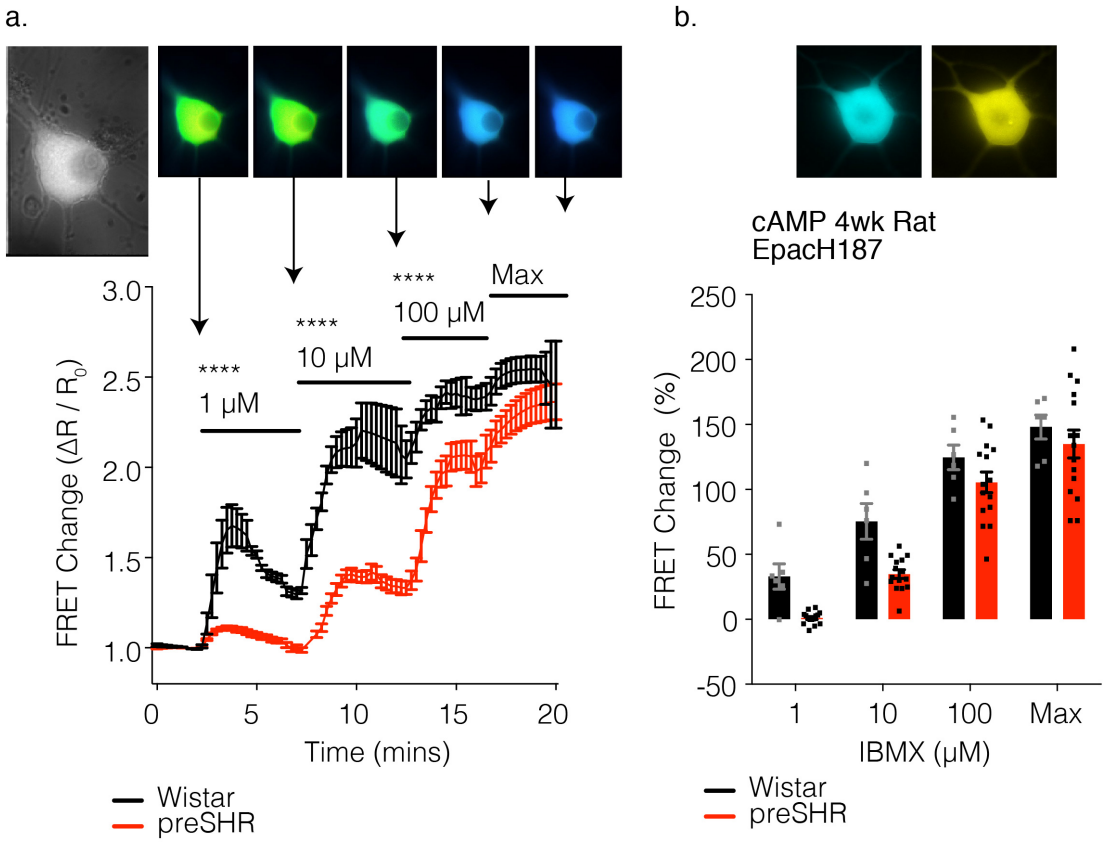


Figure 3.10. Phosphodiesterase Impairment in preSHR Sympathetic Neurons.
FRET was used to measure the levels of intracellular cAMP generated by increasing concentrations of the non-specific PDE inhibitor IBMX (1-100 μM, a, b). At all concentrations, IBMX administration led to significantly greater cAMP generation in Wistar (n=6) compared with preSHR ganglia (n=15, two-way ANOVA, $p<0.0001$). *$p<0.05$, **$p<0.01$, ***$p<0.001$, ****$p<0.0001$.

3.5 Discussion

In this chapter, RNA-seq was used to obtain an overview of transcriptome of the sympathetic ganglia from Wistar rats and SHR with established hypertension and a distinct sympathetic phenotype. The aim of this study was to identify altered gene transcripts that might be related to the elevated sympathetic phenotype observed in hypertension[210,214,281,343,344].

The main findings of this chapter are:

1. RNA-seq has highlighted alterations in the transcriptome of the SHR stellate ganglion where key changes are involved in neurotransmission, cardiac regulation, ion channel activity and phosphoric ester hydrolase activity.
2. The over-represented groups in the CC GO category correspond to families encoding neuronal projections and synapses.
3. The over-represented groups within the BP GO category included families involved in heart and blood pressure regulation, as well as synaptic transmission.
4. The over-represented groups within the MF GO category included families encoding extracellular ligand-gated ion channels, phosphoric ester hydrolase activity, in addition to and ion and protein binding.
5. Key transcripts involved in extracellular ligand-gated ion channel activity are also expressed in human stellate ganglia.
6. Differentially expressed transcripts within the phosphoric ester hydrolase activity MF GO group included PDEs in addition to protein phosphatase enzymes. Alterations in PDE regulatory transcripts resulted in impaired PDE activity in preSHR sympathetic neurons as measured by FRET.
7. Key transcripts involved in extracellular ligand-gated ion channel activity were also expressed in human stellate ganglia.

3.5.1 RNA Sequencing Reveals Differences in the SHR Stellate Ganglia

Sympathetic markers including transcripts involved in pathways governing adrenergic synthesis (e.g. *Dbh, Th*), neurotransmission (e.g. *Snap25*) and reuptake (e.g. NET, *Slc6a2)* were identified (Table 3.1), supporting recently published profiles of stellate neurons[345-347]. The differential expression analysis identified 744 differentially expressed genes where approximately 45 % of genes were upregulated and 55 % downregulated in the SHR (Fig. 3.2, Table 3.2).

The RNA-seq dataset is categorised into three parent fields (CC GO, BP GO, MF GO), and then sub-classified to reveal different themes within each parent category. The GO analysis revealed five main differential themes in the CC GO category (Table. 3.3), and implied that families involved in neuronal cell body compartments (GO:0043025, GO:0036477, GO:0048471, GO:0044297) and axonal projections (GO:0097458, GO:0043005, GO:0030424, GO:0033267, GO:0043195, GO:0043679, GO:0044306) are altered in stellate ganglia in hypertension (Fig. 3.3). These CC GO groups corresponded with the enriched GO families in the BP GO category (Table 3.4), where transcripts involved in the regulation of developmental processes (GO:0051094) and growth (GO:0040007) were differentially expressed in the SHR (Fig. 3.4), suggesting that transcripts involved in neuronal structure and development are impaired in disease.

3.5.2 Altered Transcripts Linked to Neurotransmission in the SHR

Other over-represented CC GO gene families (Table 3.3) included groups involving synapses (GO:0045202, GO:0098793), cell junctions (GO:0030054) and membrane-bounded vesicles (GO:0031988). Pronounced over-representation was also seen in families in the BP GO category (Table 3.4) corresponding to cell-cell signalling (GO:0007267, GO:0099536, GO:0099537, GO:0098916, GO:0007268) and responses to chemical stimuli (GO:0070887,

GO:0010033, GO:0010038), highlighting a potential genetic basis for an impaired response to feedback signals as well as elevated end-organ neurotransmitter release. Of interest, the transcript encoding the pro-peptide Chromogranin A (CHGA, *Chga*) was significantly downregulated in the SHR ganglia. Catestatin, the cleaved end product of CHGA is a catecholamine co-transmitter and an endogenous inhibitor of catecholamine release, that mediates its effects through potent inhibition of neuronal nicotinic acetylcholine receptor activity[348]. Catestatin has been shown to play a vital role in regulating vascular tone[349], baroreflex sensitivity[348,350], sympathetic activity[348,351], cardiac inotropy and lusiotropy[349]. Impaired catestatin production linked to catestatin polymorphisms[351] has been strongly implicated in human hypertension[349,350] and left ventricular remodelling after myocardial infarction[352]. Moreover, *Chga* knock out mice develop hypertension that is attenuated following exogenous administration of catestatin [348]. Whether downregulation of the *Chga* transcript in SHR sympathetic neurons corresponds to deficits in SHR catestatin production is not established, yet one might consider the possibility for sympathetic *Chga* gene transfer as a novel therapeutic intervention for reducing sympathetic over-activity and opposing elevated neurotransmission in hypertension.

3.5.3 Impaired Regulatory Cardiovascular Genes in SHR Stellate Ganglia

Highly enriched BP GO groups involved in cardiovascular regulation were also significantly over-represented in the SHR cardiac-sympathetic ganglia (Table 3.4, Fig. 3.4). Differentially expressed families included circulatory system and heart processes (GO:0003013, GO:0003015), regulation of blood pressure (GO:0008015, GO:0008217) and regulation of heart contraction (GO:0060047, GO:0008016), supporting a genetic basis for impaired cardiac transmission in hypertension. Interestingly, the BP GO family encoding renal system processes was also over-represented in disease, implying that the same neuronal processes might be involved in elevated renal sympathetic nerve activity further supporting the evidence for a

neurogenic basis in the aetiology of renovascular[132] as well as essential hypertension[28,353]. Moreover, BP GO families involved in stress responses and inflammation were also found to be over-represented, where altered expression of transcripts encoding chemokines (*Ccl2, Ccl7, Ccl24, Chga, Cxcr4, S100a8, S100a9*) and macrophage activating and platelet growth factors (*Mst1, Pdgfb, Pla2g7*) were identified, underpinning a possible genetic link between enhanced proinflammatory processes in diseases caused by sympathetic over-activity [30,33,145].

3.5.4 Altered Extracellular Ligand-Gated Ion Channel Activity in SHR

Enriched GO groups in the MF category (Table 3.5, Fig. 3.5) included several families representing channel activity (GO:0022836, GO:0022834, GO:0022838, GO:0015276, GO:0005230, GO:0005231) that primarily comprised transcripts involved in ligand-gated ion channel activity, phosphoric ester hydrolase activity (GO:0042578) and families involved in ion and protein binding (GO:0043168 GO:0031406 GO:0042802). Regarding the families encoding channel activity, significant differences were found in the transcript expression of glutamate-activated ion channel subunits (Table 3.6), supporting previous evidence for the role of amino acids in regulating cardiac-sympathetic activity[338-341]. For example, the NMDAR NR2 subunit (*Grin2b)* was upregulated in SHR ganglia, and is the binding site for glutamate and plays a direct role in regulating the electrophysiological properties of the channel[354-356]. Moreover, decreases in the AMPA subunit GluA2 (*Gria2)* have been associated with increased Ca^{2+} permeability in CA1 pyramidal neurons, where increased cAMP and PKA signalling shift GluA2/3-containing AMPARs to a more conductive state[357,358]. There were also significant changes in the transcript expression levels of purinergic receptors (*P2rx3, 4, 6*) and $GABA_A$ R subunits *(Gabra1, Gabra2)*. Significant downregulation of the ionotropic serotonin type 3 R subunits (*Htr3a, Htr3b*), nicotinic acetylcholine R β4 subunit (*Chrnb4)* and the chloride (Cl^-)-permeable glycine channel β subunit (*Glrb*) were also observed. The accuracy of the RNA-seq in identifying differentially expressed transcripts was validated by qRT-PCR, where trends for

up- or downregulation of each transcript were confirmed (Fig. 3.6). The presence of each transcript was also confirmed by qRT-PCR in human stellate ganglia to provide wider physiological context (Fig. 3.6). Importantly, the differential expression of ligand-gated ion channel subunits may have implications for ion permeability, channel activity and elevated neuronal excitability in sympathetic ganglia in the SHR model and diseases associated with sympathetic over-activity.

3.5.5 Altered Phosphoric Ester Hydrolase Activity Impairs PDE Function

Previous reports have demonstrated a preferential deficit in NO-cGMP signalling[113,288] and an increase in the activity of specific PDEs (e.g. PDE2a) [96,262,334]. These changes are involved in the elevated Ca^{2+} phenotype in sympathetic stellate ganglia in hypertension, yet whether transcriptomic alterations underpin changes in cN signalling is not known. Within the MF GO category, the family representing 'Phosphoric Ester Hydrolase Activity' was significantly over-represented in established hypertension [337,359]. Thirty-three genes linked to the PDE superfamily were found to be differentially expressed in the SHR stellate ganglia including downregulation of *Pde11a* and *Pde2a* transcripts and upregulation of *Pde6b.* Yet the largest number of gene transcripts observed in this family mapped to regulators of PDEs themselves[337] (Fig. 3.7) including protein phosphatases that attenuate the effects of kinase activity[342], thus altering the systems involved in cN control[298,360,361]. These data support clinical reports that have highlighted a role for impaired PDE activity in the pathophysiology of several CVDs[113,230,232,262,270,273,275,362-364]. Indeed, recent evidence suggests that 1 % of the Swedish population carry a loss-of-function mutation in PDE11a that is directly linked to hypertension, obesity and ischaemic stroke[365]. Moreover, a single nucleotide polymorphism (rs197163010) has been identified in PDE2A in the SHR/Ola rat strain and reported in the NCBI dbSNP database[366]. A full overview of the differentially expressed transcripts linked to PDEs are displayed in Table 3.7.

The KEGG functional enrichment pathway analysis illustrated the relationships between the altered transcripts and intracellular signalling pathways (Fig. 3.8) and highlighted differential expression of several transcripts that have been previously associated with hypertension and CVDs (Table 3.8). These include the class III metabotropic glutamate receptor 7 (*Grm7*)[367,368], G-protein β3 subunit (*Gnb3*)[369-372] the voltage gated L-type Ca^{2+} Cannel α subunit (*Cacna1c*)[373,374]*.* Of particular relevance to this study is the observation that the PKA Regulatory Type 1α subunit (*Prkar1a*) was found to be downregulated in the SHR stellate ganglia. *Prkar1a* transcription is integral for normal development of peripheral neurons including axonal sorting, myelination and proliferation of neurons[375]. Additional support for the importance of *Prkar1a* in peripheral neurons is found in patients with the inherited Carney Complex (CNC) syndrome[376,377]. Notably, patients with global loss-of-function mutations in *Prkar1a* develop peripheral nerve tumours and display a wide range of cardiovascular comorbidities that are often fatal, including dysregulated maintenance of blood pressure, cardiomyopathies and arrhythmia[377]. Indeed, in one study approximately 60 % of CNC patients died of cardiovascular complications[376]. Additionally, transcripts within the cGMP-PKG pathway were found to be downregulated in the SHR stellate ganglia, including the expression of PKG II (*Prkg2*) and the α1-sGC subunit (*Gucy1a3*), supporting previous reports of decreased cGMP-PKG signalling in the SHR stellate ganglia[96,288,364]. Furthermore, Genome Wide Association Studies (GWAS) have revealed a critical link between mutations in loci containing the gene *Gucy1a3* and clinical hypertension[50,378-381], myocardial infarction[382,383] atherosclerosis [384,385] and coronary artery disease[52,386,387]. Nevertheless, changes in transcript expression do not necessarily translate to changes in protein levels. For example, this RNA-seq data has revealed a decrease in *Pde2a* expression[337], whereas PDE2A activity and protein levels are reportedly raised in SHR and human stellates [262,280]. To ascertain whether the changes observed in the transcriptomic dataset translated to functional alterations in cN activity, cAMP generation and PKA activity were measured in response to an AC activator, forskolin. Evoked cAMP and PKA were not different between strains (Fig. 3.9), yet, in response to PDE inhibition, cAMP generation was found to be

diminished in preSHR neurons(Fig. 3.10). These data support previous evidence for differential PDE activity in preSHR stellate ganglia[262] suggesting that the dysfunction does not lie with the cNs themselves. Rather, these results might correspond to higher levels PDE activity in Wistar rat ganglia that chronically suppresses cAMP to prevent detrimentally elevated signals. Alternatively, these results might also reveal distinct increases in the activity of PDE isoforms insensitive to IBMX inhibition (PDE8 and PDE9) in preSHR cells. Whether this impairment is caused by dysfunction of a particular PDE isoform (e.g. *Pde2a, Pde6b* or *Pde11a*), impaired regulation of PDE activity, a mis-localisation of PDE isoforms within the intracellular compartment[298] or as a result of altered pH, oxidative stress[298] and/or other cytosolic signals remains to be established.

The *N*-type Ca^{2+} channel is the primary neuronal voltage gated Ca^{2+} channel [233,234] and plays a critical role in determining cytosolic Ca^{2+} concentrations during an action potential in sympathetic neurons[96,216,235-238]. Voltage gated Ca^{2+} channel activity is differentially regulated by kinase phosphorylation[2,74-81]. *N*-type Ca^{2+} channel conductance is elevated in preSHR neurons yet the causative mechanisms that underpin this phenotype are not known. In this chapter, a global increase in cytosolic PDE activity was recorded in preSHR sympathetic neurons, suggesting that PDE upregulation might occur as a compensatory protective mechanism to limit $[Ca^{2+}]_i$. Ascertaining the key mechanisms involved in PDE alterations may have significance for attenuating the Ca^{2+} phenotype and sympathetic over-activity in hypertension.

3.6 Limitations

This RNA-seq study was a hypothesis neutral, non-biased approach to sequencing the transcriptome of sympathetic stellate neurons of SHR and normotensive Wistar rats, nevertheless there were several limitations to this approach. First, the stellate ganglion

comprises a heterogeneous population of cell types. This was apparent in the analysis, as several markers of fibroblasts and astrocytes were identified, including vimentin and glial fibrillary acidic protein (GFAP) respectively, however; a high number of identified transcripts were of neuronal phenotype. Further studies to fully uncover the transcriptome of post-ganglionic sympathetic neurons will require single cell techniques, using tools such as *in situ* hybridisation for nucleic acids. Secondly, stellates were obtained from male rats. While there is a plethora of data regarding the sex differences in hypertension and CVD incidence[388], in this study the stellate transcriptome was investigated in the male rat stellate ganglia, given that the prevalence for hypertension and CVD is significantly higher in males compared with premenopausal women[388]. Thirdly, given the low concentration of RNA in our stellate samples, samples were amplified during the library preparation using the SMARTer amplification protocol. Low level transcripts may be under-represented in the amplification process and in our dataset via this protocol. Moreover, since the transcriptome was sequenced from rats with established hypertension, the observed transcriptomic changes may occur as compensatory rather than causative factors. Finally, the gene profiling and ontology analyses are enabled yet limited by the GO groups and KEGG enrichment pathways currently available. Notwithstanding these limitations, RNA-seq transcriptomics has revealed differential gene expression profiles in stellate neurons obtained from SHR with established hypertension and normotensive Wistar rats that was confirmed using qRT-PCR. Leading transcripts were also present in human stellate ganglia. Moreover, RNA-seq identified phosphoric ester hydrolase activity as a significantly over-represented differentially expressed GO group in SHR. This had clear functional relevance, as a PDE impairment was also identified using real-time live imaging of cAMP and PKA. Taken together, these genes require further investigation for their role in sympathetic hyperactivity and other diseases associated with autonomic dysfunction. With regard to the FRET experiments, although global cytosolic cAMP concentrations were found to be similar between control and diseased neurons, this does not in itself establish that localised control within specifically regulated microdomains is normal in the diseased neuron. It is well-

established that cNs and PDEs reside in distinct subcellular compartments [230,265,266]. Specifically, there are three splice variants of PDE2A in rat[266]. PDE2A1 has a cytosolic distribution, PDE2A2 is associated with mitochondrial membranes [265] whereas PDE2A3 is locaslised on synaptic membranes [389], although their exact roles remain to be established. Similarly, the regulation of Ca^{2+} channels by PKA/PKG occurs in distinct signalosomes, conferring site-specific regulation of Ca^{2+} entry coupled to neurotransmission. Furthermore, the rate of PDE hydrolysis is critically dependent on the concentration of both cAMP and cGMP that is reported to be different between cell types [225]. Site-specific targeted FRET sensors will be required to resolve these questions.

3.7 Conclusion

Sympathetic over-activity is a well-established contributor to hypertension and CVD. Increased $[Ca^{2+}]_i$ augments neurotransmission early in disease, before increases in arterial blood pressure develop. This Ca^{2+} phenotype is underpinned by an impaired cAMP/cGMP balance that is weighted in the favour of cAMP-PKA dependent signalling. The evidence in this chapter suggests that changes in transcripts encoding ligand-gated ion channel activity and synaptic signalling might play a role in the development of elevated sympathetic excitability and impaired transmission. Pharmacological, surgical and genetic techniques aimed at reducing sympathetic tone or raising vagal transmission have had reasonable levels of success reducing hypertension and improving cardiac function[47,98,106-108,162,390,391]; nevertheless, no prophylactic strategies have yet successfully entered the clinical arena, emphasising a critical need for translational advancements in this field. Transcriptomics might provide a useful approach for effective selection of novel targets for future validation and therapeutic targeting. These data highlight a potential area for attenuating sympathetic over-activity for prophylactic benefit in diseases associated with dysautonomia. RNA-seq is a useful tool for identifying novel targets that may play a role in the pathophysiology of dysautonomias and other diseases.

4

β-Adrenergic Signalling in Sympathetic Stellate Neurons

4.1 Introduction

Impaired neuro-hormonal regulation plays a critical role in the pathogenesis and progression of CVDs[28], where patients with familial dysautonomia suffer from catecholaminergic super-sensitivity, episodic hypertension and have a high propensity for fatal cardiac events[392]. Plasma and tissue levels of NA, Adr, AngII and aldosterone are significantly altered in hypertension and heart failure where elevated concentrations correlate with the severity of disease[76,80,193,214,393-397] and elevated cardiac adrenergic activity, specifically, is a highly negative prognostic indicator for clinical outcome[398]. Sympathetic noradrenergic transmission plays a dominant role in regulating cardiac output[66] via activation of $G\alpha_s$- coupled βARs that elevates intracellular cAMP and PKA activity[298] thus regulating a large number of phospho-sensitive processes[294]. Sustained myocardial βAR activation plays a pivotal role in the pathogenesis of many CVDs. Chronic cardiac noradrenergic stimulation leads to prolonged elevations in myocardial cAMP-PKA activity[221] that enhances Ca^{2+} influx through L-type Ca^{2+} channels[225-227], augments Ca^{2+}-induced Ca^{2+} release from sarcoplasmic endoplasmic reticulum stores[228]. Sustained cAMP-PKA activity is involved in cardiac remodelling and hypertrophy[221,230], myocyte apoptosis[103,221,397], hypertension[100 190,399], arrhythmia[102,231] and heart failure[103,104,232].

β-blockers are a mainstay treatment strategy for many CVDs and stress-related events[30], where prolonged β-blocker therapy affords patients a wide-range of beneficial effects including β_1AR re-sensitisation and restoration of intracellular cN signalling pathways[398] improvements in cardiac myocyte contractility [400] and reversal of ventricular remodelling[103,397]. The precise mechanisms and anatomical sites, that mediate and sustain the beneficial effects of β-blockers in disease is commonly thought to be via adrenergic post-synaptic sites yet the prices mechanisms remain unclear[85,401].

During 1970-1990, it was demonstrated that the activation of presynaptic β-ARs on sympathetic terminals, facilitates noradrenergic transmission within several peripheral ganglia in rat, guinea pig, cat, rabbit, dog and human [402-410], yet little is known about the precise anatomical sites nor the physiological or pathophysiological relevance of these presynaptic receptors in hypertension.

4.2 Chapter Aims

In this chapter, I used a combination of RNA-seq, qRT-PCR, protein assays and fluorescent microscopy techniques to establish whether βARs are expressed on presynaptic post-ganglionic sympathetic stellate neurons from human and rat. The aim of this study was to assess whether presynaptic βARs play a functional role in cN signalling, and contribute to the elevated sympathetic phenotype observed in hypertension. I am the first author on a manuscript describing this work that is published in Hypertension[311].

The specific aims of this chapter were to:

1. Investigate whether sympathetic βARs are present on sympathetic stellate ganglia from normotensive, prehypertensive and hypertensive rats.
2. Assess whether presynaptic βARs are also evident on human sympathetic stellate ganglia, to provide physiological context.
3. Ascertain whether the activation of sympathetic presynaptic βARs couple to the canonical cAMP-PKA intracellular signalling pathway.
4. Establish whether second messenger signalling pathways coupled to presynaptic βARs contribute to the Ca^{2+} phenotype in prehypertensive states.

4.3 Methods

4.3.1 Animals

Three- to four-week-old male prehypertensive SHRs, 16-20-week-old male SHRs with established hypertension and age-matched normotensive Wistar control rats were obtained from Envigo, UK. All experiments were performed in accordance with the UK Home Office Animal Scientific Procedures Act 1986 (ASPA) and approved by the University of Oxford (PPL 30/3131; David J. Paterson).

4.3.2 Human Donor Stellates

For clinical samples, human ganglia were extracted at UCLA and shipped on dry ice in RNA*later*® RNA Stabilization Solution (ThermoFisher). Human donor characteristics are included in Chapter Two in the General Methods section.

4.3.3 Neuronal Isolation

Sympathetic stellate ganglia from three- to four-week-old Wistar and age-matched preSHR. Stellates were dissected, de-sheathed, and dissociated into a single-cell suspension for FRET microscopy, Ca^{2+} imaging and immunocytochemistry experiments as described in Chapter Two.

4.3.4 RNA Extraction and RNA Sequencing

RNA was extracted from the left stellate from rat and left and right stellate ganglia from human donors, and the same samples were used as described in Chapter Two. The RNA-seq dataset described in Chapter Three, was used to identify the mRNA transcripts encoding adrenergic receptors in 16-week-old rat stellate ganglia.

4.3.5 Quantitative Real-Time Polymerase Chain Reaction

The presence of genes encoding adrenergic receptors identified by RNA-seq, was validated by qRT-PCR in RNA extracted from stellate ganglia from four-week and 16-week-old normotensive and hypertensive rats, as well as in human stellate ganglia. In this chapter, the RNA transcripts encoding tyrosine hydroxylase (*Th*), alpha-2 adrenoceptors (α_2AR, *Adra2a*), β_1AR (*Ardb1*) and β_2AR (*Ardb2*) were validated by qRT-PCR. A full list of the primers used and the appropriate dilutions are included in Chapter Two. Data displayed in the results section depicts the gene of interest normalised to *B2m,* however, each primer was analysed against two housekeeping genes (*B2m* and *Gapdh*) for validation and accuracy of qRT-PCR data. For qRT-PCR analysis, the relative amount of each transcript was calculated using the comparative (C_T) method ($\Delta\Delta C_T$, rat; ΔC_T, human)[332].

4.3.6 Immunocytochemistry

Cardiac-sympathetic neurons were fixed onto glass coverslips and stained with the appropriate antibodies for TH, β_1AR, β_2AR and α_{2a}AR. A full list of the antibodies used is included in Chapter Two. Neurons were imaged using 40X or 60X objectives on a confocal microscope (Live Cell Olympus Inverted Confocal or Zeiss LSM 880 Airy Scan Upright Confocal) as described in Chapter Two. Z-stack images were edited and cell sizes were measured using Fiji software (ImageJ)[2,3].

4.3.7 Enzyme-linked Immunosorbent Assays

Protein was extracted from stellate ganglia obtained from four-week and 20-week male SHR, age-matched Wistar rats and human donor stellates. 100 mg of rat stellate tissue was pooled and homogenised in ice-cold dPBS without Ca^{2+} or Mg^{2+}. In alternative experiments, 80 mg of tissue obtained from three human stellate ganglia were separately homogenised in ice-cold dPBS without Ca^{2+} or Mg^{2+}. The protein concentration in each sample was quantified using a protein assay (BioRad DC) as per the manufacturer's instructions and the total protein

concentrations in each sample were normalised. Protein concentrations of β_1AR, β_2AR and TH were established using sandwich ELISAs in rat and human stellate ganglia. A full list of the ELISAs and protein dilutions are included in Chapter Two. The concentration of proteins of interest were quantified using a standard curve generated from the supplied standards.

4.3.8 Live-Cell Förster Resonance Energy Transfer (FRET) Microscopy

FRET microscopy was utilised to monitor real-time changes in intracellular cAMP generation and PKA activity in post-ganglionic sympathetic neurons obtained from four-week preSHR and Wistar rats. Cultured stellate neurons were transduced with adenovirus particles encoding the FRET biosensors Epac1-H187 (5.1 x 10^8 PFU/ml) and AKAR4 (1.3 x 10^9 PFU/ml) for 24 hours as described in Chapter Two. During FRET experiments, stellate neurons were perfused continuously with Tyrode's solution via a gravity-fed perfusion system and the flow rate was controlled at 2–3 ml/min at room temperature. The following pharmacological compounds were diluted in Tyrode solution a non-selective βAR agonist, isoprenaline (ISO, 10 nM to 10 μM), a β_1AR agonist dobutamine (DOB, 50 μM), a β_1AR antagonist metoprolol (MET, 100 nM to 10 μM) a β_2AR agonist salbutamol (SAL, 10 μM) a β_2AR agonist ICI-118,551 (ICI, 10 nM to 10 μM). In all experiments, the maximal FRET change of each cell was recorded by exposing the cells to saturating concentrations of forskolin (25 μM) and IBMX (100 μM) to ensure that the cells responded similarly to the biosensors. In the absence of a forskolin/IBMX response cells were excluded from analysis. A stable baseline of at least two minutes was required at the start of each experiment. During analysis, the FRET changes to pharmacological stimuli were normalised to the last 30 seconds baseline period. The duration of drug administration was determined as the time until cAMP or PKA equilibrium (i.e. a recording plateau) was established.

4.3.9 Intracellular Calcium Measurements

Stellate neurons from four-week-old preSHR and Wistar rats were dissected, dissociated and incubated for four to six hours on the day of culture until fully adhered to Poly-d-Lysine / laminin-coated coverslips (37 °C , 5 % CO_2) as described in Chapter Two. Cells were incubated in neuronal plating media with the Ca^{2+} dye Indo-1 acetoxymethyl ester (Indo-1AM, 2 μM, 45 mins, RT, ThermoFisher). During Ca^{2+} imaging experiments, stellate neurons were perfused continuously with Tyrode's solution via a gravity-fed perfusion system (37 °C) and a stable baseline was recorded for 30 s prior to stimulation. Neurons were stimulated with 50 mM K^+ in bicarbonate-buffered Tyrode solution with an equimolar reduction in NaCl (S1, t = 0.25 mins,). Upon return to baseline, cells were perfused with ISO (1 μM) for 4 minutes and re-stimulated with 50 mM K^+ (S2, t = 4 mins) in the presence of ISO (1 μM). For control experiments, no ISO was administered. A list of the perfusion buffers and their constituents is included in Chapter Two. The values obtained from the peak of each KCL stimulation were averaged and baseline values were subtracted from absolute peak size. In the absence of a KCl response, cells were excluded from analysis. To determine the effect of the compound on KCl-evoked $[Ca^{2+}]_i$ the ratio 'S2 / S1' was calculated, where S2 was the response to stimulus in the presence of drug and S1 was the response to stimulus prior to drug administration. Ratios were compared to time-controlled experiments, where S1 and S2 were recorded in the absence of drug. Ratiometric data were obtained through conversion of raw data sheets into text files and fluorescence values were transformed to $[Ca^{2+}]_i$ concentrations using the equation derived by Grynkiewicz et al.,[314] as described in Chapter Two.

4.3.10 Compounds

Isoprenaline, a non-selective βAR agonist, (racemic (±)-isoproterenol hydrochloride, ISO, I5627), dobutamine hydrochloride (DOB, β_1AR agonist, D0676), salbutamol (SAL, β_2AR agonist, S8260), the metoprolol ((±)-Metoprolol (+)-tartrate, MET, β_1AR antagonist, M539), Dexmedetomidine hydrochloride ((+)-Medetomidine hydrochloride, DEX, α_2AR agonist, SML0956), forskolin (F6886) and 3-Isobutyl-1-Methylxanthine (15879) were supplied from Sigma. ICI 118,551 (ICI 118,551 hydrochloride, β_2AR antagonist, 72795-01-8) was purchased from R&DSystems.

4.3.11 Statistical Analysis

Fluorescent microscopy, qRT-PCT and ELISA data were analysed using GraphPad Prism software (v6/7). When the data passed normality tests (D'Agostino-Pearson omnibus test or Shapiro-Wilk[313]), unpaired two-tailed Student's *t*-tests, one or two-way analysis of variance (ANOVA) were performed. When the data were not normally distributed, the appropriate nonparametric tests were used with the specific statistical test reported in the figure legend. All data are expressed as the mean ± SEM. Statistical significance was accepted at $p<0.05$ unless otherwise described. RNA-seq data were analysed using a Salmon-DESeq2 protocol[322,327] as described in Chapter Two.

4.4 Results

4.4.1 Stellate Ganglia Express mRNA Encoding β-Adrenergic Receptors

The transcriptome of the sympathetic stellate ganglia was sequenced using ganglia extracted from 16-week-old male Wistar rats (n=4 stellates) and SHR (n=4 stellates) with established hypertension and sympathetic hyperactivity[150], as described in Chapter Two. Using the RNA-seq dataset, the presence of adrenergic receptors was confirmed in adult rat stellate ganglia (Fig. 4.1). Of the inhibitory $G_{i/o}$-coupled α_2ARs, mRNA transcripts encoding three isoforms were identified in the TH positive stellate ganglia, where both α_2ARs and TH are indicative of a presynaptic sympathetic phenotype[42]. These represented α_{2A}AR (*Adra2a*), α_{2B}AR (*Adra2b*), α_{2C}AR (*Adra2c*). Transcripts encoding βAR isoforms including β_1AR (*Ardb1*) and β_2AR (*Ardb2*) were also observed, where the transcript encoding *Ardb2* had the highest expression (Fig. 4.1a). Data points represent raw counts ± SEM. The RNA-seq differential expression analysis using the DESeq2 tool [327] described in Chapter Two, highlighted a significant reduction in *Adrb2* expression in SHR compared with Wistar ganglia (p.adj = 0.00945, Fig. 4.1b).

To validate the presence of adrenergic transcripts on rat stellate neurons, qRT-PCR was performed using RNA from four-week Wistar and preSHR ganglia (n=3 rats/group, unpooled), 16-week Wistar and SHR stellates (n=4 rats/group, unpooled). To validate α_2AR expression, the *Adra2a* transcript was selected in preference to *Adra2b and Adra2c,* based on the evidence that the α_{2A}AR isoform primarily regulates presynaptic sympathetic activity[42], whereas the α_{2B}AR isoform has a preferential role within the vasculature[44]. It was unexpected, however, that the transcript abundance of *Adra2b* was an order of magnitude higher than that of *Adra2a and Adra2c.* The qRT-PCR data were analysed using the $\Delta\Delta C_T$ method described by Schmittgen et al.,[332], where raw counts were first normalised to a control housekeeping gene *B2m,* and SHR data were subsequently normalised to Wistar qRT-PCR counts.

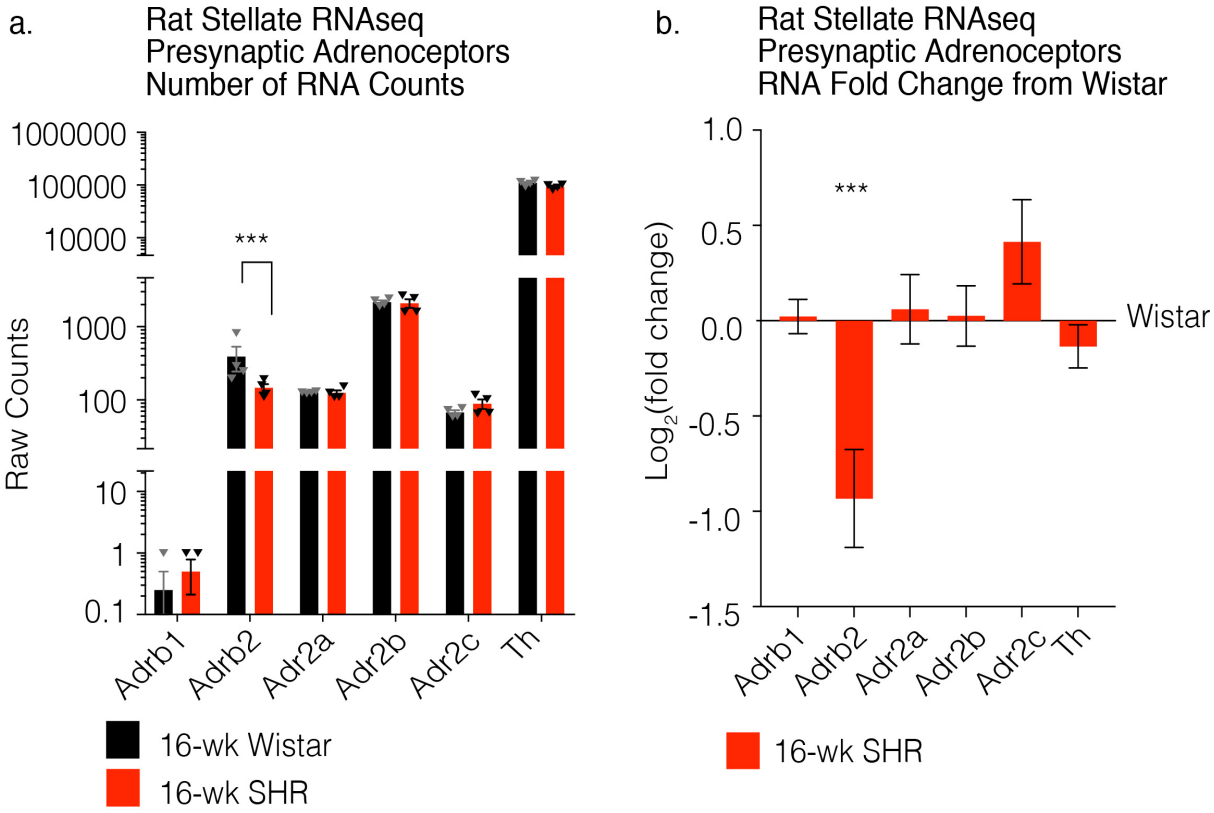


Figure 4.1. RNA-seq Depicts β-Adrenergic Receptors on Rat Stellate Ganglia
RNA-seq identified the presence of β_1AR (*Ardb1*) and β_2AR (*Ardb2*) transcripts in addition to mRNA encoding TH (*Th*) and α_{2A}AR (*Adra2a*), markers of presynaptic sympathetic neurons. Transcripts for *Adra2b* and *Adra2c* were also observed. Data points represent raw counts ± SEM (a). *Ardb2* expression was significantly lower in SHR ganglia compared with Wistar (p. adj=0.00945; Salmon-DESeq2 method[327]). Data are represented as $\log_2$(fold change) ± SEM (b). *p<0.05, **p<0.01, ***p<0.001.

Using qRT-PCR, no significant difference was found in the expression of mRNA for *Adrb1, Adrb2, Adra2a* or *Th* between strains or between age-groups in stellate RNA samples from four-week or 16-week rats (Fig.4.2a). Nevertheless, similar trends representing up or downregulation were observed in the qRT-PCR as in the RNA-seq dataset. Data are represented as $\log_2$ (fold change) ± SEM. ΔC_T values are included in the appendix (Fig. 8.6).

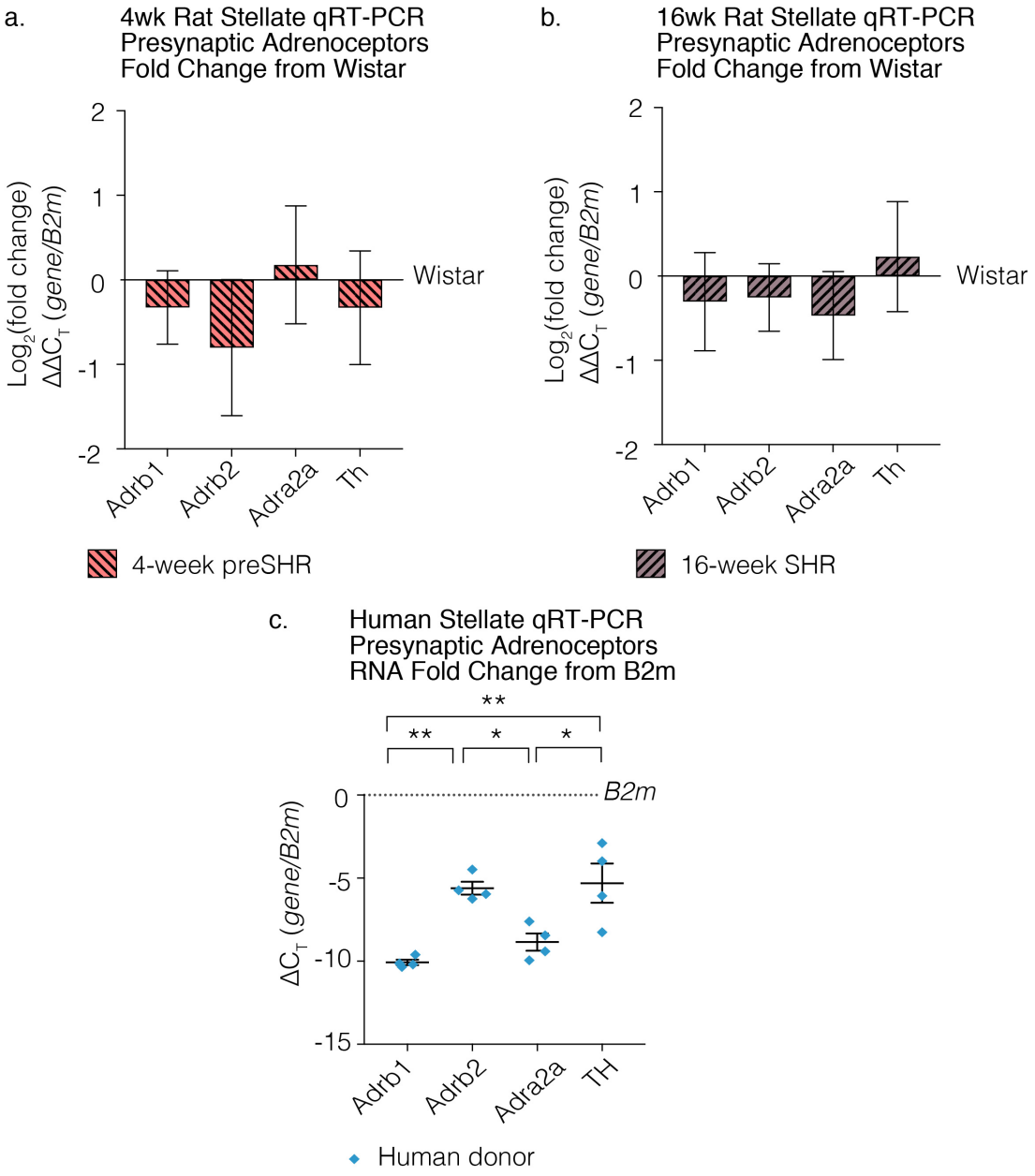


Figure 4.2. Human and Rat Stellate Ganglia Express β-Adrenergic Receptors
The presence of RNA transcripts was validated using qRT-PCR in RNA extracted from 4-week (n=3/group) and 16-week SHR and Wistar rats (n=4/group). There was no significant difference in mRNA expression for *Adrb1*, *Adrb2*, *Adra2a* or *Th* between strains (one-way ANOVA) at 4wk (a) or 16wk (b). Data were analysed using the $\Delta\Delta C_T$ method and represented as $\log_2$(fold change) ± SEM (a, b). The expression of mRNA encoding *Adrb1, Adrb2, Adra2a* and *Th* was observed in human stellate ganglia (n=4) using qRT-PCR. *Adrb1* expression was significantly lower than *Th* (p=0.002) and *Adrb2 (*p=0.0028). *Adra2a* expression was shown to be significantly lower than *Th* (p=0.0123) and *Adrb2 (*p=0.0164). Human data were analysed using a one-way ANOVA with Bonferroni's correction. Data are represented as ΔC_T normalised counts ± SEM (b). *p<0.05, **p<0.01, ***p<0.001.

The transcripts encoding the adrenergic receptors α_{2A}AR, β_1AR, β_2AR (*Adrb1, Adrb2 and Adra2a*) were also confirmed using qRT-PCR in four human stellate ganglia (two left stellates, two right stellates, unpooled were obtained from 3 patients). The ganglia were TH (*Th*) and α_{2a}AR (*Adra2a*) positive, indicative of a presynaptic sympathetic phenotype. The qRT-PCR raw counts were normalised to a control housekeeping gene *B2m,* using the ΔC_T method described by Schmittgen et al.,[332]. It was observed that *Adrb1* expression was significantly lower than *Th* (p=0.002) and *Adrb2 (*p=0.0028). Moreover, *Adra2a* expression was shown to be significantly lower than *Th* (p=0.0123) and *Adrb2 (*p=0.0164). Data were analysed using a one-way ANOVA with Bonferroni's multiple comparisons test. Graphical data points represent ΔC_T normalised counts ± SEM (Fig. 4.2c).

4.4.2 β-Adrenergic Receptors are Expressed on Human and Rat Stellate Ganglia

Immunocytochemistry confirmed the expression of β_1AR, β_2AR and α_{2A}ARs on TH positive neurons from three- to five-week-old control rats and SHR (Fig. 4.3). It was observed that β_1ARs and α_{2A}ARs primarily displayed a membrane localisation whereas the expression of β_2AR appeared cytosolic, at all levels of the Z-stack, possibly indicating internalisation of the β_2AR subtype, as has been well described [71,397,411,412].

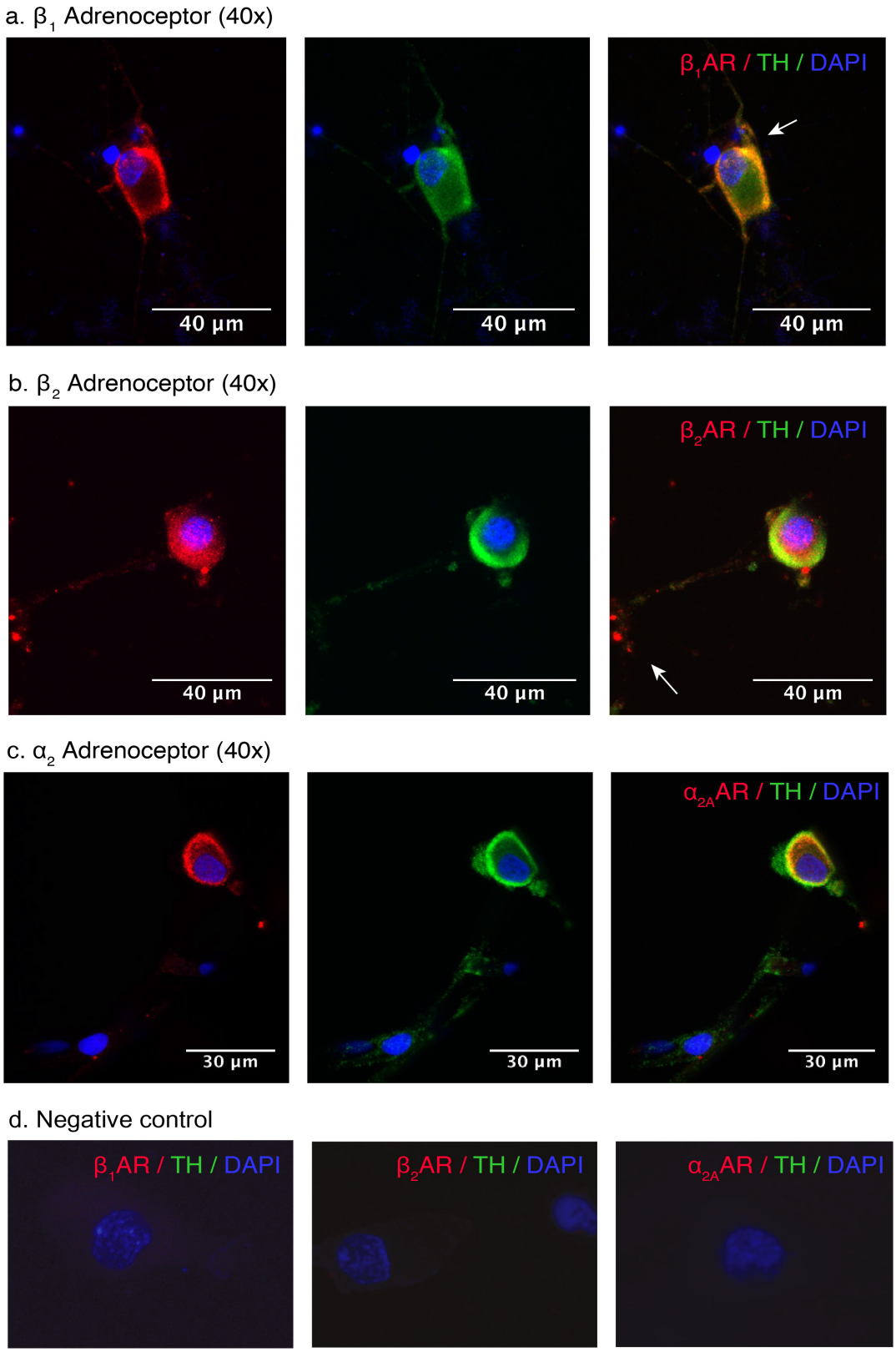


Figure 4.3. β- and α-Adrenergic Receptor Expression on Rat Stellate Neurons
Immunocytochemistry confirmed the expression of β_1AR (a) β_2AR (b) on TH positive stellate from four-week-old rats. The presence of α_{2A}ARs confirms a presynaptic phenotype (c) Images displayed are from Wistar (β_1AR, β_1AR) and preSHR (α_{2A}AR). White arrows depict the localisation of βARs on dendrites (a) and synaptic terminals (c). Negative controls with no primary antibody are depicted (d).

ELISAs were used to quantify the relative protein expression of β_1AR and β_2ARs in stellate neurons obtained from young three- to five-week-old normotensive preSHR and Wistar rats (32 stellates, 16 rats/group, pooled stellates) or adult 19- to 20-week-old SHR and Wistar rats (20 stellates, 10 rats/group, pooled stellates). The concentration of β_1AR protein in rat stellate ganglia was calculated for young Wistar (869.1 pg/ml ± 50.6), adult Wistar (674.1 pg/ml ± 44.6), young preSHR (114.2 pg/ml ± 23.7) and adult SHR (489.4 pg/ml ± 26.4, Fig. 4.4a). β_2AR protein expression in rat stellate ganglia was calculated for young Wistar (431.5 pg/ml ± 18.5), adult Wistar (348.1 pg/ml ± 5.2), young preSHR (82.2 pg/ml ± 19.6) and adult SHR (115.8 pg/ml ± 2.2, Fig. 4.4b). The samples used in the ELISA assays contained protein from 20 or 32 stellates, however, the stellates were homogenised and pooled into a single sample to obtain adequate protein concentrations for the ELISA assays therefore no statistical tests were conducted. β_1AR (516.6 pg/ml ± 60.11) and β_2AR (340 pg/ml ± 33.97) expression was also detected in human stellate ganglia, in 3 pooled stellates obtained from two patients (Fig. 4.4c). Data points indicate mean ± SEM (3-4 technical replicates).

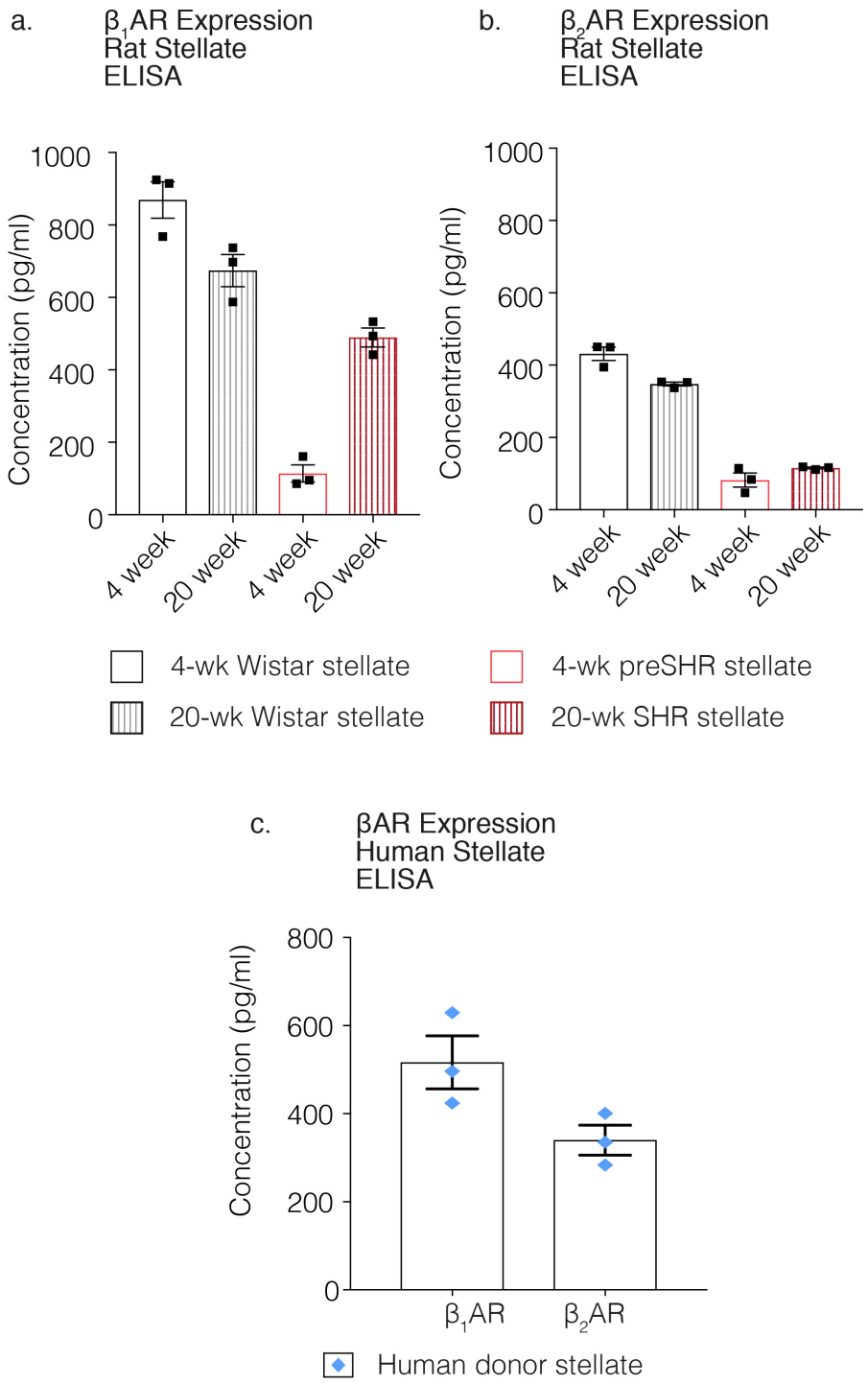


Figure 4.4. Rat and Human Stellate Ganglia Express β-Adrenergic Receptors
The protein expression of β_1AR and β_2ARs was confirmed by ELISA on three- to 5.5-week-old young Wistar and age-matched young preSHR stellates (32 stellates pooled, 16 animals/group) and 20-week-old adult Wistar and SHR stellates (32 stellates pooled, 16 animals/group). The concentration of β_1AR protein in rat stellate ganglia was calculated for (a) young Wistar (869.1 pg/ml ± 50.6), adult Wistar (674.1 pg/ml ± 44.6), young preSHR (114.2 pg/ml ± 23.7) and adult SHR (489.4 pg/ml ± 26.4). The concentration of β_2AR protein in rat stellate ganglia was calculated for (b) young Wistar (431.5 pg/ml ± 18.5), adult Wistar (348.1 pg/ml ± 5.2), young preSHR (82.2 pg/ml ± 19.6) and adult SHR (115.8 pg/ml ± 2.2). In human stellate ganglia, expression of β_1AR (516.6 pg/ml ± 60.11) and β_2AR (340 pg/ml ± 33.97) was also detected (c). Data points depict mean ± SEM (3-4 technical replicates, pooled stellates).

4.4.3 Enhanced βAR-evoked cAMP and PKA Activity in PreSHR Neurons

To determine whether the presence of presynaptic βARs on sympathetic ganglia play a functional role in modulating intracellular cN signalling pathways, FRET was used to quantify the relative levels of cAMP and PKA activity in response to a relatively non-selective βAR agonist, ISO. The rank order of potency for agonists at β_1ARs has been previously demonstrated as ISO >> Adr = NA [413]. Conversely, at β_2ARs the rank order of potency has been determined as ISO = Adr >> NA where the binding affinities for ISO were shown to be 224 nM at β_1AR and 458 nM at β_2AR[413].

To assess whether βAR mediated-cAMP generation facilitated signalling via the canonical cAMP-PKA pathway, neurons from four-week Wistar and preSHR were transduced with the loss-of-FRET sensor Epac1-H187 to measure changes in $[cAMP]_i$. ISO administration at 10 nM led to significantly greater cAMP generation in preSHR (55.6 % ± 16.8) compared with that measured in Wistar neurons (7.1 % ± 1.4 %; 2-way ANOVA, $p<0.0001$) and was also observed at higher concentrations of ISO (100 nM 2-way ANOVA, $p<0.0001$). Using the same concentration of ISO (10 nM), PKA activity was found to be significantly higher in preSHR (26.1 % ± 5.4 %) versus Wistar neurons (4.5 % ± 1.1 %; 2-way ANOVA; $p<0.0001$), and was also observed at 100 nM ISO (Fig. 4.5). Raw YFP and CFP fluorescence traces as emitted from the cytosolic loss-of FRET sensor Epac1-H187 and the gain-of-FRET sensor AKAR4 in response to ISO (10-100 nM) are displayed in Figure 4.6.

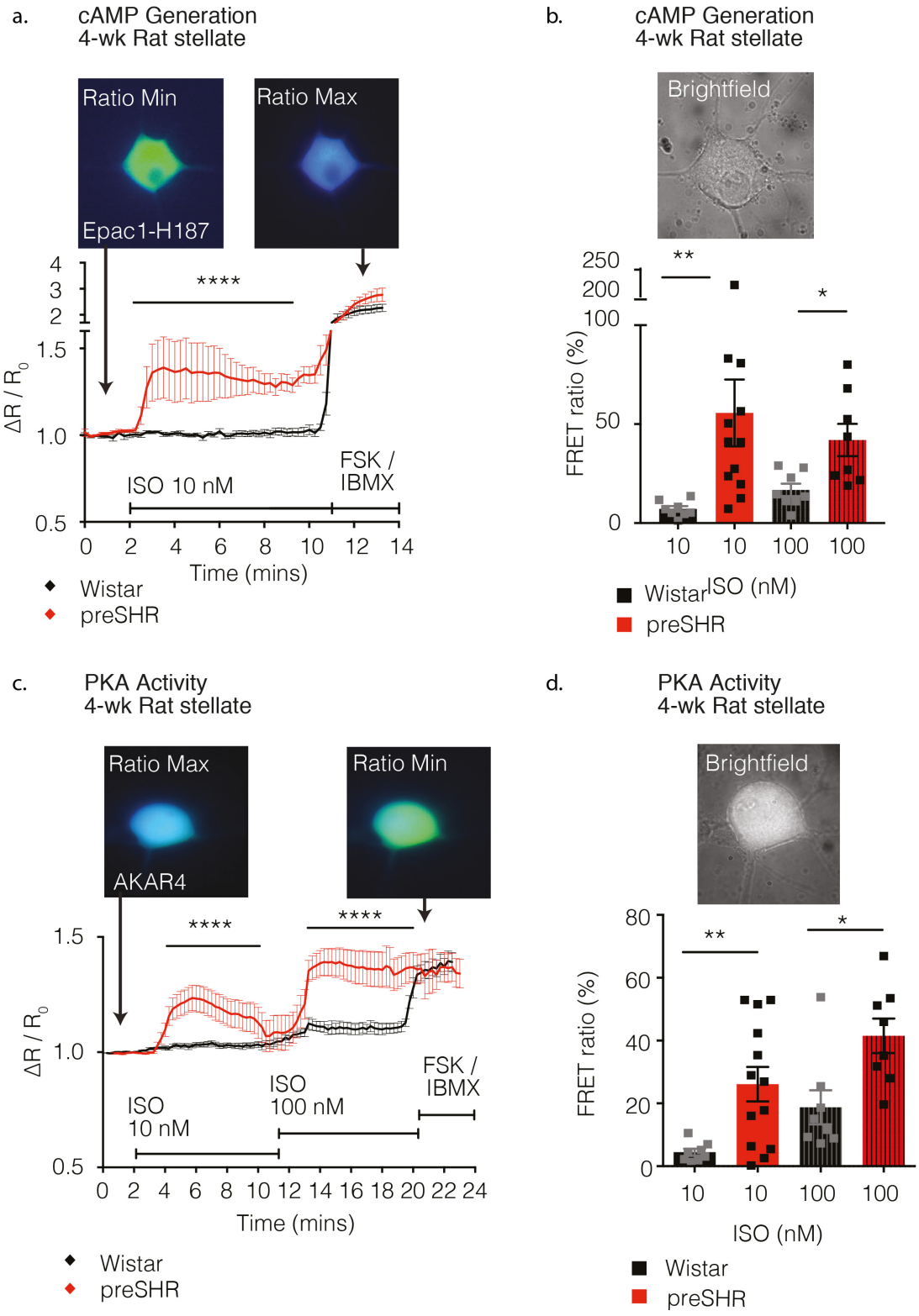


Figure 4.5. βAR Stimulation Increases cAMP-PKA in PreSHR Neurons
Isoprenaline (ISO) generated significantly higher levels of cAMP at 10 nM (a) in preSHR (55.6 % ± 16.8 %; n=12) compared with Wistar neurons (7.1 % ± 1.4 %; n=8; 2-way ANOVA, $p<0.0001$) and 100 nM (b) in preSHR (42.0 % ± 8.2 n=8) vs. Wistar (16.8 % ± 3.2 %, n=8; 2-way ANOVA, $p<0.0001$). ISO increased PKA activity to a significantly greater extent at 10 nM (c) in preSHR (26.1 % ± 5.5 %; n=13) vs. Wistar neurons (4.5 % ± 1.1 %; n=8; 2-way ANOVA; $p<0.0001$) and 100 nM (d) in preSHR (41.5 % ± 5.5, n=8) vs. Wistar (18.8 % ± 5.4 %, n=8, 2-way ANOVA; $p<0.0001$). *$p<0.05$, **$p<0.01$, ***$p<0.001$.

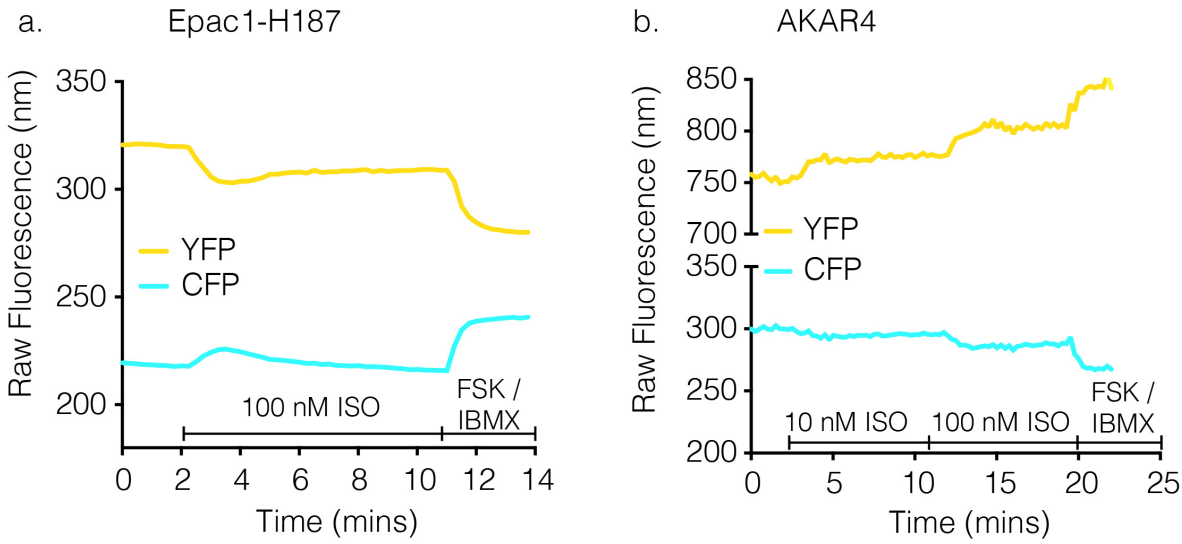


Figure 4.6. Raw Traces Representing CFP and YFP Emission Wavelength
CFP and YFP shown for Epac1-H187 (a) and AKAR4 (b) in response to ISO administration (10-100 nM).

4.4.4 βAR Activation Elevates KCl-evoked Calcium in PreSHR Neurons

To ascertain whether ISO-dependent βAR activation enhances $[Ca^{2+}]_i$, the responses to KCl were measured in the absence or presence of ISO (10 μM). Ca^{2+} recordings were obtained using Indo-1AM labelled sympathetic neurons from four-week preSHR and Wistar rats. In preSHR stellate neurons, KCl stimulation in the presence of ISO led to significantly higher $[Ca^{2+}]_i$ than KCl stimulations alone (Fig. 4.7; p=0.0272). There was also significantly higher KCl-evoked $[Ca^{2+}]_i$ in the presence of ISO in preSHR neurons, compared with that recorded in control neurons (p=0.0027).

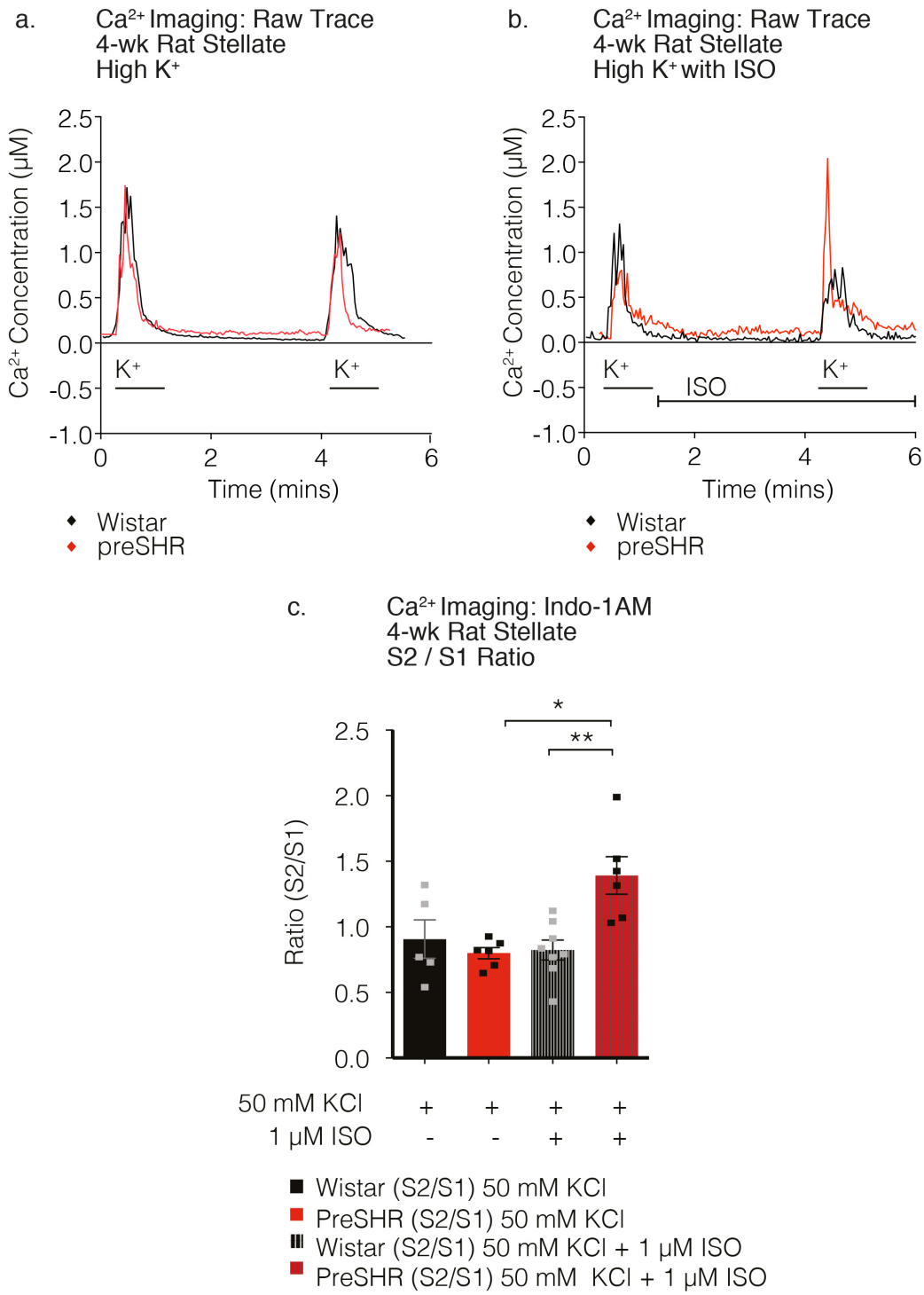


Figure 4.7. βAR Signalling Enhances Intracellular Ca^{2+} in preSHR Neurons
Intracellular Ca^{2+} imaging was conducted on neurons obtained from 4-week control and preSHR with Indo-1AM. Wistar and preSHR neurons were exposed to two KCl challenges (50 mM; stimulation S1 and S2) where S2 was conducted in the absence (Wistar, n=5; preSHR n= 6; a) or presence (Wistar, n=8; preSHR n= 6; b) of ISO (1 μM). Example traces (a, b) and S2 / S1 ratios are shown (c). There was significantly elevated $[Ca^{2+}]_i$ evoked in the presence of ISO in preSHR neurons than in the absence of ISO (p=0.0272), compared to Wistar neurons (unpaired Student's t-tests, p=0.0027). Bar charts represent mean ± SEM. *p<0.05, **p<0.01, ***p<0.001.

4.4.5 Contribution of β_1AR and β_2AR to Neuronal cAMP Generation

To determine whether the observed increases in ISO-evoked cAMP occur predominantly through either β_1AR or β_2AR activation, cells were challenged with administration of a β_1AR agonist (dobutamine, DOB, 50 μM) following β_2AR blockade with ICI-118,551 (ICI, 10 nM); or in alternative experiments, administration of a β_2AR agonist (salbutamol, SAL, 10 μM) following β_1AR antagonism (metoprolol, MET, 100 nM). Administration of the β_1AR agonist DOB, led to significantly greater cAMP generation in preSHR (15.82 % ± 2.8 %, n=5) compared with Wistar neurons (-0.31 % ± 2.4 %, n=10, 2-way ANOVA, $p<0.0001$; Fig. 4.8 a, c). Moreover, in Wistar neurons, administration of DOB did not increase cAMP from baseline.

In alterative experiments, neurons were stimulated with a β_2AR agonist salbutamol (SAL) that also led to a significantly greater cAMP generation in preSHR (63.8 % ± 16.6 %, n=12) compared with Wistar neurons (38.6 % ± 5.2 %, n=13, 2-way ANOVA, $p<0.0001$; Fig. 4.8 b, c). There was significantly higher peak SAL-evoked cAMP compared with DOB-evoked cAMP in Wistar ($p<0.0001$, Mann-Whitney, Fig. 4.8 c) and in preSHR neurons ($p=0.0173$, unpaired two-tailed Student's t-tests, Fig. 4.8 c), highlighting a greater contribution of β_2AR versus β_1AR in generating cAMP, regardless of strain.

To support the evidence that ISO-evoked cAMP was acting through β_1AR and β_2ARs rather than inducing off-target effects, ISO-evoked cAMP (ISO, 10 μM) was tested in the absence and presence of a combination of β_1AR (metoprolol, MET, 10 μM) and β_2AR antagonists (ICI 118,551, ICI, 1 μM). The dual combination of β_1AR and β_2AR antagonists (MET, ICI) abolished ISO-evoked cAMP generation entirely, in both preSHR (n=6) and Wistar neurons (n=6), regardless of the high concentration of ISO used. This observation demonstrates that ISO-dependent cAMP generation is dependent on selective β_1AR and β_2AR activation (Fig. 4.8d).

4.4.6 β_2AR Signalling Plays a Dominant Role in Neuronal cAMP

To support the observation suggesting a dominant role for β_2AR in mediating cAMP generation, β_1AR or β_2AR were selectively inhibited with metoprolol (MET, 10 µM) or ICI 118,551 (ICI, 10 nM) respectively. The resulting cAMP generation in response to ISO (10 µM) was measured in young preSHR (MET, n=14; ICI, n=6) and young Wistar stellate neurons (MET, n=13; ICI, n=7; Fig. 4.9). The selectivity and specificity of the selected β_1AR agonist dobutamine (DOB) and β_2AR agonist salbutamol (SAL) and the β_1AR and β_2AR antagonists (MET and ICI) have been previously reported[414-416].

It was observed that β_2AR blockade reduced ISO-evoked cAMP generation to a greater extent than β_1AR blockade in both Wistar and preSHR neurons, confirming the previous observations for a preferential effect of β_2AR versus β_1AR mediated cAMP generation in stellate neurons, regardless of strain (Fig. 4.9). Moreover, a slight but significantly greater ISO-evoked cAMP generation was measured in preSHR versus Wistar neurons in the presence of either MET ($p=0.0472$) or ICI ($p< 0.001$) using 2-way repeated measure ANOVAs; however, the peak FRET responses themselves were not significantly different between strains (Fig. 4.9), illustrating a slight elevation in β_1AR-mediated cAMP generation in stellate neurons in disease.

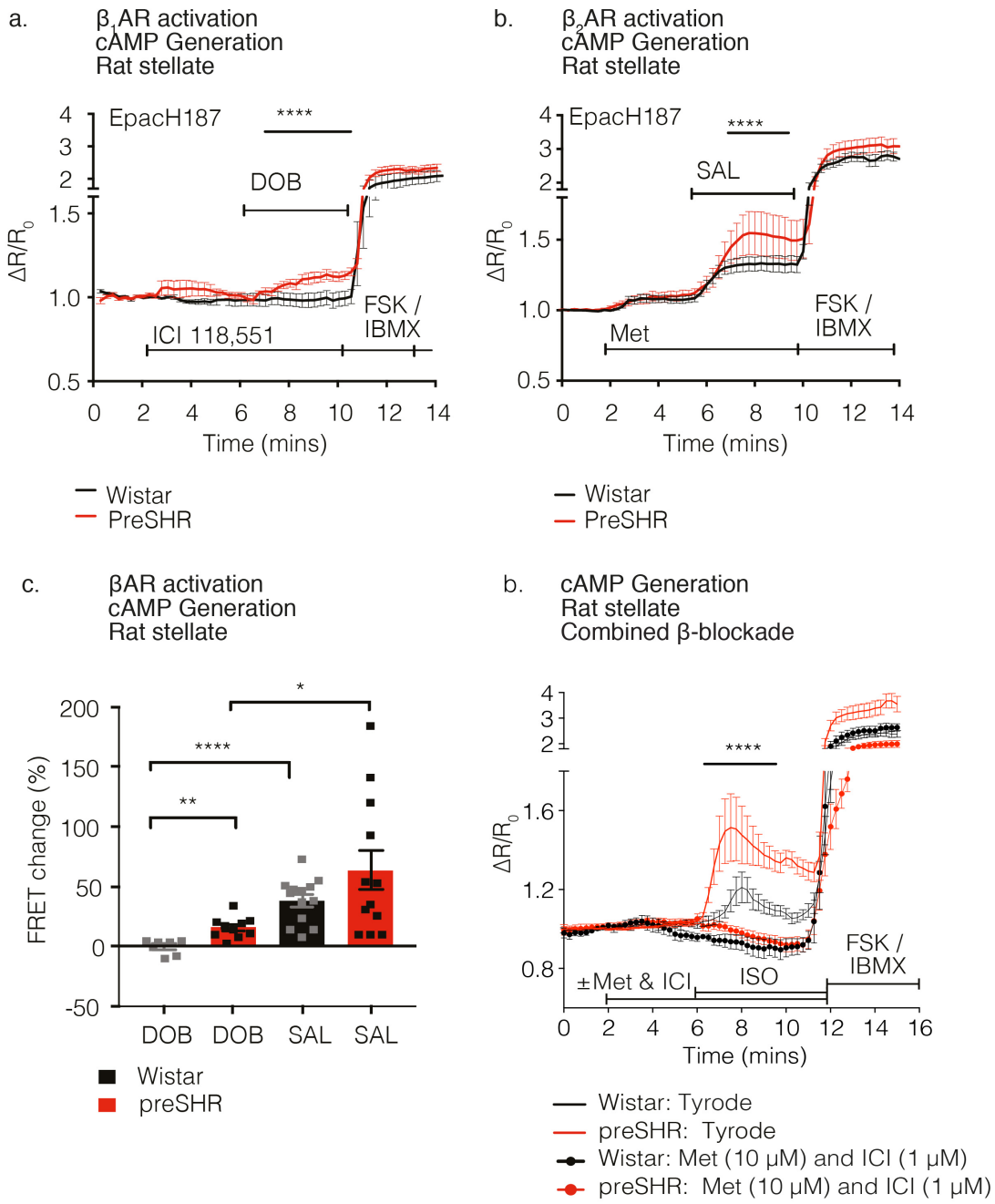


Figure 4.8. Contribution of β_1AR and β_2AR Signalling to Neuronal cAMP Generation
For measurements of cAMP generation, 4-week control and age-matched preSHR neurons were transduced with the Epac1-H187 FRET biosensor. Cells were stimulated with a β_1AR agonist, dobutamine (DOB, 50 μM) following β_2AR inhibition with a selective antagonist, ICI 118,551 (ICI, 10 nM) that led to a significantly greater increase in cAMP generation in preSHR (15.82 % ± 2.8 %; n=5) compared with Wistar neurons (-0.31 % ± 2.4 %; n=10; 2-way ANOVA, p<0.0001). In Wistar neurons, administration of DOB did not increase cAMP from baseline (a). In alterative experiments, neurons were stimulated with a β_2AR agonist salbutamol (SAL, 10 μM) following β_1AR inhibition with a selective antagonist, metoprolol (MET, 100 nM). SAL administration led to a greater increase in cAMP generation in preSHR (63.8 % ± 16.6 %; n=12) compared with Wistar neurons (38.6 % ± 5.2 %; n=13; 2-way ANOVA, p<0.0001, b). The peak FRET change (%) evoked by DOB or SAL were calculated (c). SAL administration induced significantly higher cAMP levels than DOB in Wistar (p<0.0001, Mann-Whitney) and preSHR neurons (p=0.0173, unpaired two-tailed Student's t-tests). β-blockers administration abolished ISO-induced cAMP generation in Wistar (n=6) and preSHR (n=6) neurons (d). *p<0.05, **p<0.01, ***p<0.001.

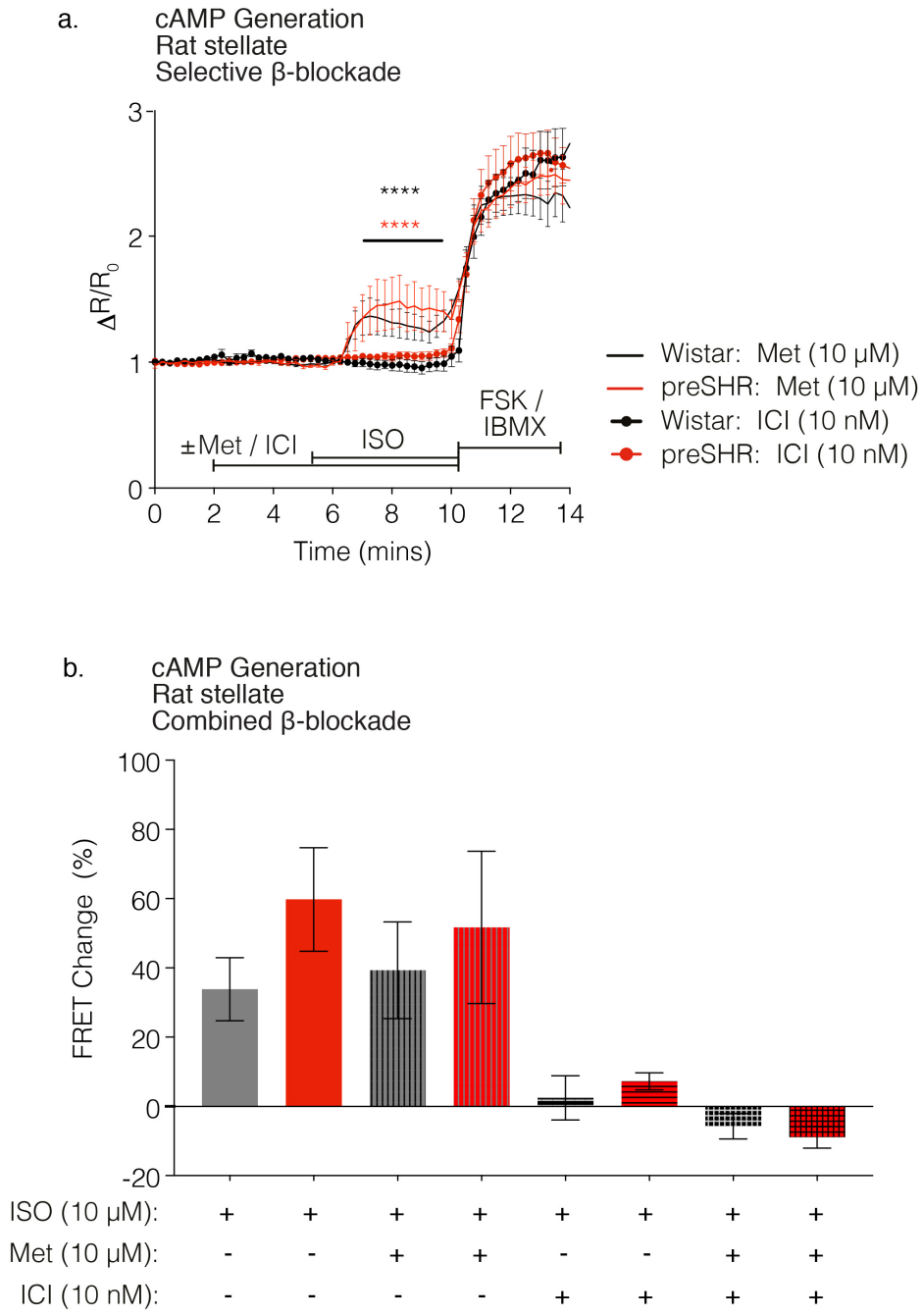


Figure 4.9. β_2AR Signalling Plays a Dominant Role in Neuronal cAMP Generation
For measurements of cAMP generation, 4-week control and age-matched preSHR neurons were transduced with the Epac1-H187 FRET biosensor. To confirm that ISO-evoked cAMP was acting downstream of βAR activation, ISO (10 μM)-evoked cAMP was tested in response to selective blockade of either β_1AR (MET, 10 μM) or β_2AR (ICI, 10 nM) in in 4-week preSHR (MET, n=14; ICI, n=6) and Wistar cells (MET, n=13; ICI, n=7). There was significantly greater inhibition of cAMP following β_2AR (ICI) compared with β_1AR inhibition (MET) in Wistar ($p<0.0001$; 2-way RM ANOVA) and preSHR PGSNs ($p<0.0001$; 2-way repeated measures ANOVA), suggesting that β_2AR plays a predominant role in cAMP generation, regardless of strain (a). *$p<0.05$, **$p<0.01$, ***$p<0.001$. Peak FRET responses are depicted (b).

4.5 Discussion

In this chapter, a combination of RNA-seq, qRT-PCR, protein assays and fluorescent microscopy techniques were applied to ascertain whether βARs are expressed on presynaptic post-ganglionic sympathetic stellate neurons from human and rat. The aim of this study was to assess whether presynaptic βARs play a functional role in cN signalling, and contribute to the elevated sympathetic phenotype observed in hypertension [96,239,311].

The main findings of this chapter are:

1. RNA-seq and qRT-PCR confirmed the expression of β_1AR and β_2AR mRNA transcripts in stellate ganglia from human and rat.
2. The protein expression of β_1AR and β_2ARs was confirmed by immunocytochemistry and concentrations were measured by ELISA in stellate ganglia from human and rat.
3. In isolated sympathetic neurons, βAR agonists elevate cAMP and raise PKA activity.
4. βAR-mediated cAMP, PKA and $[Ca^{2+}]_i$ were increased in preSHR compared with Wistar neurons.
5. βAR-mediated cAMP generation was predominantly mediated by the β_2AR isoform in both strains, and was responsible for the cAMP elevation observed in disease.

4.5.1 Sympathetic Stellate Ganglia Express β-Adrenoceptors

The RNA-seq dataset described in Chapter Two was used to identify the presence of mRNA transcripts encoding adrenergic receptors in stellate ganglia from 16-week Wistar and SHR [337,417]. The data highlighted the expression of transcripts encoding the β_1AR (*Adrb1)* and β_2AR isoforms (*Adrb2)* (Fig. 4.1). While it has been previously reported that presynaptic βARs are present and may be capable of facilitating NA release in several peripheral autonomic ganglia in rat, guinea pig, cat, rabbit, dog and human[402,406,409,410]; the role of adrenergic signalling within the sympathetic stellate ganglia remains unclear, particularly in disease. Given the well-established role of β_1AR and β_2AR myocardial signalling in CVD, the presynaptic sympathetic expression and function of the β_1AR and β_2AR isoforms were the focus of this study.

The mRNA expression of three isoforms of α_2AR were also identified in the RNA-seq dataset (*Adra2a, Adra2b, Adra2c*) that corresponded to the α_{2A}AR, α_{2B}AR, α_{2C}AR subtypes. While the expression of the α_{2A}AR and α_{2C}AR isoforms have been well-documented as important regulators of neurotransmitter feedback inhibition[418], the expression of the transcript encoding α_{2B}AR and the high abundance of this transcript was somewhat unexpected, given its previously reported role in the vasculature [418]. Nevertheless, it is unlikely that vascular tissue was extracted due to the extensive cleaning and de-sheathing protocol for the stellate ganglia under a high magnification dissection microscope. In this study, for characterisation purposes, a focus was placed on confirming the expression of the α_{2A}AR isoform, given its predominant role in protection against tachycardia[419], hypertension, cardiac hypertrophy and myocardial fibrosis in mice[420]. The expression of the transcripts encoding β_1AR, β_2AR, α_{2A}AR and TH was confirmed by qRT-PCR, immunocytochemistry and ELISA assays in rat stellate ganglia, where α_{2A}AR and TH were indicative of a presynaptic sympathetic phenotype, respectively (Fig's. 4.2-4.4). The expression of β_1AR, β_2AR, α_{2A}AR and TH mRNA transcripts were also identified by qRT-PCR and ELISA in human stellate ganglia, providing physiological context and supporting a role for

presynaptic βAR signalling in human cardiac-sympathetic ganglia (Fig's. 4.3-4.4). What is the relevance for the observation of presynaptic sympathetic βARs? Single or combinatorial administration of β-blockers are a main-stay treatment strategy for CVDs and stress-related events caused by sympathetic over-activity[421], although the precise mechanisms that underpin the long-term beneficial effects are not entirely clear[54]. Most research has focussed on the efficacy of βAR antagonists within the myocardium and vasculature, reducing cardiac work and total peripheral resistance[86]. These findings suggest that the efficacy of clinical β-blockers may be attributed, at least in part, to a reduction in sympathetic hyperactivity and neurotransmission at the end-organ.

4.5.2 Elevated β-Adrenergic Signalling in preSHR Sympathetic Neurons

What is the cause for increased sympathetic neurotransmission prior to the onset of neurogenic hypertension? Emerging evidence suggests that impaired NO synthesis and reductions in cGMP-PKG signalling lead to pathological increases in $[Ca^{2+}]_i$ and NA release at the end organ[113,335]. Recently, it has been demonstrated that decreased cGMP signalling leads to enhanced *N*-type Ca^{2+} channel ($Ca_v2.2$) currents, and that this effect may be ameliorated by artificially increasing cytosolic cGMP[96,334]. Cyclic nucleotide signalling is acutely regulated by PDE enzymes, and in early prehypertensive states PDE signalling is impaired resulting in an imbalance between cAMP and cGMP signaling[334]. We therefore sought to ask the question, could high levels of neurotransmitter release act in an autocrine and/or paracrine fashion, to increase neuronal cAMP and potentiate neurotransmission in a feed-forward manner?

In the present study, FRET was used to measure the total cytosolic cAMP and PKA activity, generated in response to administration of physiologically relevant concentrations of the non-selective βAR agonist ISO (10-100 nM) in post-ganglionic sympathetic neurons obtained from young normotensive preSHR and Wistar rats (Fig. 4.6). It was observed that both cAMP and

PKA activity were elevated in preSHR neurons in response to the βAR agonist, ISO. To assess whether βAR signalling facilitates cardiac-sympathetic neurotransmission, $[Ca^{2+}]_i$ was measured in response to KCl in the absence or presence of ISO. Consistent with the observed increases in βAR-mediated cAMP-PKA signalling in preSHR stellate neurons, ISO also increased KCl-evoked $[Ca^{2+}]_i$ in prehypertensive states; whereas there was no effect of ISO in control neurons (Fig. 4.7). Taken together, these data demonstrate that βAR-mediated signalling in sympathetic neurons contributes to the Ca^{2+} phenotype and increases sympathetic transmission. Moreover, this may occur as a direct result of altered PDE activity. Previous work has demonstrated that the *N*-type Calcium Channel (I_{CaN}) is the primary voltage-gated channel responsible for Ca^{2+} influx in sympathetic neurons; and carries a significantly larger Ca^{2+} current in preSHR neurons compared with controls[96,216], where its activity is differentially regulated by PKA and PKG[96,334]. Therefore, it is probable that the ISO-potentiated increases in $[Ca^{2+}]_i$ in preSHR neurons primarily occurs as a result of βAR-cAMP activation that increases PKA-dependent phosphorylation of I_{CaN} ($Ca_v2.2$).

4.5.3 β_2AR Plays a Dominant Role in Sympathetic cAMP Generation

To establish whether the observed increases in cAMP-PKA activity occur downstream of β_1AR and/or β_2AR signalling, cultured stellate neurons were perfused with selective agonists for either β_1 or β_2AR subtypes. The selective activation of β_1AR or β_2AR led to significantly greater increases in cAMP in preSHR neurons compared with Wistar. Indeed, there was no measurable effect of β_1AR activation on $[cAMP]_i$ in normotensive controls (Fig. 4.8). Furthermore, stimulation of preSHR neurons with the β_2AR agonist salbutamol, led to cAMP generation that was almost twice as high as β_1AR-evoked cAMP within preSHR neurons, suggesting a dominant role for β_2AR compared with β_1AR signalling in these neurons. Importantly, elevated cAMP-PKA- Ca^{2+} activity did not result from an increase βAR transcription or protein levels, as it was observed that mRNA transcripts and protein expression are reduced in preSHR stellates as well as in

aged SHR with established hypertension compared to age-matched Wistar neurons; in a similar manner to that reported in the myocardium[422]. Moreover, it was observed that in healthy ganglia, β_1AR expression decreases with age (Fig. 4.3) much like in the heart. Together, these data suggest that in diseased states, the potentiating effects of βAR agonists are mediated by impaired second messengers coupled to cAMP and/or its effector PKA rather than the GPCRs themselves; that may be exacerbated by the impairment of PDEs to hydrolyse cAMP[96,334].

In support of a role for elevated cAMP-PKA activity in stellate ganglia in disease, the RNA-seq dataset highlighted a significant reduction in the gene encoding the type Iα regulatory subunit of PKA (*Prkar1a*) as discussed in Chapter Two. This subunit plays a dominant role as an endogenous inhibitor of kinase activity[337] where loss-of-function mutations in *Prkar1a* are associated with a two-fold greater responsiveness to cAMP and an excess of PKA type II activity [376]. Moreover, in humans, *Prkar1a* mutations are characterised by endocrine over-activity, neural dysfunction and cardiac complications, that results in dysregulation of arterial blood pressure homeostasis, arrhythmia and cardiomyopathies [377,423], highlighting the importance of cAMP-PKA signalling in neuronal and cardiovascular regulation. Consequently, it appears that in cardiac sympathetic nerves from prehypertensive rats, several processes that favour excitatory cAMP-PKA signalling are upregulated, whereas, pathways that are coupled to NO are critically impaired early in disease, thus exacerbating or underpinning the observed Ca^{2+} phenotype [96,113,262].

4.6 Limitations

In this study, the role and mechanisms involved in feed-forward presynaptic signalling in the cardiac-sympathetic ganglia were investigated. The limitations of the RNA-seq study have been described in detail in Chapter Three so will not be further discussed here. To assess the functional relevance of βAR expression, several techniques were utilised including qRT-PCR, immunocytochemistry, ELISA, FRET and Ca^{2+} imaging. There were several limitations to these approaches. Firstly, the stellate ganglion comprises a heterogeneous population of cell types that might influence the transcripts identified by qRT-PCR. Nevertheless, immunocytochemistry highlighted the localisation of β- and αARs on the soma and dendrites of TH-positive neurons. In support of these data, our collaborators have also identified the presence of transcripts encoding presynaptic βARs in sorted sympathetic mouse neurons (personal communication Ana Domingos). Moreover, sympathetic neurons displayed a cAMP and PKA FRET response to βAR agonists. Secondly, in the absence of cardiac tracing experiments, anatomical literature[218,424,425] and our own previous observations[100,112,333,426] are relied upon, suggesting that the results presented here are relevant to 'cardiac-sympathetic' communication; since significant myocardial sympathetic innervation has been shown to arise from the cervicothoracic ganglia (T1-T4)[107,162]. Thirdly, stellates were obtained from male rats only. While sex differences in hypertension and CVD incidence have been widely reported[114], in this study the role of presynaptic βAR signalling in the male rat stellate ganglia was investigated, given that the prevalence for CVDs is significantly higher in males than premenopausal women[115]. Fourthly, although protein concentrations of βARs were measured, limited datasets were acquired due to the high requirement of protein in each sample, therefore no statistical analyses could be conducted. Moreover, total protein concentrations cannot inform us as to the localisation of receptors. Whether altered membrane receptor expression or adrenoceptor activity resulting from desensitisation or internalisation of βARs plays a role in the altered cAMP-PKA-Ca^{2+} responses cannot be determined from the data presented in this chapter. As such, the cAMP-

PKA phenotype in preSHR neurons described here, provides a target for further investigation. Fifthly, β_2AR mRNA expression levels were found to be more highly expressed than β_1AR mRNA expression SHR stellate ganglia, however this trend was not reflected in the protein concentrations. Finally, cNs and PDEs reside in distinct subcellular compartments and their localisation with βARs receptors is acutely regulated[230,265,266]. Similarly, the regulation of Ca^{2+} channels by PKA/PKG occurs in distinct signalosomes, conferring site-specific regulation of Ca^{2+} entry coupled to neurotransmission. Furthermore, the rate of PDE hydrolysis is critically dependent on the concentration of both cAMP and cGMP that is reported to be different between cell types[225]. In this study, global cytosolic cAMP, PKA and Ca^{2+} concentrations were measured, therefore whether alterations preferentially occur within specific subcellular compartments is not known. Site-specific FRET and Ca^{2+} sensors will be required to resolve the question of microdomain impairments in cN and effector signalling.

4.7 Conclusion

This chapter provides evidence for presynaptic βARs signalling that increases cAMP generation, PKA activity and $[Ca^{2+}]_i$ levels in disease, in a manner akin to positive feedback. Figure 4.10 depicts the model signalling pathways in healthy (a) and prehypertensive states (b) and highlights potential sites for neural phenotypic targeting in disease. Presynaptic activation of β_2ARs (and β_1ARs to a lesser extent) has been demonstrated to enhance neurotransmission in a potentiating feed-forward manner, with activation of α_2ARs playing a role in negative feedback. This may be caused by altered G-protein activation coupled to the receptors themselves, or as a result of impaired PDE activity in disease, supporting a role for impaired cN regulation by PDEs in hypertension. These findings may have implications beyond neurogenic hypertension, and may offer benefit in other diseases of sympathetic over-activity such as modulation of renin-angiotensin-aldosterone release, chronic inflammatory diseases and heart

failure. β-blockers, particularly with β_2AR selectivity may also have beneficial effects by decreasing sympathetic transmission at the end-organ.

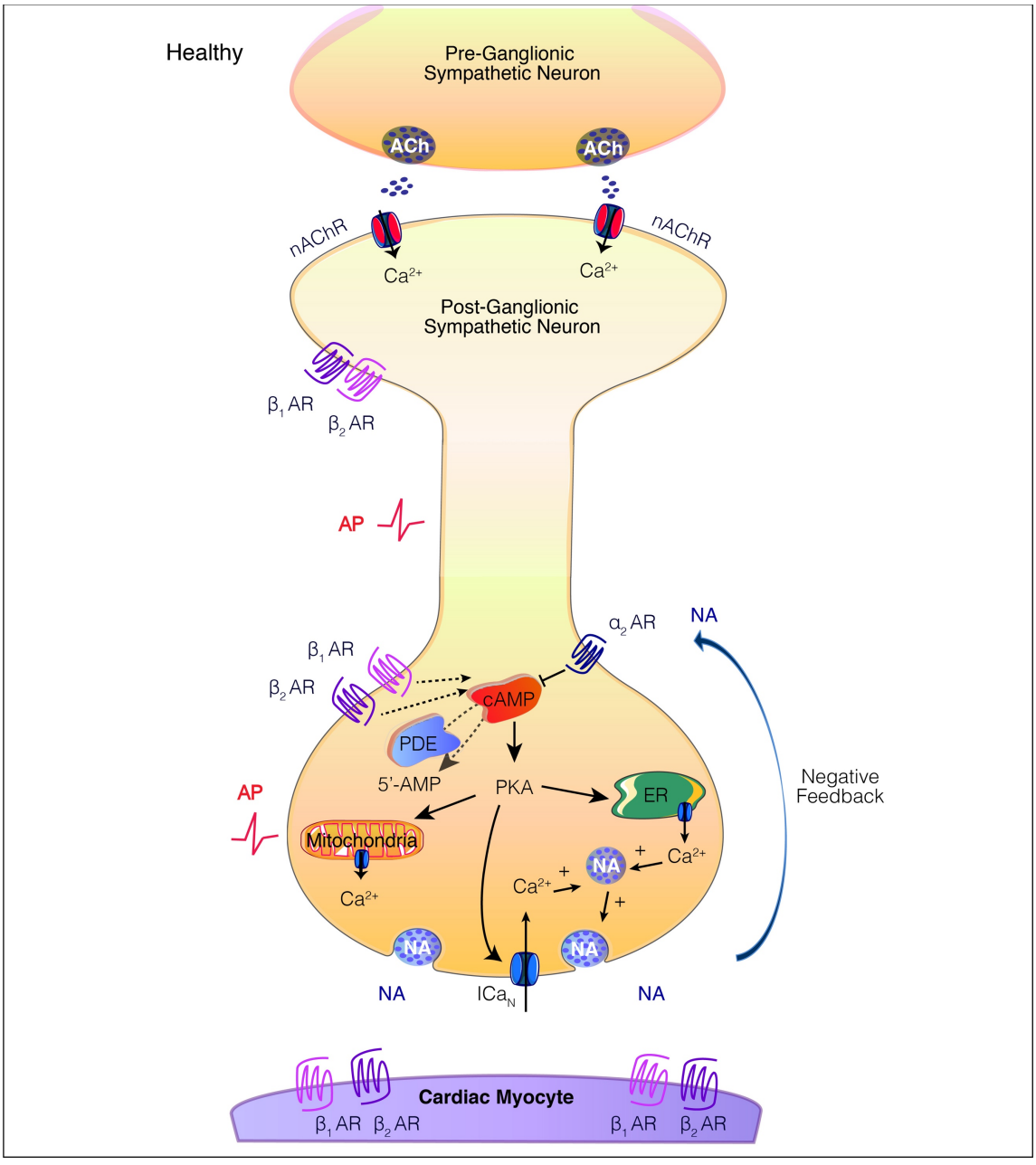


Figure 4.10a. Intracellular Signalling in Healthy Neurons
In healthy sympathetic neurons, Ca^{2+} dependent exocytosis facilitates the release of NA onto cardiac myocytes, where post-synaptic β_1ARs and β_2ARs are activated. Increases in extracellular NA acts on presynaptic α_2ARs, reducing AC activity through activation of inhibitory $G\alpha_{i/o}$ G-proteins. Acute regulation of cAMP is maintained by PDEs. cAMP generation and PKA activity increase $[Ca^{2+}]_i$ via phosphorylation of the *N*-type Ca^{2+} Channel (I_{CaN}; $Ca_V2.2$); ER store and mitochondrial Ca^{2+} release.

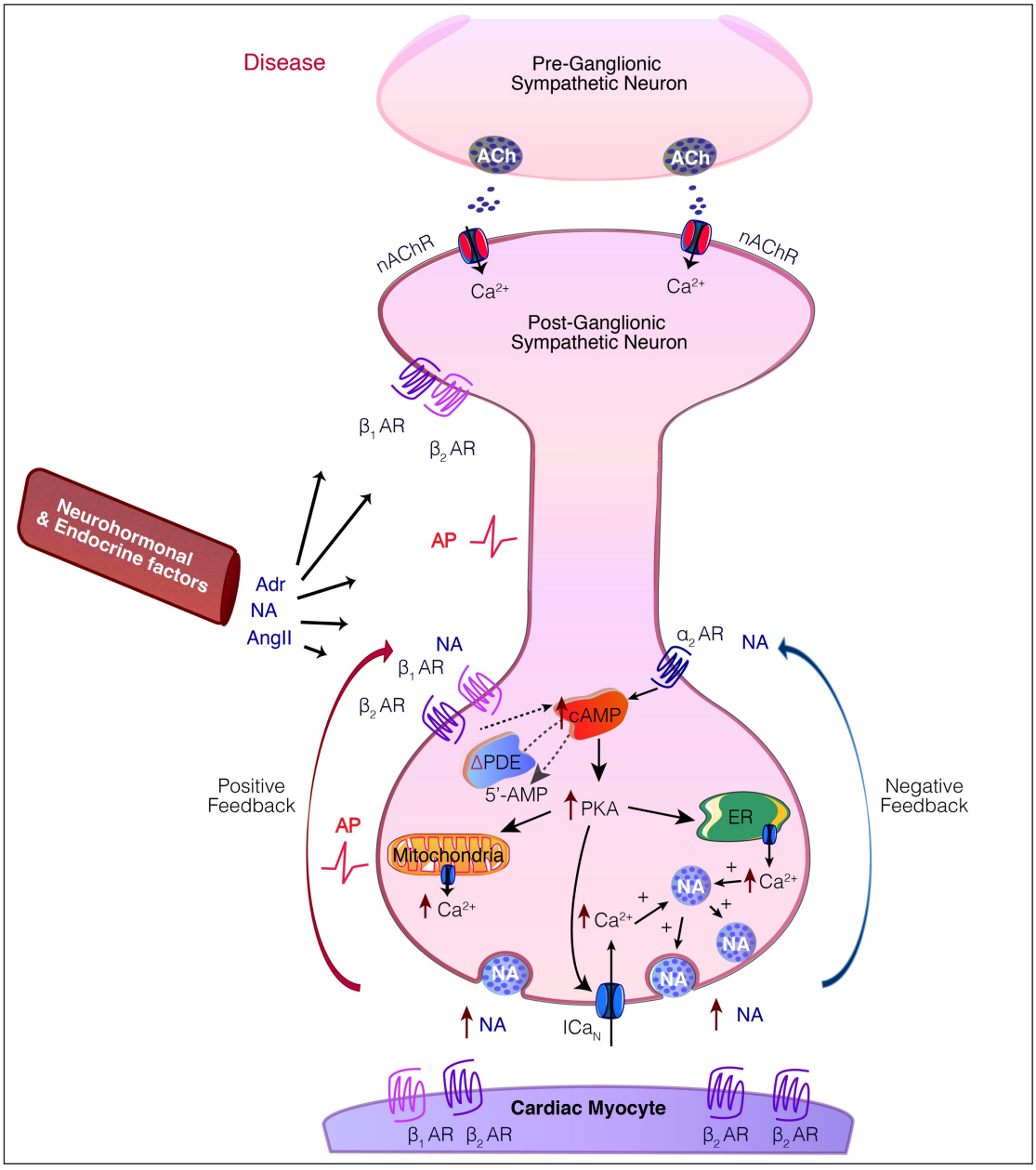


Figure 4.10b. Intracellular Signalling in Diseased Neurons
In diseased neurons, activation of presynaptic βARs augments cAMP generation, PKA activity and $[Ca^{2+}]_i$ via elevated phosphorylation of the *N*-type Ca^{2+} Channel (I_{CaN}; $Ca_V2.2$). This facilitates neurotransmission in a potentiating feedforward manner. Catecholamines may also be supplied from the circulation. As such, β-blockers may also have efficacy at βARs expressed on peripheral neurons, by reducing cardiac-sympathetic communication in hypertension and dysautonomias.

5

Adrenaline Synthesis in the Sympathetic Stellate Ganglia

5.1 Introduction

The autonomic nervous system (ANS) comprising the parasympathetic and sympathetic branches provide a communicatory link between the CNS and the regulation of peripheral organ activity[66].The relationship between psychological factors and blood pressure regulation is well known, and has been a topic of interest since Ancient Greeks when a critical link between mental stress and heart rate was first reported "…*distress, fear, rage, worry…and all those sorts of thing... in common to all of them, the pulse increases in speed and frequency…*"[427]. Epidemiological evidence now supports a strong role for chronic stress in the aetiology of essential hypertension[181,428], where biomarkers of stress identified in patients with panic disorder are also found to be strongly represented in patients with essential hypertension [429]. Although the aetiology of hypertension is not known, there are a number of shared characteristics between chronic mental stress and essential hypertension, where evidence points to a primary role for neurohormonal dysfunction as a key determinant of blood pressure. Observations in patients with mental stress or essential hypertension include enhanced hypothalamic and amygdala activity linked to central sympathetic outflow [429], elevated peripheral sympathetic nerve firing rates [429], and increased plasma concentrations of Adr.

The 'Adrenaline Hypothesis' of essential hypertension argues that small incremental increases in plasma Adr enhance sympathetic activity through sustained activation of presynaptic sympathetic βARs, leading to the development of hypertension[430] yet the source of Adr, however, is not clear [209,403,430-434]. Recent evidence has pointed to the possible synthesis of Adr in sympathetic nerves in patients with stress disorder[435], however, the *in situ* synthesis of Adr and a role for cardiac sympathetic Adr in the aetiology of hypertension is far from well-established.

5.2 Chapter Aims

In this chapter, I aimed to investigate the concentrations and classes of catecholaminergic neurotransmitters present within the cardiac-sympathetic ganglia in healthy and diseased states, to test the idea that Adr may act as the preferential sympathetic neurotransmitter in disease. I am the first author on a manuscript describing this work that is published in Hypertension[311].

The specific aims of this chapter were to:

1. Identify the mRNA transcripts encoding enzymes involved in the synthesis of catecholamine neurotransmitters, NA and Adr in human and rat stellate ganglia.
2. Determine whether the abundance of the transcripts encoding enzymes involved in the synthesis of catecholamine transmitters correlates with elevated catecholamine release in the SHR directly.
3. Assess whether the enzyme Phenylethanolamine N-methyl transferase involved in the synthesis of Adr is detectable at protein levels in human and rat stellate ganglia
4. Quantify concentrations of catecholamines synthesised in rat stellate ganglia.
5. To assess whether electrical field stimulation leads to quantifiable concentrations of NA and / or Adr release from sympathetic stellate ganglia.

5.3 Methods

5.3.1 Animals

Three- to five-week-old male prehypertensive SHRs, 16- to 20-week-old male SHRs with established hypertension and age-matched normotensive Wistar control rats were obtained from Envigo, UK. All experiments were performed in accordance with the UK Home Office Animal Scientific Procedures Act 1986 (ASPA) and approved by the University of Oxford (PPL 30/3131; David J. Paterson).

5.3.2 Human Donor Stellates

For clinical samples, human ganglia were extracted at UCLA and shipped on dry ice in RNA*later*® RNA Stabilization Solution (ThermoFisher). Human donor characteristics are included in Chapter Two in the General Methods section.

5.3.3 RNA Extraction and RNA-seq

RNA was extracted from rat and human stellate ganglia using the protocols described in Chapter Two. The RNA-seq dataset described in Chapter Three, was used to identify the mRNA transcripts encoding catecholamine-synthesising enzymes and precursors in 16-week-old rat stellate ganglia.

5.3.4 Quantitative Real-Time Polymerase Chain Reaction

The genes encoding catecholamine-synthesising enzymes and precursors identified by RNA-seq, were validated by qRT-PCR using the same RNA samples used in Chapter Four. RNA samples were extracted from stellate ganglia from four-week and 16-week-old normotensive and hypertensive rats, as well as in human stellate ganglia. In this chapter, the RNA transcripts encoding phenylalanine hydroxylase (*Pah*), TH (*Th*), L-DOPA decarboxylase (*Ddc*), Dopamine

β-hydroxylase (*Dbh*) and Phenylethanolamine N-methyltransferase (*Pnmt*) were validated by qRT-PCR A full list of primers used and the appropriate dilutions are included in Chapter Two. Data displayed in the results section depicts the gene of interest normalised to *B2m,* however, each primer was analysed against two housekeeping genes (*B2m* and *Gapdh*) for validation and accuracy of qRT-PCR data. For qRT-PCR analysis, the relative amount of each transcript was calculated using the comparative (C_T) method ($\Delta\Delta C_T$, rat; ΔC_T, human)[332].

5.3.5 Enzyme-linked Immunosorbent Assays

Protein was extracted from stellate ganglia obtained from four-week and 20-week male SHR, age-matched Wistar rats and human donor stellates. 100 mg of rat stellate tissue was pooled and homogenised in ice-cold dPBS without Ca^{2+} or Mg^{2+}. In alternative experiments, 80 mg of tissue obtained from three human PGSNs were separately homogenised in ice-cold dPBS without Ca^{2+} or Mg^{2+}. The protein concentration in each sample was quantified using a protein assay (BioRad DC) as per the manufacturer's instructions and total protein concentrations in each sample were normalised. Protein concentrations of PNMT and TH were established via sandwich ELISA using rat and human stellate ganglia. A full list of the ELISAs, protein dilutions and the manufacturers are included in Chapter Two. The concentration of proteins of interest were quantified using a standard curve generated from the supplied standards.

5.3.6 Whole Ganglia and Electrical Release of Catecholamines

To investigate concentrations of NA or Adr in cardiac-sympathetic ganglia, whole fresh ganglia were dissected from four-week preSHR (n=4 rats) and four-week Wistar (n=8 rats). For each experiment, a single ganglion was cleaned, de-sheathed and allowed to recover in carbogenated bicarbonate-buffered Tyrode's solution (5 min, 37 °C , 95 % O_2 / 5 % CO_2). The ganglia were subsequently incubated in fresh bicarbonate-buffered Tyrode's (95 % O_2, 5 % CO_2) containing the norepinephrine transport (NET)-reuptake inhibitor, desipramine (1 µM, 10

min, 37 °C). A list of the buffer constituents is included in Chapter Two. Stellate ganglia were electrically stimulated (3 mA, 5 Hz, 5 mins) using parameters that were adapted from previous electrical stimulation methods[262]. The perfusate was removed and perchloric acid (PCA, 0.1 M) was added at each step to prevent the oxidation of catecholamines. Perfusate samples were kept on ice before freezing at -80 °C. At the end of each experiment, whole stellate ganglia were homogenised in bicarbonate-buffered Tyrode's solution containing PCA (0.1 M), centrifuged (15,000 x g, 15 min, 4 °C) and the supernatant was stored at -80 °C.

5.3.7 High-Pressure Liquid Chromatography with Electrochemical Detection

For detection and quantification of NA and Adr, the samples were loaded into an autosampler (JASCO, Model AS-2055/2057) and detected with an isocratic HPLC system using a C18 reverse-phase column (CP30710 Microsorb 100-5 C18 S250 x4.6mm, Agilent). The details describing the HPLC-EC protocol for the quantification of catecholamines are included in Chapter Two. The concentrations of NA were calculated against a 50 mg standard of NA and Adr dissolved in bicarbonate-buffered Tyrode's containing PCA (0.1 M). Concentrations from the homogenate and the concentrations measured in the perfusate were added, to obtain concentrations reflecting the total content of catecholamines in the stellate ganglia

5.3.8 Statistical Analysis

Data were analysed using GraphPad Prism software (v6/7). When the data passed normality tests, unpaired two-tailed Student *t*-tests, one or two-way analysis of variance (ANOVA) were used. When the data were not normally distributed, the appropriate nonparametric tests were used with the specific statistical test reported in the figure legend. All data are expressed as the mean ± SEM. Statistical significance was accepted at $p<0.05$ unless otherwise described.

5.4 Results

5.4.1 RNA Sequencing Illustrates Catecholamine Synthesising Pathway

RNA-seq was conducted using sympathetic stellate ganglia from 16-week-old male Wistar rats (n=4 stellates) and SHR (n=4 stellates) with established hypertension and sympathetic hyperactivity[150] as described in Chapter Two. RNA encoding the enzymes involved in the synthesis of catecholamines were identified, where relevant transcripts included phenylalanine hydroxylase (*Pah*), TH (*Th*), L-DOPA decarboxylase (*Ddc*) and dopamine β-hydroxylase (*Dbh*) (Fig. 5.1). The high transcript abundance of the enzymes required for NA synthesis indicates that a high population of the stellate ganglia cells are of a sympathetic phenotype. The RNA-seq dataset highlighted the presence of the mRNA transcript encoding PNMT (*Pnmt*); the enzyme required for the conversion of NA to Adr in both Wistar and SHR stellate ganglia (Fig. 5.1). Data points represent raw counts ± SEM. The RNA-seq differential expression analysis using the DESeq2 tool[327] described in Chapter Two, highlighted a significant reduction in *Pah* and *Ddc* expression in SHR compared with Wistar ganglia (*p*.adj = 0.0719; 6.64×10^{-15}; *Pah*, *Ddc* respectively, Fig. 5.1b).

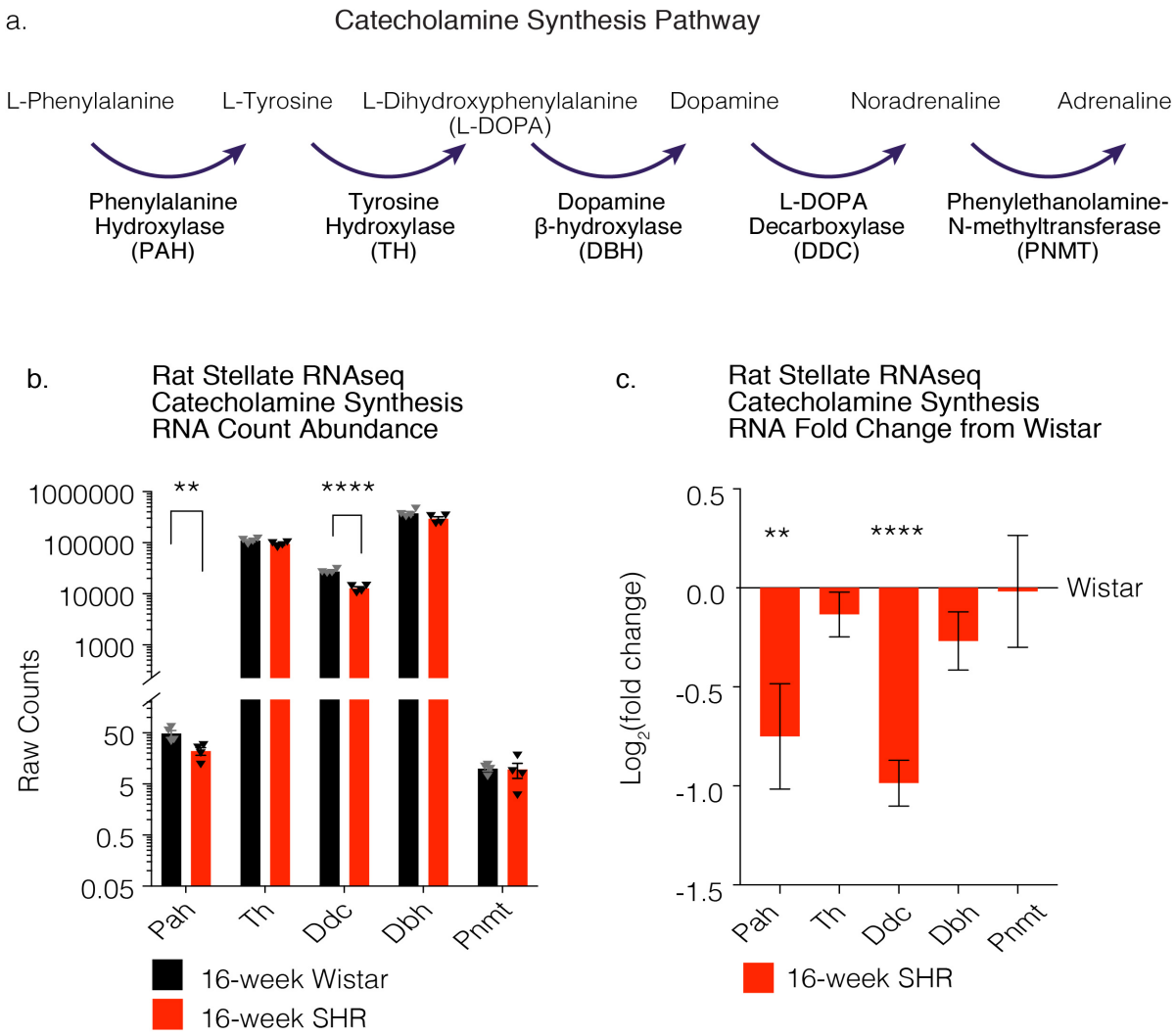


Figure 5.1. RNA-seq Highlights Catecholamine Synthesis Pathway
The catecholamine synthesis pathway is outlined (a). RNA-seq identified the presence phenylalanine hydroxylase (*Pah*), TH (*Th*), L-DOPA decarboxylase (*Ddc*) and dopamine β-hydroxylase (*Dbh*) transcripts in addition to mRNA encoding PNMT (*Pnmt*), the enzyme required for the conversion of NA to Ad. Data points represent raw counts ± SEM (a). *Pah* and *Ddc* expression were significantly lower in SHR ganglia compared with Wistar (p.adj = 0.0719; 6.64 x 10^{-15}; *Pah*, *Ddc* respectively; Salmon-DESeq2 method[327]). Data are represented as $\log_2$(fold change) ± SEM (b). *p<0.05, **p<0.01, ***p<0.001.

5.4.2 Stellate Ganglia Express Phenylethanolamine N-Methyltransferase

To validate the presence and relative levels of catecholamine enzyme transcripts in rat stellate neurons, qRT-PCR was performed using RNA from four-week Wistar and preSHR ganglia (n=3 rats/group, unpooled Fig. 5.2). Additionally, given the absence of previous evidence, reporting the presence of *Pnmt* expression in sympathetic neurons, qRT-PCR was also carried out to probe for *Pnmt* and *Th* in RNA from 16-week Wistar and SHR stellates (n=3-4 rats/group, unpooled, Fig. 5.2). The qRT-PCR data were analysed using the $\Delta\Delta C_T$ method described by Schmittgen et al., [332] where raw counts were first normalised to a control housekeeping gene *B2m,* and SHR data were subsequently normalised to Wistar qRT-PCR counts. ΔC_T values are included in the appendix (Fig. 8.6).

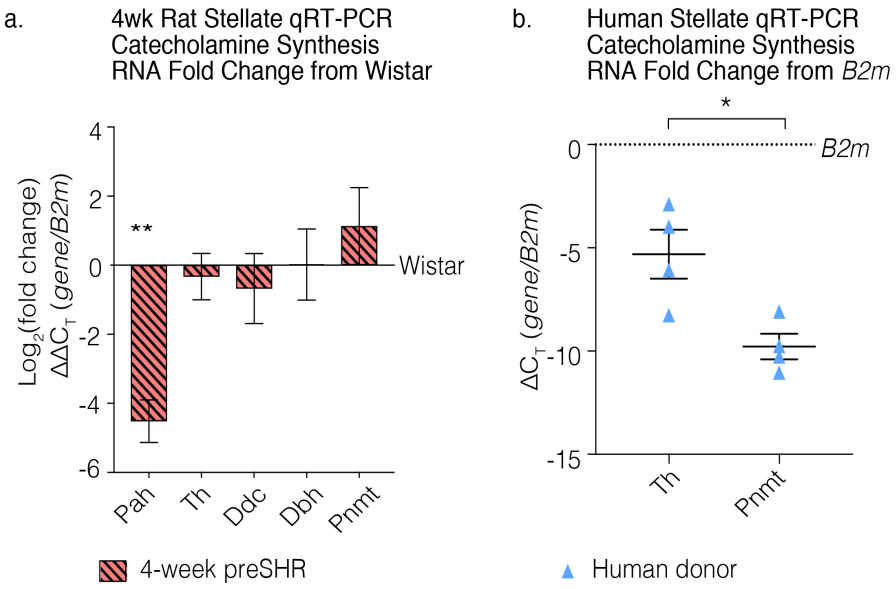


Figure 5.2. Catecholamine Synthesising Enzyme mRNA Validation by qRT-PCR
The presence of RNA transcripts was validated using qRT-PCR in RNA extracted from 4-week (n=3/group) preSHR and Wistar rats (n=3-4/group). There was no significant difference in mRNA expression for *Th, Ddc, Dbh* or *Th* between strains. Data were analysed using the $\Delta\Delta C_T$ method and are represented as $\log_2$(fold change) ± SEM (a). A significant four-fold reduction in *Pah* mRNA expression in preSHR ganglia was observed compared to the expression in Wistar ganglia (p=0.0098, two-tailed unpaired Student's t-test). The expression of mRNA encoding *Th* and *Pnmt* was observed in human stellate ganglia (n=4) using qRT-PCR. *Pnmt* expression was significantly lower than *Th* (p=0.0308, two-tailed paired Student's t-test). Data are represented as ΔC_T normalised counts ± SEM (b). *p<0.05, **p<0.01, ***p<0.001.

There was no significant difference in the levels of mRNA for *Th, Ddc, Dbh* or *Pnmt* between strains using stellate RNA samples from four-week rats. Conversely, a significant four-fold reduction in *Pah* mRNA expression in preSHR ganglia was observed compared to the expression in Wistar ganglia (p=0.0098, unpaired Student's t-test, Fig. 5.2a), mirroring the significant downregulation of this transcript in the RNA-seq dataset, further supporting the validity of these results. The transcripts encoding *Pnmt* and *Th* were also confirmed using qRT-PCR in four male human stellate ganglia (two left stellates, two right stellates, unpooled were obtained from 3 patients). The qRT-PCR raw counts were normalised to a control housekeeping gene *B2m,* using the ΔC_T method described by Schmittgen et al.,[332] and expressed as normalised count values. It was observed that *Pnmt* expression was significantly lower than *Th* (p=0.0308). Data were analysed using a paired Student's t-test and the graphical data points represent ΔC_T normalised counts ± SEM (Fig. 5.2b).

ELISAs were used to quantify the protein expression of TH and PNMT in stellate ganglia from young three- to five-week-old normotensive preSHR and Wistar (32 stellates, 16 rats/group, pooled stellates) or adult 19- to 20-week-old SHR and Wistar (20 stellates, 10 rats/group, pooled stellates). The concentration of TH was calculated for young Wistar (460.9 pg/ml ± 8.0 pg/ml), adult Wistar (406.6 pg/ml ± 31.6) young preSHR (89.1 pg/ml ± 11.4 pg/ml) and adult SHR (215.7 pg/ml ± 21.7 pg/ml, Fig. 5.3a). PNMT protein expression was calculated for young Wistar (525.7 pg/ml ± 8.7 pg/ml), adult Wistar (352.8 pg/ml ± 39.7 pg/ml), young preSHR (117.0 pg/ml ± 3.7 pg/ml) and adult SHR (362.7 pg/ml ± 70.1 pg/ml, Fig. 5.3b).

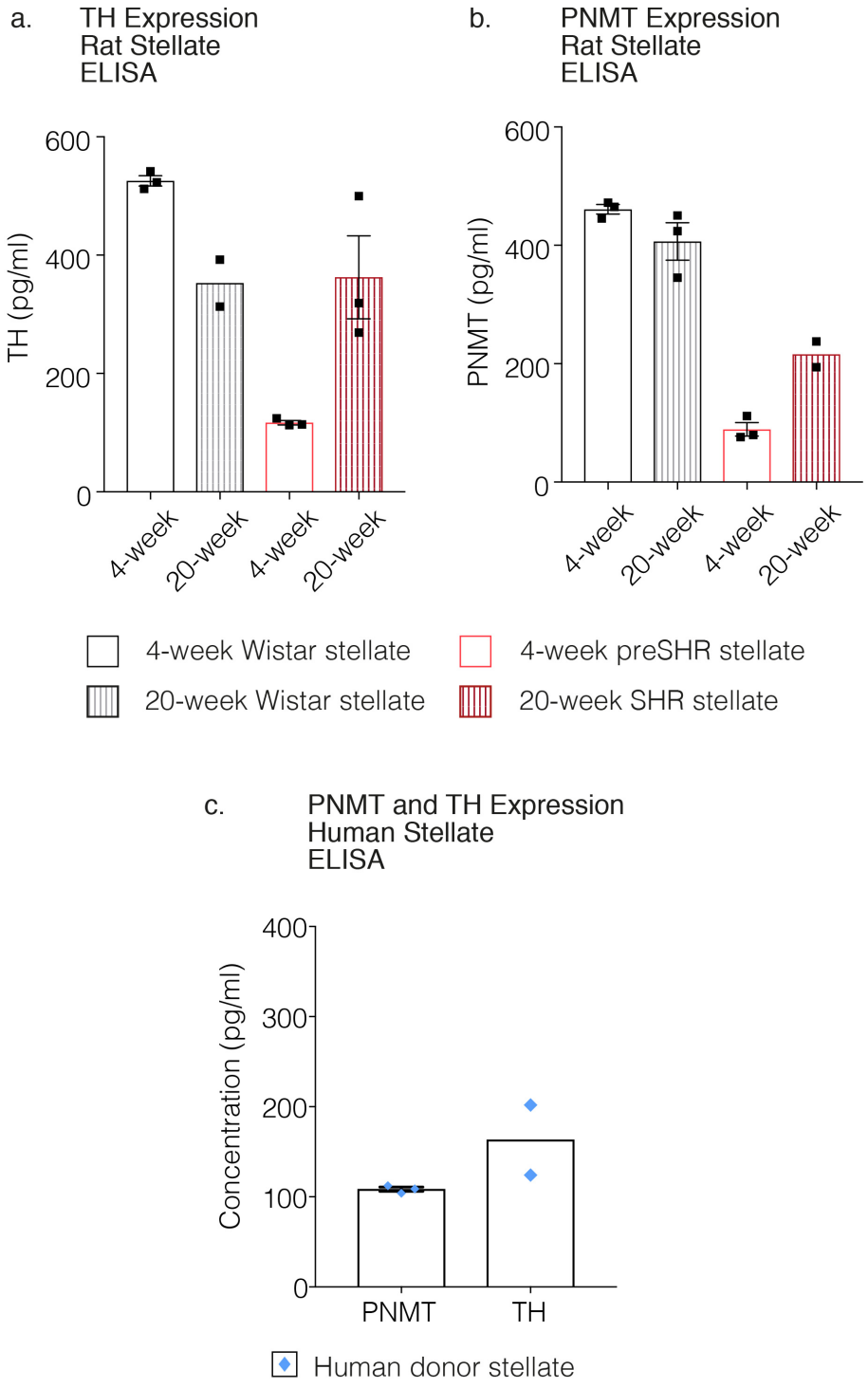


Figure 5.3. Rat and Human Stellate Ganglia Express PNMT
The protein expression of TH and PNMT was confirmed by ELISA on 3.5- to 5-week-old Wistar and preSHR stellates (32 stellates pooled, 16 animals/group) and 20-week-old Wistar and SHR stellates (32 stellates pooled, 16 animals/group). The concentration of β_1AR protein in rat stellate ganglia was calculated for (a) 4-week Wistar (460.9 pg/ml ± 8.0), 20-week Wistar (406.6 pg/ml ± 31.6), 4-week preSHR (89.1 pg/ml ± 11.4) and 20-week SHR (215.7 pg/ml ± 21.7). The concentration of PNMT protein in rat stellate ganglia was calculated for (b) 4-week Wistar (525.7 pg/ml ± 8.7), 20-week Wistar (352.8 pg/ml ± 39.7), 4-week preSHR (117.0 pg/ml ± 3.7) and 20-week SHR (362.7 pg/ml ± 70.1). In human stellate ganglia, expression of TH (163.0 pg/ml ± 38.8) and PNMT (108.4 pg/ml ± 2.4) was also detected (c). Data points depict mean ± SEM (2-3 technical replicates, pooled stellates).

TH (163.0 pg/ml ± 38.8 pg/ml) and PNMT (108.4 pg/ml ± 2.4 pg/ml) expression was also detected in human stellate ganglia, in 3 pooled stellates obtained from two patients (Fig. 5.3c). The data points indicate mean ± SEM (2-3 technical replicates). The samples used in the ELISA assays contained protein from 20 or 32 stellates, however, the stellates were homogenised and pooled into a single sample to obtain adequate protein concentrations for the ELISA assays therefore no statistical tests were conducted.

5.4.3 Total Catecholamine Concentration in Rat Stellate Ganglia

Elevated cardiac neurotransmission plays a key role in the pathophysiology of hypertension[436], therefore, to assess whether the presence of TH or PNMT in the stellate ganglia lead to physiological alterations in neurotransmitter production, cardiac-sympathetic ganglia from four-week preSHR and Wistar rats were homogenised and the total catecholamine content was quantified by HPLC-EC. The presence of both NA and Adr was observed in the rat stellate ganglia (Fig. 5.4). Unexpectedly, the concentration of NA was significantly greater in Wistar stellates (43.3 pg ± 2.2, n=8) compared with that measured in the preSHR stellate ganglia (29.8 pg ± 6.4, n=4, two-tailed unpaired Student's t-test, p=0.0294). Conversely, the concentration of Adr measured in the same samples was shown to be significantly elevated in the preSHR ganglia (14.1 pg ± 5.4, n=4) compared with that measured in Wistar stellates (3.9 pg ± 0.8, n=8, two-tailed unpaired Student's t-test, p=0.0332). Together, these data illustrate that a significant amount of NA is converted to Adr in prehypertensive states (Fig. 5.4).

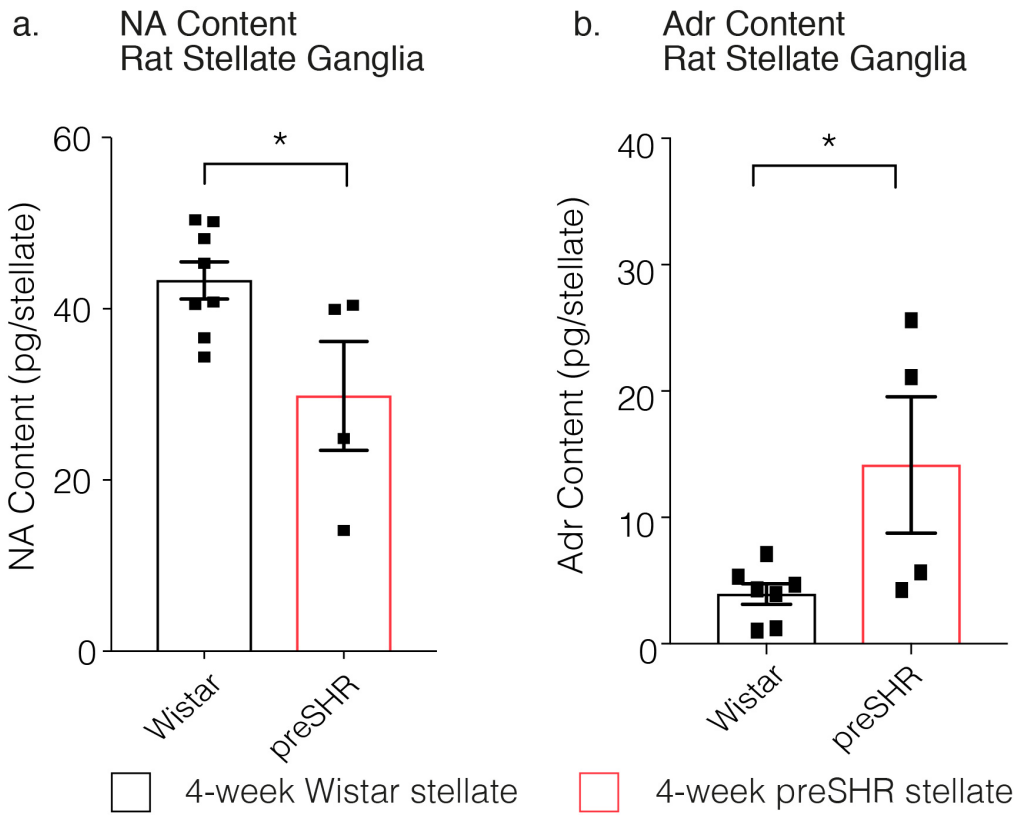


Figure 5.4. Total Catecholamine Concentration in Rat Stellate Ganglia
The presence of both NA and Adr was observed in the rat stellate ganglia (Fig. 5.4). Using HPLC-EC, it was observed that the concentration of NA was significantly greater in homogenised Wistar stellates (43.3 pg ± 2.2, n=8) compared with that measured in the preSHR stellate ganglia (29.8 pg ± 6.4, n=4, two-tailed unpaired Student's t-test, p=0.0294, a). Conversely, the concentration of Adr measured was shown to be significantly elevated in the preSHR ganglia (14.1 pg ± 5.4, n=4) compared with that measured in Wistar stellates (3.9 pg ± 0.8, n=8, two-tailed unpaired Student's t-test, p=0.0332, b). Data represents mean ± SEM. *p<0.05, **p<0.01, ***p<0.001. Each data point represents the concentration of NA or Adr measured in a single stellate, from a different rat.

5.4.4 Evoked Catecholamine Release from Rat Stellate Ganglia.

To determine whether the concentrations of NA and Adr measured in the rat stellate ganglia reflect the neurotransmitter-release profile, four-week Wistar and preSHR stellate ganglia were subject to electrical field stimulations. The ganglia were pre-bathed in desipramine (1 µM) to inhibit NA reuptake via the norepinephrine transporter (NET) for 10 minutes prior to electrical stimulation. Electrical-stimulation was conducted on single stellates and the experiments were at 37 °C in bicarbonate-buffered Tyrode's solution to mimic physiological conditions. A protocol of 5 Hz stimulations at 3 mA for 5 minutes was selected based on previous reported stimulation

parameters[333]. The presence of NA and Adr was observed in the perfusate from both preSHR and Wistar stellates (Fig. 5.4). A comparison of the concentrations of the released catecholamines from Wistar and preSHR stellate ganglia revealed a significant elevation in the levels of NA in the perfusate obtained from preSHR (4.3 pg ± 1.5, n=4) compared with Wistar (1.5 pg ± 0.3, n=8, two-tailed unpaired Student's t-test, p=0.0396). Moreover, in the same samples the concentrations of electrically-evoked Adr were significantly higher in preSHR ganglia (4.4 pg ± 1.4) compared with that measured in Wistar stellates (0.3 pg ± 0.03, two-tailed unpaired Student's t-test, p=0.0028), illustrating an alteration in neurotransmitter release profiles in disease (Fig. 5.5).

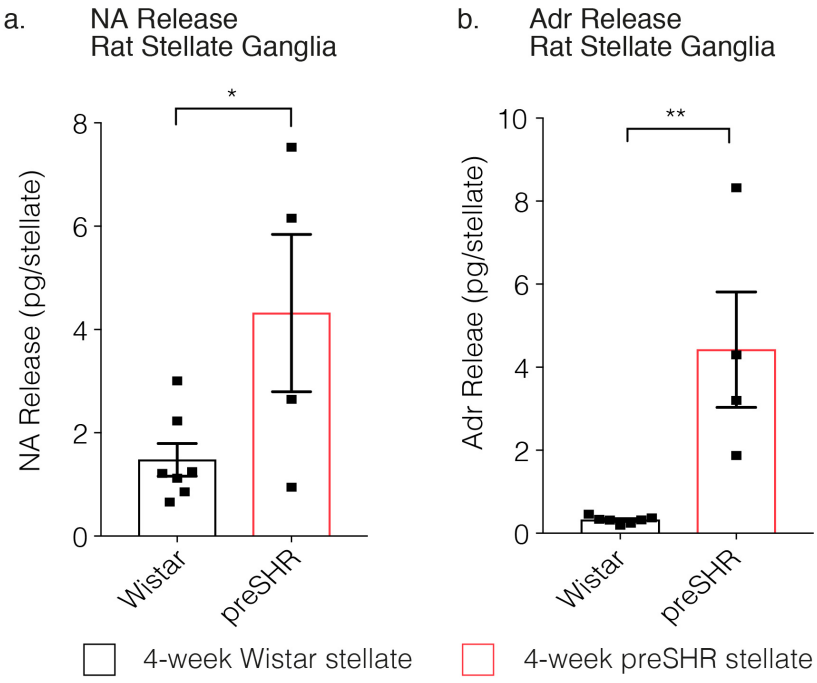


Figure 5.5. Evoked Catecholamine Release from Rat Stellate Ganglia
The presence of both NA and Adr was observed by HPLC-EC in the perfusate from both preSHR and Wistar stellates. Significantly higher concentrations of NA were measured in the perfusate obtained from preSHR (4.3 pg ± 1.5, n=4) compared with Wistar stellates (1.5 pg ± 0.3, n=8, two-tailed unpaired Student's t-test, p=0.0396, a). In the same samples, the concentrations of electrically-evoked Adr were significantly higher in preSHR ganglia (4.4 pg ± 1.4) compared with that measured in Wistar stellates (0.3 pg ± 0.03, two-tailed unpaired Student's t-test, p=0.0028, b). Data represents mean ± SEM. *p<0.05, **p<0.01, ***p<0.001. Each data point represents the concentration of NA or Adr measured in a single stellate, from a different rat.

5.5 Discussion

In this chapter, a combination of RNA-seq data, qRT-PCR, protein assays and HPLC-EC were applied to ascertain whether alterations in catecholamine synthesis are evident in the stellate ganglia of prehypertensive rats. The aim of this study was to assess whether the identification of PNMT expression in human and rat stellate ganglia led to the functional synthesis and release of physiological concentrations of Adr, that might play a role in the pathophysiology of hypertension.

The main findings of this chapter are:

1. RNA-seq and qRT-PCR confirmed the expression of the mRNA transcript encoding PNMT involved in the synthesis of Adr in stellate ganglia from human and rat.
2. The protein expression of PNMT was also confirmed and the concentration was measured by ELISA in stellate ganglia from human and rat.
3. HPLC-EC demonstrated detectable concentrations of Adr in Wistar and preSHR cardiac-stellate ganglia.
4. Total Adr content was increased in preSHR compared with Wistar stellate ganglia.
5. Evoked release concentrations of NA and Adr were increased in preSHR compared with Wistar stellate ganglia.

5.5.1 Stellate Ganglia Express Phenylethanolamine N-Methyltransferase

Elevated cardiac-sympathetic noradrenergic transmission plays a critical role in the aetiology of hypertension, yet a genetic basis underpinning elevated catecholamine synthesis has not been established. The RNA-seq dataset was used to identify the presence of mRNA transcripts encoding the catecholamine synthesising enzymes in stellate ganglia from 16-week Wistar and SHR[337,417]. As expected, the data highlighted the expression of all relevant transcripts, including phenylalanine hydroxylase (*Pah*), TH (*Th*), L-DOPA decarboxylase (*Ddc*) and dopamine β-hydroxylase (*Dbh*) (Fig. 5.1). Within this group, the transcripts encoding *Th*, *Ddc* and *Dbh* had the highest abundance where the level of expression fell within the most highly expressed genes in the rat stellate ganglia (Chapter Two, Table 3.2) thus reflecting a sympathetic catecholaminergic phenotype. The RNA-seq dataset also highlighted, somewhat unexpectedly, the expression of the mRNA transcript encoding PNMT (*Pnmt*), the enzyme required for the conversion of NA to Adr in Wistar and SHR stellate ganglia (Fig. 5.1).

The expression of transcripts involved in catecholamine synthesis was confirmed by qRT-PCR in human and rat stellate ganglia (Fig. 5.2), where together with the RNA-seq dataset, it was determined that there was no increase in mRNA transcript expression of *Th*, *Ddc*, *Dbh* or *Pnmt* in the hypertensive rat model. Indeed, if anything the mRNA expression tended towards a decrease in the SHR, where a significant four-fold reduction was observed in the transcript encoding *Pah* by qRT-PCR. Nevertheless, transcript levels do not necessarily correlate with protein expression, and the activity of enzymes are known to be critically dependent on pH[437], substrate concentration, co-factor activity[438] and spatial proximity to their substrates. Moreover, catecholamine biosynthesis is subject to further regulatory processes including sensitivity to nerve stimulation[438], allosteric influence particularly via kinase phosphorylation [438-440], and is also sensitive to feedback inhibition via transcriptional regulation[439]. As such, the aims of this chapter were to measure the concentrations of NA in Wistar and preSHR stellate ganglia, and

to ascertain whether the mRNA expression of *Pnmt* leads to detectable PNMT protein concentrations.

ELISA assays confirmed the presence of PNMT protein within rat and human stellate ganglia providing physiological context and supporting a role for PNMT-dependent activity in human cardiac-sympathetic ganglia (Fig. 5.3). What is the relevance for the observation of presynaptic PNMT? In 1981, Brown and Macquin proposed the 'Adrenaline Hypothesis' of essential hypertension[430], that highlights a dominant role for Adr in facilitating NA release through actions at presynaptic βARs[441]. Two simultaneous observations led to the concept of Adr as a pathological entity in the progression of hypertension. First, it was observed that Adr infusions underpin sustained increases in blood pressure post-infusion[441-443]; and secondly, that plasma Adr is elevated in hypertensive patients[430,444]. This hypothesis was strongly supported by clinical and preclinical observations [203,442,445-448]. The source of Ad, however, has not yet been resolved, with most reports suggesting chronic neuronal uptake and enhanced release of circulating Adr derived from the adrenals[209,403,430-434]. Emerging evidence has pointed to the possible synthesis of Adr in sympathetic nerves in the forearm of patients with stress disorder[435], however, the *in situ* synthesis of Adr and a role for cardiac-sympathetic Adr in the aetiology of hypertension is far from well-established. Our identification of PNMT mRNA and protein expression in human and rat cardiac-sympathetic ganglia supports the findings of these earlier studies that Adr is synthesized in sympathetic stellate ganglia in disease. Additionally, a recurrent feature in human and animal models of hypertension is a reduction in norepinephrine reuptake transport (NET), leading to larger and sustained extracellular catecholamine concentrations[284,435,449,450]. Emerging evidence suggests that PNMT may also act as a DNA methylase, silencing NET transcription that may underpin the observed NET phenotype previously identified in the preSHR[435] and human cardiac stellate ganglia in hypertension[284].

5.5.2 Adrenaline Synthesis and Release from Stellate Ganglia

In the present study, HPLC-EC was used to investigate whether the presence of PNMT plays a functional role in converting NA to Adr in rat stellate ganglia. The total catecholamine content was measured in samples obtained from preSHR and Wistar rats (Fig. 5.4) where a significant decrease in total NA content was observed in preSHR ganglia (74.8 % of total catecholamine content) compared to the NA content calculated in Wistar ganglia (91.5 % of total catecholamine content). Conversely, Adr content was found to be significantly elevated in preSHR ganglia (25.2 % of total catecholamine content) compared with that measured in Wistar stellate ganglia (8.5 % of total catecholamines), highlighting a switch in neurotransmitter profiles in prehypertension that occurs prior to overt increases in arterial blood pressure. In addition to measuring the total catecholamine content, the concentrations of evoked-catecholamines released from preSHR and Wistar ganglia were quantified following an electrical field stimulation protocol. It was observed that both Adr and NA evoked-release were significantly elevated in the perfusate collected from the preSHR ganglia compared with Wistar. This alteration in neurotransmitter profiles is further demonstrated by considering the ratios for NA:Adr release, where the percentage ratio of NA:Adr released from Wistar ganglia was calculated as 91 % : 9 %; whereas in preSHR ganglia the ratio of catecholamines released (NA:Adr) was 44 % : 56 % respectively (Fig. 5.4). Interestingly, the total amount of catecholamines released from a single stellate ganglion during electrical stimulation remained fairly similar between the strains (~11-12 pg).

What is the relevance of elevated Adr synthesis in preSHR stellate ganglia, prior to overt increases in arterial blood pressure? The ‘Adrenaline Hypothesis’ of hypertension proposes that stress and subsequent small incremental increases in Adr plays a major role in the aetiology of hypertension, through chronic stimulation of sympathetic nerves that elevates NA release [430]. The presence of presynaptic βARs on the cardiac-sympathetic ganglia of human and rat has

been previously described in Chapter Four. It was observed that activation of sympathetic βARs with ISO led to pathological elevations in cAMP-PKA-Ca^{2+} activity in the prehypertensive rat strain, and a dominant effect of β_2AR activity was demonstrated. Importantly, Adr has a ten-fold higher affinity for β_2AR than NA (EC_{50} 5.2 nM, 53.7 nM respectively) and is capable of generating three times more cAMP than NA via β_2AR activation; a feature that may be mimicked by ISO due to similarities in efficacy[451]. Subsequently, the high efficacy of Adr (and the relatively low efficacy of NA) at β_2ARs has been shown to result in significant Adr-dependent NA release that has been identified in a wide variety of peripheral tissues in rat, rabbit and human[404,405,431]. Indeed, low concentrations of Adr (0.1-10 nM) have been shown to be 100-500 times more potent than NA for enhancing NA transmission[404,452-454], where Adr may have a more sustained effect on NA release, due to the extended tissue half-life of Adr compared with NA[452].

Support for a pathological role involving elevated sympathetic β_2AR activation may also be seen in patients treated for chronic asthma and COPD with β_2AR agonists; where tachycardia is a common side effect of short-term administration, and long-term treatment is associated with several CVD and adverse cardiac events[455-457]. Moreover, a 20-year follow-up of the Oslo study on normotensive, prehypertensive and male patients with established hypertension has identified arterial Adr as an significant independent predictor of blood pressure elevation[433]. Together, these studies support the observations in this chapter that highlight a role for Adr in the pathophysiology of sympathetic over-activity in hypertension[458].

5.6 Limitations

In this study, the enzymes involved in catecholamine synthesis in the cardiac-sympathetic ganglia were investigated. The limitations of the RNA-seq and qRT-PCR analyses have been described in detail in Chapter Three and Chapter Four so will not be described in further detail here. There were several limitations to this study. First, researchers in the field of hypertension

are strongly divided in the cause and aetiology of chronically elevated blood pressure due to the polygenic nature of the disease. As such, the Adr hypothesis of essential hypertension never gained full traction despite being strongly supported by clinical and preclinical observations[203,442,445-448]. Secondly, the SHR, a model of hypertension, is also a model of attention-deficit/hyperactivity disorder (ADHD), a disease commonly associated with stress[32,33]. In this study, the presence of Adr was observed in sympathetic stellate ganglia, however, a relationship between chronic stress and sympathetic PNMT has been previously described[428,435], therefore the use of a stress-related model may affect Adr synthesis and activity-dependent sympathetic neurotransmission. Nevertheless, PNMT mRNA and protein expression was also detected in stellate ganglia obtained from human donors, maintaining the integrity of the SHR model in this context. Thirdly, although protein concentrations of PNMT were measured, limited datasets were obtained due to the high requirement of protein in each sample, therefore, no statistical analyses could be conducted. Fourthly, the activity of catecholamine synthesising enzymes may not be directly related to transcript and protein expression levels. In light of this, catecholamine concentrations were measured using a sensitive approach (HPLC-EC) to assess the net effect of transmitter synthesis pathways. Therefore, although the mRNA expression of catecholamine synthesising enzymes appeared to trend towards a reduction in disease, the overall outcome was an elevation in catecholamine release in preSHR ganglia, that did not directly reflect the intracellular concentrations of NA and Adr. In addition, the concentrations of NA and Adr measured by HPLC-EC cannot be explained as pg/mg total protein, as the total protein in one stellate ganglion could not be measured prior to running through the HPLC column, therefore catecholamine content measured in this chapter may be influenced by the size of the stellate ganglion; nevertheless, the absolute catecholamine concentration found in a single stellate was measured using accurately by HPLC-EC. Further experiments are required to investigate the regulators involved in catecholamine release that underpin elevated transmission in stellate ganglia from preSHR.

5.7 Conclusion

This chapter provides evidence for presynaptic synthesis of Adr within the cardiac-sympathetic ganglia of human and rat, where elevated concentrations of Adr are synthesised and released at the end-organ in prehypertension. NA and Adr were shown to be released in an activity-dependent manner from preSHR sympathetic ganglia and Wistar rat, where higher concentrations of both catecholamines were released from preSHR rat stellates. Elevated Adr transmission may act preferentially on presynaptic sympathetic β_2ARs to increase cAMP generation and PKA activity, that enhances $[Ca^{2+}]_i$ levels and sympathetic neurotransmission in disease, in a manner akin to positive feedback. Together these data raise the possibility for a causal role for Adr in the aetiology of neurogenic hypertension. These data also suggest that neurotransmitter switching occurs prior to increases in arterial blood pressure, where elevated Adr may play a role in sympathetic over-activity through the activation of presynaptic sympathetic β_2ARs, elevating neurotransmission in hypertension. Figure 5.6 depicts a model figure describing the current hypothesis for a presynaptic role for Adr in healthy and prehypertensive states, and highlights potential sites for neural phenotypic targeting in disease.

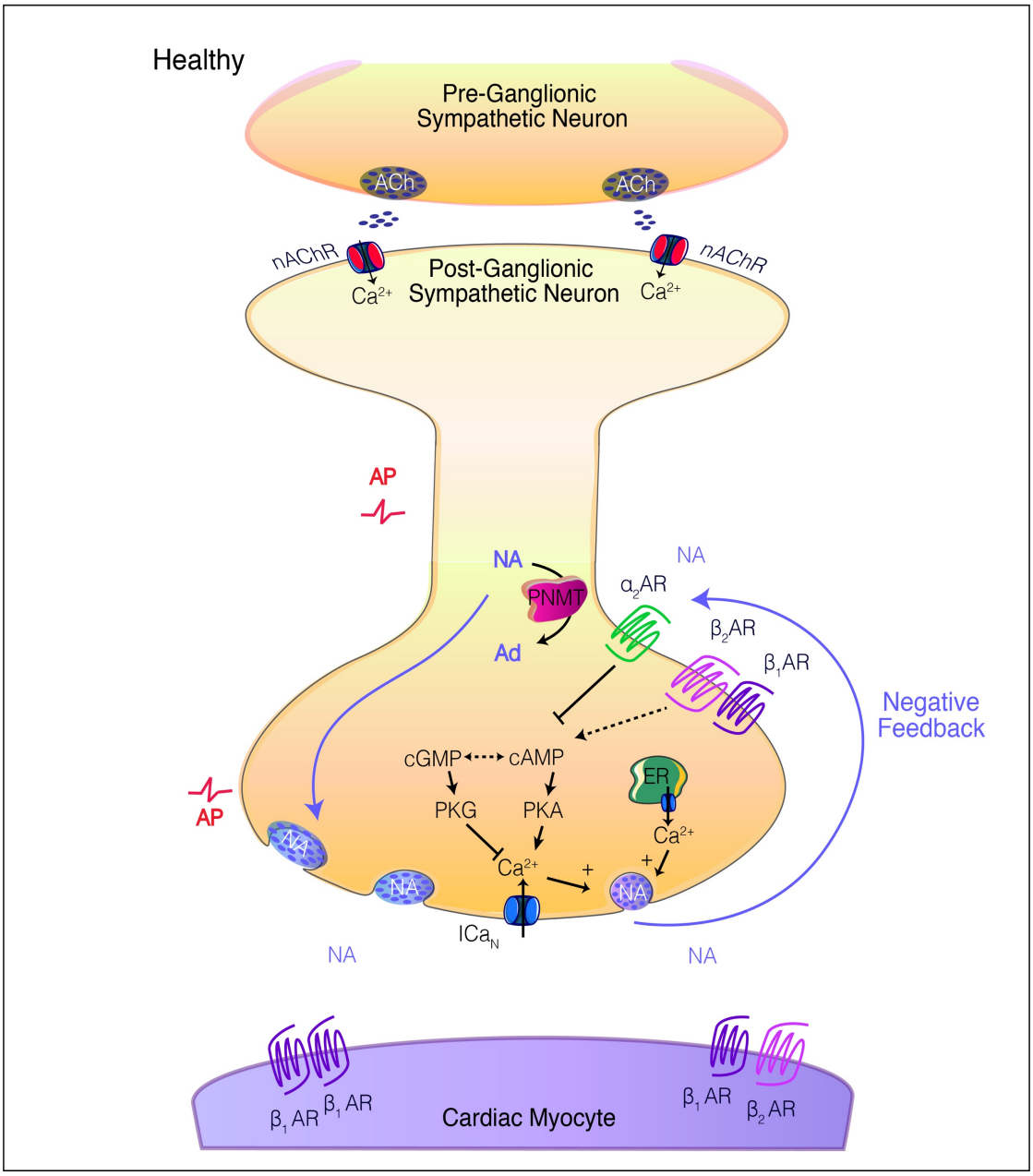


Figure 5.6a. Intracellular Signalling in Healthy Neurons
In healthy sympathetic stellate neurons, Ca^{2+} dependent exocytosis facilitates the release of NA onto cardiac myocytes, where post-synaptic β_1ARs and β_2ARs are activated. Increases in extracellular NA acts on presynaptic α_2ARs, and presynaptic β_1ARs and β_2ARs to a small degree. Acute regulation of cAMP and cGMP signalling is maintained by PDEs. cAMP generation and PKA activity increases $[Ca^{2+}]_i$ via phosphorylation of the *N*-type Ca^{2+} Channel (I_{CaN}; $Ca_V2.2$); endoplasmic reticulum (ER) store and mitochondrial Ca^{2+} release.

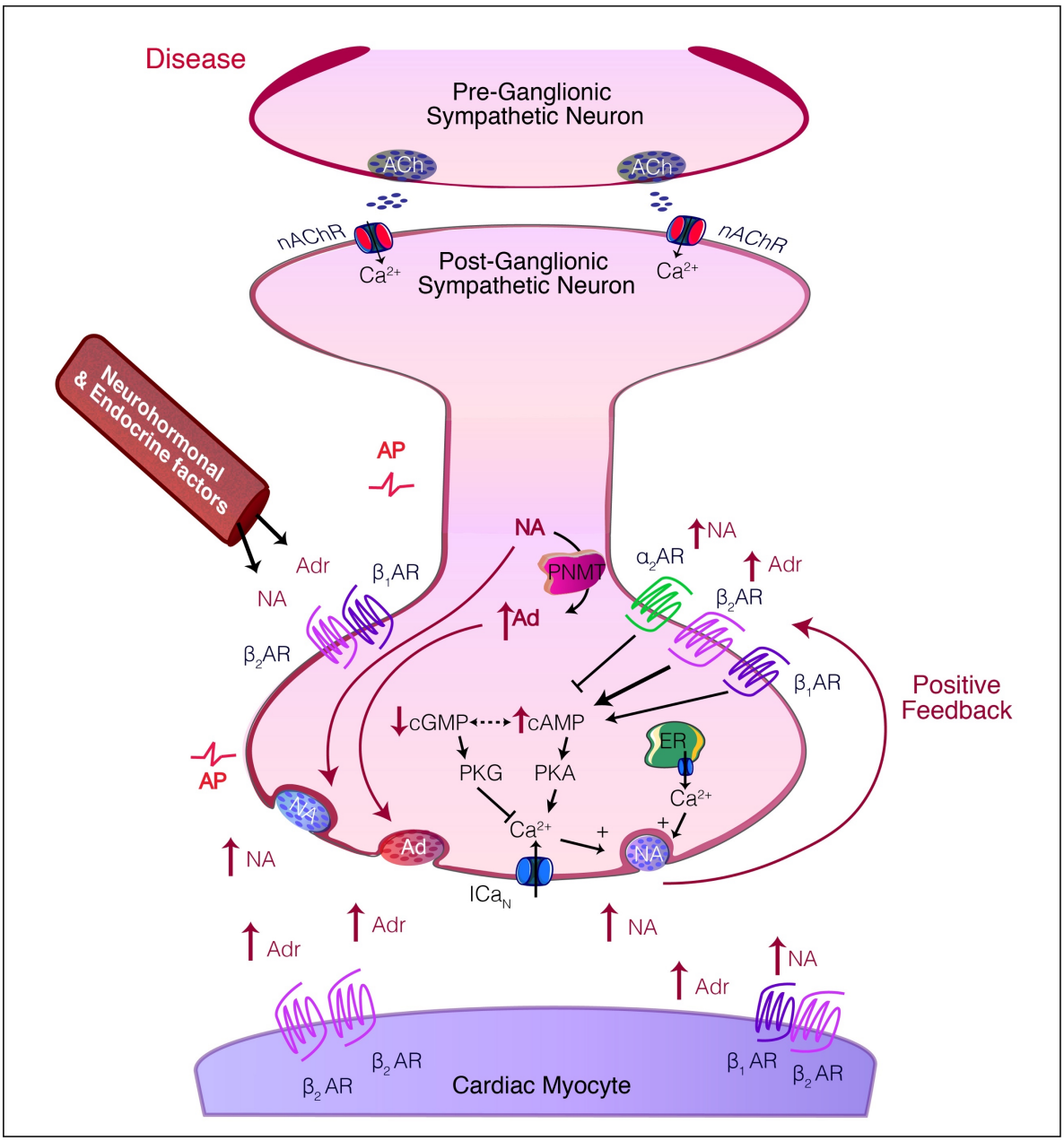


Figure 5.6b. Intracellular Signalling in Diseased Neurons
In diseased sympathetic stellate neurons, Ca^{2+} dependent exocytosis facilitates the release of NA and Adr onto cardiac myocytes, where post-synaptic β_2ARs are upregulated and preferentially activated. Elevations in NA and Ad release acts on presynaptic βARs, where Ad preferentially stimulates β_2ARs, augmenting cAMP generation and PKA activity in prehypertension. Increased PKA activity raises $[Ca^{2+}]_i$ via phosphorylation of the *N*-type Ca^{2+} Channel (I_{CaN}; $Ca_V2.2$), exacerbating the Ca^{2+} phenotype that may contribute to the initiation of hypertension.

6

Angiotensin Synthesis in the Sympathetic Stellate Ganglia

6.1 Introduction

The Renin-Angiotensin-Aldosterone system plays a central role in the physiological regulation of arterial blood pressure and fluid volume homeostasis[66,459]. AngII is a major effector of the RAS that mediates its effects in a wide range of organs via selective activation of AngII receptors type 1 and 2 (AT_1R, AT_2R) [78,460-464]. Plasma and tissue levels of NA, Adr, AngII, aldosterone and other mediators are significantly altered in hypertension and heart failure and correlate with the severity of disease[76,80,193,214,393-397]. Indeed, increased RAS signalling is evident in hypertension[76,214,394,395,465-467], heart failure[80,200,468-470] and post-myocardial infarction[471-477], where AngII-AT_1R activation impairs Ca^{2+} handling[465,471,478], and elevates sympathetic transmission[81,472,479-481], cardiac hypertrophy[200,214,467,482-486] vascular remodelling[461,487-490], and pro-inflammatory events[88,145,491].

In contrast, Angiotensin 1-7 (Ang1-7) a bioactive metabolite of AngII, opposes the effects of AT_1R via activation its partner receptor, Mas[492-494], a GPCR coupled to NO generation and cGMP signalling pathways[494]. Mas receptor knock out and Ang1-7 overexpression transgenic models have highlighted the importance of Ang1-7-Mas signalling in regulating cardiovascular physiology and haemodynamics through actions in the CNS[494-497], myocardium[498-500], vasculature[494,501-504] and kidney[494]. This axis is now considered a major counter-regulatory pathway for endogenous protection against several CVDs[474,496-501,504-512]. Therapeutic inhibition of classical RAS signalling is an effective tool for the treatment and management of renal and CVDs[459,513-517] and blood pressure maintenance[5,85,86,401,459,513,514,517-520]. Nevertheless, the precise mechanisms, source/s of angiotensins and site/s of action are not clear[76,513,518,521].

6.2 Chapter Aims

This chapter investigated the potential for an intracrine RAS within cardiac-sympathetic stellate ganglia of human and rat and to assess whether concentrations of RAS proteins are altered in models of hypertension. A range of techniques were applied to demonstrate the expression of key proteins and enzymes involved in the synthesis of AngII, including RNA-seq, qRT-PCR, ELISA assays, in addition to enzyme immunoassays and fluorometric enzyme activity assays. To assess the release of angiotensin peptides in an activity-dependent manner, rat stellates were electrically stimulated and release concentrations were measured. I am the first author on a manuscript describing this work that is currently in review.

The specific aims of this chapter were to:

1. Investigate whether the key enzymes involved in AngII including angiotensinogen (*Agt*), renin (*Ren*), and the Angiotensin Converting Enzymes (*Ace, Ace2*) are present in the rat cardiac-sympathetic ganglia, providing evidence for an intracrine RAS system.
2. Assess whether key AngII synthesising enzymes and precursor proteins are also evident on human sympathetic stellate ganglia, to provide physiological context.
3. Establish whether the activity of AngII synthesising enzymes are impaired in the stellate ganglia in hypertension leading to alterations in AngII synthesis.
4. Investigate whether there exists an Ang1-7-Mas receptor signalling axis in sympathetic stellate ganglia of human and rat, and establish whether this is altered in hypertension.
5. Assess whether AngII or Ang1-7 are released in an activity dependent manner from stellate ganglia and ascertain whether these concentrations are altered in hypertension.
6. Establish whether angiotensin-related receptors are present on sympathetic ganglia of human and rat, that may provide context for AngII and Ang1-7 local autocrine or paracrine signalling within the cardiac-sympathetic stellate ganglia.

6.3 Methods

6.3.1 Animals

Three- to four-week-old young male prehypertensive SHRs, 12-to 16-week or 18- to 20-week-old adult male SHRs with established hypertension and age-matched normotensive Wistar control rats were obtained from Envigo, UK. All experiments were performed in accordance with the UK Home Office Animal Scientific Procedures Act 1986 (ASPA) and approved by the University of Oxford (PPL 30/3131; David J. Paterson).

6.3.2 Human Donor Stellates

For clinical samples, human ganglia were extracted at UCLA and shipped on dry ice in RNA*later*® RNA Stabilization Solution (ThermoFisher). Human donor characteristics are included in Chapter Two in the General Methods section.

6.3.3 Rat Sympathetic Stellate Ganglia Extraction

Rats were anaesthetised in an induction chamber (3-5 % isoflurane) and humanely killed by a Home Office approved Schedule 1 method, overdose of pentobarbital (Euthatal, 200 mg/ml) and exsanguination prior to stellate ganglia dissection.

6.3.4 Neuronal Isolation

For neuronal cultures, sympathetic stellate ganglia were extracted from three- to four-week-old Wistar and age-matched preSHR. Stellates were dissected, de-sheathed, and dissociated into a single-cell suspension for immunocytochemistry experiments as described in Chapter Two.

6.3.5 Immunocytochemistry

Cardiac-sympathetic neurons were fixed onto glass coverslips and stained with the appropriate antibodies for TH and AT_1R. Neurons were imaged using 40X or 60X objectives on a confocal microscope (Live Cell Olympus Inverted Confocal or Zeiss LSM 880 Airy Scan Upright Confocal) as described in Chapter Two. Z-stack images were edited and cell sizes were measured using Fiji software (ImageJ)[2,3].

6.3.6 RNA Extraction and RNA Sequencing Analysis

RNA was extracted from rat and human stellate ganglia using the protocols described in Chapter Two. The RNA-seq dataset described in Chapter Three, was used to identify the mRNA transcripts encoding the key enzymes involved in RAS synthesis and angiotensin receptors in 16-week-old rat stellate ganglia. Differentially expressed genes at the Benjamini-Hochburg p.adj<0.05 level were imported into The Database for Annotation, Visualization and Integrated Discovery (DAVID, v6.8) [329] to obtain information intracellular pathway enrichment using the Kyoto Encyclopedia of Genes and Genome (KEGG) analysis tool[331,522,523] using the parameters described in Chapter Two. The count filter was set to a minimum limit of 5 genes per group.

6.3.7 Quantitative Real-Time Polymerase Chain Reaction

The presence of genes encoding angiotensin-synthesising enzymes and precursors identified by RNA-seq, was validated by qRT-PCR in RNA extracted from stellate ganglia from four-week and 16-week-old normotensive and hypertensive rats, as well as in human stellate ganglia. In this chapter, the RNA transcripts encoding angiotensinogen *(Agt),* renin *(Ren)* angiotensin converting enzyme (ACE, *Ace*), angiotensin converting enzyme 2 (ACE2, *Ace2),* human AngII type 1 receptor (AT_1R, *Agtr1*), rat AngII type 1A receptor ($AT_{1A}R$, *Agtr1a;* rat), rat AngII type 1B receptor ($AT_{1B}R$, *Agtr1b;* rat), AngII type 2 receptor (AT_2R, *Agtr2*) and the Ang1-7 receptor (Mas,

Mas1) were validated by qRT-PCR. A full list of the primers and appropriate dilutions are included in Chapter Two. Data displayed in the results section depicts the gene of interest normalised to *B2m,* however, each primer was analysed against two housekeeping genes (*B2m* and *Gapdh*) for validation and accuracy of qRT-PCR data. For qRT-PCR analysis, the relative amount of each transcript was calculated using the comparative (C_T) method ($\Delta\Delta C_T$, rat; ΔC_T, human)[332].

6.3.8 Protein Extraction

Protein was extracted from 12-14 stellates obtained from three- to four-week young Wistar or preSHR stellate ganglia. In alternative experiments, protein was extracted from 10-12 stellates obtained from 12- to 14-week-old adult rats or 16- to 20-week-old adult Wistar or SHR. Rat stellates were pooled and homogenised to obtain adequate protein concentrations and samples were normalised using a protein assay (BioRad DC). Three separate samples were acquired per strain (Wistar, SHR) within each age group (three- to four-week, 13- to 15-week, 16-to 18-week). Where no significant difference was observed in the protein or enzyme activity assays between the 13-week and 16-week age-groups, datasets were combined to increase the power of the data, as hypertension and sympathetic hyperactivity are already established[125,139,143,145,147-149,151]. Protein from one human stellate (80 mg) was used per sample and the concentration normalised. Rat and human stellates were cleaned, de-sheathed and homogenised in ice-cold dPBS without Ca^{2+} or Mg^{2+}.

6.3.9 Evoked-Release of Angiotensin Peptides by Field Stimulation

To investigate the concentrations of AngII or Ang1-7 electrically released from cardiac-sympathetic ganglia, whole fresh ganglia were dissected from young three- to four-week-old young preSHR (n=3), age-matched Wistar rats (n=3), adult 14- to 15-week-old SHR (n=8) and age-matched Wistar rats (n=6). For each experiment, one ganglion was cleaned, de-sheathed

and allowed to recover in carbogenated bicarbonate-buffered Tyrode's solution (5 min, 37 °C, 95 % O_2 / 5 % CO_2). A list of the buffer constituents is included in Chapter Two. For the AngII release experiments, stellate ganglia were incubated in fresh carbogenated bicarbonate-buffered Tyrode's containing an ACE2 inhibitor (DX600 100 µM; BioVision) to prevent AngII degradation (5 min, 37 °C). Ganglia were electrically stimulated (5x) using a DG2A train generator and DS3 constant current stimulator (Digitimer Ltd.) using parameters that were adapted from a previous electrical stimulation method[311](3 mA, 5 Hz, 30 s pulse every 90 s, 7.5 minutes). The perfusate was collected, snap frozen in liquid nitrogen and stored at -80 °C .

6.3.10 Enzyme-Linked Immunosorbent Assay and Enzyme Immunoassay

In rat stellate samples, the protein concentrations of Agt and Ang1-7 were established using sandwich ELISAs and in human stellate ganglia, the protein concentrations of Agt, Ren, Ang1-7 and ACE2 were measured by ELISA. In human and rat stellate samples, AngII concentrations were established using EIA. Each assay was conducted as per the manufacturer's recommendations. A full list of the assay kits, as well as protein dilutions are included in Chapter Two. The concentration and activity of the proteins of interest were quantified using a standard curve generated from the supplied standards.

6.3.11 Fluorometric Enzyme Activity Assays

The enzymatic activity of Ren, ACE and ACE2 in rat stellate ganglia were established using fluorometric activity assays. The enzyme activity of ACE was also established in human stellates. A full list of the assay kits, as well as protein dilutions and the manufacturers are included in Chapter Two. The activity of the proteins of interest were quantified by first constructing a standard curve (0-100 %) obtained from the supplied standards. The data was fit to a sigmoidal $\log_{10}$(molar concentration) curve and each of the sample values were interpolated (GraphPad Prism, v7). The interpolated values were un-logged to calculate the

concentration in each sample (pmol), and the three technical replicates were averaged. The values were divided by the mass of protein in each well (mg) to obtain a value for enzyme concentration (pmol/mg) as calculated using Equation 5. Enzyme concentration was divided by time (minutes) to calculate enzyme activity (mU/mg) using Equation 6.

Equation 5.

$$(\mathrm{E})\ \text{Enzyme concentration}\ (\mathrm{pmol/mg}) = \frac{B * D}{\text{Tissue mass}}$$

Where:

B= Interpolated value based on standard curve slope (pmol)

D = Sample dilution factor

Tissue mass = Milligrams of tissue in the sample

Equation 6.

$$\text{Enzyme activity}\ (\mathrm{mU/mg}) = \frac{E}{\Delta \mathrm{T}}$$

Where:

E = Enzyme concentration (pmol/mg)

ΔT = reaction time (minutes). The reaction times were 20 minutes for calculating renin activity, 35 minutes for calculating ACE activity and 25 minutes for calculating ACE2 activity.

6.3.12 Statistical Analysis

Fluorescent microscopy, qRT-PCT and ELISA data were analysed using GraphPad Prism software (v6/7). When the data passed normality tests (D'Agostino-Pearson omnibus or Shapiro-Wilk test [313]) unpaired or paired two-tailed Student *t*-tests, or a one or two-way analysis of variance (ANOVA) were used. When the data were not normally distributed, the appropriate nonparametric tests were used with the specific statistical test reported in the figure legend. All

data are expressed as the mean ± SEM. Statistical significance was accepted at $p<0.05$ unless otherwise described. RNA-seq data were analysed using a Salmon-DESeq2 protocol[322,327] as described in Chapter Two.

6.4 Results

6.4.1 Angiotensin II Synthesis Pathway in Sympathetic Stellate Ganglia

The transcriptome of the sympathetic stellate ganglia was sequenced using ganglia extracted from 16-week-old male Wistar rats (n=4 stellates) and age-matched SHR (n=4 stellates) with established hypertension and sympathetic hyperactivity[150], as described in Chapter Two. In the RNA-seq dataset, mRNA encoding the enzymes classically involved in the synthesis of the AngII peptides were identified in adult rat stellate ganglia, where relevant transcripts included Angiotensinogen (*Agt),* Renin (*Ren*) and Angiotensin Converting Enzyme (*Ace*) (Fig. 6.1). The KEGG group 'Renin Secretion' was found to be significantly under-represented in the SHR ganglia ($p<0.01$). The differentially expressed genes in this group associated with Renin Secretion, included *Adrb2, Ptger2, Gnai3, Gucy1a3, Prkacb, Prkg2, Cacna1c, Adora1, Adcyap1* (Fig. 6.1). A list of the gene names, respective fold changes and levels of significance are reported in Tables 6.1 and 6.2.

6.4.2 Ang II Precursor Transcripts in Stellate Ganglia

To validate the presence and relative levels of the classical AngII synthesising enzyme transcripts *(Ren, Ace)* and its precursor *(Agt)* in rat stellate neurons, qRT-PCR was performed using RNA from young four-week Wistar and preSHR ganglia (n=4 rats/group, unpooled), and 16-week adult SHR (n=4 rats/group), relative to age-matched Wistar rats (n=5 rats, Fig. 6.2). The mRNA expression of *Agt* and *Ace* were significantly decreased in young preSHR (n=3-4 samples/group, two-tailed unpaired Student's t-test, $p=0.0045$, $p=0.0048$) and adult SHR (n=4 samples/group, two-tailed unpaired Student's t-test, $p=0.0212$, $p=0.0469$) relative to age-

matched Wistar rats (n=4 samples/group). *Ren* mRNA expression was significantly upregulated in 16-week-old SHR (n=4 samples/group) compared with the expression recorded in adult Wistar rats (n=5 samples/group, unpaired two-tailed Student's t-test, $p<0.0001$, Fig. 6.2). The qRT-PCR data were analysed using the $\Delta\Delta C_T$ method[332] where raw counts were first normalised to a control housekeeping gene *B2m,* and SHR data were subsequently normalised to Wistar qRT-PCR counts. ΔC_T values are included in the appendix (Fig. 8.6). The presence of the transcripts encoding *Agt, Ren* and *Ace* were confirmed by qRT-PCR in four human stellate ganglia (two left, two right unpooled stellates from 3 patients). Data were expressed as normalised count values and analysed by one-way ANOVA using a Bonferroni post-hoc test. In the human stellates, *Ren* expression was found to be significantly lower than *Agt* ($p<0.0001$) and *Ace* ($p=0.0204$), where *Ace* expression was also significantly lower than *Agt* ($p=0.0005$; Fig. 6.2). The qRT-PCR raw counts were normalised to a control housekeeping gene *B2m,* using the ΔC_T method described by Schmittgen et al., [332].

Table 6.1. The KEGG Group 'Renin Secretion' (rno04924)

KEGG ID	KEGG Description	Count	Fold Enrichment	p. value	p. adjusted
rno04924	Renin secretion	9	3.50	3.85E-03	1.07E-01

The KEGG functional enrichment pathway representing 'Renin Secretion' (rno04924) was significantly under-represented in the SHR ganglia in the RNA-seq data

.

Table 6.2. Differentially Expressed Genes in KEGG Group 'Renin Secretion'

Gene Name	Description	RNAseq	
		Log_2 Fold Change	p. adjusted
Adcyap1	adenylate cyclase activating polypeptide 1	-1.564	3.69E-11
Prkg2	protein kinase, cGMP-dependent, type II	-1.314	1.81E-09
Cacna1c	calcium voltage-gated channel subunit alpha1 C	-1.125	8.53E-06
Prkacb	protein kinase cAMP-activated catalytic subunit beta	-0.499	2.26E-03
Gucy1a3	guanylate cyclase 1 soluble subunit alpha 3	-0.422	7.51E-03
Adrb2	adrenoceptor beta 2	-0.932	9.45E-03
Adora1	adenosine A1 receptor	-0.773	2.34E-02
Gnai3	G protein subunit alpha i3	-0.388	2.38E-02
Ptger2	prostaglandin E receptor 2	-0.850	4.19E-02

Nine genes within the KEGG group representing 'Renin Secretion' (rno04924) were downregulated. These genes highlight the involvement of adenylyl/guanylyl cyclase, cN and protein kinase activity in the regulation of renin secretion.

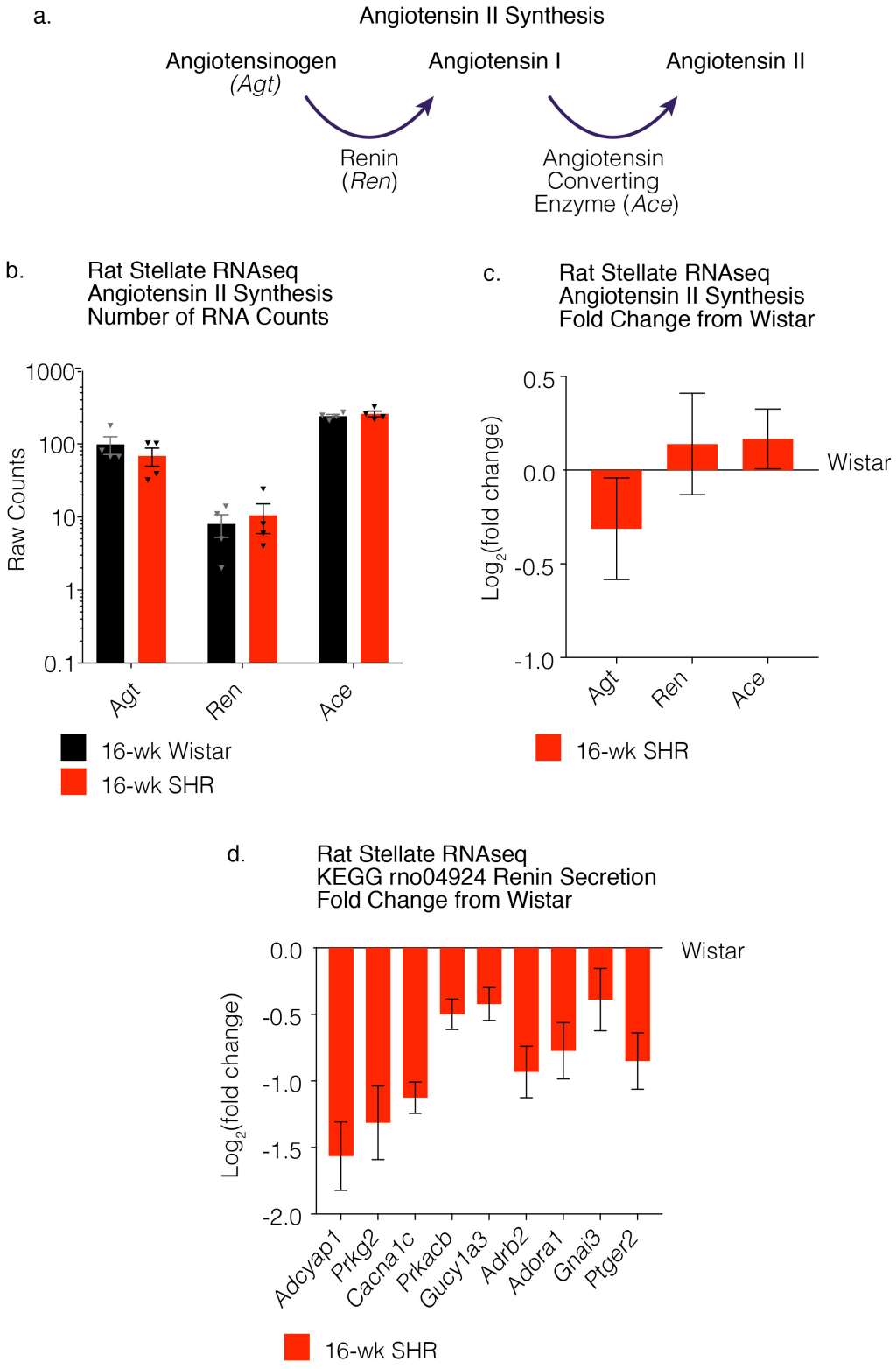


Figure 6.1. RNA-seq Highlights Angiotensin synthesis in Rat Stellate Ganglia
The AngII synthesis pathway is outlined (a). RNA-seq identified the presence of transcripts involved in AngII synthesis including Angiotensinogen (Agt), Renin (Ren), Angiotensin Converting Enzyme (Ace) transcripts. Transcript abundances were not found to be differentially expressed in SHR vs. Wistar ganglia (Salmon-DESeq2 method[327]). Data points represent raw counts ± SEM (b). RNA-seq transcripts are represented as log2(fold change) ± SEM normalised to Wistar (c). The differentially expressed genes in the KEGG group (rno04924) representing 'Renin Secretion' are depicted as $\log_2$(fold change) ± SEM (d).

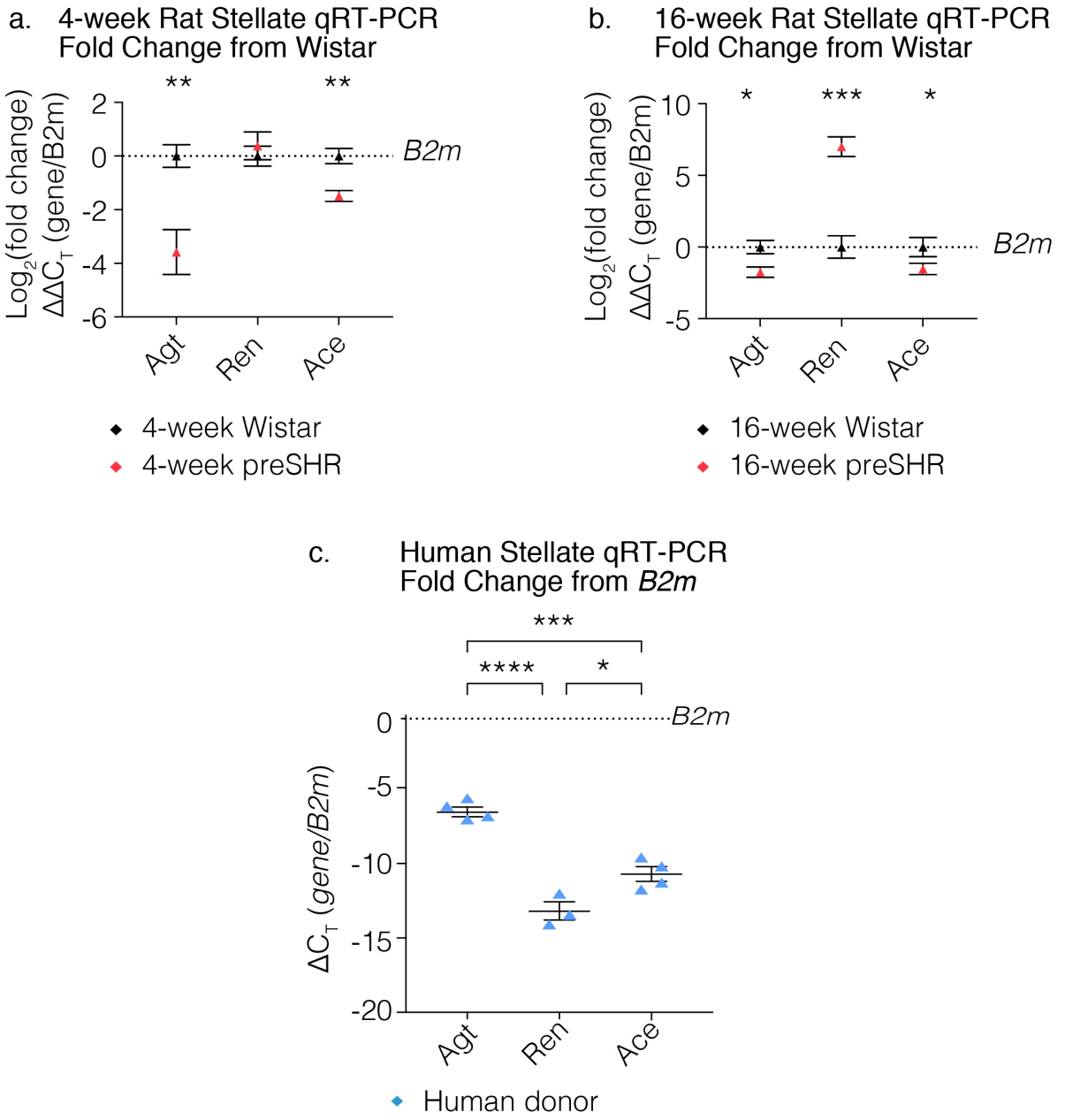


Figure 6.2. Angiotensin II Synthesising Enzyme mRNA in Stellate Ganglia.
The presence of RNA transcripts was validated using qRT-PCR in RNA extracted from four-week Wistar and preSHR ganglia (n=4 rats/group, unpooled, a), and 16-week adult SHR (n=4 rats/group, b), relative to age-matched Wistar rats (n=5 rats). The expression of *Agt* and *Ace* were significantly decreased in young preSHR compared to age-matched Wistar (n=3-4 samples; two-tailed unpaired Student's t-test p=0.0045, p=0.0048, a) and in adult SHR (n=4 samples) relative to age-matched Wistar rats (n=4 samples/group, two-tailed unpaired Student's t-test; p=0.0212, p=0.0469, b). *Ren* mRNA expression in 16-week SHR was also significantly upregulated compared to 16-week Wistar rats (p<0.0001, unpaired two-tailed Student's t-test, b). Data were analysed using the $\Delta\Delta C_T$ method. The expression of mRNA encoding *Agt*, *Ren* and *Ace* were observed in human stellate ganglia (n=3-4) using qRT-PCR. *Ren* expression was significantly lower than *Agt* (p<0.0001) and *Ace* (p=0.0005), and *Ace* was significantly lower than *Agt* (p=0.0005). Data were analysed by one-way ANOVA with Bonferroni's post-hoc tests. Data are represented as $\Delta\Delta C_T$ (rat), ΔC_T (human) normalised counts ± SEM. *p<0.05, **p<0.01, ***p<0.00, ****p<0.0001.

6.4.3 Stellate Ganglia Express Ang II Synthesising Enzymes and Precursors

ELISAs were used to quantify the relative protein expression of Agt and renin (Ren) whereas fluorometric activity assays were used to measure ACE activity in human and adult rat stellate ganglia. To obtain adequate protein concentrations young rat stellates (12-14 stellates per sample), or adult rat stellates (10-12 stellates per sample) were pooled. Agt was highly expressed in young Wistar (16750 ± 3472 pg/ml, n=3 samples), young preSHR (14928 ± 1990 pg/ml, n=3 samples), adult Wistar (16924 ± 1312 pg/ml, n=5 samples) and adult SHR (15071 ± 1572 pg/ml, n=6 samples), however there was no significant difference in Agt expression between strains at any age (one-way ANOVA, Fig. 6.3a). Angiotensin I (AngI) was not detectable by ELISA, as concentrations fell below assay detection limit.

Ren activity was detected in young Wistar (101.0 ± 14.8 mU/ml, n=3 samples), young preSHR (85.3 ± 11.7 mU/ml, n=3 samples), adult Wistar (97.4 ± 12.9 mU/ml, n=6 samples) and adult SHR (95.7 ± 9.0 mU/ml, n=5 samples) calculated at 20 minutes. ACE activity was also detected in young Wistar (74.3 ± 2.8 mU/ml, n=3 samples), young preSHR (79.4 ± 1.7 mU/ml, n=3 samples), adult Wistar (70.1 ± 1.9 mU/ml, n=3 samples) and adult SHR (74.9 ± 0.5 mU/ml, n=3 samples) calculated at 35 minutes, however there was no significant difference in Ren activity (Fig. 6.3 b, c) or ACE activity (Fig. 6.3 d, e) between strains at any age (one-way ANOVA with Bonferroni's multiple comparisons). In human stellate ganglia (three pooled stellates obtained from two patients) Agt (53694 ± 1351 pg/ml), Ren (2006 ± 388 pg/ml) and ACE activity (50.5 ± 2.8 mU/ml, calculated at 35 minutes) were also detected (Fig. 6.4).

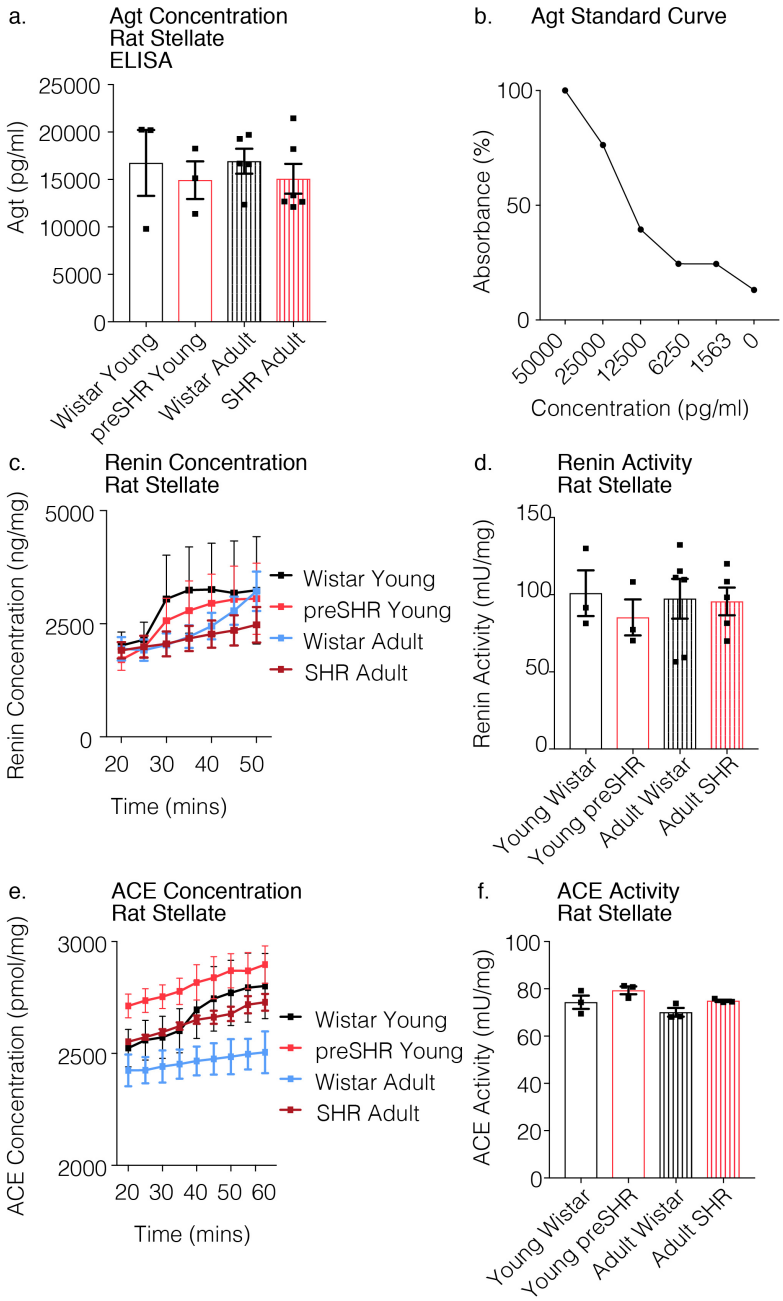


Figure 6.3. Rat Stellate Ganglia Express Angiotensin II Synthesising Enzymes
The concentration of Agt (a) with calibration curve (b) and activity of Ren (c, d) and ACE (e, f) were identified in young Wistar (n=3), preSHR (n=3) and adult Wistar (n=3-6) and SHR (n=3-6) stellate ganglia. Agt concentration (14,000-17,000 pg/ml, a), Ren concentration (b) and activity (85-101 pg/mg/min or mU/mg, c), ACE concentration (d) and activity (70-75 pg/mg/min or mU/mg, e) were not significantly different between or within strains at any age (one-way ANOVA for a, d, f). Data are represented as mean ± SEM. To calculate Ren and ACE concentrations and activity (c-f), standard curves were constructed (0-100 %) from the supplied standards in each assay. The data were fit to a sigmoidal $\log_{10}$(molar concentration) curve and each of the sample values were interpolated (GraphPad Prism, v7). The interpolated values were un-logged to determine the amount of Ren or ACE in each sample (ng or pmol respectively), multiplied by the dilution factor, and the three technical replicates were averaged. The amount of Ren or ACE in each sample was divided by the total mass of protein in each well (mg) to obtain a value for enzyme concentration (pmol/mg) (c, e). Enzyme concentrations were divided by the reaction time (in minutes) to calculate enzyme activity (mU/mg). The reaction times were 20 min and 35 min for Ren or ACE activity, respectively.

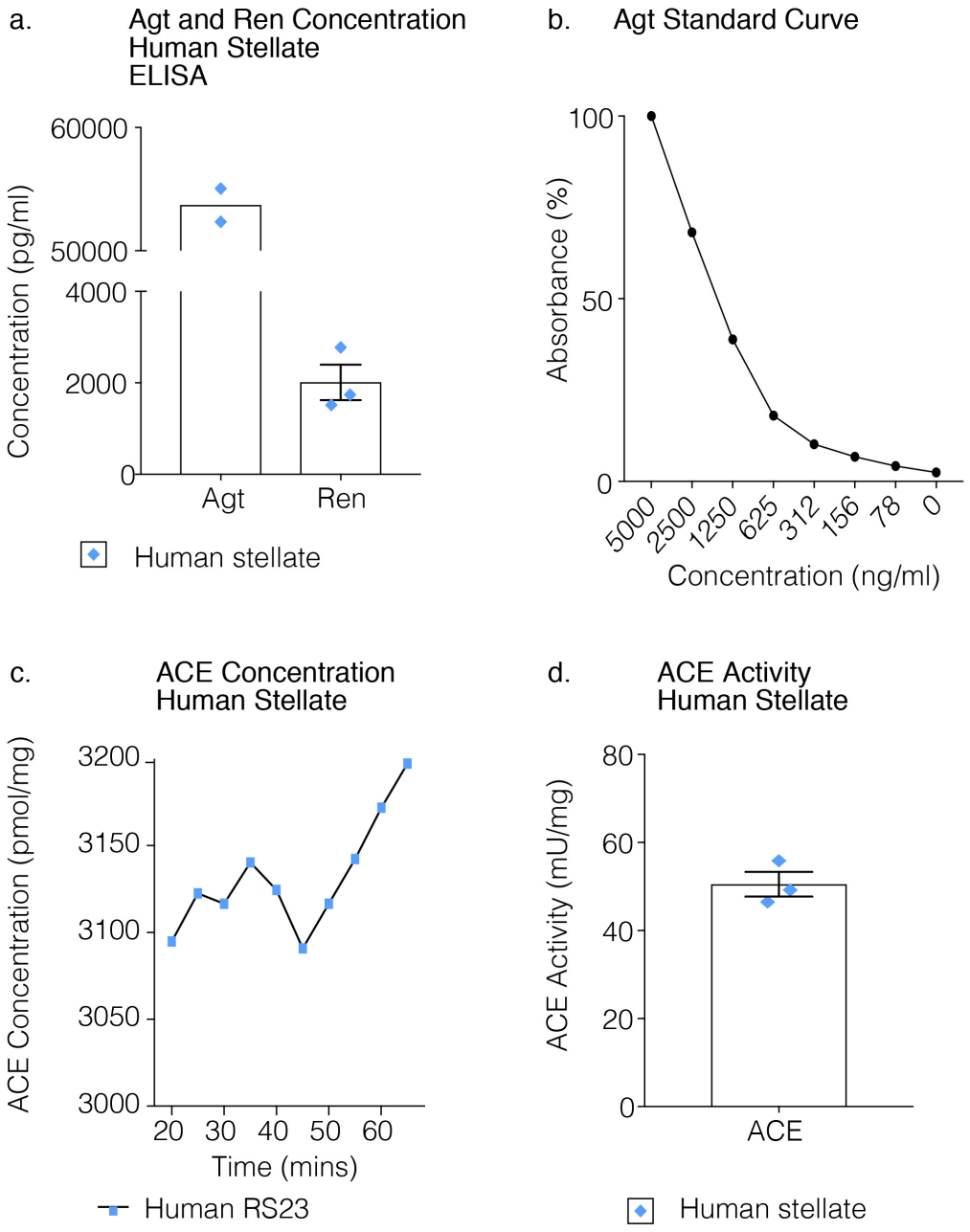


Figure 6.4. Human Stellates Express AngII Synthesising Enzymes and Precursors
Agt expression (53694 ± 1351 pg/ml, a), Ren expression (2006 ± 388 pg/ml, a) standard curve for Agt (b) and ACE (50.5 ± 2.8 pmol/mg/min or mU/ml, c, d) were detected in human stellate ganglia, in two or three stellates obtained from two patients. Agt and Ren values were multiplied by a dilution factor of 10, as the stellate samples were diluted 1:10 prior to assaying to fit within the range of the standard curve. Data depicts mean ± SEM (2-3 technical replicates). To calculate ACE concentrations and activity, standard curves were constructed (0-100 %) from the supplied standards. The data were fit to a sigmoidal $\log_{10}$(molar concentration) curve and each of the sample values were interpolated (GraphPad Prism, v7). The interpolated values were un-logged to determine ACE in each sample (pmol), and the three technical replicates were averaged. The amount of ACE in each sample was divided by the total mass of protein in each well (mg) to obtain a value for enzyme concentration (pmol/mg) (c, e). Enzyme concentrations were divided by time (in minutes) to calculate enzyme activity (mU/mg). The reaction times was 35 minutes for calculating ACE activity.

6.4.4 Angiotensin II is Synthesised in Human and Rat Stellate Ganglia

Plasma and tissue levels of AngII are significantly altered in hypertension and heart failure and correlate with the severity of disease[76,80,193,214,393-397]. To assess whether the presence of proteins that synthesise AngII have physiological relevance in the generation of neuronal AngII, protein was extracted from cardiac-sympathetic ganglia of from young preSHR (n=12-14 stellates), adult SHR (n=10-12 stellates) and an equal number of age-matched Wistar rats. A slightly greater concentration of AngII was measured in stellate ganglia protein samples from young preSHR (423.5 pg/ml ± 14.65, n=3) compared with that measured in young Wistar stellate samples (274.5 pg/ml ± 13.06, n=3) although this was not found to be significant (p=0.0577, one-way ANOVA with Bonferroni corrections). A significantly greater total content of AngII was also observed in adult SHR stellate ganglia (465.8 pg/ml ± 38.67; n=6) compared with AngII measured in Wistar stellate ganglia (282.4 pg/ml ± 19.31, n=6, one-way ANOVA with Bonferroni post-hoc tests, p=0.0011). There was no significant difference in AngII measured in the stellate ganglia samples obtained from rats in the 12-week or 16-week-old groups, therefore these datasets were combined as described in the methods section (Fig. 6.5a). The presence of AngII was also confirmed in stellate ganglia obtained from human donors at similar levels to that measured in rat (114.3 pg/ml ± 11.79; n=3 stellates, unpooled).

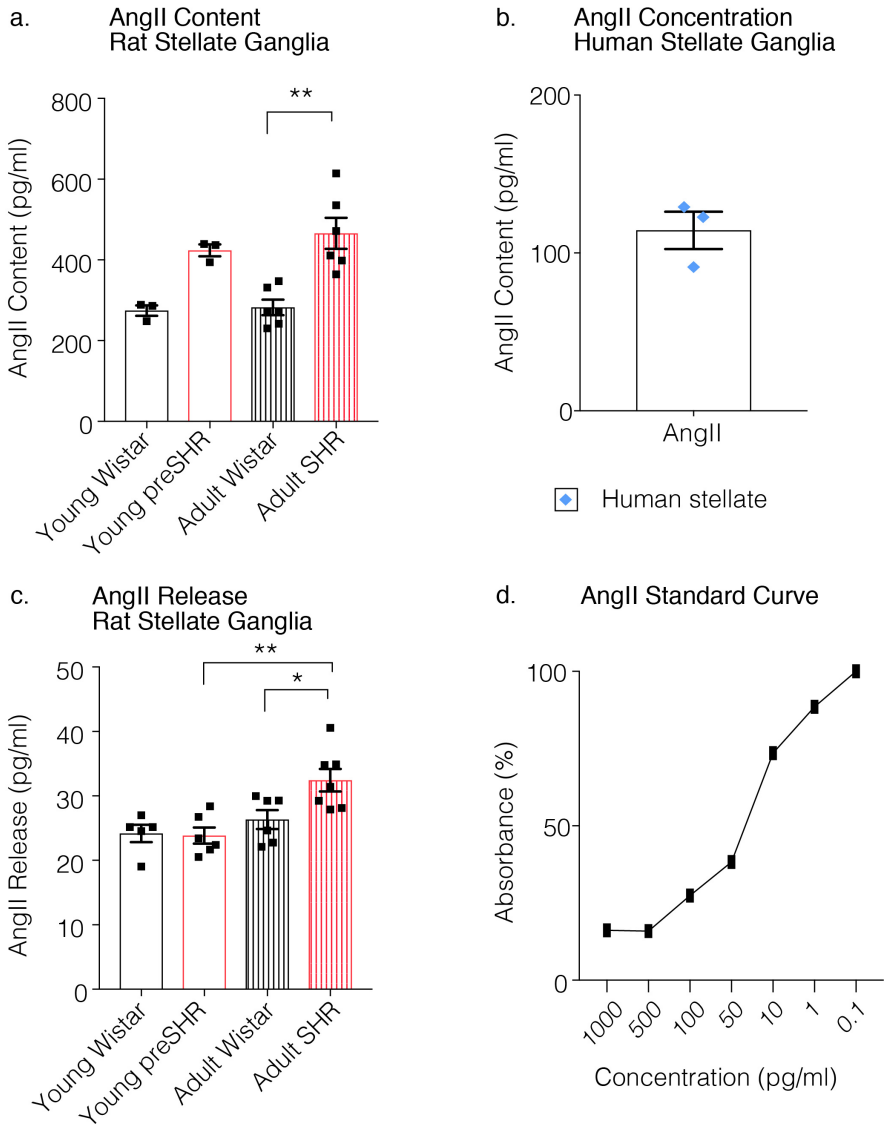


Figure 6.5. Angiotensin II Content in Stellate Ganglia

AngII was observed in the rat stellate ganglia. Slightly higher levels of AngII was measured in stellate ganglia protein samples from young preSHR (423.5 pg/ml ± 14.65, n=3) compared with that measured in age-matched young Wistar stellate samples (274.5 pg/ml ± 13.06, n=3) although this was not found to be significant (p=0.0577, one-way ANOVA with Bonferroni post-hoc tests). A significantly greater AngII content was observed in adult SHR stellate ganglia (465.8 pg/ml ± 38.67; n=6) compared with that measured in adult Wistar stellate ganglia (282.4 pg/ml ± 19.31, n=6, one-way ANOVA with Bonferroni post-hoc tests, p=0.0011). AngII was also detected in stellate ganglia obtained from human donors (114.3 pg/ml ± 11.79; n=3 stellates, unpooled, b). Following electrical stimulation AngII was detected in the perfusate from both preSHR and Wistar stellates (c). There was no significant difference in the concentration of AngII obtained from young preSHR stellate perfusate (23.86 pg/ml ± 1.252; n=6) compared with that released from Wistar ganglia (24.18 pg/ml ± 1.349; n=5; p=ns). Conversely, significantly higher concentrations of Ang II were measured in the adult SHR perfusate (32.42 pg/ml ± 1.748; n=7) compared with that measured in the age-matched adult Wistar perfusate (26.33 pg/ml ± 1.46; n=6; p=0.0366). The concentration of electrically-evoked AngII was also significantly greater in adult SHR perfusate than that released from young preSHR ganglia (p=0.0026). Each data point represents the concentration of AngII measured from 5-7 individual stellates (c). All data represents mean ± SEM. *p<0.05, **p<0.01.*p<0.05, **p<0.01. A calibration curve for the assay is included for reference (d).

6.4.5 Angiotensin II Evoked-Release from Rat Stellate Ganglia

To determine whether AngII is released from stellate neurons, sympathetic stellate ganglia were removed from young four-week Wistar and preSHR and subjected to electrical field stimulations. The ganglia were pre-bathed in an ACE2 inhibitor DX600 (100 µM) to inhibit AngII hydrolysis for 5 minutes prior to and during electrical stimulation. Electrical stimulation was conducted on single stellates and the experiments were conducted at 37 °C in bicarbonate-buffered Tyrode's solution to mimic physiological conditions (95 % O_2 / 5 % CO_2). A list of the buffer constituents is included in Chapter Two. A stimulation protocol involving 5 Hz stimulations at 3 mA with 30 s pulses every 90 s for 7.5 minutes was applied to each stellate as an adaptation from previously reported stimulation parameters[333]. The presence of AngII was observed in the perfusate from individually stimulated preSHR and Wistar stellates (Fig. 6.5). There was no significant difference in electrically-evoked concentrations of AngII obtained from young (three- to four-week-old) preSHR stellate ganglia perfusate (23.86 pg/ml ± 1.252; n=6) compared with that released from age-matched Wistar ganglia (24.18 pg/ml ± 1.349; n=5; p=ns). Conversely, significantly higher concentrations of electrically-evoked Ang II were measured in the adult SHR (12- to 14-week-old) perfusate (32.42 pg/ml ± 1.748; n=7) compared with that measured in the age-matched adult Wistar perfusate (26.33 pg/ml ± 1.46; n=6; p=0.0366). The concentration of electrically-evoked AngII was also significantly greater in adult SHR perfusate than that released from young preSHR ganglia (p=0.0026). Data were analysed by one way ANOVA with Bonferroni corrections.

6.4.6 Angiotensin Converting Enzyme 2 Expression in Stellate Ganglia

To ascertain whether impaired metabolism of AngII underpins the elevated AngII levels measured in the hypertensive rat stellate ganglia, the presence and activity of Angiotensin Converting Enzyme 2 (ACE2) was investigated, as the primary enzyme responsible for the hydrolysis of AngII into Ang1-7 (Fig. 6.6a). The transcript encoding ACE2 (*Ace2*) was identified in Wistar and SHR stellates using the RNA-seq dataset (Fig. 6.7b) and was validated using qRT-PCR (Fig. 6.6b). Data were analysed using the $\Delta\Delta C_T$ method where the counts reflecting the gene of interest were normalised to the counts obtained from the control housekeeping gene (*B2m*), and SHR were subsequently normalised to Wistar using the $\Delta\Delta C_T$ method[332]. The qRT-PCR analysis revealed a significant reduction in *Ace2* mRNA expression in samples obtained from young preSHR ganglia (n=3 stellates/group, unpooled) compared with *Ace2* measured in Wistar ganglia (n=3 stellates/group, unpooled, two-tailed unpaired Student's t-test, $p<0.0007$). Moreover, *Ace2* mRNA expression was decreased in adult 16-week SHR ganglia (n=4 stellates/group, unpooled) compared with *Ace2* measured in the Wistar samples (n=3 stellates/group, unpooled, $p=0.0390$, Fig. 6.6c). The reduction in *Ace2* mRNA expression mirrored the trend in the RNA-seq dataset[417]. The transcript encoding *Ace2* was also confirmed by qRT-PCR in four male human stellate ganglia (two left stellates, two right stellates, unpooled were obtained from 3 patients) for physiological context. The qRT-PCR raw counts were normalised to a control housekeeping gene *B2m,* using the ΔC_T method described by Schmittgen et al.,[332] and expressed as normalised count values (Fig. 6.6d).

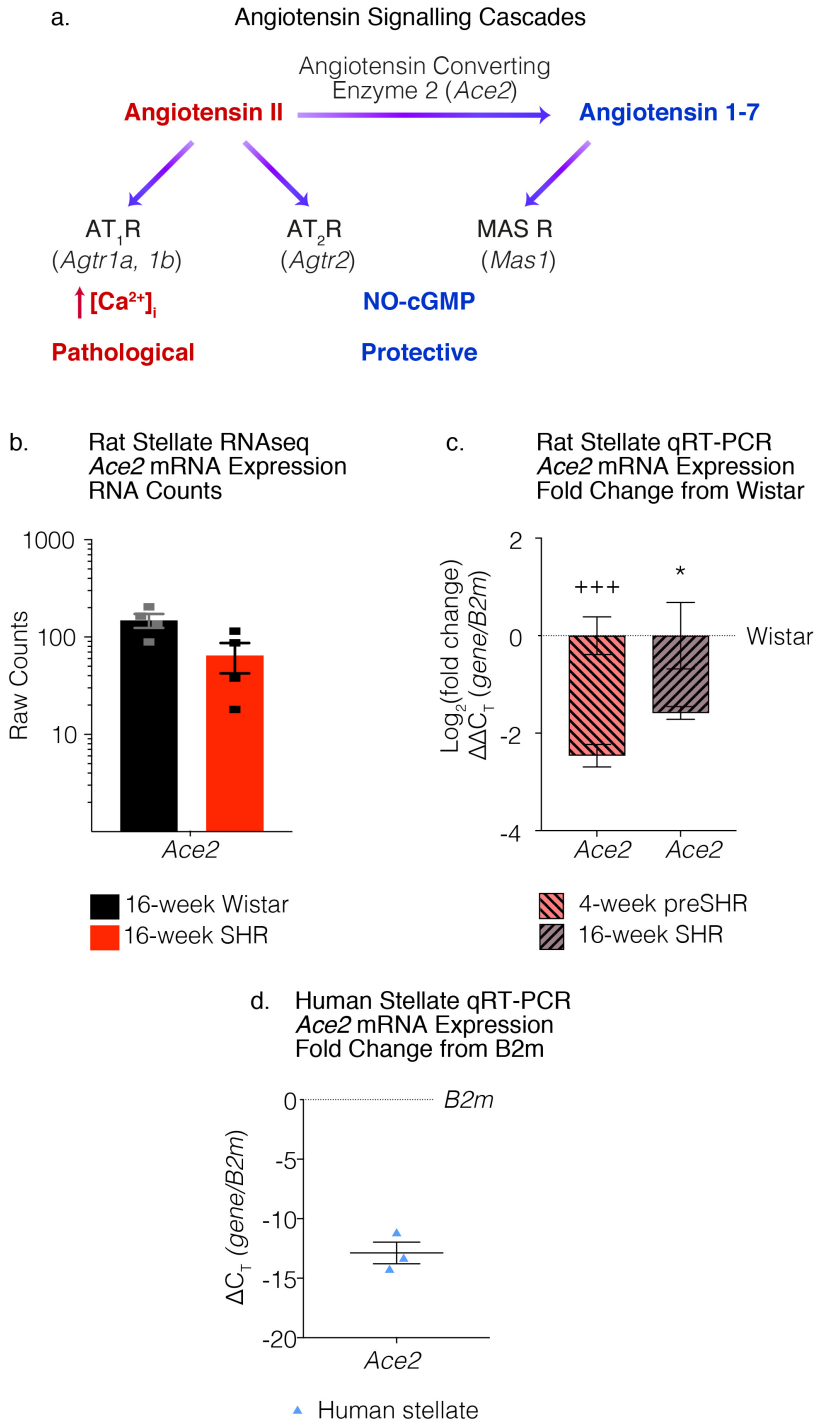


Figure 6.6. Angiotensin Converting Enzyme 2 Expression in Stellate Ganglia
The AngII/Ang1-7 signalling cascades and their receptor pathways are outlined (a). RNA-seq identified the presence of the Angiotensin Converting Enzyme 2 (*Ace2*) transcript in adult stellate ganglia using the Salmon-DESeq2 method [322,327] (b). The presence of *Ace2* was validated using qRT-PCR in RNA extracted from 4-week (n=3/group) and 16-week SHR and Wistar rats (n=3-4/group). There was a significant reduction in *Ace2* mRNA expression in RNA samples from young preSHR (n=3 stellates/group, unpooled) versus Wistar ganglia (n=3 stellates/group, unpooled, two-tailed unpaired Student's t-test, +++p<0.0007, c). *Ace2* was also decreased in adult 16-week SHR ganglia (n=4 stellates/group, unpooled) compared with *Ace2* expression measured in the Wistar samples (n=3 stellates/group, unpooled, *p=0.0390, c). *Ace2* mRNA in human stellate ganglia (n=3, d). The qRT-PCR data were analysed using $\Delta\Delta C_T$ (rat) or ΔC_T (human). Data are expressed as normalised counts ± SEM. *p<0.05, **p<0.01, ***p<0.001.

6.4.7 ACE2 Activity is Elevated in the Hypertensive Rat Stellate Ganglia

To assess whether decreased *Ace2* transcription is reflected in impaired ACE2 activity and decreased AngII metabolism, an ACE2 activity assay was conducted using young rat stellate samples (12-14 stellates/sample) and adult rat stellate samples (10-11 stellates/samples). ACE2 activity was detected in young Wistar (3557 ± 315.2 mU/ml, n=3 samples), young preSHR (3383 ± 151.6 mU/ml, n=3 samples), adult Wistar (3317 ± 88.3 mU/ml, n=3 samples) and adult SHR (5040 ± 187.6 mU/ml, n=3 samples) calculated at 25 minutes. There was no significant difference in ACE2 activity between strains at four-weeks of age, however ACE2 activity was found to be significantly elevated in adult SHR ganglia compared with young preSHR ganglia ($p=0.0019$) and between adult SHR compared with age-matched Wistar rats ($p=0.0015$). Groups were analysed using a one-way ANOVA with Bonferroni post-hoc multiple comparisons tests (Fig. 6.7). ACE2 expression was also identified in human stellate ganglia (171.9 ± 2.1 pg/ml, n=2 stellate samples, unpooled, Fig. 6.7).

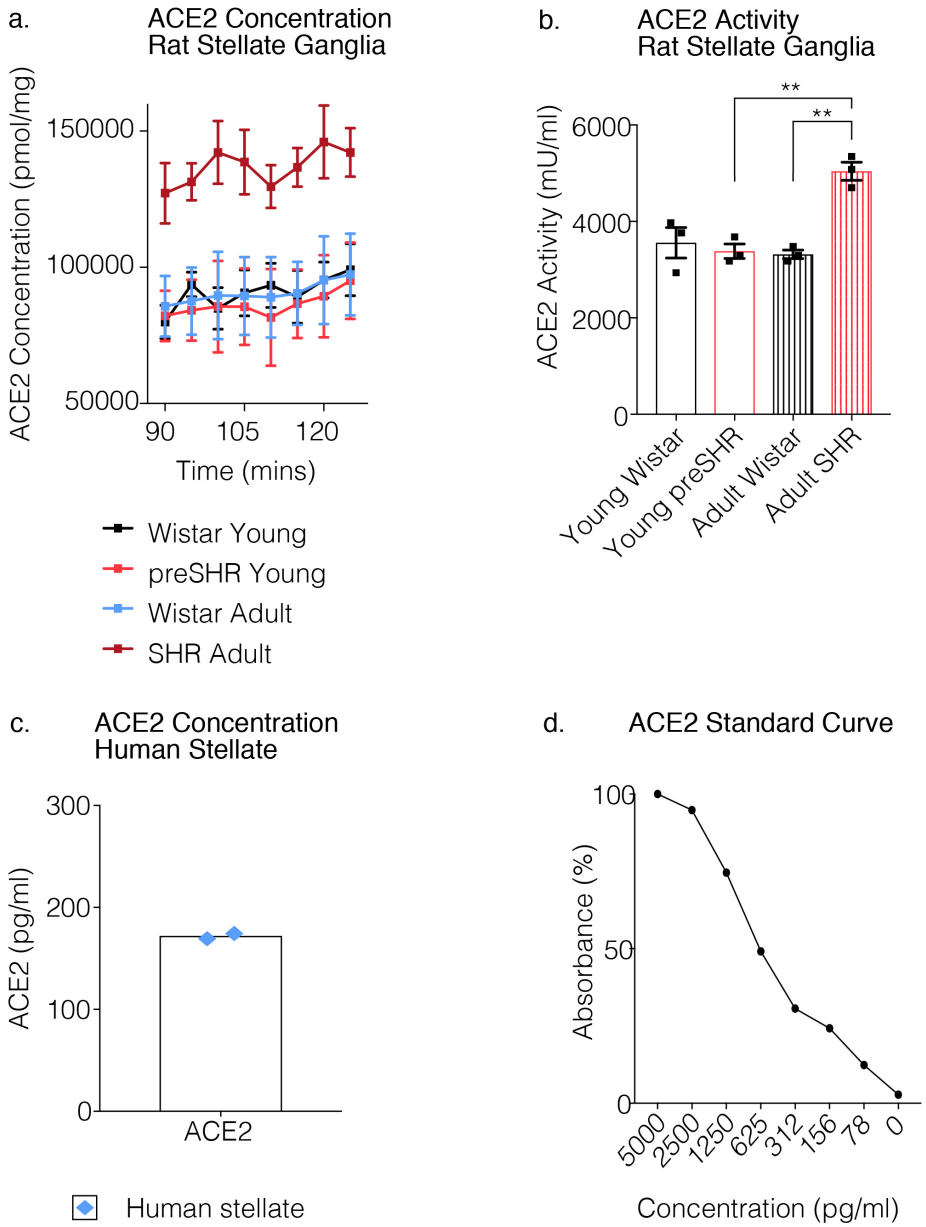


Figure 6.7. ACE2 Activity is Elevated in the Hypertensive Rat Stellate Ganglia
The concentration (a) and activity of ACE2 (b, c) was identified in stellate ganglia from young Wistar (3557 ± 315.2 mU/ml, n=3 samples), young preSHR (3383 ± 151.6 mU/ml, n=3 samples), adult Wistar (3317 ± 88.3 mU/ml, n=3 samples) and adult SHR (5040 ± 187.6 mU/ml, n=3 samples). To calculate ACE2 concentrations and activity (a, b), standard curves were constructed (0-100 %) from the supplied standards in each assay. The data were fit to a sigmoidal $\log_{10}$(molar concentration) curve and each of the sample values were interpolated (GraphPad Prism, v7). The interpolated values were un-logged to determine the amount of Ren or ACE in each sample (pmol), multiplied by the dilution factor, and the three technical replicates were averaged. The amount of ACE2 in each sample was divided by the total mass of protein in each well (mg) to obtain a value for enzyme concentration (pmol/mg; a). Enzyme concentrations were divided by time (in minutes) to calculate enzyme activity (mU/mg; b). The reaction times was 25 minutes for calculating ACE2 activity. There was no significant difference in ACE2 activity between strains at 4-weeks. ACE2 activity was significantly elevated in adult SHR vs. young preSHR ganglia (p=0.0019) and between adult SHR vs. age-matched Wistar (p=0.0015), using one-way ANOVA with Bonferroni post-hoc tests. ACE2 was identified in human stellate ganglia (171.9 ± 2.1 pg/ml, n=2 stellate samples, unpooled, c). Data with error bars are depicted as mean ± SEM. *p<0.05, **p<0.01.

6.4.8 Angiotensin 1-7 is Synthesised in Human and Rat Stellate Ganglia

To determine whether ACE2 activity within the stellate ganglia leads to detectable levels of the bioactive AngII metabolite Ang1-7, ELISA assays were carried out using young rat stellate samples (12-14 stellates/sample) and adult rat stellate samples (10-11 stellates/sample). Ang1-7 concentrations were detected in rat stellate ganglia (Fig. 6.8a),

A significant increase in Ang1-7 expression was observed in preSHR ganglia(104.3 pg/ml ± 14.0, n=3 samples), compared with Ang1-7 concentrations measured in age-matched young Wistar ganglia (40.2 pg/ml ± 13.9, n=3 samples, p=0.0132, Fig. 6.8). It was observed that the total concentration of Ang1-7 was no longer significantly elevated in adult SHR ganglia (53.6 pg/ml ± 2.7, n=3 samples) compared with Ang1-7 measured in adult Wistar ganglia (42.8 pg/ml ± 4.9, n=3 samples). Moreover, significantly lower levels of Ang1-7 were measured in the adult SHR ganglia compared with young preSHR ganglia (p=0.0481), indicating that the concentrations of stellate Ang1-7 decrease with disease progression. A one-way ANOVA was performed with Bonferroni corrections test for analysis.

Ang1-7 was also identified in human stellate ganglia obtained from donors (179.9 pg/ml ± 6.1 n=3 stellate samples, unpooled, Fig. 6.9b). Moreover, electrical stimulation led to detectable levels of Ang1-7 released into the perfusate from young preSHR (5.1 pg/ml ± 0.9; n=7) and young Wistar ganglia (3.0 pg/ml ± 0.7; n=7) where an elevated trend was observed in the young preSHR compared to Wistar samples although this difference was not significant (two-tailed unpaired Student's t-test, p=0.0799; Fig. 6.8b).

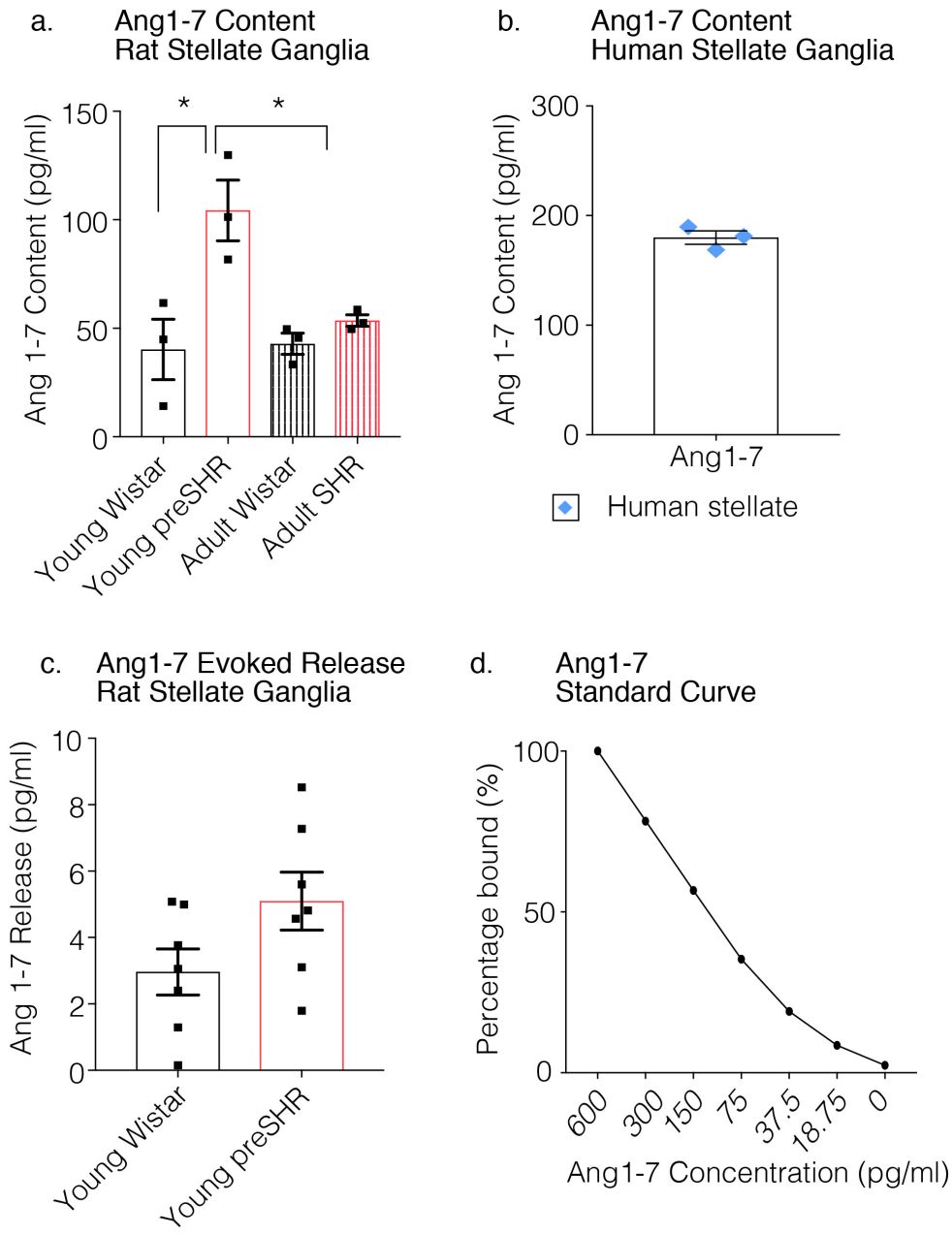


Figure 6.8. Angiotensin 1-7 is Synthesised in Human and Rat Stellate Ganglia
Ang1-7 was detected rat stellate ganglia. A significant increase in Ang1-7 was observed in preSHR ganglia (104.3 pg/ml ± 14.0, n=3 samples), compared with Ang1-7 concentrations measured in age-matched young Wistar ganglia (40.2 pg/ml ± 13.9, n=3 samples, p=0.0132) and levels measured in the adult SHR ganglia (53.6 pg/ml ± 2.7, n=3 samples, p=0.0481). Conversely, Ang1-7 expression was no longer significantly elevated in adult SHR ganglia compared to adult Wistar ganglia (42.8 pg/ml ± 4.9, n=3 samples, a). A one-way ANOVA was performed with Bonferroni corrections test for analysis of rat Ang1-7 concentrations. Ang1-7 was also identified in human stellate ganglia obtained from donors (179.9 ± 6.1 n=3 stellate samples, unpooled, b). Electrical stimulation led to detectable levels of Ang1-7 released into the perfusate from young preSHR (5.1 pg/ml ± 0.9; n=7) and young Wistar ganglia (3.0 pg/ml ± 0.7; n=7) where an elevated trend was observed in the young preSHR compared to Wistar samples, although this difference was not significant (two-tailed unpaired Student's t-test, p=0.0799, c). Data are depicted as mean ± SEM. *p<0.05.

6.4.9 AngII and Ang1-7 Receptors are Expressed on Stellate Ganglia

Immunocytochemistry illustrated the expression of the AngII receptor type I A ($AT_{1A}R$) on TH positive rat stellate ganglia (Fig. 6.9). The RNA-seq dataset revealed the expression of mRNA encoding AngII and Ang1-7 receptors (Fig. 6.10) in samples from 16-week male SHR and Wistar rats, suggesting that AngII and Ang1-7 peptides may have autocrine effects on the stellate ganglia itself and thus play a role in modulating transmission. To validate the presence of angiotensin receptor transcripts in rat stellate neurons, qRT-PCR was performed using RNA from four-week Wistar and preSHR ganglia (n=3 rats/group, unpooled) in addition to 16-week Wistar and age-matched SHR stellates (n=4 rats/group, unpooled). The transcripts encoding the AngII receptor type I subtypes, $AT_{1A}R$ (*Agtr1a)* and $AT_{1B}R$ (*Agtr1b*), in addition to the AngII receptor type II (AT_2R, *Agtr2*) and Ang1-7 receptor Mas (*Mas1*) were identified by qRT-PCR (Fig. 6.12a). There was no difference in *Agtr1a* or *Agtr1b* transcript expression between Wistar and SHR at any age, however, *Agtr2* mRNA expression was significantly decreased in preSHR ganglia at four-weeks of age (unpaired two-tailed Student's t-test, p=0.0003), yet elevated two-fold in adult SHR ganglia relative to that measured in age-matched Wistar (unpaired two-tailed Student's t-test, p=0.0361). Whilst no significant difference was measured in *Mas1* expression in young rats between strains, a four-fold upregulation in *Mas1* was observed in adult SHR stellate compared with Wistar ganglia (p=0.0084). The expression of the human AngII receptor type I homologue (*Agtr1*) was identified in donor stellates (n=4 samples, unpooled, Fig. 6.11b). Moreover, mRNA encoding the AngII type II receptor (AT_2R, *Agtr2*) and the Ang1-7 receptor Mas (*Mas1*) were identified in human ganglia (n=3-4 samples, unpooled) where *Mas1* expression was found to be significantly higher than *Agtr2* expression (one-way ANOVA, p=0.0046). The human qRT-PCR data were analysed using the ΔC_T method[332] where gene counts were normalised to the control gene counts for *B2m*.

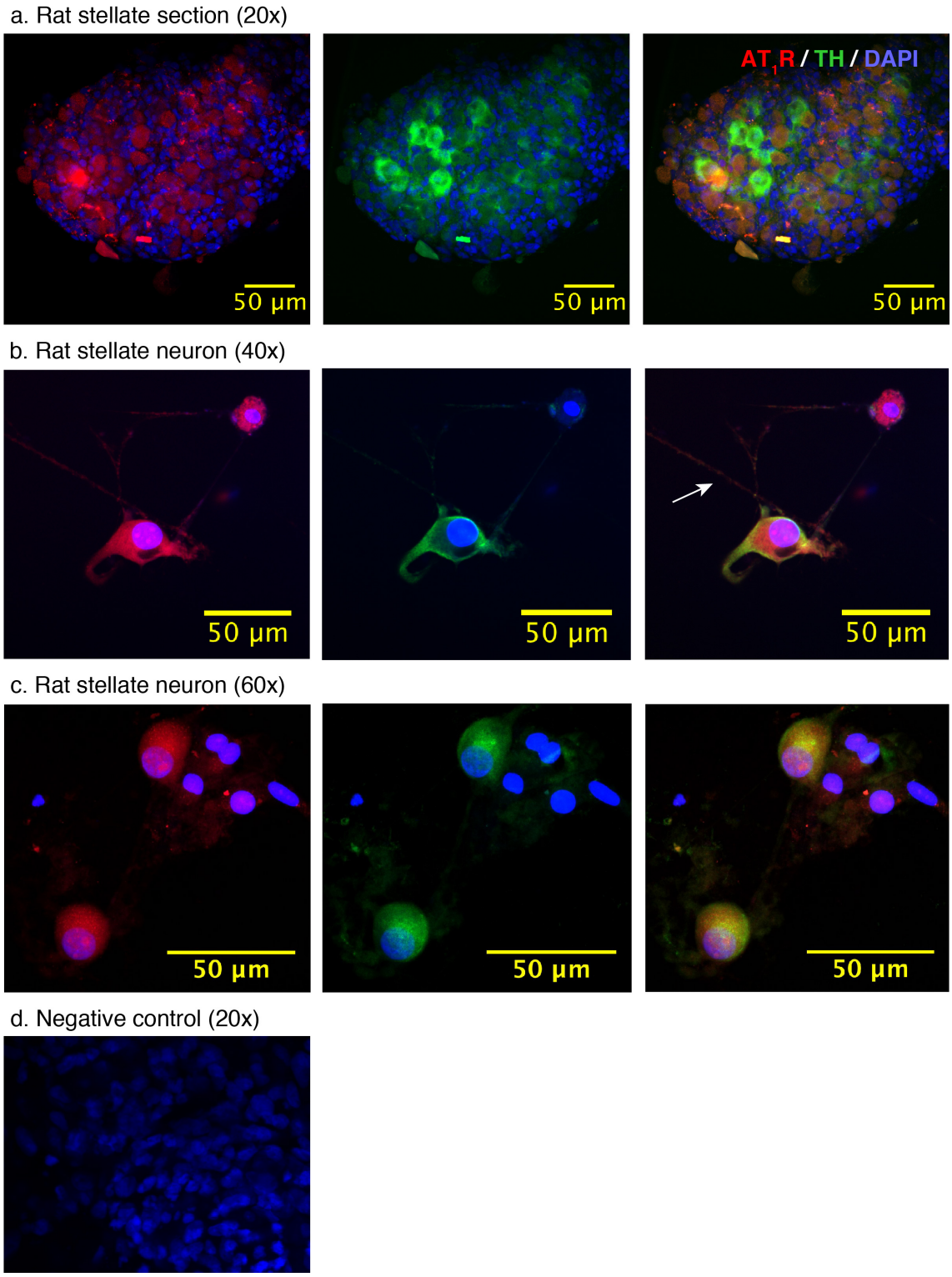


Figure 6.9. $AT_{1A}R$ Expression on Rat Stellate Ganglia
Immunocytochemistry illustrates the expression of the AngII receptor type I A (AT_1R, red) on TH positive (green) rat stellate ganglia on 20x to 60x objectives (Zeiss Airy Scan, Confocal Microscope, a-d). White arrows depict the localisation of AT_1R on dendrites (b). Negative controls with no primary antibody are depicted (d). AT_1R is internalised in a β-arrestin-dependent manner, which might explain the lack of localisation of AT_1R to the membrane.

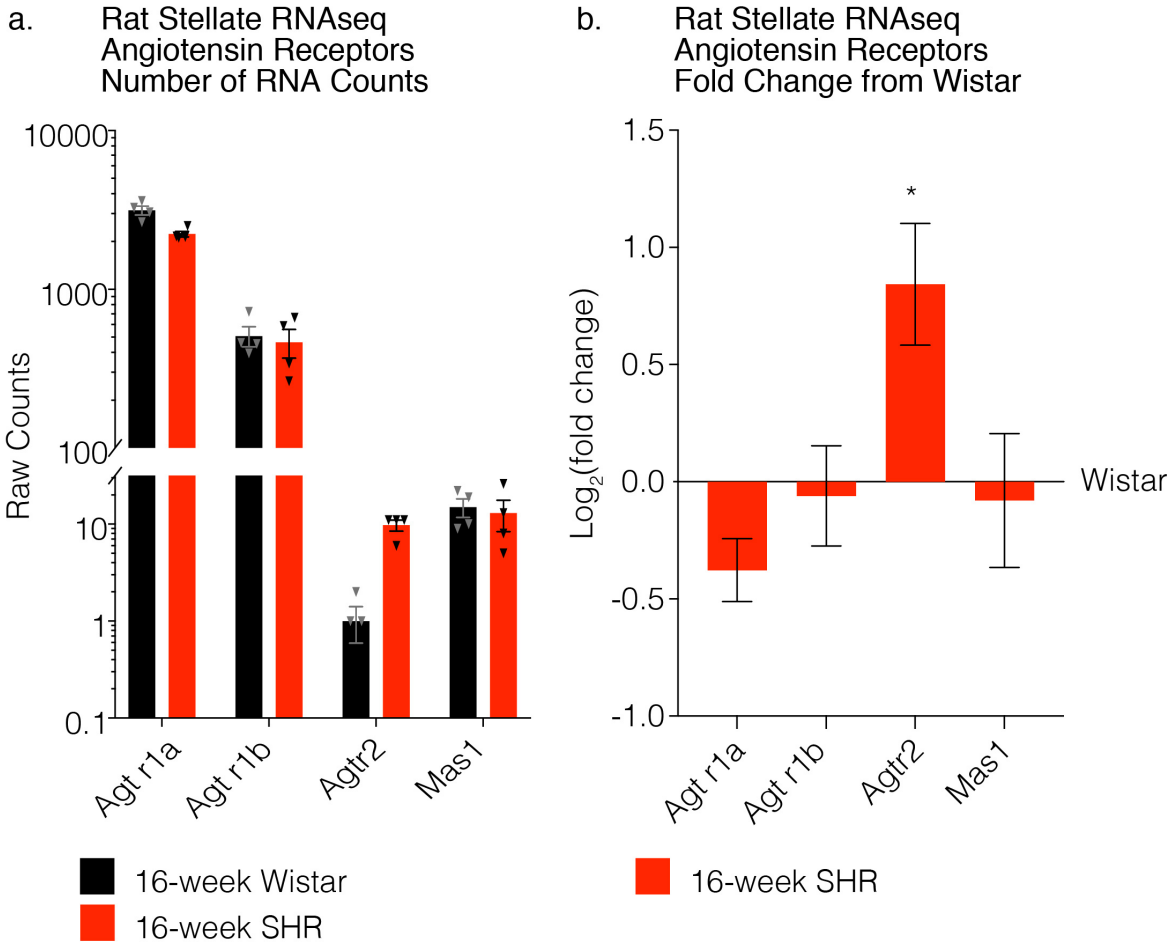


Figure 6.10. AngII and Ang1-7 Receptor mRNA in Rat Stellate Ganglia
RNA-seq identified the presence of transcripts encoding the AngII type 1 receptor $AT_{1A}R$ (*Agtr1a, Agtr1b),* the AngII type 2 receptor AT_2R (*Agtr2*) and the Ang1-7 receptor (*Mas1*). Transcript abundances of *Agtr1a, Agtr2a* and *Mas1* were not found to be differentially expressed in SHR vs. Wistar ganglia, however, *Agtr2a* expression significantly upregulated in SHR ganglia (p. adj=0.0274, Salmon-DESeq2 method [327], b, c). Data points represent raw counts ± SEM (a) and log_2(fold change) ± SEM normalised to Wistar (b). *p<0.05.

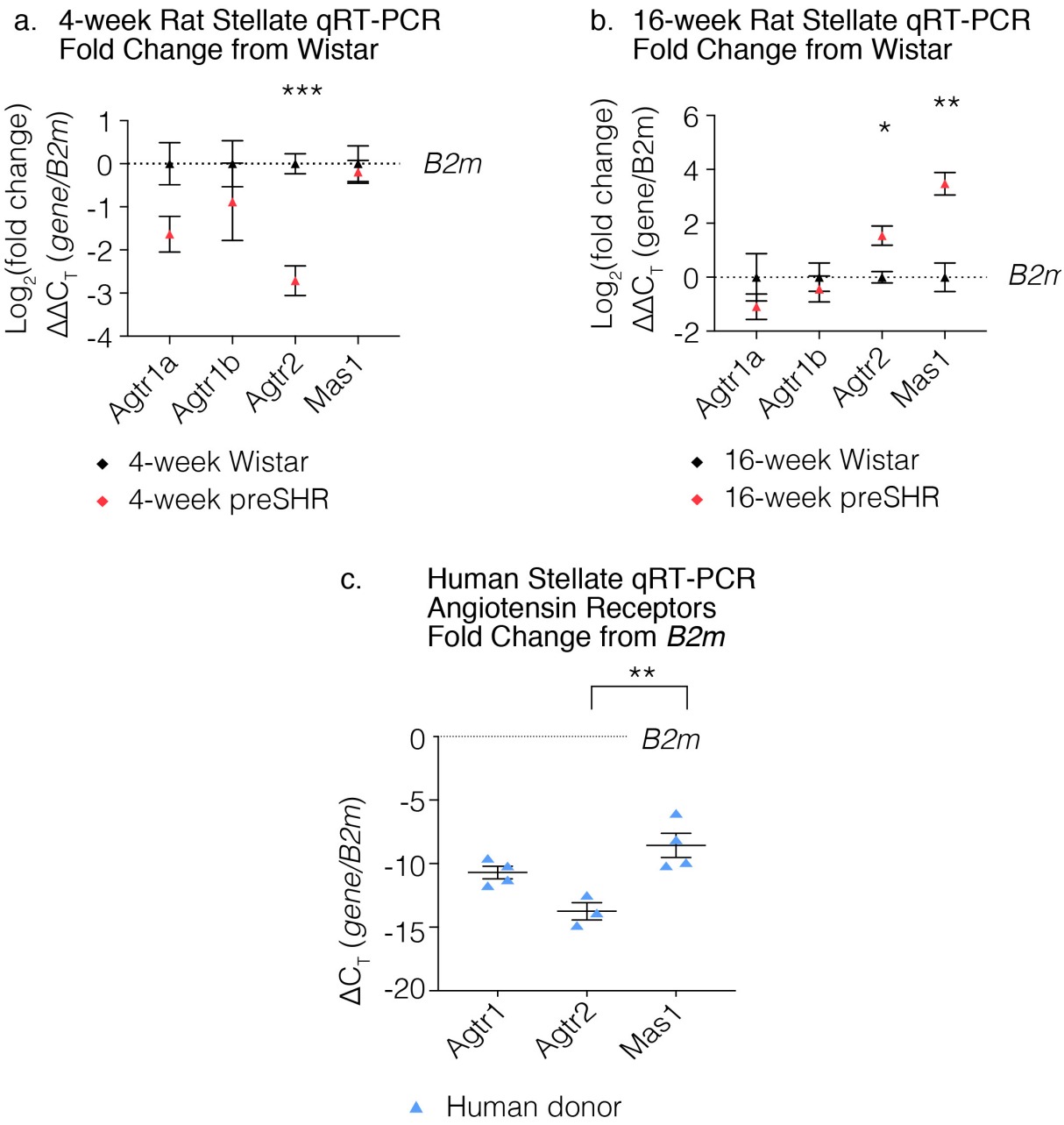


Figure 6.11. AngII and Ang1-7 Receptor mRNA in Human Stellate Ganglia
qRT-PCR confirmed the expression of the angiotensin peptide receptor mRNA transcripts AngII type 1 receptor AT1AR (*Agtr1a, Agtr1b*), the AngII type 2 receptor AT2R (*Agtr2*), and the Ang1-7 receptor (*Mas1*) in RNA from 4-week Wistar and preSHR ganglia (n=3 rats/group, unpooled, a), and 16-week Wistar and age-matched SHR stellates (n=4 rats/group, unpooled, b). There was no significant difference in *Agtr1a* or *Agtr1b* transcript expression between Wistar and SHR at any age, however, *Agtr2* mRNA expression was significantly decreased in preSHR ganglia at 4-weeks of age (unpaired two-tailed Student's t-test, p=0.0003), and increased two-fold in adult SHR ganglia relative age-matched Wistar (unpaired two-tailed Student's t-test, p=0.0361). There was no significant difference in *Mas1* expression between strains at 4-weeks (a), however a four-fold upregulation in *Mas1* was observed in adult SHR stellate compared with the relative expression in Wistar ganglia (unpaired two-tailed Student's t-test, p=0.0084, b). The expression of *Agtr1*, *Agtr2* and *Mas1* were also identified in human ganglia (n=3-4 samples, unpooled), where *Mas1* expression was found to be significantly higher than *Agtr2* expression (one-way ANOVA, Bonferroni's post-hoc tests, p=0.0046, c). Data are represented as $\Delta\Delta C_T$ (rat), ΔC_T (human) normalised counts ± SEM. *p<0.05, **p<0.01, ***p<0.001.

6.5 Discussion

In this chapter, a combination of RNA-seq, qRT-PCR, electrical field stimulation, protein measurements and enzyme activity assays were applied to investigate the potential for an intracellular RAS synthesis pathway in cardiac-sympathetic stellate ganglia of human and rat, thus providing a novel source of angiotensins to the heart. This chapter also aimed to investigate whether angiotensin peptide concentrations are altered in models of disease that may play a role in the aetiology of hypertension.

The main findings of this chapter are:

1. Key proteins involved in angiotensin peptide synthesis are present in cardiac-stellate ganglia from human and rat.
2. AngII and Ang1-7 were observed in the cardiac-stellate ganglia of human and rat and released from the rat stellate ganglia during electrical field stimulation.
3. AngII and Ang1-7 concentrations (intracellular and released) were elevated in the prehypertensive model compared with healthy counterparts. AngII was also elevated in the SHR with established hypertension.
4. AngII receptors (AT_1R, AT_2R) were expressed on cardiac-sympathetic ganglia of human and rat; where mRNA expression levels of AT_2R were shown to be upregulated in adult SHR with established hypertension.
5. The Ang1-7 receptor Mas as expressed on cardiac-sympathetic ganglia of human and rat; where expression levels of Mas receptor was upregulated in adult SHR with established hypertension

6.5.1 The Angiotensin II Synthesis Pathway is Present in Stellate Ganglia

AngII is a major effector of the classical RAS that mediates its effects via a signalling cascade following selective activation of AngII receptors type 1 and 2 (AT_1R, AT_2R); where activation of AT_1R underpins increases in $[Ca^{2+}]_i$ via G_q-coupled pathways[462]. Conversely, AT_2R is commonly coupled to NO-cGMP and is thought to oppose AT_1R mediated effects, although its physiological function is less well-characterised[524,525]. Emerging evidence highlights a dominant role for local rather than systemic angiotensin signalling, where key proteins are synthesised intracellularly and act in an autocrine and/or paracrine manner on local and neighbouring tissues[464,488,526,527], however the key source/s and local sites of angiotensin peptides are not fully established.

The RNA-seq dataset was used to identify the presence of mRNA transcripts encoding angiotensin synthesising enzymes in stellate ganglia from 16-week Wistar and SHR[337,417]. The dataset highlighted the expression of all relevant transcripts suggestive of an intracrine RAS, including angiotensinogen (*Agt*), renin (*Ren*), and Angiotensin Converting Enzyme (*Ace*), where transcript abundances were not differentially expressed between strains (Fig. 6.1)[337,359]. Importantly, the KEGG functional annotation analysis highlighted a significant under-representation in the pathway involved in 'Renin Secretion' (rno04924) in the SHR ganglia (Fig. 6.1). Indeed, all of the transcripts identified in this group were downregulated (Table 6.1a) where key transcripts preferentially mapped to adenylyl / guanylyl cyclases (*Adcyap1, Gucy1a3*) coupled to cNs (*Gnai3*) and the associated protein kinases (*Prkacb, Prkg2)* highlighting the importance of cN signalling in the synthesis of angiotensins (Table 6.1). The key genes involved in angiotensin synthesis (*Agt, Ren, Ace*) were identified using qRT-PCR and highlighted alterations in prehypertensive and hypertensive models (Fig. 6.2), although no functional alterations were observed in protein expression levels or enzyme activity (Fig. 6.3). *Agt, Ren* and *Ace* were also found to be expressed in human stellate ganglia by qRT-PCR (Fig. 6.2),

where protein expression was observed by ELISA and enzyme activity assays (Fig. 6.4). Together, these data provide evidence for an intracrine RAS in sympathetic-cardiac ganglia in human, although the relevance to human hypertension is not yet established.

What is the relevance for the observation of presynaptic sympathetic intracrine RAS system? Plasma and tissue levels of AngII are significantly altered in hypertension and correlate with the severity of disease [76,80,193,214,393-397]. Inhibitors of RAAS include angiotensin receptor antagonists, renin antagonists, mineralocorticoid receptor blockers and non-selective ACE inhibitors, that are gold-standard treatment strategies for hypertension[5,459,513,514,517,519,520]. Therapeutic benefit is primarily achieved through opposition of AngII-mediated effects including vasodilation, reduced aldosterone secretion and natriuresis[76,475]. Nevertheless, their mechanism of action, is not fully understood as ACE inhibitors reduce blood pressure via actions that do not necessarily correlate with a fall in systemic AngII, and drugs of this class are most effective in patients with low-to-medium circulating RAAS concentrations[76,477,513,518,521]. Emerging evidence now suggests that alterations in local RAS signalling within key organs or a collection of tissues may confer more pathophysiological specificity, compared with global changes in AngII. Our findings suggest that the presence of an intracrine RAS within the stellate ganglia of human and rat may provide an opportunity for precise therapeutic targeting[473,488,494,497,528].

6.5.2 Angiotensin II is Present in Rat and Human Stellate Ganglia

In this chapter, enzyme immunosorbent assays were used to investigate whether the presence of AngII synthesising enzymes plays a physiological role in the generation of a functional intracrine RAS system within the stellate ganglia of human and rat. AngII concentrations were found to be detectable both human and rat stellate ganglia (Fig. 6.5). Moreover, elevated AngII concentrations were observed in the prehypertensive and hypertensive phenotypes (Fig. 6.5). In addition to measuring the total AngII content, the concentrations of evoked-AngII released

from young and adult Wistar and SHR stellate ganglia were quantified following an electrical field stimulation protocol. It was observed that AngII release was significantly elevated in the perfusate collected from SHR ganglia compared with AngII measured in the young preSHR normotensive rat ganglia perfusate (Fig. 6.5). These data suggest that elevated AngII synthesis occurs early in hypertension where release is limited by regulatory mechanisms conferring protection against chronically elevated end-organ AngII. Increased sympathetic AngII release may coincide with the maintenance rather than the initiation of hypertension, although the concentrations measured here fell within the lower end of the assay detection limits, where a more sensitive technique might be required to reveal more subtle changes i.e. in the earlier stages of hypertension.

What are the local sites of action for AngII that have been proposed to play a role in the pathophysiology of disease? It is widely established that clinical morbidity and mortality associated with many CVDs are underpinned by dysautonomia (i.e. sympathetic over-activity and vagal impairment) [28,29,95,101,190,529]. This may occur prior to overt clinical signs, facilitating chronic end-organ damage. AngII-AT_1R signalling is linked to enhanced sympathetic outflow from the CNS[88,200,469,530,531] but also has a direct stimulatory effect on peripheral sympathetic neurons themselves[469,480,481,532-535]. We demonstrate the presence of mRNA transcripts encoding sympathetic AT_1R and AT_2Rs in human and rat stellate ganglia; and demonstrate that AT_2R is significantly increased in SHR with established hypertension, supporting previous findings[536,537]. Whether activation of sympathetic AT receptors plays a dominant role in the pathophysiology and progression of hypertension is not known[538]. Local AngII signalling is also evident within the myocardium, where receptor mediated signalling cascades are involved in the physiological and pathophysiological regulation of myocardial processes [462,473,474,488,528,539]. In normal conditions, activation of myocardial AT_1R regulates cardiac contractility, cell-cell signalling and impulse propagation [473,488,528]. Conversely, in models of CVDs, elevated local plasma and/or tissue concentrations of AngII, ACE and/or AT_1R expression associated left

ventricular hypertrophy[200,214,467,482-486], post-myocardial infarction remodelling[471-477] and heart failure[80,200,468-470].

The close relationship between elevated AngII and sympathetic over-activity in CVD is intriguing [81,481,534,540] and has raised questions surrounding membrane level receptor-receptor interactions and cross-talk between AngII and adrenergic signalling cascades [541-547]. Specifically, AT_1R-$\alpha_{2c}AR$ heterodimers have been observed, where activation by NA promotes atypical enhanced cAMP-PKA signalling by converting an $\alpha_{2c}AR$ auto-inhibitory signal to excitatory positive feedback signalling [546]. Moreover, activation of the AT_1R-$\alpha_{2c}AR$ heterodimer facilitates NA hyper-secretion and sympathetic over-activity in sympathetic neurons *in vivo* [546]. Heterodimer formation has also been found to occur between AT_1R-β_2AR [541,548] that enhances the membrane stability of β_2AR and prolongs cAMP signalling, suggesting a potential synergistic role for NA-AngII-mediated effects in provoking sympathetic over-activity in hypertension and cardiovascular pathophysiology [481,541,544,546,547,549,550].

6.5.3 Angiotensin 1-7 is Present in Rat and Human Stellate Ganglia

In addition to the classical AngII-AT_1R Ca^{2+}-coupled signalling pathways, the metabolism of AngII is also associated with generation of alternative signalling cascades. One such pathway known as the Ang1-7-Mas receptor signalling axis, physiologically antagonises AngII-AT_1R signalling[551] through NO and cGMP generation; where Ang1-7 is produced by ACE2 hydrolysis of AngII [493]. In this chapter, the expression of ACE2 was confirmed using a combination of RNA-seq, qRT-PCR and ACE2 activity assays in rat stellate (Fig. 6.6), and by ELISA for human stellate ganglia (Fig. 6.7). One possible cause for the elevated levels of AngII measured in the adult SHR could result from impaired ACE2 activity and reduced AngII metabolism. Contrary to the initial expectations, however, the activity of ACE2 was significantly raised in the adult SHR samples (Fig. 6.7), although this observation may not be entirely counterintuitive if the

concentrations of substrate (AngII) are sufficiently high enough to saturate ACE2 activity. Other lines of evidence point to a significant role for soluble ACE2 (sACE2) that is found within the cardiac interstitium to hydrolyse extracellular AngII. Although the physiological role of sACE is not fully understood, upregulated sACE2 activity has been identified in patients with heart failure [552] post-myocardial infarction remodelling [553] and cardiac dysfunction [553], and correlates with disease severity [552]. Whether sACE2 is also released from the cardiac-stellate ganglia and plays a significant role in altered sympathetic-derived AngII metabolism remains to be investigated. In this chapter, the activity of ACE2 was shown to play a functional role in the rat sympathetic stellate ganglia, where AngII was converted into detectable concentrations of Ang1-7 in human and rat (Fig. 6.8), where Ang1-7 was also released from rat stellate ganglia with electrical field stimulation. Moreover, Ang1-7 concentrations were increased in the prehypertensive rat stellate ganglia, but were no longer elevated with established hypertension, suggesting that compensatory upregulation of Ang1-7 occurs early in disease to counteract increases in AngII production, where reduced Ang1-7 synthesis correlates with disease progression.

What are the possible target organs for Ang1-7 released from the sympathetic stellate ganglia? Physiological responses to Ang1-7 have been identified within the myocardium, where administration of Ang1-7 facilitates NO synthesis through activation of nNOS and eNOS enzymes[511]. The beneficial effects of NO-cGMP signalling within the myocardium are well-established, where tools that increase NO-cGMP signalling reduce $[Ca^{2+}]_i$ via inhibition of the L-type Ca^{2+} channel and increase reuptake into the sarcoplasmic reticulum attenuating end-organ chronotropy and inotropy [99,112,554,555]. Moreover, peripheral and central actions of Ang1-7 exert potent anti-hypertensive[494,503,507,512,556] and cardio-protective effects[494,498,511,557] including attenuated sympathetic outflow[495,496], vasodilation[501,502,509], anti-arrhythmic effects[558], reduced remodelling[474,511,559-561], anti-proliferative processes [562-564], improvements in baroreflex sensitivity[154,505,506], and decreased pro-inflammatory events [565-568]. In the brain, Ang1-7 reduces TH activity, attenuates presynaptic NA release, and reduces peripheral sympathetic nerve

outflow [495,508,569] in an NO-PKG dependent manner[508]. Conversely, Ang1-7 has been shown to increase the release of atrial [^{3}H]-NA in an NO-dependent manner[570,571]; however, the importance of NO-cGMP signalling in reducing $[Ca^{2+}]_i$ [96,334] and end-organ transmission in peripheral sympathetic stellate nerves has been previously demonstrated [96,113,260,261,272,572,573]; although bi-phasic concentration-dependent effects of Ang1-7 have also been described[558].

In this chapter, the transcripts encoding AngII and Ang1-7 receptors were identified on human and rat stellate ganglia (Fig. 6.9-6.11), suggesting a possible site for an autocrine/paracrine effect of Ang1-7-mediated signalling within peripheral nerves. Although no changes were observed in expression of the AngII type 1 receptors (*Agtr1a, Agtr1b*), the Ang1-7 receptor, Mas (*Mas1*) was increased four-fold in hypertension, alongside a concomitant decrease in Ang1-7 generation. These data suggest that a decrease in agonist production may lead to selective upregulation of the Mas receptor to counteract increases in pathological AngII signalling, supporting previous findings [500]. Whether Ang1-7 directly modulates sympathetic transmission in an NO-dependent manner remains to be determined. A model diagram is depicted in Fig. 6.12a, b.

6.6 Limitations

In this chapter, the presence of the enzymes involved in AngII and Ang1-7 synthesis in the stellate ganglia was explored. There were several limitations to this study. First, to assess the pathways involved in AngII and Ang1-7 synthesis, the classical enzymes ACE and ACE2 were investigated. Recent literature has highlighted the importance of other enzymatic pathways involved in AngII synthesis and breakdown including neprilysin, endopeptidases and other metalloproteases that haven't been considered in this chapter[494], although their transcripts were identified in the RNA-seq dataset. Moreover, new angiotensin-derived metabolites are regularly identified[494] that may influence the results described. Nevertheless, this study provides an

overview of a classical intracrine RAS synthesis pathway within the stellate ganglia of human and rat, within the context of hypertension. Secondly, enzyme activity is sensitive to several parameters including pH and oxidative stress. In these experiments, the pH in the samples is determined by the assay and the kit selected that may not necessarily reflect the physiological environment for the enzymes *in vivo*. Indeed, SHR neurons reportedly have a cytosolic environment with lower pH and increased levels of oxidative signalling. In addition, although accuracy and selectivity of the chosen assay kits were verified by the manufacturer, the cross-reactivity of these assays for other proteins cannot be ruled out. Thirdly, changes in mRNA expression levels may not necessarily reflect protein concentrations or indeed enzyme activity given the number of regulatory processes involved in mediating enzymatic behaviour, however the net effect resulted in increased AngII release and changes in the release profile of Ang1-7 at different stages of disease. Finally, renin and angiotensinogen have been identified in neurons and glial cells in the brain; where expression in both cell types has been shown to regulate resting arterial pressure[531,574]. In this study, the precise cell-type/s responsible for angiotensin synthesis within the stellate ganglia are not known; however, the angiotensin genes were observed in the RNA-seq dataset alongside high abundance transcripts specific to sympathetic nerves, suggesting that the primary cell type within these ganglia is of sympathetic phenotype. Moreover, the net effect of the expression of these enzymes resulted in the release of angiotensins in an activity-dependent manner from the cardiac-stellate ganglia, regardless of cellular origin.

6.7 Conclusion

This chapter provides evidence for presynaptic synthesis of AngII and Ang1-7 within the cardiac sympathetic ganglia of human and rat, where elevated concentrations of AngII were released at the end-organ in an activity-dependent manner. Moreover, stellate ganglion synthesis of the NO-generating peptide Ang1-7 was found to be upregulated early in prehypertension but was no longer elevated in hypertension, suggesting that the potential beneficial effects of Ang1-7 may be lost with disease progression. Together, these data suggest that neurotransmitter and neuropeptides profiles may be more complex than the classical 'noradrenergic-sympathetic' signalling. Changes in neuropeptide production occurs prior to increases in arterial blood pressure, where elevated Ang1-7 synthesis may play a role in to counteracting the processes contributing to sympathetic over-activity through the activation of the presynaptic sympathetic NO-coupled Mas receptor. These results may have implications for future therapeutic targeting of diseases associated with dysautonomia and sympathetic over-activity. Whether the physiological activity of these angiotensin peptides resides entirely within the heart, or plays a role in feedback/feedforward signalling within the stellate ganglia itself remains to be established.

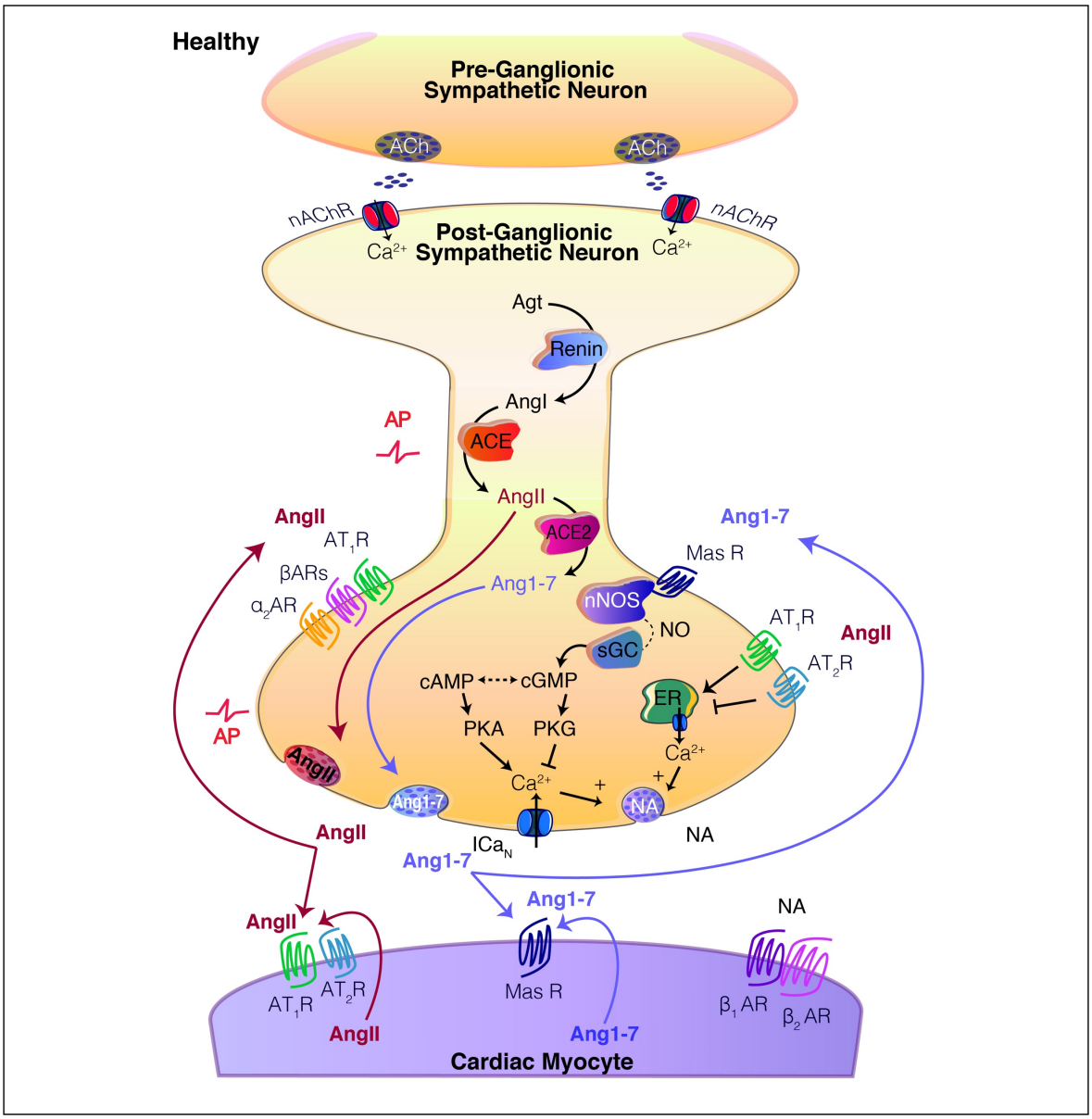


Figure 6.12a. Angiotensin Synthesis in Sympathetic Stellate Neurons
The sympathetic stellate ganglia (cervicothoracic ganglia) are located alongside vertebrate T1 to T4. They are the primary sympathetic ganglia that innervate the heart and have been shown to exert the greatest control over increases in heart rate and contractility[218,424,425,575]. In healthy neurons, AngII synthesis occurs by sequential enzymatic cleavage of Angiotensinogen (Agt) by Renin and Angiotensin Converting Enzymes (ACE). AngII is hydrolysed by the activity of ACE2 into Ang1-7. The synthesis and release of AngII and Ang1-7 is highly regulated, where release occurs in an activity dependent manner.

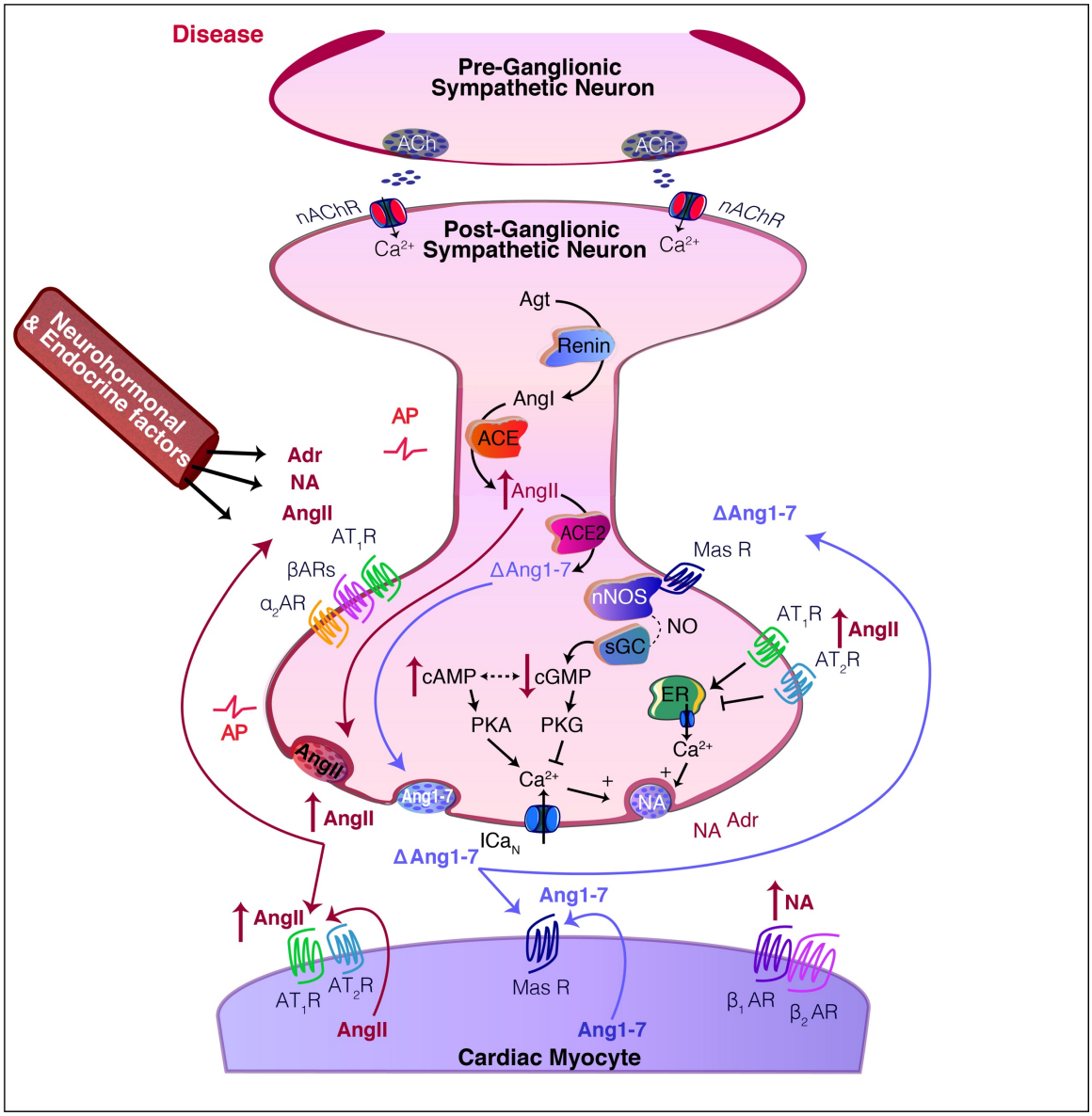


Figure 6.12b. Angiotensin Synthesis in Stellate Neurons in Hypertension
In diseased neurons, AngII synthesis occurs by sequential enzymatic cleavage of Angiotensinogen (Agt) by Renin and Angiotensin Converting Enzymes (ACE). AngII is hydrolysed by the activity of ACE2 into Ang1-7. The regulatory mechanisms controlling the synthesis and release of AngII and Ang1-7 are dysregulated in disease. In young prehypertensive rat neurons, the synthesis of AngII is elevated that occurs alongside a concomitant rise in the synthesis of the 'protective' Ang1-7 peptide. This results in no detectable elevation in activity-dependent release of AngII is observed in young prehypertensive rats. In adult hypertensive rat neurons, the synthesis of AngII is elevated, however, synthesis of the 'protective' Ang1-7 peptide is no longer increased. This results in a significant elevation in activity-dependent release of AngII in adult SHR with established hypertension.

7

Concluding Discussion

7.1 Introduction

Dysautonomia is a key feature of hypertension and is present early in disease; however, the mechanisms that underpin altered neuronal function are not known. The first objective of this thesis was to profile the transcriptome of the cardiac-stellate ganglia from normotensive healthy Wistar rats and SHR with established hypertension, using a non-biased, hypothesis neutral, RNA-seq approach. The identified transcriptomic changes were subsequently validated using quantitative real-time polymerase chain reaction using stellate ganglia from rat and humans, thus emphasising the translational relevance of these studies. The associated cellular and molecular consequences of these transcriptomic alterations were investigated using a combination of protein and activity assays, real-time fluorescence microscopy and HPLC-EC. The observations in this thesis suggest that many changes in the stellate ganglia observed in the hypertensive model occur prior to the onset of hypertension that may predispose to sympathetic over-activity providing novel targets for therapeutic intervention.

7.2 The Main Findings of this Thesis

1. The genetic profile of the sympathetic stellate ganglia is altered in the SHR compared to its normotensive genetic counterpart, where key genes are conserved in human stellates.
2. Disruptions in the SHR stellate transcriptome affect ion channel excitability and alter cN signalling via impaired PDE regulation.
3. Genetic alterations led to disrupted intracellular cN signalling that was validated using real-time fluorescence microscopy, highlighting advantages for transcriptomics in understanding disease pathophysiology.
4. Presynaptic βARs were identified on sympathetic stellate ganglia of human and rat. Activation of neuronal βARs elevated cAMP-PKA signalling, and exacerbated the Ca^{2+} phenotype. These data suggest that cN signalling may be a useful therapeutic target for hypertension.
5. In early disease states, a neurotransmitter profile switch was identified where increased Adr was released alongside NA, highlighting an augmented feed-forward signalling pathway coupled to βARs that contributes to sympathetic over-activity.
6. Angiotensin synthesis occurs within the cardiac-sympathetic stellate ganglia of human and rat highlighting a role for local intracrine RAS synthesis.
7. Elevated AngII release and altered Ang1-7 synthesis in the cardiac-stellate ganglia were observed in the preSHR and SHR model of hypertension, demonstrating a novel source of AngII that might play a role in the aetiology of sympathetic impairment associated with hypertension.

7.3 RNA Sequencing Highlights a Genetic Component for Sympathetic Over-activity in the Spontaneously Hypertensive Rat

In Chapter Three, the results from the RNA-seq study provided an overview of the transcriptomic changes evident in the stellate ganglia of adult SHR with established hypertension. This study demonstrated a potential genetic basis for sympathetic over-activity and elevated end-organ transmission. The RNA-seq dataset also highlighted a wide range of targets that directed the experimental objectives of this thesis and guided the successive investigations.

7.3.1 RNA Sequencing Highlights a Genetic Component for Impaired Cardiovascular Regulation in the Spontaneously Hypertensive Rat

The differentially expressed genes in the RNA-seq dataset were assembled into three parent GO categories, that were sub-categorised into over-represented GO groups reflecting significant transcriptomic changes in hypertension. In the CC category, changes were identified in GO groups representing ‘cell junctions’, ‘axonal projections’, ‘synapse’ and ‘membrane-bounded vesicles’. These over-represented families correlated with alterations identified in the BP category that demonstrated disruptions in genes involved in ‘cell-cell signalling’ and ‘responses to chemical stimuli’, highlighting a potential genetic basis for an altered response to feedback signals as well as impaired neurotransmitter release in hypertension. Other highly enriched GO groups in the BP category were found to be involved in cardiovascular regulation, where transcriptomic changes in SHR ganglia corresponded to ‘circulatory system processes’, ‘heart processes’, ’regulation of blood pressure’ and ‘regulation of heart contraction’ supporting a genetic basis for impaired cardiac transmission in hypertension. GO groups involved in ‘stress responses’ and inflammatory or ‘defence processes’ were also over-represented in the SHR ganglia reflecting a possible genetic link between diseases caused by sympathetic over-activity and increased proinflammatory events[30,33,145].

7.3.2 RNA Sequencing Highlights a Genetic Component for Elevated Neuronal Excitability in the Spontaneously Hypertensive Rat

Within the sympathetic stellate ganglia, several molecular processes have been previously shown to underpin or exacerbate sympathetic hyper-activity in prehypertensive and hypertensive states. These include a preferential deficit in NO-cGMP signalling[113,288], increased $[Ca^{2+}]_i$ [96,260,335] and an alteration in the activity of specific PDEs (e.g. PDE2a) [96,262,334]. Given the mounting evidence that these molecular perturbations both precipitate and provoke sympathetic over-activity, Chapter Three focussed on investigating the functional relevance of the altered genes within the MF category, by correlating the transcriptomic observations with cellular and molecular biochemistry techniques. It was observed that in the GO MF category, families encoding 'extracellular ligand gated ion channel activity' and 'phosphoric ester hydrolase activity' were critically altered in ganglia from SHR with established hypertension. Importantly, the differential expression of ligand-gated ion channel subunits may have implications for ion permeability, channel activity and elevated neuronal excitability in sympathetic ganglia in the SHR model and diseases associated with sympathetic over-activity. The differentially expressed transcripts in the MF group 'extracellular ligand-gated ion channel activity' highlighted the presence of glutamate (AMPA, NMDA and Kainate) and GABA receptor subunits in addition to purinergic, glycinergic and serotonergic receptors; most of which have not previously been shown to play a role within the sympathetic stellate ganglia nor have they been considered as potential therapeutic targets for cardiovascular or autonomic diseases. The expression of these transcripts was confirmed using qRT-PCR and translational context was demonstrated by validation of these transcripts within human stellates.

7.3.3 RNA Sequencing Highlights a Genetic Component for Altered Phosphodiesterase Activity in the Spontaneously Hypertensive Rat

The differentially expressed MF GO Group 'phosphoric ester hydrolase activity' was shown to comprise a group of transcripts predominantly encoding phosphatases involved in the regulation of PDE activity. PDEs play a key role in the regulation of cNs, where the deleterious effects of impaired PDE activity is well-documented and underpins a wide-range of diseases[265,275,277,278,576,577]. The second aim of Chapter Three was to establish whether the observed transcriptomic adaptations in the 'phosphoric ester hydrolase activity' group translated to altered PDE activity in cultured stellate neurons from preSHR and Wistar rats. Using FRET microscopy, it was established that changes to the stellate transcriptome resulted in functional alterations in PDE activity that disrupted cN signalling. The observation was characterised by distinct differences in cAMP generation following PDE inhibition. Indeed, abrogated cross-talk between the two cN signalling pathways has been previously reported [96]. These findings suggest that approaches aimed at modulating the activity of specific PDE isoforms or, alternatively, targeting regulators of PDE function may provide a novel strategy for regulating neuronal excitability.

7.4 Elevated Presynaptic β-Adrenergic Signalling in the Stellate Ganglia of Prehypertensive Spontaneously Hypertensive Rat

Disruptions to βAR signalling are a well-documented characteristic of human hypertension, where a plethora of literature has identified alterations in cAMP-PKA signalling within the myocardium that is exacerbated by perturbations in PDE activity[265,266,578]. As such, chronic β-blocker therapy remains a mainstay intervention for clinical hypertension, although the precise mechanisms by which β-blockers improve all-cause mortality is less than clear[401,421].

In Chapter Four, the RNA-seq dataset highlighted the expression of transcripts encoding presynaptic neuronal βARs that was validated in stellate ganglia from human and rat using qRT-PCR and ELISA assays. Using FRET microscopy, the presence of presynaptic neuronal βARs in rat stellate ganglia were found to be functionally relevant where pharmacological activation led to a detectable rise in cAMP generation and PKA activity. Moreover, the cAMP-PKA- Ca^{2+} signalling pathway coupled to βAR activation was significantly elevated in ganglia obtained from young preSHR, where a preferential role for β_2AR was observed. Previous work has demonstrated that the *N*-type Calcium Channel (I_{CaN}) is the primary voltage-gated channel responsible for Ca^{2+} influx in sympathetic neurons; and carries a significantly larger Ca^{2+} current in preSHR neurons compared with controls[96,216]. I_{CaN} activity is differentially regulated by PKA and PKG[96,334], therefore, βAR-potentiated increases in $[Ca^{2+}]_i$ in preSHR stellate neurons are likely to occur as a result of βAR-cAMP activation that increases PKA-dependent phosphorylation of I_{CaN} ($Ca_v2.2$). Together, these data demonstrate that βAR-mediated signalling in sympathetic neurons contributes to the Ca^{2+} phenotype and increases sympathetic activity, highlighting an additional efficacious target for the use of β-blockers in CVD.

7.5 The 'Adrenaline Hypothesis' of Essential Hypertension: Adrenaline Synthesis in Sympathetic Stellate Ganglia

In Chapter Five the concentrations of catecholamines in the rat stellate ganglia was investigated, to provide physiological context relating to the functional relevance of presynaptic sympathetic βARs. The aim of this chapter was to investigate the potential for a feed-forward mechanism that contributes to elevated neurotransmission in prehypertension. The expression of mRNA transcripts encoding the enzymes involved in NA synthesis were confirmed using the RNA-seq dataset and were validated via qRT-PCR in human and rat stellate ganglia RNA

samples. Moreover, the enzyme PNMT required for the conversion of NA to Adr was also found to be expressed in both rat and human stellate ganglia. ELISA assays were performed to measure the relative concentrations of PNMT in TH positive stellate ganglia from human and rat. High levels of TH confirmed the validity of the expression of PNMT within a population of sympathetic neurons.

Following the identification of the catecholamine synthesising enzymes, concentrations of NA and Adr were measured from a single, freshly dissected stellate ganglion, extracted from healthy Wistar rats and prehypertensive SHR. A significant decrease in total NA content was observed in the preSHR ganglia (74.8 % of total catecholamine content) compared to the NA content calculated in Wistar ganglia (91.5 % of total catecholamine content). Conversely, Adr content was found to be significantly elevated in preSHR stellate ganglia (25.2 % of total catecholamines measured) compared with that measured in Wistar ganglia (8.5 % of total catecholamines), highlighting a switch in neurotransmitter synthesis in prehypertension, that was evident prior to increases in arterial blood pressure. In addition to measuring the total catecholamine content, the concentrations of evoked-catecholamines released from preSHR and Wistar ganglia were quantified following electrical field stimulation. In the perfusate samples from preSHR ganglia, it was observed that NA concentrations were significantly elevated compared with concentrations measured in the Wistar, reflecting the widely established literature [190,436]. Conversely, it was also observed that in preSHR stellate ganglia, equivalent amounts Adr were found to be released alongside NA (44 % : 56 %, NA:Adr) that was not evident in the Wistar stellate perfusate (91 % : 9 %, NA:Adr), establishing a critical alteration in catecholamine neurotransmission in the cardiac-stellate ganglia early disease states.

The presence of presynaptic βARs on the cardiac-sympathetic ganglia of human and rat was described in Chapter Four, where presynaptic β_2AR activity was shown to play a dominant role in cAMP generation that was disproportionately elevated in preSHR compared with Wistar

stellate neurons. These results have significance in the context of the results from Chapter Five where significantly elevated concentrations of Adr were released from preSHR ganglia. Indeed , the high efficacy of Adr at β_2ARs facilitates Ad-dependent NA transmission in a wide number of peripheral ganglia[404,405,431] [404,452-454]. As such, elevated Adr transmission may act preferentially on presynaptic cardiac-sympathetic β_2ARs, increasing cAMP-PKA-Ca^{2+} signalling and neurotransmission in disease, in a manner akin to positive feedback. Inhibitors of Adr synthesis or release may provide novel therapeutic benefit in diseases characterised by enhanced sympathetic activity.

7.6 Intracrine Angiotensin Synthesis in the Stellate Ganglia

Elevated RAS signalling is evident in hypertension[76,214,394,395,465-467], heart failure[80,200,468-470] and post-myocardial infarction[471-477], where AngII signalling is involved in enhanced sympathetic transmission[81,472,479-481], cardiac hypertrophy[200,214,467,482-486] impaired calcium handling[465,471,478], vascular remodelling[461,487-490] and pro-inflammatory events[88,145,491]. Conversely, the peptide Ang1-7 opposes the effects of AngII via activation of its cognate receptor Mas, that couples to NO-cGMP[492-494] and is now considered a major counter-regulatory pathway for endogenous protection against several CVDs[474,496-501,504-512]. Emerging evidence suggests that alterations in local RAS signalling within key organs or a collection of tissues may confer more pathophysiological specificity, compared with global changes in AngII[464,527]. Chapter Six was conducted to investigate the potential for a functional intracrine AngII / Ang1-7 system within cardiac-stellate ganglia in prehypertensive and hypertensive states.

The intracrine AngII synthesis pathway was identified in human and rat stellate ganglia using a combination of RNA-seq, qRT-PCR and ELISA assays. This sympathetic intracrine RAS system was shown to be physiologically functional, where detectable concentrations of AngII and Ang1-7 were measured in human and rat stellate ganglia. Moreover, AngII concentrations were found

to be significantly elevated in stellates extracted from preSHR and SHR compared to their normotensive counterparts, that resulted in enhanced electrically-evoked AngII release from adult SHR ganglia. Unexpectedly, normal levels of AngII were found to be released from the preSHR ganglia, however, lower levels of AngII release was found to coincide with a significant elevation in Ang1-7 synthesis, suggesting that Ang1-7 might play a protective role by limiting AngII release through negative feedback mechanisms. Indeed, the presence of the Ang1-7 receptor, Mas, was observed on sympathetic stellate ganglia of human and rat.

In support of this hypothesis, lower concentrations of Ang1-7 were measured in the adult SHR ganglia with established hypertension that correlated with augmented AngII release. Clearly, correlation does not imply causation, however, AngII and Ang1-7 are well established opposing regulators of neuronal transmission in the brain[494,495,508,569,579], and a potentiating role for AngII has been identified within peripheral sympathetic ganglia directly [28,540,580]. Moreover, strong evidence supports a role for NO-cGMP signalling in attenuating peripheral cardiac-sympathetic transmission[96,113,260,261,272,572,573]. Nevertheless, whether the expression of neuronal Mas receptors functionally couple to NO-cGMP and are activated by autocrine and/or paracrine sources of Ang1-7 remains to be established. A model diagram is depicted in Figure 7.1.

7.7 Clinical Significance

Hypertension is central in determining cardiovascular risk and is a strong predictive indicator of morbidity and mortality; however, there still remains an unmet clinical need for disease-modifying and prophylactic interventions. Cardiac-sympathetic hyper-activity is a key feature of human hypertension that is also seen in animal models of CVD[95,96] yet interventions that target this sympathetic phenotype are problematic to develop, due to the anatomical location of the cardiac-sympathetic ganglia[105] and the challenges involved in unravelling the underlying pathophysiological mechanisms. Surgical techniques such as sympathectomy per se, provide symptomatic relief and lead to fewer cardiovascular co-morbidities in hypertension[106] and reduce the incidence of ventricular arrhythmia[107,108], yet these techniques are not without risk[107]. Current pharmacological approaches including β-blockers and AngII inhibitors are mainstay therapeutic strategies for early hypertension and many other CVDs associated with dysautonomia[421]. However, the results described in this thesis suggest that β-blockers may also reduce cardiac-sympathetic excitability in models of hypertension. Approaches that aim to modulate sympathetic over-activity may have both a therapeutic and physiological advantage over surgical techniques, where the results described in this thesis provide a number of potential therapeutic targets. Optimal neuromodulation of sympathetic tone will counteract hypertension-induced cardiovascular damage, whilst retaining a level of sympathetic reserve that will still enable cardiac performance during physical exertion. Gene transfer approaches that modulate cN activity have had some success in improving neuronal activity, and a new era of genetic and protein modification techniques might be predicted to underpin the primary areas of advancement in this field. Moreover, the application of bioinformatics and the integration of machine-learning techniques with primary research may provide novel approaches for assisting diagnoses and prediction[120-123] as well as clarity regarding the complex interactions between pathways and the associated molecular processes[114-119] as a way to facilitate precise therapeutic targeting.

7.8 Conclusion

This thesis supports the notion that elevated cardiac-sympathetic activity and enhanced end-organ transmission are underpinned by increased ion channel activity and alterations in cN and protein kinase signalling that arises from perturbations in PDE activity in the SHR model of hypertension. Moreover, changes in neurotransmitter profiles from a noradrenergic to an adrenergic phenotype in the preSHR, in addition to an alteration in angiotensin-mediated signalling, may exacerbate or play a causative role in sympathetic over-activity via enhanced activation of presynaptic cAMP-coupled βARs and Ca^{2+}-coupled AT_1Rs, thus predisposing to myocardial dysfunction and the development of hypertension. This work describes the differences in the SHR stellate ganglia compared with the Wistar normotensive stellate ganglia, yet the functional significance of these differences in higher mammals remains to be established.

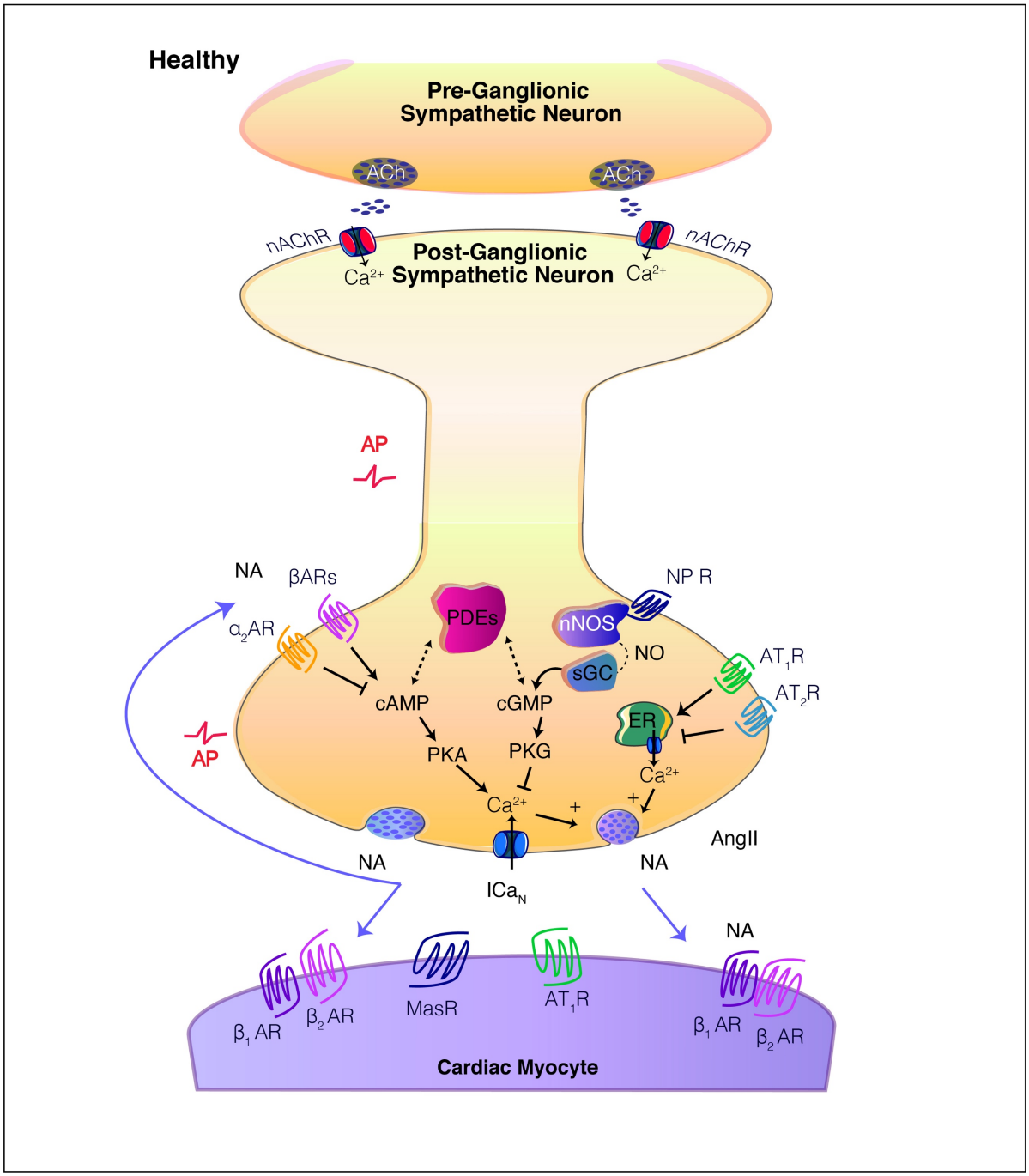


Figure 7.1a. Model Figure: Cardiac-Sympathetic Neurotransmission

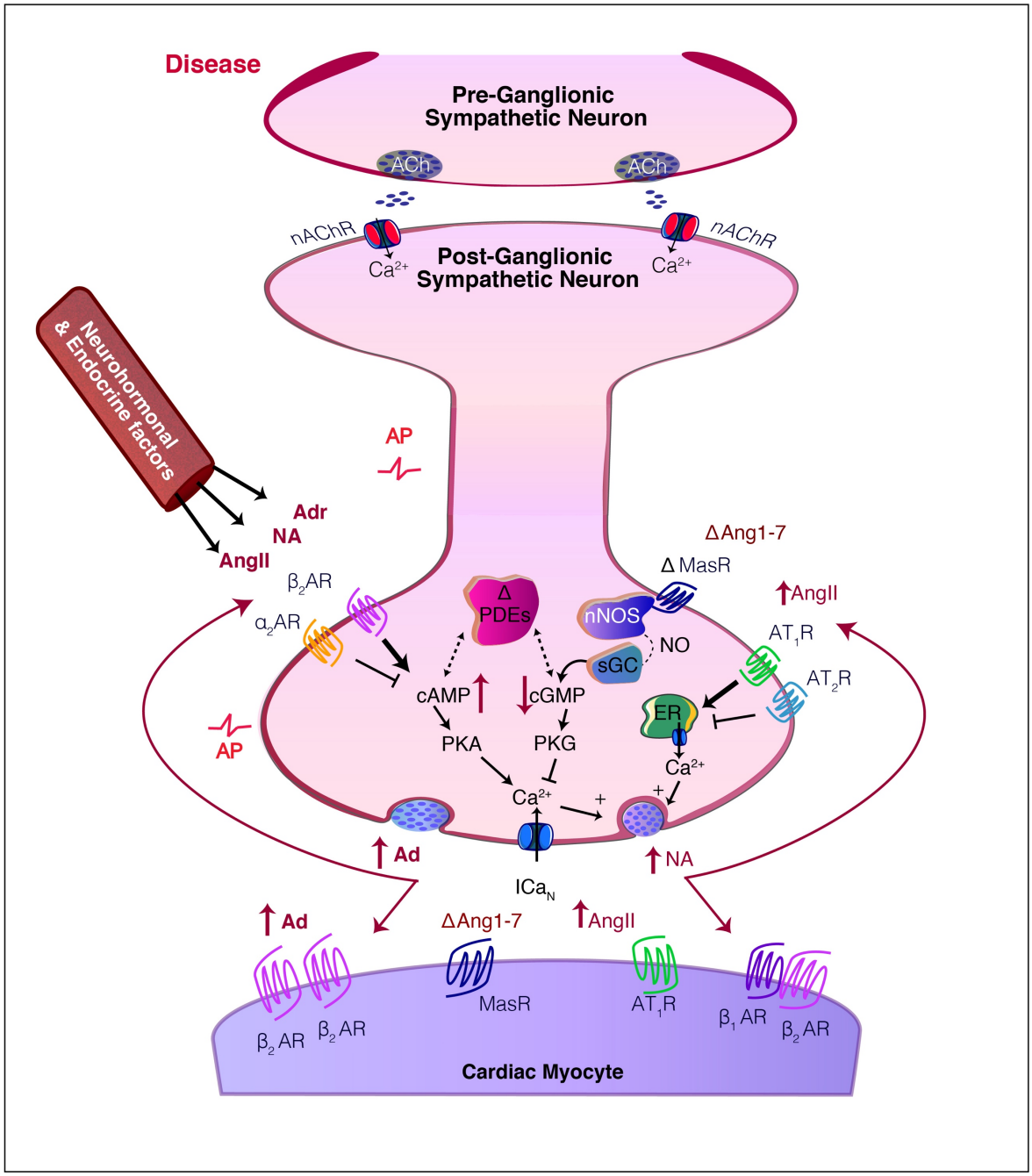


Figure 7.1b. Model Figure: Cardiac-Sympathetic Dysfunction in Hypertension

References

1. World Health Organization. A global brief on hypertension. Silent killer, global public health crisis. 2013:1-40.
2. World Health Organization. The global burden of disease 2004 update. 2004:1-160.
3. NICE: National Institute for Health and Care Excellence. Cardiovascular disease: risk assessment and reduction, including lipid modification. 2014:1-44.
4. Beevers DG, Lip GYH, O'Brien ET. *ABC of Hypertension*. 5 ed. (Beevers DG, Gregory YL, O'Brien ET, eds.). BMJ Books. Blackwell Publishing; 2007.
5. Flack JM, Atlas SA, Pool JL, White WB. Renin-angiotensin aldosterone system and hypertension: current approaches and future directions. *J Manag Care Spec Pharm*. 2007;13(8 Supp B):1-39. doi:10.18553/jmcp.2007.13.s8-b.1.
6. Whelton PK, Carey RM, Aronow WS, Casey DE, Collins KJ, Dennison Himmelfarb C, DePalma SM, Gidding S, Jamerson KA, Jones DW, MacLaughlin EJ, Muntner P, Ovbiagele B, Smith SC, Spencer CC, Stafford RS, Taler SJ, Thomas RJ, Williams KA, Williamson JD, Wright JT. 2017 ACC/ AHA/ AAPA/ ABC/ CPM/ AGS/ APhA/ ASH/ ASPC/ NMA/ PCNA guideline for the prevention, detection, evaluation, and management of high blood pressure in adults: executive summary: a report of the american college of cardiology/american heart association task force on clinical practice guidelines. *Hypertension*. 2018;71(6):1269-1324. doi:10.1161/HYP.0000000000000066.
7. Bakris G, Sorrentino M. Redefining hypertension - assessing the new blood-pressure guidelines. *N Engl J Med*. 2018;378(6):497-499. doi:10.1056/NEJMp1716193.
8. Kjeldsen SE. Hypertension and cardiovascular risk: general aspects. *Pharmacol Res*. 2018;129:95-99. doi:10.1016/j.phrs.2017.11.003.
9. Dunlay SM, Weston SA, Jacobsen SJ, Roger VL. Risk factors for heart failure: a population-based case-control study. *Am J Med*. 2009;122(11):1023-1028. doi:10.1016/j.amjmed.2009.04.022.
10. Cressman MD, Gifford RW. Hypertension and stroke. *J Am Coll Cardiol*. 1983;1(2):521-527. doi:10.1016/S0735-1097(83)80083-7.
11. Kannan A, Janardhanan R. Hypertension as a risk factor for heart failure. *Curr Hypertens Rep*. 2014;16(7):447. doi:10.1007/s11906-014-0447-7.
12. Subramaniam V, Lip GYH. Hypertension to heart failure: a pathophysiological spectrum relating blood pressure, drug treatments and stroke. *Expert Rev Cardiovasc Ther*. 2009;7(6):703-713. doi:10.1586/erc.09.43.
13. Levy D, Larson MG, Vasan RS, Kannel WB, Ho K. The progression from hypertension to congestive heart failure. *JAMA*. 1996;275(20):1557-1562. doi:10.1001/jama.275.20.1557.
14. Dunn FG. Hypertension and myocardial infarction. *J Am Coll Cardiol*. 1983;1(2):528-532. doi:10.1016/s0735-1097(83)80084-9.

15. Pedrinelli R, Ballo P, Fiorentini C, Denti S, Galderisi M, Ganau A, Germanò G, Innelli P, Paini A, Perlini S, Salvetti M, Zacka V, Cardiologia SI. Hypertension and acute myocardial infarction: an overview. *J Cardiovasc Med (Hagerstown)*. 2012;13(3):194-202. doi:10.2459/JCM.0b013e3283511ee2.

16. Stamler J, Vaccaro O, Neaton JD, Wentworth D. Diabetes, other risk-factors, and 12-yr cardiovascular mortality for men screened in the multiple risk factor intervention trial. *Diabetes Care*. 1993;16(2):434-444. doi:10.2337/diacare.16.2.434.

17. Gaede P, Vedel P, Larsen N, Jensen G, Parving H, Pedersen O. Multifactorial intervention and cardiovascular disease in patients with type 2 diabetes. *N Engl J Med*. 2003;348(5):383-393. doi:10.1056/NEJMoa021778.

18. Conde SV, Sacramento JF, Guarino MP, Gonzalez C, Obeso A, Diogo LN, Monteiro EC, Ribeiro MJ. Carotid body, insulin, and metabolic diseases: unraveling the links. *Front Physiol*. 2014;5(51):418. doi:10.3389/fphys.2014.00418.

19. Coresh J, Astor BC, Greene T, Eknoyan G, Levey AS. Prevalence of chronic kidney disease and decreased kidney function in the adult US population: Third National Health and Nutrition Examination Survey. *Am J Kidney Dis*. 2003;41(1):1-12. doi:10.1053/ajkd.2003.50007.

20. The SPRINT Research Group. A randomized trial of intensive versus standard blood-pressure control. *N Engl J Med*. 2015;373(22):2103-2116. doi:10.1056/nejmoa1511939.

21. Everett B, Zajacova A. Gender differences in hypertension and hypertension awareness among young adults. *Biodemography Soc Biol*. 2015;61(1):1-17. doi:10.1080/19485565.2014.929488.

22. Zhang Y, Moran AE. Trends in the prevalence, awareness, treatment, and control of hypertension among young adults in the united states, 1999 to 2014. *Hypertension*. 2017;70(4):736-742. doi:10.1161/HYPERTENSIONAHA.117.09801.

23. Komolova M, Friberg P, Adams MA. Altered vascular resistance properties and acute pressure-natriuresis mechanism in neonatal and weaning spontaneously hypertensive rats. *Hypertension*. 2012;59(5):979-984. doi:10.1161/HYPERTENSIONAHA.111.178194.

24. Higashi Y, Kihara Y, Noma K. Endothelial dysfunction and hypertension in aging. *Hypertens Res*. 2012;35(11):1039-1047. doi:10.1038/hr.2012.138.

25. Schulz E, Gori T, Münzel T. Oxidative stress and endothelial dysfunction in hypertension. *Hypertens Res*. 2011;34(6):665-673. doi:10.1038/hr.2011.39.

26. Guyton AC, Coleman TG, Cowley AW, Liard JF, Norman RA, Manning RD. Systems analysis of arterial pressure regulation and hypertension. *Ann Biomed Eng*. 1972;1(2):254-281. doi:10.1007/BF02584211.

27. Guyenet PG. The sympathetic control of blood pressure. *Nat Rev Neurosci*. 2006;7(5):335-346. doi:10.1038/nrn1902.

28. Malpas SC. Sympathetic nervous system overactivity and its role in the development of cardiovascular disease. *Physiol Rev*. 2010;90(2):513-557. doi:10.1152/physrev.00007.2009.

29. Grassi G, Mark A, Esler M. The sympathetic nervous system alterations in human hypertension. *Circ Res*. 2015;116(6):976-990. doi:10.1161/CIRCRESAHA.116.303604.

30. Solak Y, Afsar B, Vaziri ND, Aslan G, Yalcin CE, Covic A, Kanbay M. Hypertension as an autoimmune and inflammatory disease. *Hypertens Res*. 2016;39(8):567-573. doi:10.1038/hr.2016.35.

31. Lim SS, Vos T, Flaxman AD, Danaei G, Shibuya K, Adair-Rohani H, Amann M, Anderson HR, Andrews KG, Aryee M, Atkinson C, Bacchus LJ, Bahalim AN, Balakrishnan K, Balmes J, Barker-Collo S, Baxter A, Bell ML, Blore JD, Blyth F, Bonner C, Borges G, Bourne R, Boussinesq M, Brauer M, Brooks P, Bruce NG, Brunekreef B, Bryan-Hancock C, Bucello C, Buchbinder R, Bull F, Burnett RT, Byers TE, Calabria B, Carapetis J, Carnahan E, Chafe Z, Charlson F, Chen H, Chen JS, Cheng AT-A, Child JC, Cohen A, Colson KE, Cowie BC, Darby S, Darling S, Davis A, Degenhardt L, Dentener F, Jarlais Des DC, Devries K, Dherani M, Ding EL, Dorsey ER, Driscoll T, Edmond K, Ali SE, Engell RE, Erwin PJ, Fahimi S, Falder G, Farzadfar F, Ferrari A, Finucane MM, Flaxman S, Fowkes FGR, Freedman G, Freeman MK, Gakidou E, Ghosh S, Giovannucci E, Gmel G, Graham K, Grainger R, Grant B, Gunnell D, Gutierrez HR, Hall W, Hoek HW, Hogan A, Hosgood HDI, Hoy D, Hu H, Hubbell BJ, Hutchings SJ, Ibeanusi SE, Jacklyn GL, Jasrasaria R, Jonas JB, Kan H, Kanis JA, Kassebaum N, Kawakami N, Khang Y-H, Khatibzadeh S, Khoo J-P, et al. A comparative risk assessment of burden of disease and injury attributable to 67 risk factors and risk factor clusters in 21 regions, 1990-2010: a systematic analysis for the Global Burden of Disease Study 2010. *Lancet*. 2012;380(9859):2224-2260. doi:10.1016/S0140-6736(12)61766-8.

32. Page IH. The mosaic theory of arterial hypertension—: It's interpretation. *Perspect Biol Med*. 1967;10(3):325-333. doi:10.1353/pbm.1967.0031.

33. Harrison DG. The mosaic theory revisited: common molecular mechanisms coordinating diverse organ and cellular events in hypertension. *J Am Soc Hypertens*. 2013;7(1):68-74. doi:10.1016/j.jash.2012.11.007.

34. Garfinkle MA. Salt and essential hypertension: pathophysiology and implications for treatment. *J Am Soc Hypertens*. 2017;11(6):385-391. doi:10.1016/j.jash.2017.04.006.

35. Hall JE, do Carmo JM, da Silva AA, Wang Z, Hall ME. Obesity-induced hypertension: interaction of neurohumoral and renal mechanisms. *Circ Res*. 2015;116(6):991-1006. doi:10.1161/CIRCRESAHA.116.305697.

36. Johncy SS, Karthik CS, Bondade SY, Jayalakshmi MK. Altered cardiovascular autonomic function in young normotensive offspring of hypertensive parents-Is obesity an additional risk factor? *J Basic Clin Physiol Pharmacol*. 2015;26(6):531-537. doi:10.1515/jbcpp-2014-0068.

37. Re RN. Obesity-related hypertension. *Ochsner J*. 2009;9(3):133-136.

38. Sleight P. Smoking and hypertension. *Clin Exp Hypertens*. 1993;15(6):1181-1192. doi:10.3109/10641969309037104.

39. Leone A. Smoking and hypertension. *Journal of Cardiology & Current Research*. 2015;2(2). doi:10.15406/jccr.2015.02.00057.

40. Diaz KM, Shimbo D. Physical activity and the prevention of hypertension. *Curr Hypertens Rep*. 2013;15(6):659-668. doi:10.1007/s11906-013-0386-8.

41. Sohn MW, Manheim LM, Chang RW, Greenland P, Hochberg MC, Nevitt MC, Semanik PA, Dunlop DD. Sedentary behavior and blood pressure control among osteoarthritis initiative participants. *Osteoarthr Cartil*. 2014;22(9):1234-1240. doi:10.1016/j.joca.2014.07.007.

42. Bennett A, Parto P, Krim SR. Hypertension and ethnicity. *Curr Opin Cardiol*. 2016;31(4):381-386. doi:10.1097/HCO.0000000000000293.

43. Ventura HO, Lavie CJ. Impact of comorbidities in hypertension. *Curr Opin Cardiol*. 2016;31(4):374-375. doi:10.1097/HCO.0000000000000302.

44. Hausberg M, Sinkey CA, Mark AL, Hoffman RP, Anderson EA. Sympathetic nerve activity and insulin sensitivity in normotensive offspring of hypertensive parents. *Am J Hypertens*. 1998;11(11):1312-1320.

45. Hamer M. The effects of exercise on haemodynamic function in relation to the familial hypertension risk model. *J Hum Hypertens*. 2006;20(5):313-319. doi:10.1038/sj.jhh.1001999.

46. Pal GK, Pal P, Nanda N, Lalitha V, Dutta TK, Adithan C. Sympathovagal imbalance in prehypertensive offspring of two parents versus one parent hypertensive. *Int J Hypertens*. 2011;2011:263170. doi:10.4061/2011/263170.

47. Rathi P, Agarwal V, Kumar A. Sympathetic hyperactivity in children of hypertensive parents. *Ann Neurosci*. 2013;20(1):4-6. doi:10.5214/ans.0972.7531.200103.

48. Kessler T, Vilne B, Schunkert H. The impact of genome-wide association studies on the pathophysiology and therapy of cardiovascular disease. *EMBO Mol Med*. 2016;8(7):688-701. doi:10.15252/emmm.201506174.

49. Levy D, Ehret GB, Rice K, Verwoert GC, Launer LJ, Dehghan A, Glazer NL, Morrison AC, Johnson AD, Aspelund T, Aulchenko Y, Lumley T, Köttgen A, Vasan RS, Rivadeneira F, Eiriksdottir G, Guo X, Arking DE, Mitchell GF, Mattace-Raso FUS, Smith AV, Taylor K, Scharpf RB, Hwang S-J, Sijbrands EJG, Bis J, Harris TB, Ganesh SK, O'Donnell CJ, Hofman A, Rotter JI, Coresh J, Benjamin EJ, Uitterlinden AG, Heiss G, Fox CS, Witteman JCM, Boerwinkle E, Wang TJ, Gudnason V, Larson MG, Chakravarti A, Psaty BM, van Duijn CM. Genome-wide association study of blood pressure and hypertension. *Nat Genet*. 2009;41(6):677-687. doi:10.1038/ng.384.

50. Ehret GB, Munroe PB, Rice KM, Bochud M, Johnson AD, Chasman DI, Smith AV, Tobin MD, Verwoert GC, Hwang S-J, Pihur V, Vollenweider P, O'Reilly PF, Amin N, Bragg-Gresham JL, Teumer A, Glazer NL, Launer L, Zhao JH, Aulchenko Y, Heath S, Sõber S, Parsa A, Luan J, Arora P, Dehghan A, Zhang F, Lucas G, Hicks AA, Jackson AU, Peden JF, Tanaka T, Wild SH, Rudan I, Igl W, Milaneschi Y, Parker AN, Fava C, Chambers JC, Fox ER, Kumari M, Go MJ, van der Harst P, Kao WHL, Sjögren M, Vinay DG, Alexander M, Tabara Y, Shaw-Hawkins S, Whincup PH, Liu Y, Shi G, Kuusisto J, Tayo B, Seielstad M, Sim X, Nguyen K-DH, Lehtimäki T, Matullo G, Wu Y, Gaunt TR, Onland-Moret NC, Cooper MN, Platou CGP, Org E, Hardy R, Dahgam S, Palmen J, Vitart V, Braund PS, Kuznetsova T, Uiterwaal CSPM, Adeyemo A, Palmas W, Campbell H, Ludwig B, Tomaszewski M, Tzoulaki I, Palmer ND, Aspelund T, Garcia M, Chang Y-PC, O'Connell JR, Steinle NI, Grobbee DE, Arking DE, Kardia SL, Morrison AC, Hernandez D, Najjar S, McArdle WL, Hadley D, Brown MJ, Connell JM, Hingorani AD, Day INM, Lawlor DA, Beilby JP, et al. Genetic variants in novel pathways

influence blood pressure and cardiovascular disease risk. *Nature*. 2011;478(7367):103-109. doi:10.1038/nature10405.

51. Dehghan A, Bis JC, White CC, Smith AV, Morrison AC, Cupples LA, Trompet S, Chasman DI, Lumley T, Völker U, Buckley BM, Ding J, Jensen MK, Folsom AR, Kritchevsky SB, Girman CJ, Ford I, Dörr M, Salomaa V, Uitterlinden AG, Eiriksdottir G, Vasan RS, Franceschini N, Carty CL, Virtamo J, Demissie S, Amouyel P, Arveiler D, Heckbert SR, Ferrières J, Ducimetière P, Smith NL, Wang YA, Siscovick DS, Rice KM, Wiklund P-G, Taylor KD, Evans A, Kee F, Rotter JI, Karvanen J, Kuulasmaa K, Heiss G, Kraft P, Launer LJ, Hofman A, Markus MRP, Rose LM, Silander K, Wagner P, Benjamin EJ, Lohman K, Stott DJ, Rivadeneira F, Harris TB, Levy D, Liu Y, Rimm EB, Jukema JW, Völzke H, Ridker PM, Blankenberg S, Franco OH, Gudnason V, Psaty BM. Genome-wide association study for incident myocardial infarction and coronary heart disease in prospective cohort studies: The CHARGE consortium. *PLoS ONE*. 2016;11(3):e0144997. doi:10.1371/journal.pone.0144997.

52. Nikpay M, Goel A, Won H-H, Hall LM, Willenborg C, Kanoni S, Saleheen D, Kyriakou T, Nelson CP, Hopewell JC, Webb TR, Zeng L, Dehghan A, Alver M, Armasu SM, Auro K, Bjonnes A, Chasman DI, Chen S, Ford I, Franceschini N, Gieger C, Grace C, Gustafsson S, Huang J, Hwang S-J, Kim YK, Kleber ME, Lau KW, Lu X, Lu Y, Lyytikäinen L-P, Mihailov E, Morrison AC, Pervjakova N, Qu L, Rose LM, Salfati E, Saxena R, Scholz M, Smith AV, Tikkanen E, Uitterlinden A, Yang X, Zhang W, Zhao W, de Andrade M, de Vries PS, van Zuydam NR, Anand SS, Bertram L, Beutner F, Dedoussis G, Frossard P, Gauguier D, Goodall AH, Gottesman O, Haber M, Han B-G, Huang J, Jalilzadeh S, Kessler T, König IR, Lannfelt L, Lieb W, Lind L, Lindgren CM, Lokki M-L, Magnusson PK, Mallick NH, Mehra N, Meitinger T, Memon F-U-R, Morris AP, Nieminen MS, Pedersen NL, Peters A, Rallidis LS, Rasheed A, Samuel M, Shah SH, Sinisalo J, Stirrups KE, Trompet S, Wang L, Zaman KS, Ardissino D, Boerwinkle E, Borecki IB, Bottinger EP, Buring JE, Chambers JC, Collins R, Cupples LA, Danesh J, Demuth I, Elosua R, Epstein SE, et al. A comprehensive 1,000 Genomes-based genome-wide association meta-analysis of coronary artery disease. *Nat Methods*. 2015;47(10):1121-1130. doi:10.1038/ng.3396.

53. Milan DJ, Lubitz SA, Kääb S, Ellinor PT. Genome-wide association studies in cardiac electrophysiology: Recent discoveries and implications for clinical practice. *Heart Rhythm*. 2010;7(8):1141-1148. doi:10.1016/j.hrthm.2010.04.021.

54. Napier MD, Franceschini N, Gondalia R, Stewart JD, Méndez-Giráldez R, Sitlani CM, Seyerle AA, Highland HM, Li Y, Wilhelmsen KC, Yan S, Duan Q, Roach J, Yao J, Guo X, Taylor KD, Heckbert SR, Rotter JI, North KE, Reiner AP, Zhang Z-M, Tinker LF, Liao D, Laurie CC, Gogarten SM, Lin HJ, Brody JA, Bartz TM, Psaty BM, Sotoodehnia N, Soliman EZ, Avery CL, Whitsel EA. Genome-wide association study and meta-analysis identify loci associated with ventricular and supraventricular ectopy. *Sci Rep*. 2018;8(1):5675. doi:10.1038/s41598-018-23843-z.

55. Nielsen JB, Thorolfsdottir RB, Fritsche LG, Zhou W, Skov MW, Graham SE, Herron TJ, McCarthy S, Schmidt EM, Sveinbjornsson G, Surakka I, Mathis MR, Yamazaki M, Crawford RD, Gabrielsen ME, Skogholt AH, Holmen OL, Lin M, Wolford BN, Dey R, Dalen H, Sulem P, Chung JH, Backman JD, Arnar DO, Thorsteinsdottir U, Baras A, O'Dushlaine C, Holst AG, Wen X, Hornsby W, Dewey FE, Boehnke M, Kheterpal S, Mukherjee B, Lee S, Kang HM, Holm H, Kitzman J, Shavit JA, Jalife J, Brummett CM, Teslovich TM, Carey DJ, Gudbjartsson DF,

Stefansson K, Abecasis GR, Hveem K, Willer CJ. Biobank-driven genomic discovery yields new insight into atrial fibrillation biology. *Nat Methods*. 2018;49(Suppl.):1593. doi:10.1038/s41588-018-0171-3.

56. Krogh A, Lindhard J. The regulation of respiration and circulation during the initial stages of muscular work. *J Physiol (Lond)*. 1913;47(1-2):112-136. doi:10.1113/jphysiol.1913.sp001616.

57. Hamer M, Taylor A, Steptoe A. The effect of acute aerobic exercise on stress related blood pressure responses: a systematic review and meta-analysis. *Biological Psychology*. 2006;71(2):183-190. doi:10.1016/j.biopsycho.2005.04.004.

58. Trapp M, Trapp E-M, Egger JW, Domej W, Schillaci G, Avian A, Rohrer PM, Hörlesberger N, Magometschnigg D, Cervar-Zivkovic M, Komericki P, Velik R, Baulmann J. Impact of mental and physical stress on blood pressure and pulse pressure under normobaric versus hypoxic conditions. *PLoS ONE*. 2014;9(5):e89005. doi:10.1371/journal.pone.0089005.

59. Brook RD. The environment and blood pressure. *Cardiol Clin*. 2017;35(2):213-221. doi:10.1016/j.ccl.2016.12.003.

60. Brook RD, Weder AB, Rajagopalan S. “Environmental hypertensionology” the effects of environmental factors on blood pressure in clinical practice and research. *J Clin Hypertens (Greenwich)*. 2011;13(11):836-842. doi:10.1111/j.1751-7176.2011.00543.x.

61. Harvey W, Willis R. *The Works of William Harvey*. 1847. https://archive.org/details/worksofwilliamha00harviala.

62. Harvey W, Leake CD. *Anatomical Studies on the Motion of the Heart and Blood (Exertitation Anatomica De Motu Cordis Et Sanguinis in Animalibus)*. Southern Medical Journal; 1929.

63. Patterson SW, Starling EH. On the mechanical factors which determine the output of the ventricles. *J Physiol (Lond)*. 1914;48(5):357-379. doi:10.1113/jphysiol.1914.sp001669.

64. Guyton AC, Lindsey AW, Abernathy B, Richardson T. Venous return at various right atrial pressures and the normal venous return curve. *Am J Physiol*. 1957;189(3):609-615. doi:10.1152/ajplegacy.1957.189.3.609.

65. Heymans C. Reflexogenic areas of the cardiovascular system. *Perspect Biol Med*. 1960;3(3):409-417. doi:10.1353/pbm.1960.0038.

66. Herring N, Paterson DJ. *Levick's Introduction to Cardiovascular Physiology*. CRC Press Taylor and Francis Group; 2018.

67. Pilowsky PM, Goodchild AK. Baroreceptor reflex pathways and neurotransmitters: 10 Years on. *J Hypertens*. 2002;20(9):1675-1688. doi:10.1097/00004872-200209000-00002.

68. Spyer KM. Neural organisation and control of the baroreceptor reflex. *Rev Physiol Biochem Pharmacol*. 1981;88:24-124.

69. Marshall JM. Peripheral chemoreceptors and cardiovascular regulation. *Physiol Rev*. 1994;74(3):543-594. doi:10.1152/physrev.1994.74.3.543.

70. Peers C, Kumar P, Wyatt C, Gauda E, Nurse CA, Prabhakar N. *Arterial Chemoreceptors in Physiology and Pathophysiology*. Vol 860. Springer; 2015. doi:10.1007/978-3-319-18440-1.

71. Jones JE, Natarajan AR, Jose PA. Cardiovascular and Autonomic Influences on Blood Pressure. In: *Pediatric Hypertension*. Totowa, NJ: Humana Press, Totowa, NJ; 2004:23-43. doi:10.1007/978-1-59259-797-0_2.

72. Spyer KM. Central nervous integration of cardiovascular control. *J Exp Biol*. 1982;100:109-128.

73. Rowell LB, O'Leary DS. Reflex control of the circulation during exercise: chemoreflexes and mechanoreflexes. *Journal of Applied Physiology*. 1990;69(2):407-418. doi:10.1152/jappl.1990.69.2.407.

74. Cowley AW. Long-term control of arterial blood pressure. *Physiol Rev*. 1992;72(1):231-300. doi:10.1152/physrev.1992.72.1.231.

75. Guyton AC. Blood pressure control - Special role of the kidneys and body fluids. *Science*. 1991;252(5014):1813-1816. doi:10.1126/science.2063193.

76. Riet Te L, Van Esch JHM, Roks AJM, Van Den Meiracker AH, Danser AHJ. Hypertension: renin-angiotensin-aldosterone system alterations. *Circ Res*. 2015;116(6):960-975. doi:10.1161/CIRCRESAHA.116.303587.

77. Granger JP, Alexander BT, Llinas M. Mechanisms of pressure natriuresis. *Curr Hypertens Rep*. 2002;4(2):152-159. doi:10.1007/s11906-002-0040-3.

78. de Gasparo M, Catt KJ, Inagami T, Wright JW, Unger T. International union of pharmacology. XXIII. The angiotensin II receptors. *Pharmacol Rev*. 2000;52(3):415-472.

79. Crowley SD, Gurley SB, Coffman TM. AT1 receptors and control of blood pressure: the kidney and more…. *Trends Cardiovasc Med*. 2007;17(1):30-34. doi:10.1016/j.tcm.2006.11.002.

80. Rupp H, Jäger B. The renin-angiotensin system and the sympathetic nervous system in hypertension and congestive heart failure: Implications for therapeutic interventions. *Journal of Clinical & Basic Cardiology*. 2001;4(1):47-51.

81. Hilgers KF, Veelken R, Rupprecht G, Reeh PW, Luft FC, Mann JF. Angiotensin II facilitates sympathetic transmission in rat hind limb circulation. *Hypertension*. 1993;21(3):322-328. doi:10.1161/01.hyp.21.3.322.

82. Ritz E, Tomaschitz A. Aldosterone and the kidney: A rapidly moving frontier (an update). *Nephrol Dial Transplant*. 2014;29(11):2012-2019. doi:10.1093/ndt/gft035.

83. Muï oz-Durango N, Fuentes CBA, Castillo ASE, Gonzï lez-Gï mez LMN, Vecchiola A, Fardella CE, Kalergis AM. Role of the renin-angiotensin-aldosterone system beyond blood pressure regulation: Molecular and cellular mechanisms involved in end-organ damage during arterial hypertension. *Int J Mol Sci*. 2016;17(7). doi:10.3390/ijms17070797.

84. Spät A, Hunyady L. Control of aldosterone secretion: a model for convergence in cellular signaling pathways. *Physiol Rev*. 2004;84(2):489-539. doi:10.1152/physrev.00030.2003.

85. Frishman WH. Beta-adrenergic receptor blockers in hypertension: alive and well. *Prog Cardiovasc Dis*. 2016;59(3):247-252. doi:10.1016/j.pcad.2016.10.005.

86. Ram CVS. Beta-blockers in hypertension. *Asian-australas J Anim Sci*. 2010;106(12):1819-1825. doi:10.1016/j.amjcard.2010.08.023.

87. Jackson RE, Bellamy MC. Antihypertensive drugs. *BJA Education*. 2015;15(6):280-285. doi:10.1093/bjaceaccp/mku061.

88. Ferrario CM, Strawn WB. Role of the renin-angiotensin-aldosterone system and proinflammatory mediators in cardiovascular disease. *Am J Cardiol*. 2006;98(1):121-128. doi:10.1016/j.amjcard.2006.01.059.

89. Eriksson U, Danilczyk U, Penninger JM. Just the beginning: novel functions for angiotensin-converting enzymes. *Current Biology*. 2002;12(21):R745-R752. doi:10.1016/S0960-9822(02)01255-1.

90. Piepho RW, Beal J. An overview of antihypertensive therapy in the 20th century. *J Clin Pharmacol*. 2013;40(9):967-977. doi:10.1177/00912700022009693.

91. Berridge MJ. Elementary and global aspects of calcium signalling. *J Exp Biol*. 1997;200(Pt 2):315-319. doi:10.1111/(ISSN)1469-7793.

92. Opie LH. Pharmacological differences between calcium antagonists. *Eur Heart J*. 1997;18(SUPPL. A):A71-A79.

93. Sanguinetti MC, Kass RS. Voltage-dependent block of calcium-channel current in the calf cardiac purkinje-fiber by dihydropyridine calcium-channel antagonists. *Circ Res*. 1984;55(3):336-348. doi:10.1161/01.RES.55.3.336.

94. Sica DA. Alpha1-adrenergic blockers: current usage considerations. *J Clin Hypertens (Greenwich)*. 2005;7(12):757-762. doi:10.1111/j.1524-6175.2005.05300.x.

95. Esler M. Sympathetic nervous activation in essential hypertension: commonly neglected as a therapeutic target, usually ignored as a drug side effect. *Hypertension*. 2010;55(5):1090-1091. doi:10.1161/HYPERTENSIONAHA.110.151506.

96. Larsen HE, Bardsley EN, Lefkimmiatis K, Paterson DJ. Dysregulation of neuronal Ca^{2+} channel linked to heightened sympathetic phenotype in prohypertensive states. *J Neurosci*. 2016;36(33):8562-8573. doi:10.1523/JNEUROSCI.1059-16.2016.

97. Oliveira-Sales EB, Toward MA, Campos RR, Paton JFR. Revealing the role of the autonomic nervous system in the development and maintenance of Goldblatt hypertension in rats. *Auton Neurosci*. 2014;183:23-29. doi:10.1016/j.autneu.2014.02.001.

98. Heaton DA, Li D, Almond SC, Dawson TA, Wang L, Channon KM, Paterson DJ. Gene transfer of neuronal nitric oxide synthase into intracardiac ganglia reverses vagal impairment in hypertensive rats. *Hypertension*. 2007;49(2):380-388. doi:10.1161/01.HYP.0000255792.97033.f7.

99. Danson EJ, Li D, Wang L, Dawson TA, Paterson DJ. Targeting cardiac sympatho-vagal imbalance using gene transfer of nitric oxide synthase. *J Mol Cell Cardiol*. 2009;46(4):482-489. doi:10.1016/j.yjmcc.2008.12.013.

100. Shanks J, Manou-Stathopoulou S, Lu C-J, Li D, Paterson DJ, Herring N. Cardiac sympathetic dysfunction in the prehypertensive spontaneously hypertensive rat. *Am J Physiol Heart Circ Physiol*. 2013;305(7):H980-H986. doi:10.1152/ajpheart.00255.2013.

101. Parati G, Esler M. The human sympathetic nervous system: Its relevance in hypertension and heart failure. *Eur Heart J*. 2012;33(9):1058-1066. doi:10.1093/eurheartj/ehs041.

102. Meredith IT, Broughton A, Jennings GL, Esler MD. Evidence of a selective increase in cardiac sympathetic activity in patients with sustained ventricular arrhythmias. *N Engl J Med*. 1991;325(9):618-624. doi:10.1056/nejm199108293250905.

103. Florea VG, Cohn JN. The autonomic nervous system and heart failure. *Circ Res*. 2014;114(11):1815-1826. doi:10.1161/CIRCRESAHA.114.302589.

104. Kaye DM, Lefkovits J, Jennings GL, Bergin P, Broughton A, Esler MD. Adverse consequences of high sympathetic nervous activity in the failing human heart. *J Am Coll Cardiol*. 1995;26(5):1257-1263. doi:10.1016/0735-1097(95)00332-0.

105. Kwon OJ, Pendekanti S, Fox JN, Yanagawa J, Fishbein MC, Shivkumar K, Lambert HW, Ajijola OA. Morphological spectra of adult human stellate ganglia: implications for thoracic sympathetic denervation. *Anat Rec (Hoboken)*. 2018;301:1244-1250. doi:10.1002/ar.23797.

106. Morrissey DM, Brookes VS, Cooke WT. Sympathectomy in the treatment of hypertension - review of 122 cases. *Lancet*. 1953;264:403-412.

107. Ajijola OA, Vaseghi M, Mahajan A, Shivkumar K. Bilateral cardiac sympathetic denervation: why, who and when? *Expert Rev Cardiovasc Ther*. 2014;10(8):947-949. doi:10.1586/erc.12.93.

108. Irie T, Yamakawa K, Hamon D, Nakamura K, Shivkumar K, Vaseghi M. Cardiac sympathetic innervation via middle cervical and stellate ganglia and antiarrhythmic mechanism of bilateral stellectomy. *Am J Physiol Heart Circ Physiol*. 2017;312(3):H392-H405. doi:10.1152/ajpheart.00644.2016.

109. Iliescu R, Lohmeier TE, Tudorancea I, Laffin L, Bakris GL. Renal denervation for the treatment of resistant hypertension: review and clinical perspective. *Am J Physiol Renal Physiol*. 2015;309(7):F583-F594. doi:10.1152/ajprenal.00246.2015.

110. Azizi M. Catheter-based renal denervation for treatment of hypertension. *Lancet*. 2017;390(10108):2124-2126. doi:10.1016/S0140-6736(17)32293-6.

111. Specialised Commissioning Team. Clinical Commissioning Policy: Renal denervation for resistant hypertension. https://www.england.nhs.uk/wp-content/uploads/2018/07/Renal-denervation-for-resistant-hypertension.pdf. https://www.england.nhs.uk/wp-content/uploads/2018/07/Renal-denervation-for-resistant-hypertension.pdf. Published 2016.

112. Choate JK, Paterson DJ. Nitric oxide inhibits the positive chronotropic and inotropic responses to sympathetic nerve stimulation in the isolated guinea-pig atria. *J Auton Nerv Syst*. 1999;75(2-3):100-108. doi:10.1016/S0165-1838(98)00173-8.

113. Li D, Nikiforova N, Lu C-J, Wannop K, McMenamin M, Lee C-W, Buckler KJ, Paterson DJ. Targeted neuronal nitric oxide synthase transgene delivery into stellate neurons reverses impaired intracellular calcium transients in prehypertensive rats. *Hypertension*. 2013;61(1):202-207. doi:10.1161/HYPERTENSIONAHA.111.00105.

114. Xie Z-R, Chen J, Wu Y. Predicting protein-protein association rates using coarse-grained simulation and machine learning. *Sci Rep*. 2017;7(1):1-17. doi:10.1038/srep46622.

115. Wang W, Yang Y, Yin J, Gong X. Different protein-protein interface patterns predicted by different machine learning methods. *Sci Rep*. 2017;7(1):16023. doi:10.1038/s41598-017-16397-z.

116. Pavillon N, Hobro AJ, Akira S, Smith NI. Noninvasive detection of macrophage activation with single-cell resolution through machine learning. *Proc Natl Acad Sci USA*. 2018;115(12):E2676-E2685. doi:10.1073/pnas.1711872115.

117. Costello Z, Martin HG. A machine learning approach to predict metabolic pathway dynamics from time-series multiomics data. *NPJ Syst Biol Appl*. 2018;4(1):19. doi:10.1038/s41540-018-0054-3.

118. Cunningham RJ. The application of deep convolutional neural networks to ultrasound for modelling of dynamic states within human skeletal muscle. *bioRxiv*. 2017. doi:http://dx.doi.org/10.1101/157479.

119. Cholley P-E, Moehlin J, Rohmer A, Zilliox V, Nicaise S, Gronemeyer H, Mendoza-Parra MA. Modeling gene-regulatory networks to describe cell fate transitions and predict master regulators. *NPJ Syst Biol Appl*. 2018;29:1-5. doi:10.1038/s41540-018-0066-z.

120. Savage N. Machine learning: Calculating disease. *Nature*. 2017;550(7676):S115-S117. doi:10.1038/550S115a.

121. Poplin R, Varadarajan AV, Blumer K, Liu Y, McConnell MV, Corrado GS, Peng L, Webster DR. Prediction of cardiovascular risk factors from retinal fundus photographs via deep learning. *Nat Biomed Eng*. 2018;2(3):158-164. doi:10.1038/s41551-018-0195-0.

122. LaFreniere D, Zulkernine F, Barber D, Martin K. Using machine learning to predict hypertension from a clinical dataset. In: IEEE; 2016:1-7. doi:10.1109/ssci.2016.7849886.

123. Kublanov VS, Dolganov AY, Belo D, Gamboa H. Comparison of machine learning methods for the arterial hypertension diagnostics. *Appl Bionics Biomech*. 2017;2017(1). doi:https://doi.org/10.1155/2017/5985479.

124. Franco NH. Animal experiments in biomedical research: a historical perspective. *Animals (Basel)*. 2013;3(1):238-273. doi:10.3390/ani3010238.

125. Doggrell SA, Brown L. Rat models of hypertension, cardiac hypertrophy and failure. *Cardiovasc Res*. 1998;39(1):89-105.

126. Pinto YM, Paul M, Ganten D. Lessons from rat models of hypertension: from Goldblatt to genetic engineering. *Cardiovasc Res*. 1998;39(1):77-88. doi:10.1016/S0008-6363(98)00077-7.

127. Dornas WC, Silva ME. Animal models for the study of arterial hypertension. *J Biosci*. 2011;36(4):731-737. doi:10.1007/s12038-011-9097-y.

128. Navar LG, Zou L, Thun Von A, Tarng Wang C, Imig JD, Mitchell KD. Unraveling the Mystery of Goldblatt Hypertension. *Physiology*. 1998;13:170-176.

129. Lerman LO, Chade AR, Sica V, Napoli C. Animal models of hypertension: an overview. *J Lab Clin Med*. 2005;146(3):160-173. doi:10.1016/j.lab.2005.05.005.

130. Petersson MJ, Rundqvist B, Johansson M, Eisenhofer G, Lambert G, Herlitz H, Jensen G, Friberg P. Increased cardiac sympathetic drive in renovascular hypertension. *J Hypertens*. 2002;20(6):1181-1187. doi:10.1097/00004872-200206000-00031.

131. Johansson M, Elam M, Rundqvist B, Eisenhofer G, Herlitz H, Lambert G, Friberg P. Increased sympathetic nerve activity in renovascular hypertension. *Circulation*. 1999;99(19):2537-2542. doi:10.1161/01.CIR.99.19.2537.

132. Tromp TR, Mahesh D, Joles JA, Ramchandra R. Direct recording of cardiac and renal sympathetic nerve activity shows differential control in renovascular hypertension. *Hypertension*. 2018;71(6):1108-1116. doi:10.1161/HYPERTENSIONAHA.117.10749.

133. Pijacka W, McBryde FD, Marvar PJ, Lincevicius GS, Abdala APL, Woodward L, Li D, Paterson DJ, Paton JFR. Carotid sinus denervation ameliorates renovascular hypertension in adult Wistar rats. *J Physiol (Lond)*. 2016;594(21):6255-6266. doi:10.1113/JP272708.

134. Monassier L, Combe R, Fertak LE. Mouse models of hypertension. *Drug Discov Today Dis Models*. 2006;3(3):273-281. doi:10.1016/j.ddmod.2006.10.008.

135. Okamoto K, Aoki K. Development of a strain of spontaneously hypertensive rats. *Jpn Circ J*. 1963;27(3):282-293. doi:10.1253/jcj.27.282.

136. Doris PA. Genetics of hypertension: An assessment of progress in the spontaneously hypertensive rat. *Physiol Genomics*. 2017;49(11):601-617. doi:10.1152/physiolgenomics.00065.2017.

137. Oliveira-Sales EB, Colombari E, Abdala AP, Campos RR, Paton JFR. Sympathetic overactivity occurs before hypertension in the two-kidney, one-clip model. *Exp Physiol*. 2016;101(1):67-80. doi:10.1113/EP085390.

138. Abdala AP, McBryde FD, Marina N, Hendy EB, Engelman ZJ, Fudim M, Sobotka PA, Gourine AV, Paton JFR. Hypertension is critically dependent on the carotid body input in the spontaneously hypertensive rat. *J Physiol (Lond)*. 2012;590(17):4269-4277. doi:10.1113/jphysiol.2012.237800.

139. Smith TL, Hutchins PM. Central hemodynamics in the developmental stage of spontaneous hypertension in the unanesthetized rat. *Hypertension*. 1979;1(5):508-517. doi:10.1161/01.HYP.1.5.508.

140. Sanada LS, Tavares MR, Maia Neubern MC, Salgado HC, Sassoli Fazan VP. Can Wistar rats be used as the normotensive controls for nerve morphometry investigations in spontaneously hypertensive rats (SHR)? *Acta Cir Bras*. 2011;26(6):514-520.

141. Wilson AJ, Wang VY, Sands GB, Young AA, Nash MP, LeGrice IJ. Increased cardiac work provides a link between systemic hypertension and heart failure. *Physiol Rep*. 2017;5(1). doi:10.14814/phy2.13104.

142. Adams MA, Bobik A, Korner PI. Differential development of vascular and cardiac hypertrophy in genetic hypertension. Relation to sympathetic function. *Hypertension*. 1989;14(2):191-202. doi:10.1161/01.HYP.14.2.191.

143. Sundaram A, Keah LS, Sirajudeen KNS, Singh HJ. Upregulation of catalase and downregulation of glutathione peroxidase activity in the kidney precede the development of hypertension in pre-hypertensive SHR. *Hypertens Res*. 2013;36(3):213-218. doi:10.1038/hr.2012.163.

144. Cabassi A, Vinci S, Calzolari M, Bruschi G, Borghetti A. Regional sympathetic activity in pre-hypertensive phase of spontaneously hypertensive rats. *Life Sci*. 1998;62(12):1111-1118. doi:10.1016/S0024-3205(98)00034-4.

145. Heijnen BF, Van Essen H, Schalkwijk CG, Janssen BJ, Struijker-Boudier HA. Renal inflammatory markers during the onset of hypertension in spontaneously hypertensive rats. *Hypertens Res*. 2014;37(2):100-109. doi:10.1038/hr.2013.99.

146. Lee RM. Vascular changes at the prehypertensive phase in the mesenteric arteries from spontaneously hypertensive rats. *Blood Vessels*. 1985;22(3):105-126.

147. Lee RM. Structural alterations of blood vessels in hypertensive rats. *Can J Physiol Pharmacol*. 1987;65(8):1528-1535.

148. Safar M, Chamiot-Clerc P, Dagher G, Renaud JF. Pulse pressure, endothelium function, and arterial stiffness in spontaneously hypertensive rats. *Hypertension*. 2001;38(6):1416-1421. doi:10.1161/hy1201.096538.

149. Cunha RS, Dabiré H, Bezie I, Weiss AM, Chaouche-Teyara K, Laurent S, Safar ME, Lacolley P. Mechanical stress of the carotid artery at the early phase of spontaneous hypertension in rats. *Hypertension*. 1997;29(4):992-998. doi:10.1161/01.HYP.29.4.992.

150. Ely DL, Friberg P, Nilsson H, Folkow B. Blood pressure and heart rate responses to mental stress in spontaneously hypertensive (SHB) and normotensive (WKY) rats on various sodium diets. *Acta Physiol Scand*. 1985;123(2):159-169. doi:10.1111/j.1748-1716.1985.tb07573.x.

151. Dickhout JG, Lee RMKW. Structural and functional analysis of small arteries from young spontaneously hypertensive rats. *Hypertension*. 1997;29(3):781-789. doi:10.1161/01.HYP.29.3.781.

152. Bazil MK, Krulan C, Webb RL. Telemetric monitoring of cardiovascular parameters in conscious spontaneously hypertensive rats. *J Cardiovasc Pharmacol*. 1993;22(6):897-905. doi:10.1097/00005344-199312000-00019.

153. Minami N, Imai Y, Munakata M, Sasaki S, Sekino H, Abe K, Yoshinaga K. Age-related changes in blood pressure, heart rate and baroreflex sensitivity in SHR. *Clin Exp Pharmacol Physiol*. 1989;15:85-87.

154. Oliveira DR, Santos R, Santos G, Khosla MC, Campagnole-Santos MJ. Changes in the baroreflex control of heart rate produced by central infusion of selective angiotensin antagonists in hypertensive rats. *Hypertension*. 1996;27(6):1284-1290. doi:10.1161/01.HYP.27.6.1284.

155. Tan Z-Y, Lu Y, Whiteis CA, Simms AE, Paton JFR, Chapleau MW, Abboud FM. Chemoreceptor hypersensitivity, sympathetic excitation, and overexpression of ASIC and TASK channels before the onset of hypertension in SHR. *Circ Res*. 2010;106(3):536-545. doi:10.1161/CIRCRESAHA.109.206946.

156. Barbieri M, Varani K, Cerbai E, Guerra L, Li Q, Borea PA, Mugelli A. Electrophysiological basis for the enhanced cardiac arrhythmogenic effect of isoprenaline in aged spontaneously hypertensive rats. *J Mol Cell Cardiol*. 1994;26(7):849-860. doi:10.1006/jmcc.1994.1102.

157. Langley JN. On the union of cranial autonomic (visceral) fibres with the nerve cells of the superior cervical ganglion. *J Physiol (Lond)*. 1898;23(3):240-270. doi:10.1113/jphysiol.1898.sp000726.

158. Moreira TS, Takakura AC, Colombari E, Guyenet PG. Central chemoreceptors and sympathetic vasomotor outflow. *J Physiol (Lond)*. 2006;577(1):369-386. doi:10.1113/jphysiol.2006.115600.

159. Costa KM, Accorsi-Mendonça D, Moraes DJA, Machado BH. Evolution and physiology of neural oxygen sensing. *Front Physiol*. 2014;5:302. doi:10.3389/fphys.2014.00302.

160. Dempsey B, Le S, Turner A, Bokiniec P, Ramadas R, Bjaalie JG, Menuet C, Neve R, Allen AM, Goodchild AK, McMullan S. Mapping and analysis of the connectome of sympathetic premotor neurons in the rostral ventrolateral medulla of the rat using a volumetric brain atlas. *Front Neural Circuits*. 2017;11:9. doi:10.3389/fncir.2017.00009.

161. Hanna P, Rajendran PS, Ajijola OA, Vaseghi M, Armour JA, Ardell JL, Shivkumar K. Cardiac neuroanatomy - Imaging nerves to define functional control. *Auton Neurosci*. 2017;207:48-58. doi:10.1016/j.autneu.2017.07.008.

162. Shivkumar K, Ajijola OA, Anand I, Armour JA, Chen P-S, Esler M, De Ferrari GM, Fishbein MC, Goldberger JJ, Harper RM, Joyner MJ, Khalsa SS, Kumar R, Lane R, Mahajan A, Po S, Schwartz PJ, Somers VK, Valderrabano M, Vaseghi M, Zipes DP. Clinical neurocardiology defining the value of neuroscience-based cardiovascular therapeutics. *J Physiol (Lond)*. 2016;594(14):3911-3954. doi:10.1113/JP271870.

163. Panegyres KP, Panegyres PK. The Ancient Greek discovery of the nervous system: Alcmaeon, Praxagoras and Herophilus. *J Clin Neurosci*. 2016;29:21-24. doi:10.1016/j.jocn.2015.10.047.

164. Bay NS-Y, Bay B-H. Greek anatomist Herophilus: the father of anatomy. *Anat Cell Biol*. 2010;43(4):280-283. doi:10.5115/acb.2010.43.4.280.

165. Tomey MI, Komotar RJ, Mocco J. Herophilus, Erasistratus, Aretaeus, and Galen: ancient roots of the Bell–Magendie Law. *Neurosurgical Focus*. 2007;23(1):1-3. doi:10.3171/foc-07/07/e12.

166. van Gijn J. Charles Bell (1774-1842). *J Neurol*. 2011;258(6):1189-1190. doi:10.1007/s00415-011-5912-5.

167. Schuetze SM. The discovery of the action potential. *Trends Neurosci*. 1983;6(C):164-168. doi:10.1016/0166-2236(83)90078-4.

168. Finkelstein G. Mechanical neuroscience: Emil du Bois-Reymond's innovations in theory and practice. *Front Syst Neurosci*. 2015;9:133. doi:10.3389/fnsys.2015.00133.

169. Zimmer HG. Sydney Ringer, serendipity, and hard work. *Clin Cardiol*. 2005;28(1):55-56.

170. Danielli JF, Rosenberg MD, Cadenhead DA. *Progress in Surface and Membrane Science*. Elsevier Science; 2013.

171. Burdon-Sanderson J, Page FJM. On the Time-relations of the Excitatory Process in the Ventricle of the Heart of the Frog. *J Physiol (Lond)*. 1880;2(5-6):52.

172. Finger S. *Minds Behind the Brain: a History of the Pioneers and Their Discoveries*. Oxford University Press, USA; 2005.

173. Schwiening CJ. A brief historical perspective: Hodgkin and Huxley. *J Physiol (Lond)*. 2012;590(11):2571-2575. doi:10.1113/jphysiol.2012.230458.

174. Hodgkin AL, Huxley AF. The components of membrane conductance in the giant axon of Loligo. *J Physiol (Lond)*. 1952;116(4):473-496. doi:10.1113/jphysiol.1952.sp004718.

175. Hodgkin AL, Huxley AF. Currents carried by sodium and potassium ions through the membrane of the giant axon of Loligo. *J Physiol (Lond)*. 1952;116(4):449-472. doi:10.1113/jphysiol.1952.sp004717.

176. Hodgkin AL, Huxley AF. The dual effect of membrane potential on sodium conductance in the giant axon of Loligo. *J Physiol (Lond)*. 1952;116(4):497-506. doi:10.1113/jphysiol.1952.sp004719.

177. Hodgkin AL, Huxley AF, Katz B. Measurement of current-voltage relations in the membrane of the giant axon of Loligo. *J Physiol (Lond)*. 1952;116(4):424-448. doi:10.1113/jphysiol.1952.sp004716.

178. Südhof TC. The molecular machinery of neurotransmitter release (Nobel lecture). *Angew Chem Int Ed*. 2014;53(47):12696-12717. doi:10.1002/anie.201406359.

179. Südhof TC. A molecular machine for neurotransmitter release: synaptotagmin and beyond. *Nat Methods*. 2013;19(10):1227-1231. doi:10.1038/nm.3338.

180. Rozanski A, Blumenthal JA, Kaplan J. Impact of psychological factors on the pathogenesis of cardiovascular disease and implications for therapy. *Circulation*. 1999;99(16):2192-2217. doi:10.1161/01.cir.99.16.2192.

181. Steptoe A, Kivimaki M. Stress and cardiovascular disease. *Nat Rev Cardiol*. 2012;9(6):360-370. doi:10.1038/nrcardio.2012.45.

182. Tahsili-Fahadan P, Geocadin RG. Heart-brain axis: effects of neurologic injury on cardiovascular function. *Circ Res*. 2017;120(3):559-572. doi:10.1161/CIRCRESAHA.116.308446.

183. Celsus AC, Spencer WG. *De Medicina (on Medicine).* Vol 1. Loeb Classical Library Ed.; 1935:219-351.

184. Gaskell WH. On the structure, distribution and function of the nerves which innervate the visceral and vascular systems. *J Physiol (Lond)*. 1886;7(1):1-80. doi:10.1113/jphysiol.1886.sp000207.

185. Hoff HE. The history of vagal inhibition. *Bulletin of the History of Medicine*. 1940:461-496. https://www.jstor.org/stable/44440526.

186. Woollard HH. The Innervation of the heart. *J Anat*. 1926;60(Pt 4):345-373.

187. Sheehan D. Discovery of the autonomic nervous system. *Arch Neurol Psychiatry*. 1936;35(5):1081-1115. doi:10.1001/archneurpsyc.1936.02260050155011.

188. Brook RD, Julius S. Autonomic imbalance, hypertension, and cardiovascular risk. *Am J Hypertens*. 2000;13(S4):112S–122S. doi:10.1016/S0895-7061(00)00228-4.

189. Palatini P, Julius S. Elevated heart rate: a major risk factor for cardiovascular disease. *Clin Exp Hypertens*. 2004;26(7-8):637-644. doi:10.1081/CEH-200031959.

190. Mancia G, Grassi G. The autonomic nervous system and hypertension. *Circ Res*. 2014;114(11):1804-1814. doi:10.1161/CIRCRESAHA.114.302524.

191. Sverrisdottir YB, Rundqvist B, Johannsson G, Elam M. Sympathetic neural burst amplitude distribution: A more specific indicator of sympathoexcitation in human heart failure. *Circulation*. 2000;102(17):2076-2081.

192. Smith PA, Graham LN, Mackintosh AF, Stoker JB, Mary DASG. Relationship between central sympathetic activity and stages of human hypertension. *Am J Hypertens*. 2004;17(3):217-222. doi:10.1016/j.amjhyper.2003.10.010.

193. Grassi G, Esler M. How to assess sympathetic activity in humans. *J Hypertens*. 1999;17(6):719-734. doi:10.1097/00004872-199917060-00001.

194. Watson AMD, Hood SG, Ramchandra R, McAllen RM, May CN. Increased cardiac sympathetic nerve activity in heart failure is not due to desensitization of the arterial baroreflex. *Am J Physiol Heart Circ Physiol*. 2007;293(1):H798-H804. doi:10.1152/ajpheart.00147.2007.

195. Ramchandra R, Hood SG, Denton DA, Woods RL, McKinley MJ, McAllen RM, May CN. Basis for the preferential activation of cardiac sympathetic nerve activity in heart failure. *Proc Natl Acad Sci USA*. 2009;106(3):924-928. doi:10.1073/pnas.0811929106.

196. Sun SY, Wang W, Zucker IH, Schultz HD. Enhanced activity of carotid body chemoreceptors in rabbits with heart failure: role of nitric oxide. *Journal of Applied Physiology*. 1999;86(4):1273-1282.

197. Li Y-L, Li Y-F, Liu D, Cornish KG, Patel KP, Zucker IH, Channon KM, Schultz HD. Gene transfer of neuronal nitric oxide synthase to carotid body reverses enhanced chemoreceptor function in heart failure rabbits. *Circ Res*. 2005;97(3):260-267. doi:10.1161/01.RES.0000175722.21555.55.

198. Pijacka W, Moraes DJA, Ratcliffe LEK, Nightingale AK, Hart EC, da Silva MP, Machado BH, McBryde FD, Abdala AP, Ford AP, Paton JFR. Purinergic receptors in the carotid body as a new drug target for controlling hypertension. *Nat Med*. 2016;22(10):1151-1159. doi:10.1038/nm.4173.

199. Moraes DJA, Machado BH, Paton JFR. Carotid body overactivity induces respiratory neurone channelopathy contributing to neurogenic hypertension. *J Physiol (Lond)*. 2015;593(14):3055-3063. doi:10.1113/JP270423.

200. Zhu G-Q, Gao L, Li Y, Patel KP, Zucker IH, Wang W. AT1 receptor mRNA antisense normalizes enhanced cardiac sympathetic afferent reflex in rats with chronic heart failure. *Am J Physiol Heart Circ Physiol*. 2004;287(4):H1828-H1835. doi:10.1152/ajpheart.01245.2003.

201. Grassi G, Giannattasio C, ClÉroux J, Cuspidi C, Sampieri L, Battista Bolla G, Mancia G. Cardiopulmonary reflex before and after regression of left ventricular hypertrophy in essential hypertension. *Hypertension*. 1988;12(3):227-237. doi:10.1161/01.HYP.12.3.227.

202. Ferrara LA, Moscato TS, Pisanti N, Marotta T, Krogh V, Capone D, Mancini M. Is the sympathetic nervous system altered in children with familial history of arterial hypertension? *Cardiology*. 1988;75(3):200-205. doi:10.1159/000174371.

203. Dominiak P, Grobecker H. Elevated plasma catecholamines in young hypertensive and hyperkinetic patients: effect of pindolol. *Br J Clin Pharmacol*. 1982;13(2 S):381S–390S. doi:10.1111/j.1365-2125.1982.tb01945.x.

204. Bianchetti MG, Weidmann P, Beretta-Piccoli C. Disturbed noradrenergic blood pressure control in normotensive members of hypertensive families. *Br Heart J*. 1984;51(3):306-311.

205. Maver J, Štrucl M, Accetto R. Autonomic nervous system activity in normotensive subjects with a family history of hypertension. *Clin Auton Res*. 2004;14(6):369-375. doi:10.1007/s10286-004-0185-z.

206. Piccirillo G, Viola E, Nocco M, Durante M, Tarantini S, Marigliano V. Autonomic modulation of heart rate and blood pressure in normotensive offspring of hypertensive subjects. *J Lab Clin Med*. 2000;135(2):145-152. doi:10.1067/mlc.2000.103428.

207. Lopes HF, Silva HB, Consolim-Colombo FM, Barreto Filho JA, Riccio GM, Giorgi DM, Krieger EM. Autonomic abnormalities demonstrable in young normotensive subjects who are children of hypertensive parents. *Braz J Med Biol Res*. 2000;33(1):51-54.

208. Perini C, Muller FB, Rauchfleisch U, Battegay R, Hobi V, Buhler FR. Psychosomatic factors in borderline hypertensive subjects and offspring of hypertensive parents. *Hypertension*. 1990;16(6):627-634. doi:10.1161/01.HYP.16.6.627.

209. Horikoshi Y, Tajima I, Igarashi H, Inui M, Kasahara K, Noguchi T. The adreno-sympathetic system, the genetic predisposition to hypertension, and stress. *Am J Med Sci*. 1985;289(5):186-191. doi:10.1097/00000441-198505000-00002.

210. Judy WV, Watanabe AM, Murphy WR, Aprison BS, Yu PL. Sympathetic nerve activity and blood pressure in normotensive backcross rats genetically related to the spontaneously hypertensive rat. *Hypertension*. 1979;1(6):598-604. doi:10.1161/01.HYP.1.6.598.

211. Esler M, Jennings G, Lambert G, Meredith I, Horne M, Eisenhofer G. Overflow of catecholamine neurotransmitters to the circulation: Source, fate, and functions. *Physiol Rev*. 1990;70(4):963-985. doi:10.1152/physrev.1990.70.4.963.

212. Vaz M, Jennings G, Turner A, Cox H, Lambert G, Esler M. Regional sympathetic nervous activity and oxygen consumption in obese normotensive human subjects. *Circulation*. 1997;96(10):3423-3429. doi:10.1161/01.CIR.96.10.3423.

213. Friberg P, Meredith I, Jennings G, Lambert G, Fazio V, Esler M. Evidence for increased renal norepinephrine overflow during sodium restriction in humans. *Hypertension*. 1990;16(2):121-130. doi:10.1161/01.hyp.16.2.121.

214. Dang AM, Zheng DY, Wang B, Zhang YQ, Zhang PH, Yu MF, Liu GZ, Liu LS. The role of the renin-angiotensin and cardiac sympathetic nervous systems in the development of hypertension and left ventricular hypertrophy in spontaneously hypertensive rats. *Hypertens Res*. 1999;22(3):217-221.

215. Rundqvist B, Elam M, Bergmann-Sverrisdottir YB, Eisenhofer G, Friberg P. Increased cardiac adrenergic drive precedes generalized sympathetic activation in human heart failure. *Circulation*. 1997;95(1):169-175. doi:https://doi.org/10.1161/01.CIR.95.1.169.

216. Tu H, Liu J, Zhang D, Zheng H, Patel KP, Cornish KG, Wang W-Z, Muelleman RL, Li Y-L. Heart failure-induced changes of voltage-gated Ca2+ channels and cell excitability in rat cardiac postganglionic neurons. *Am J Physiol, Cell Physiol*. 2014;306(2):C132-C142. doi:10.1152/ajpcell.00223.2013.

217. Souza HC, Ballejo G, Salgado MC, Da Silva VJ, Salgado HC. Cardiac sympathetic overactivity and decreased baroreflex sensitivity in L-NAME hypertensive rats. *Am J Physiol Heart Circ Physiol*. 2001;280(2):H844-H850.

218. Korzina MB, Korobkin AA, Vasilieva OA, Maslyukov PM. Morphological characteristics of the stellate ganglion in white rats. *Neurosci Behav Physiol*. 2011;41(4):436-439. doi:10.1007/s11055-011-9433-6.

219. DiFrancesco D. The role of the funny current in pacemaker activity. *Circ Res*. 2010;106(3):434-446. doi:10.1161/CIRCRESAHA.109.208041.

220. DiFrancesco D, Tortora P. Direct activation of cardiac pacemaker channels by intracellular cyclic AMP. *Nature*. 1991;351(6322):145-147. doi:10.1038/351145a0.

221. Sprenger JU, Perera RK, Steinbrecher JH, Lehnart SE, Maier LS, Hasenfuss G, Nikolaev VO. In vivo model with targeted cAMP biosensor reveals changes in receptor-microdomain communication in cardiac disease. *Nat Commun*. 2015;6:1-11. doi:10.1038/ncomms7965.

222. Heaton DA, Lei M, Li D, Golding S, Dawson TA, Mohan RM, Paterson DJ. Remodeling of the cardiac pacemaker L-type calcium current and its beta-adrenergic responsiveness in hypertension after neuronal NO synthase gene transfer. *Hypertension*. 2006;48(3):443-452. doi:10.1161/01.HYP.0000233383.04280.3c.

223. Dawson TA, Li D, Woodward T, Barber Z, Wang L, Paterson DJ. Cardiac cholinergic NO-cGMP signaling following acute myocardial infarction and nNOS gene transfer. *Am J Physiol Heart Circ Physiol*. 2008;295(3):H990-H998. doi:10.1152/ajpheart.00492.2008.

224. Baliga RS, Preedy MEJ, Dukinfield MS, Chu SM, Aubdool AA, Bubb KJ, Moyes AJ, Tones MA, Hobbs AJ. Phosphodiesterase 2 inhibition preferentially promotes NO/guanylyl cyclase/cGMP signaling to reverse the development of heart failure. *Proc Natl Acad Sci USA*. July 2018. doi:10.1073/pnas.1800996115.

225. Zhao CY, Greenstein JL, Winslow RL. Roles of phosphodiesterases in the regulation of the cardiac cyclic nucleotide cross-talk signaling network. *J Mol Cell Cardiol*. 2016;91:215-227. doi:10.1016/j.yjmcc.2016.01.004.

226. Zhao CY, Greenstein JL, Winslow RL. Mechanisms of the cyclic nucleotide cross-talk signaling network in cardiac L-type calcium channel regulation. *J Mol Cell Cardiol*. 2017;106:29-44. doi:10.1016/j.yjmcc.2017.01.013.

227. Leiser M, Fleischer N. cAMP-dependent regulation of cardiac L-type Ca^{2+} channels requires membrane targeting of PKA and phosphorylation of channel subunits. *Diabetes*. 1996;45(10):1412-1418. doi:10.2337/diabetes.45.10.1412.

228. Mattiazzi A, Kranias EG. The role of CaMKII regulation of phospholamban activity in heart disease. *Front Pharmacol*. 2014;5. doi:10.3389/fphar.2014.00005.

229. Larsen HE, Lefkimmiatis K, Paterson DJ. Sympathetic neurons are a powerful driver of myocyte function in cardiovascular disease. *Sci Rep*. 2016;6:1-11. doi:10.1038/srep38898.

230. Zoccarato A, Surdo NC, Aronsen JM, Fields LA, Mancuso L, Dodoni G, Stangherlin A, Livie C, Jiang H, Sin YY, Gesellchen F, Terrin A, Baillie GS, Nicklin SA, Graham D, Szabo-Fresnais N, Krall J, Vandeput F, Movsesian M, Furlan L, Corsetti V, Hamilton G, Lefkimmiatis K, Sjaastad I, Zaccolo M. Cardiac hypertrophy is inhibited by a local pool of cAMP regulated by phosphodiesterase 2. *Circ Res*. 2015;117(8):707-719. doi:10.1161/CIRCRESAHA.114.305892.

231. Kalla M, Chotalia M, Coughlan C, Hao G, Crabtree MJ, Tomek J, Bub G, Paterson DJ, Herring N. Protection against ventricular fibrillation via cholinergic

receptor stimulation and the generation of nitric oxide. *J Physiol (Lond)*. 2016;594(14):3981-3992. doi:10.1113/JP271588.

232. Mehel H, Emons J, Vettel C, Wittköpper K, Seppelt D, Dewenter M, Lutz S, Sossalla S, Maier LS, Lechêne P, Leroy J, Lefebvre F, Varin A, Eschenhagen T, Nattel S, Dobrev D, Zimmermann W-H, Nikolaev VO, Vandecasteele G, Fischmeister R, El-Armouche A. Phosphodiesterase-2 is up-regulated in human failing hearts and blunts β-adrenergic responses in cardiomyocytes. *J Am Coll Cardiol*. 2013;62(17):1596-1606. doi:10.1016/j.jacc.2013.05.057.

233. Catterall WA. International union of pharmacology. XL. Compendium of voltage-gated ion channels: calcium channels. *Pharmacol Rev*. 2003;55(4):579-581. doi:10.1124/pr.55.4.8.

234. Catterall WA. Voltage-gated calcium channels. *Cold Spring Harb Perspect Biol*. 2011;3(8):a003947-a003947. doi:10.1101/cshperspect.a003947.

235. Uhrenholt TR, Nedergaard OA. Calcium channels involved in noradrenaline release from sympathetic neurones in rabbit carotid artery. *Pharmacol Toxicol*. 2003;92(5):226-233.

236. Pruneau D, Bélichard P. Haemodynamic and humoral effects of ω-conotoxin GVIA in normotensive and spontaneously hypertensive rats. *Eur J Pharmacol*. 1992;211(3):329-335. doi:10.1016/0014-2999(92)90389-l.

237. Ino M, Yoshinaga T, Wakamori M, Miyamoto N, Takahashi E, Sonoda J, Kagaya T, Oki T, Nagasu T, Nishizawa Y, Tanaka I, Imoto K, Aizawa S, Koch S, Schwartz A, Niidome T, Sawada K, Mori Y. Functional disorders of the sympathetic nervous system in mice lacking the alpha$_{1B}$ subunit ($Ca_V2.2$) of N-type calcium channels. *Proc Natl Acad Sci USA*. 2001;98(9):5323-5328. doi:10.1073/pnas.081089398.

238. Mori Y, Nishida M, Shimizu S, Ishii M, Ino M, Sawada K, Niidome T. Ca^{2+} channel α1B subunit ($Ca_V2.2$) knockout mouse reveals a predominant role of N-type channels in the sympathetic regulation of the circulatory system. *Trends Cardiovasc Med*. 2002. doi:10.1016/S1050-1738(02)00173-1.

239. Briant LJB, Paton JFR, Pickering AE, Champneys AR. Modelling the vascular response to sympathetic postganglionic nerve activity. *J Theor Biol*. 2015;371(C):102-116. doi:10.1016/j.jtbi.2015.01.037.

240. Mahapatra S, Marcantoni A, Zuccotti A, Carabelli V, Carbone E. Equal sensitivity of Cav1.2 and Cav1.3 channels to the opposing modulations of PKA and PKG in mouse chromaffin cells. *J Physiol (Lond)*. 2012;590(20):5053-5073. doi:10.1113/jphysiol.2012.236729.

241. Schroder F. Single L-type Ca2+ channel regulation by cGMP-dependent protein kinase type I in adult cardiomyocytes from PKG I transgenic mice. *Cardiovasc Res*. 2003;60(2):268-277. doi:10.1016/S0008-6363(03)00546-7.

242. Sandoval A, Duran P, Gandini MA, Andrade A, Almanza A, Kaja S, Felix R. Regulation of L-type $Ca_V1.3$ channel activity and insulin secretion by the cGMP-PKG signaling pathway. *Cell Calcium*. 2017;66:1-9. doi:10.1016/j.ceca.2017.05.008.

243. Brown AM, Birnbaumer L. Direct G protein gating of ion channels. *Am J Physiol*. 1988;254(3 Pt 2):H401-H410. doi:10.1152/ajpheart.1988.254.3.H401.

244. D'Ascenzo M, Martinotti G, Azzena GB, Grassi C. cGMP/protein kinase G-dependent inhibition of N-type Ca^{2+} channels induced by nitric oxide in human neuroblastoma IMR32 cells. *J Neurosci*. 2002;22(17):7485-7492.

245. Zamponi GW, Striessnig J, Koschak A, Dolphin AC. The physiology, pathology, and pharmacology of voltage-gated calcium channels and their future therapeutic potential. Sibley DR, ed. *Pharmacol Rev*. 2015;67(4):821-870. doi:10.1124/pr.114.009654.

246. Molderings GJ, Likungu J, Göthert M. N-Type calcium channels control sympathetic neurotransmission in human heart atrium. *Circulation*. 2000;101(4):403-407.

247. Yamada Y, Kinoshita H, Kuwahara K, Nakagawa Y, Kuwabara Y, Minami T, Yamada C, Shibata J, Nakao K, Cho K, ARAI Y, Yasuno S, Nishikimi T, Ueshima K, Kamakura S, Nishida M, Kiyonaka S, Mori Y, Kimura T, Kangawa K, Nakao K. Inhibition of N-type Ca^{2+} channels ameliorates an imbalance in cardiac autonomic nerve activity and prevents lethal arrhythmias in mice with heart failure. *Cardiovasc Res*. 2014;104(1):183-193. doi:10.1093/cvr/cvu185.

248. Tanaka S, Tanaka R, Harada S, Kohda Y, Matsumura H, Shimamoto C, Sawabe Y, Marunaka Y, Kuwabara H, Takahashi Y, Ito S, Nakahari T. A PKG inhibitor increases Ca^{2+}-regulated exocytosis in guinea pig antral mucous cells: cAMP accumulation via PDE2A inhibition. *Am J Physiol Gastrointest Liver Physiol*. 2013;304(9):G773-G780. doi:10.1152/ajpgi.00281.2012.

249. Sato K, Park NG, Kohno T, Maeda T, Kim JI, Kato R, Takahashi M. Role of basic residues for the binding of omega-conotoxin GVIA to N-type calcium channels. *Biochem Biophys Res Commun*. 1993;194(3):1292-1296. doi:10.1006/bbrc.1993.1964.

250. Marsh N, Marsh A. A short history of nitroglycerine and nitric oxide in pharmacology and physiology. *Clin Exp Pharmacol Physiol*. 2000;27(4):313-319. doi:10.1046/j.1440-1681.2000.03240.x.

251. Lauder Brunton T. On the use of nitrite of amyl in angina pectoris. *Lancet*. 1867;90(2291):97-98. doi:10.1016/S0140-6736(02)51392-1.

252. Brunton TL. The action of nitrate of amyl on the circulation. *J Anat Physiol*. 1870;5(Pt 1):92-101.

253. Arnold WP, Mittal CK, Katsuki S, Murad F. Nitric oxide activates guanylate cyclase and increases guanosine 3“ : 5-”cyclic monophosphate levels in various tissue preparations. *Proc Natl Acad Sci USA*. 1977;74(8):3203-3207. doi:10.1073/pnas.74.8.3203.

254. Furchgott RF, Zawadzki JV. The obligatory role of endothelial cells in the relaxation of arterial smooth muscle by acetylcholine. *Nature*. 1980;288(5789):373-376. doi:10.1038/288373a0.

255. Furchgott RF. Endothelium-derived relaxing factor: Discovery, early studies, and identification as nitric oxide. In: Vol 19. Portland Press Limited; 1999:235-251. doi:10.1023/A:1020537506008.

256. Palmer RMJ, Ferrige AG, Moncada S. Nitric oxide release accounts for the biological activity of endothelium-derived relaxing factor. *Nature*. 1987;327(6122):524-526. doi:10.1038/327524a0.

257. Ignarro LJ, Buga GM, Wood KS, Byrns RE, Chaudhuri G. Endothelium-derived relaxing factor produced and released from artery and vein is nitric oxide. *Proc Natl Acad Sci USA*. 1987;84(24):9265-9269. doi:10.1073/pnas.84.24.9265.

258. Howlett R. *Nobel Award Stirs Up Debate on Nitric Oxide Breakthrough.* Vol 395. 1998:625-626. doi:10.1038/27019.

259. Sears CE, Choate JK, Paterson DJ. Effect of nitric oxide synthase inhibition on the sympatho-vagal control of heart rate. *J Auton Nerv Syst*. 1998;73(1):63-73. doi:10.1016/S0165-1838(98)00123-4.

260. Wang L, Henrich M, Buckler KJ, McMenamin M, Mee CJ, Sattelle DB, Paterson DJ. Neuronal nitric oxide synthase gene transfer decreases $[Ca^{2+}]_i$ in cardiac sympathetic neurons. *J Mol Cell Cardiol*. 2007;43(6):717-725. doi:10.1016/j.yjmcc.2007.09.005.

261. Lee C-W, Li D, Channon KM, Paterson DJ. L-arginine supplementation reduces cardiac noradrenergic neurotransmission in spontaneously hypertensive rats. *J Mol Cell Cardiol*. 2009;47(1):149-155. doi:10.1016/j.yjmcc.2009.03.023.

262. Li D, Lu C-J, Hao G, Wright H, Woodward L, Liu K, Vergari E, Surdo NC, Herring N, Zaccolo M, Paterson DJ. Efficacy of B-type natriuretic peptide is coupled to phosphodiesterase 2a in cardiac sympathetic neurons. *Hypertension*. 2015;66(1):190-198. doi:10.1161/HYPERTENSIONAHA.114.05054.

263. Lu C-J, Hao G, Nikiforova N, Larsen HE, Liu K, Crabtree MJ, Li D, Herring N, Paterson DJ. CAPON modulates neuronal calcium handling and cardiac sympathetic neurotransmission during dysautonomia in hypertension. *Hypertension*. 2015;65(6):1288-1297. doi:10.1161/HYPERTENSIONAHA.115.05290.

264. Briant LJB, Stalbovskiy AO, Nolan MF, Champneys AR, Pickering AE. Increased intrinsic excitability of muscle vasoconstrictor preganglionic neurons may contribute to the elevated sympathetic activity in hypertensive rats. *J Neurophysiol*. 2014;112(11):2756-2778. doi:10.1152/jn.00350.2014.

265. Stangherlin A, Zaccolo M. Phosphodiesterases and subcellular compartmentalized cAMP signaling in the cardiovascular system. *Am J Physiol Heart Circ Physiol*. 2012;302(2):H379-H390. doi:10.1152/ajpheart.00766.2011.

266. Zaccolo M, Movsesian MA. cAMP and cGMP signaling cross-talk: role of phosphodiesterases and implications for cardiac pathophysiology. *Circ Res*. 2007;100(11):1569-1578. doi:10.1161/CIRCRESAHA.106.144501.

267. Maurice DH, Ke H, Ahmad F, Wang Y, Chung J, Manganiello VC. Advances in targeting cyclic nucleotide phosphodiesterases. *Nat Methods*. 2014;13(4):290-314. doi:10.1038/nrd4228.

268. Francis SH, Blount MA, Corbin JD. Mammalian cyclic nucleotide phosphodiesterases: molecular mechanisms and physiological functions. *Physiol Rev*. 2011;91(2):651-690. doi:10.1152/physrev.00030.2010.

269. Maurice DH. Cyclic nucleotide phosphodiesterase activity, expression, and targeting in cells of the cardiovascular system. *Mol Pharmacol*. 2003;64(3):533-546. doi:10.1124/mol.64.3.533.

270. Bender AT. Cyclic nucleotide phosphodiesterases: molecular regulation to clinical use. *Pharmacol Rev*. 2006;58(3):488-520. doi:10.1124/pr.58.3.5.

271. Levy FO. Cardiac PDEs and crosstalk between cAMP and cGMP signalling pathways in the regulation of contractility. *Naunyn Schmiedebergs Arch Pharmacol*. 2013;386(8):665-670. doi:10.1007/s00210-013-0874-z.

272. Li D, Paterson DJ. Cyclic nucleotide regulation of cardiac sympatho-vagal responsiveness. *J Physiol (Lond)*. 2016;594(14):3993-4008. doi:10.1113/JP271827.

273. Boda H, Uchida H, Takaiso N, Ouchi Y, Fujita N, Kuno A, Hata T, Nagatani A, Funamoto Y, Miyata M, Yoshikawa T, Kurahashi H, Inagaki H. A PDE3A mutation in familial hypertension and brachydactyly syndrome. *J Hum Genet*. 2016;61(8):701-703. doi:10.1038/jhg.2016.32.

274. Maass PG, Aydin A, Luft FC, Schächterle C, Weise A, Stricker S, Lindschau C, Vaegler M, Qadri F, Toka HR, Schulz H, Krawitz PM, Parkhomchuk D, Hecht J, Hollfinger I, Wefeld-Neuenfeld Y, Bartels-Klein E, Mühl A, Kann M, Schuster H, Chitayat D, Bialer MG, Wienker TF, Ott J, Rittscher K, Liehr T, Jordan J, Plessis G, Tank J, Mai K, Naraghi R, Hodge R, Hopp M, Hattenbach LO, Busjahn A, Rauch A, Vandeput F, Gong M, Rüschendorf F, Hübner N, Haller H, Mundlos S, Bilginturan N, Movsesian MA, Klussmann E, Toka O, Bähring S. PDE3A mutations cause autosomal dominant hypertension with brachydactyly. *Nat Methods*. 2015;47(6):647-653. doi:10.1038/ng.3302.

275. Lee DI, Zhu G, Sasaki T, Cho G-S, Hamdani N, Holewinski R, Jo S-H, Danner T, Zhang M, Rainer PP, Bedja D, Kirk JA, Ranek MJ, Dostmann WR, Kwon C, Margulies KB, Van Eyk JE, Paulus WJ, Takimoto E, Kass DA. Phosphodiesterase 9A controls nitric-oxide- independent cGMP and hypertrophic heart disease. *Nature*. 2015;519(7544):472-476. doi:10.1038/nature14332.

276. Katz SD, Balidemaj K, Homma S, Wu H, Wang J, Maybaum S. Acute type 5 phosphodiesterase inhibition with sildenafil enhances flow-mediated vasodilation in patients with chronic heart failure. *J Am Coll Cardiol*. 2000;36(3):845-851. doi:10.1016/S0735-1097(00)00790-7.

277. Nagendran J, Archer SL, Soliman D, Gurtu V, Moudgil R, Haromy A, St Aubin C, Webster L, Rebeyka IM, Ross DB, Light PE, Dyck JRB, Michelakis ED. Phosphodiesterase type 5 is highly expressed in the hypertrophied human right ventricle, and acute inhibition of phosphodiesterase type 5 improves contractility. *Circulation*. 2007;116(3):238-248. doi:10.1161/CIRCULATIONAHA.106.655266.

278. Assenza MR, Barbagallo F, Barrios F, Cornacchione M, Campolo F, Vivarelli E, Gianfrilli D, Auletta L, Soricelli A, Isidori AM, Lenzi A, Pellegrini M, Naro F. Critical role of phosphodiesterase 2A in mouse congenital heart defects. *Cardiovasc Res*. 2018;114(6):830-845. doi:10.1093/cvr/cvy030.

279. Vettel C, Lindner M, Dewenter M, Lorenz K, Schanbacher C, Riedel M, Lämmle S, Meinecke S, Mason FE, Sossalla S, Geerts A, Hoffmann M, Wunder F, Brunner FJ, Wieland T, Mehel H, Karam S, Lechêne P, Leroy J, Vandecasteele G, Wagner M, Fischmeister R, El-Armouche A. Phosphodiesterase 2 protects against catecholamine-induced arrhythmia and preserves contractile function after myocardial infarction. *Circ Res*. 2017;120(1):120-132. doi:10.1161/CIRCRESAHA.116.310069.

280. Liu K, Li D, Hao G, McCaffary D, Neely O, Woodward L, Ioannides D, Lu C-J, Brescia M, Zaccolo M, Tandri H, Ajijola OA, Ardell JL, Shivkumar K, Paterson DJ. Phosphodiesterase 2A as a therapeutic target to restore cardiac

neurotransmission during sympathetic hyperactivity. *JCI Insight*. 2018;3(9):1-17. doi:10.1172/jci.insight.98694.

281. Iriuchijima J. Sympathetic discharge rate in spontaneously hypertensive rats. *Jpn Heart J*. 1973;14(4):350-356. doi:10.1536/ihj.14.350.

282. Shanks J, Herring N, Johnson E, Liu K, Li D, Paterson DJ. Overexpression of sarcoendoplasmic reticulum calcium ATPase 2a promotes cardiac sympathetic neurotransmission via abnormal endoplasmic reticulum and mitochondria Ca^{2+} regulation. *Hypertension*. 2017;69(4):625-632. doi:10.1161/HYPERTENSIONAHA.116.08507.

283. Rumantir MS, Kaye DM, Jennings GL, Vaz M, Hastings JA, Esler MD. Phenotypic evidence of faulty neuronal norepinephrine reuptake in essential hypertension. *Hypertension*. 2000;36(5):824-829.

284. Shanks J, Mane S, Ryan R, Paterson DJ. Ganglion-specific impairment of the norepinephrine transporter in the hypertensive rat. *Hypertension*. 2013;61:197–193. doi:10.1161/HYPERTENSIONAHA.112.202184/-/DC1.

285. Esler MD, Wallin G, Dorward PK, Eisenhofer G, Westerman R, Meredith I, Lambert G, Cox HS, Jennings G. Effects of desipramine on sympathetic nerve firing and norepinephrine spillover to plasma in humans. *Am J Physiol*. 1991;260(4 Pt 2):R817-R823. doi:10.1152/ajpregu.1991.260.4.R817.

286. Kimura S, Miura Y, Adachi M, Nezu M, Toriyabe S, Sugawara T, Ishizuka Y, Noshiro T, Takahashi M. The effect of sodium depletion on plasma norepinephrine kinetics in patients with essential hypertension. *Jpn Circ J*. 1983;47(10):1232-1241.

287. Esler M, Jackman G, Bobik A, Leonard P, Kelleher D, Skews H, Jennings G, Korner P. Norepinephrine kinetics in essential hypertension. Defective neuronal uptake of norepinephrine in some patients. *Hypertension*. 1981;3(2):149-156. doi:10.1161/01.HYP.3.2.149.

288. Wang L, Li D, Plested CP, Dawson T, Teschemacher AG, Paterson DJ. Noradrenergic neuron-specific overexpression of nNOS in cardiac sympathetic nerves decreases neurotransmission. *J Mol Cell Cardiol*. 2006;41(2):364-370. doi:10.1016/j.yjmcc.2006.05.007.

289. Orike N, Thrasivoulou C, Cowen T. Serum-free culture of dissociated, purified adult and aged sympathetic neurons and quantitative assays of growth and survival. *Journal of Neuroscience Methods*. 2001;106(2):153-160. doi:10.1016/S0165-0270(01)00344-2.

290. He Y, Baas PW. Growing and working with peripheral neurons. *Methods Cell Biol*. 2003;71(71):17-35.

291. Schindelin J, Arganda-Carreras I, Frise E, Kaynig V, Longair M, Pietzsch T, Preibisch S, Rueden C, Saalfeld S, Schmid B, Tinevez J-Y, White DJ, Hartenstein V, Eliceiri K, Tomancak P, Cardona A. Fiji: an open-source platform for biological-image analysis. *Nat Methods*. 2012;9(7):676-682. doi:10.1038/nmeth.2019.

292. Schindelin J, Rueden CT, Hiner MC, Eliceiri KW. The ImageJ ecosystem: an open platform for biomedical image analysis. *Mol Reprod Dev*. 2015;82(7-8):518-529. doi:10.1002/mrd.22489.

293. Bollen E, Prickaerts J. Phosphodiesterases in neurodegenerative disorders. *IUBMB Life*. 2012;64(12):965-970. doi:10.1002/iub.1104.

294. Lefkimmiatis K, Zaccolo M. cAMP signaling in subcellular compartments. *Pharmacol Ther*. 2014;143(3):295-304. doi:10.1016/j.pharmthera.2014.03.008.

295. Steiner AL, Parker CW, Kipnis DM. Radioimmunoassay for cyclic nucleotides. I. Preparation of antibodies and iodinated cyclic nucleotides. *J Biol Chem*. 1972;247(4):1106-1113.

296. Gilman AG. A protein binding assay for adenosine 3“ :5” -cyclic monophosphate. *Proc Natl Acad Sci USA*. 1970;67(1):305-312. doi:10.1073/pnas.67.1.305.

297. Zaccolo M, De Giorgi F, Cho CY, Feng L, Knapp T, Negulescu PA, Taylor SS, Tsien RY, Pozzan T. A genetically encoded, fluorescent indicator for cyclic AMP in living cells. *Nat Cell Biol*. 2000;2(1):25-29. doi:10.1038/71345.

298. Musheshe N, Schmidt M, Zaccolo M. cAMP: from long-range second messenger to nanodomain signalling. *Trends Pharmacol Sci*. 2018;39(2):209-222. doi:10.1016/j.tips.2017.11.006.

299. Kaupp UB, Seifert R. Cyclic nucleotide-gated ion channels. *Physiol Rev*. 2002;82(3):769-824. doi:10.1152/physrev.00008.2002.

300. Schmidt M, Dekker FJ, Maarsingh H. Exchange protein directly activated by cAMP (epac): A multidomain cAMP mediator in the regulation of diverse biological functions. *Pharmacol Rev*. 2013;65(2):670-709. doi:10.1124/pr.110.003707.

301. Schindler RFR, Brand T. The Popeye domain containing protein family--A novel class of cAMP effectors with important functions in multiple tissues. *Prog Biophys Mol Biol*. 2016;120(1-3):28-36. doi:10.1016/j.pbiomolbio.2016.01.001.

302. Zaccolo M, Pozzan T. Discrete microdomains with high concentration of cAMP in stimulated rat neonatal cardiac myocytes. *Science*. 2002;295(5560):1711-1715. doi:10.1126/science.1069982.

303. Nikolaev VO, Bünemann M, Hein L, Hannawacker A, Lohse MJ. Novel single chain cAMP sensors for receptor-induced signal propagation. *J Biol Chem*. 2004;279(36):37215-37218. doi:10.1074/jbc.C400302200.

304. DiPilato LM, Cheng X, Zhang J. Fluorescent indicators of cAMP and Epac activation reveal differential dynamics of cAMP signaling within discrete subcellular compartments. *Proc Natl Acad Sci USA*. 2004;101(47):16513-16518. doi:10.1073/pnas.0405973101.

305. Ponsioen B, Zhao J, Riedl J, Zwartkruis F, van der Krogt G, Zaccolo M, Moolenaar WH, Bos JL, Jalink K. Detecting cAMP-induced Epac activation by fluorescence resonance energy transfer: Epac as a novel cAMP indicator. *EMBO reports*. 2004;5(12):1176-1180. doi:10.1038/sj.embor.7400290.

306. Zaccolo M. *cAMP Signaling: Methods and Protocols*. Vol 1294. (Zaccolo M, ed.). New York, NY: Springer New York; 2015:1-222. doi:10.1007/978-1-4939-2537-7.

307. Klarenbeek J, Goedhart J, van Batenburg A, Groenewald D, Jalink K. Fourth-generation Epac-based FRET sensors for cAMP feature exceptional brightness, photostability and dynamic range: characterization of dedicated sensors for FLIM, for ratiometry and with high affinity. Anderson KI, ed. *PLoS ONE*. 2015;10(4):1-11. doi:10.1371/journal.pone.0122513.

308. van der Krogt GNM, Ogink J, Ponsioen B, Jalink K. A comparison of donor-acceptor pairs for genetically encoded FRET sensors: application to the Epac

cAMP sensor as an example. Koch K-W, ed. *PLoS ONE*. 2008;3(4):e1916-e1919. doi:10.1371/journal.pone.0001916.

309. Depry C, Allen MD, Zhang J. Visualization of PKA activity in plasma membrane microdomains. *Mol BioSyst*. 2011;7(1):52-58. doi:10.1039/C0MB00079E.

310. Zhou X, Herbst-Robinson KJ, Zhang J. Visualizing dynamic activities of signaling enzymes using genetically encodable FRET-based biosensors. *Meth Enzymol*. 2012;504:317-340. doi:10.1016/B978-0-12-391857-4.00016-1.

311. Bardsley EN, Davis H, Buckler KJ, Paterson DJ. Neurotransmitter switching coupled to β-adrenergic signaling in sympathetic neurons in prehypertensive states. *Hypertension*. 2018;71(6):1226-1238. doi:10.1161/HYPERTENSIONAHA.118.10844.

312. Burdyga A, Surdo NC, Monterisi S, Di Benedetto G, Grisan F, Penna E, Pellegrini L, Bortolozzi M, Swietach P, Pozzan T, Lefkimmiatis K. Phosphatases control PKA-dependent functional microdomains at the outer mitochondrial membrane. *Proc Natl Acad Sci USA*. 2018;115(28):E6497-E6506. doi:10.1073/pnas.1806318115.

313. Ghasemi A, Zahediasl S. Normality tests for statistical analysis: A guide for non-statisticians. *Int J Endocrinol Metab*. 2012;10(2):486-489. doi:10.5812/ijem.3505.

314. Grynkiewicz G, Poenie M, Tsien RY. A new generation of Ca^{2+} indicators with greatly improved fluorescence properties. *J Biol Chem*. 1985;260(6):3440-3450.

315. McGettigan PA. Transcriptomics in the RNA-seq era. *Curr Opin Chem Biol*. 2013;17(1):4-11. doi:10.1016/j.cbpa.2012.12.008.

316. Zhu YY, Machleder EM, Chenchik A, Li R, Siebert PD. Reverse transcriptase template switching: A SMART™ approach for full-length cDNA library construction. *BioTechniques*. 2001;30(4):892-897. doi:10.1098/rspb.1991.0037.

317. Conesa A, Madrigal P, Tarazona S, Gomez-Cabrero D, Cervera A, McPherson A, Szcześniak MW, Gaffney DJ, Elo LL, Zhang X, Mortazavi A. A survey of best practices for RNA-seq data analysis. *Genome Biol*. February 2017:1-19. doi:10.1186/s13059-016-0881-8.

318. Pertea M, Kim D, Pertea GM, Leek JT, Salzberg SL. Transcript-level expression analysis of RNA-seq experiments with HISAT, StringTie and Ballgown. *Nat Protoc*. 2016;11(9):1650-1667. doi:10.1038/nprot.2016-095.

319. Kukurba KR, Montgomery SB. RNA sequencing and analysis. *Cold Spring Harb Protoc*. 2015;2015(11):pdb.top084970–29. doi:10.1101/pdb.top084970.

320. Srivastava A, Sarkar H, Gupta N, Patro R. RapMap: a rapid, sensitive and accurate tool for mapping RNA-seq reads to transcriptomes. *Bioinformatics*. 2016;32(12):i192-i200. doi:10.1093/bioinformatics/btw277.

321. Patro R, Duggal G, Love MI, Irizarry RA, Kingsford C. Salmon documentation release 0.11.2. https://salmon.readthedocs.io/en/latest/index.html. Published 2018. Accessed August 16, 2018.

322. Patro R, Duggal G, Love MI, Irizarry RA, Kingsford C. Salmon provides fast and bias-aware quantification of transcript expression. *Nat Methods*. 2017;14(4):417-419. doi:10.1038/nmeth.4197.

323. Tse D. Fast and accurate single-cell RNA-seq analysis by clustering of transcript-compatibility counts. *Genome Biol*. May 2016:1-14. doi:10.1186/s13059-016-0970-8.

324. Dong X. How to tell which library type to use (fr-firststrand or fr-secondstrand)? http://onetipperday.sterding.com/2012/07/how-to-tell-which-library-type-to-use.html. Published 2012. Accessed August 24, 2018.

325. Kallio MA, Tuimala JT, Hupponen T, Klemelä P, Gentile M, Scheinin I, Koski M, Käki J, Korpelainen EI. Directional RNA-seq data -which parameters to choose? https://chipster.csc.fi/manual/library-type-summary.html.

326. Soneson C, Love MI, Robinson MD. Differential analyses for RNA-seq: transcript-level estimates improve gene-level inferences. *F1000Res*. 2015;4:1521. doi:10.12688/f1000research.7563.1.

327. Love MI, Huber W, Anders S. Moderated estimation of fold change and dispersion for RNA-seq data with DESeq2. *Genome Biol*. 2014;15(12):31-62. doi:10.1186/s13059-014-0550-8.

328. Ashburner M, Ball CA, Blake JA, Botstein D, Butler H, Cherry JM, Davis AP, Dolinski K, Dwight SS, Eppig JT, Harris MA, Hill DP, Issel-Tarver L, Kasarskis A, Lewis S, Matese JC, Richardson JE, Ringwald M, Rubin GM, Sherlock G. Gene ontology: tool for the unification of biology. *Nat Genet*. 2000;25(1):25-29. doi:10.1038/75556.

329. Huang DW, Sherman BT, Lempicki RA. Systematic and integrative analysis of large gene lists using DAVID bioinformatics resources. *Nat Protoc*. 2009;4(1):44-57. doi:10.1038/nprot.2008.211.

330. Huang DW, Sherman BT, Lempicki RA. Bioinformatics enrichment tools: paths toward the comprehensive functional analysis of large gene lists. *Nucleic Acids Res*. 2008;37(1):1-13. doi:10.1093/nar/gkn923.

331. Kanehisa M, Goto S. KEGG: kyoto encyclopedia of genes and genomes. *Nucleic Acids Res*. 2000;28(1):27-30.

332. Schmittgen TD, Livak KJ. Analyzing real-time PCR data by the comparative CT method. *Nat Protoc*. 2008;3(6):1101-1108. doi:10.1038/nprot.2008.73.

333. Buttgereit J, Shanks J, Li D, Hao G, Athwal A, Langenickel TH, Wright H, da Costa Goncalves AC, Monti J, Plehm R, Popova E, Qadri F, Lapidus I, Ryan B, Özcelik C, Paterson DJ, Bader M, Herring N. C-type natriuretic peptide and natriuretic peptide receptor B signalling inhibits cardiac sympathetic neurotransmission and autonomic function. *Cardiovasc Res*. 2016;112(3):637-644. doi:10.1093/cvr/cvw184.

334. Bardsley EN, Larsen HE, Paterson DJ. Impaired cAMP-cGMP cross-talk during cardiac sympathetic dysautonomia. *Channels (Austin)*. 2016;11(3):178-180. doi:10.1080/19336950.2016.1259040.

335. Li D, Lee CW, Buckler K, Parekh A, Herring N, Paterson DJ. Abnormal intracellular calcium homeostasis in sympathetic neurons from young prehypertensive rats. *Hypertension*. 2012;59(3):642-649. doi:10.1161/HYPERTENSIONAHA.111.186460.

336. Albrecht MA, Colegrove SL, Hongpaisan J, Pivovarova NB, Andrews SB, Friel DD. Multiple modes of calcium-induced calcium release in sympathetic neurons I: Attenuation of endoplasmic reticulum Ca^{2+} accumulation at low $[Ca^{2+}]i$ during

weak depolarization. *J Gen Physiol*. 2001;118(1):83-100. doi:10.1085/jgp.118.1.83.

337. Bardsley EN, Davis H, Ajijola OA, Buckler KJ, Ardell JL, Shivkumar K, Paterson DJ. RNA sequencing reveals novel transcripts from sympathetic stellate ganglia during cardiac sympathetic hyperactivity. *Sci Rep*. 2018;8(1):8633. doi:10.1038/s41598-018-26651-7.

338. Huang MH, Smith FM, Armour JA. Amino acids modify activity of canine intrinsic cardiac neurons involved in cardiac regulation. *Am J Physiol*. 1993;264(4 Pt 2):H1275-H1282. doi:10.1152/ajpheart.1993.264.4.H1275.

339. Huang MH, Wolf SG, Armour JA. Ventricular arrhythmias induced by chemically modified intrinsic cardiac neurones. *Cardiovasc Res*. 1994;28(5):636-642.

340. Butler CK, Smith FM, Nicholson J, Armour JA. Cardiac effects induced by chemically activated neurons in canine intrathoracic ganglia. *Am J Physiol*. 1990;259(4 Pt 2):H1108-H1117. doi:10.1152/ajpheart.1990.259.4.H1108.

341. Gill SS, Pulido OM, Mueller RW, McGuire PF. Molecular and immunochemical characterization of the ionotropic glutamate receptors in the rat heart. *Brain Res Bull*. 1998;46(5):429-434.

342. Sun H, Tonks NK. The coordinated action of protein tyrosine phosphatases and kinases in cell signaling. *Trends Biochem Sci*. 1994;19(11):480-485.

343. Shanks J, Herring N. Peripheral cardiac sympathetic hyperactivity in cardiovascular disease: role of neuropeptides. *Am J Physiol Regul Integr Comp Physiol*. 2013;305(12):R1411-R1420. doi:10.1152/ajpregu.00118.2013.

344. Lee RMKW, Borkowski KR, Leenen FHH, Tsoporis J, Coughlin M. Combined effect of neonatal sympathectomy and adrenal demedullation on blood pressure and vascular changes in spontaneously hypertensive rats. *Circ Res*. 1991;69(3):714-721. doi:10.1161/01.RES.69.3.714.

345. Ernsberger U, Kramer M, Tsarovina K, Deller T, Rohrer H. Coordinate expression of pan-neuronal and functional signature genes in sympathetic neurons. *Cell Tissue Res*. 2017;370(2):227-241. doi:10.1007/s00441-017-2688-7.

346. Stanzel S, Stubbusch J, Pataskar A, Howard MJ, Deller T, Ernsberger U, Tiwari VK, Rohrer H, Tsarovina K. Distinct roles of hand2 in developing and adult autonomic neurons. *Dev Neurobiol*. 2016;76(10):1111-1124. doi:10.1002/dneu.22378.

347. Furlan A, La Manno G, Lübke M, Häring M, Abdo H, Hochgerner H, Kupari J, Usoskin D, Airaksinen MS, Oliver G, Linnarsson S, Ernfors P. Visceral motor neuron diversity delineates a cellular basis for nipple- and pilo-erection muscle control. *Nat Neurosci*. 2016;19(10):1331-1340. doi:10.1038/nn.4376.

348. Mahapatra NR. Catestatin is a novel endogenous peptide that regulates cardiac function and blood pressure. *Cardiovasc Res*. 2008;80(3):330-338. doi:10.1093/cvr/cvn155.

349. Angelone T, Quintieri AM, Brar BK, Limchaiyawat PT, Tota B, Mahata SK, Cerra MC. The antihypertensive chromogranin a peptide catestatin acts as a novel endocrine/paracrine modulator of cardiac inotropism and lusitropism. *Endocrinology*. 2008;149(10):4780-4793. doi:10.1210/en.2008-0318.

350. O'Connor DT, Kailasam MT, Kennedy BP, Ziegler MG, Yanaihara N, Parmer RJ. Early decline in the catecholamine release-inhibitory peptide catestatin in humans at genetic risk of hypertension. *J Hypertens*. 2002;20(7):1335-1345. doi:10.1097/00004872-200207000-00020.

351. Mahata SK, Mahata M, Wen G, Wong WB, Mahapatra NR, Hamilton BA, O'Connor DT. The catecholamine release-inhibitory “catestatin” fragment of chromogranin A: Naturally occurring human variants with different potencies for multiple chromaffin cell nicotinic cholinergic responses. *Mol Pharmacol*. 2004;66(5):1180-1191. doi:10.1124/mol.104.002139.

352. Zhu D, Xie H, Wang X, Liang Y, Yu H, Gao W. Catestatin-a novel predictor of left ventricular remodeling after acute myocardial infarction. *Sci Rep*. 2017;7(1):44168. doi:10.1038/srep44168.

353. Philipp T, Distler A, Cordes U. Sympathetic nervous system and blood-pressure control in essential hypertension. *Lancet*. 1978;2(8097):959-963.

354. Tang Y-P, Shimizu E, Dube GR, Rampon C, Kerchner GA, Zhuo M, Liu G, Tsien JZ. Genetic enhancement of learning and memory in mice. *Nature*. 1999;401(6748):63-69. doi:10.1038/43432.

355. Riedel G, Platt B, Micheau J. Glutamate receptor function in learning and memory. *Behav Brain Res*. 2003;140(1-2):1-47. doi:10.1016/S0166-4328(02)00272-3.

356. Loftis JM, Janowsky A. The N-methyl-D-aspartate receptor subunit NR2B: localization, functional properties, regulation, and clinical implications. *Pharmacol Ther*. 2003;97(1):55-85.

357. Gutierrez-Castellanos N, Da Silva-Matos CM, Zhou K, Canto CB, Renner MC, Koene LMC, Ozyildirim O, Sprengel R, Kessels HW, De Zeeuw CI. Motor Learning Requires Purkinje Cell Synaptic Potentiation through Activation of AMPA-Receptor Subunit GluA3. *Neuron*. 2017;93(2):409-424. doi:10.1016/j.neuron.2016.11.046.

358. Renner MC, Albers EH, Gutierrez-Castellanos N, Reinders NR, van Huijstee AN, Xiong H, Lodder TR, Kessels HW. Synaptic plasticity through activation of GluA3-containing AMPA-receptors. *Elife*. 2017;6:265. doi:10.7554/eLife.25462.

359. Davis H, Bardsley EN, Paterson DJ. Data descriptor: Transcriptional profiling of stellate ganglia from normotensive and spontaneously hypertensive rat strains. *Sci Data*. 2018;5. doi:10.1038/sdata.2018.123.

360. Sassone-Corsi P. The cyclic AMP pathway. *Cold Spring Harb Perspect Biol*. 2012;4(12):a011148-a011148. doi:10.1101/cshperspect.a011148.

361. Torres-Quesada O, Mayrhofer JE, Stefan E. The many faces of compartmentalized PKA signalosomes. *Cell Signal*. 2017;37:1-11. doi:10.1016/j.cellsig.2017.05.012.

362. Abi-Gerges A, Richter W, Lefebvre F, Mateo P. Decreased expression and activity of cAMP phosphodiesterases in cardiac hypertrophy and its impact on β-adrenergic cAMP signals. *Circulation*. 2009. doi:10.1161/CIRCRESAHA.109.197947.

363. Wilkins MR, Wharton J, Grimminger F, Ghofrani HA. Phosphodiesterase inhibitors for the treatment of pulmonary hypertension. *Eur Respir J*. 2008;32(1):198-209. doi:10.1183/09031936.00124007.

364. Li D, Wang L, Lee CW, Dawson TA, Paterson DJ. Noradrenergic cell specific gene transfer with neuronal nitric oxide synthase reduces cardiac sympathetic neurotransmission in hypertensive rats. *Hypertension*. 2007;50(1):69-74. doi:10.1161/HYPERTENSIONAHA.107.088591.

365. Ohlsson T, Lindgren A, Engström G, Jern C, Melander O. A stop-codon of the phosphodiesterase 11A gene is associated with elevated blood pressure and measures of obesity. *J Hypertens*. 2016;34(3):445–51–discussion451. doi:10.1097/HJH.0000000000000821.

366. Yates A, Akanni W, Amode MR, Barrell D, Billis K, Carvalho-Silva D, Cummins C, Clapham P, Fitzgerald S, Gil L, Girón CG, Gordon L, Hourlier T, Hunt SE, Janacek SH, Johnson N, Juettemann T, Keenan S, Lavidas I, Martin FJ, Maurel T, McLaren W, Murphy DN, Nag R, Nuhn M, Parker A, Patricio M, Pignatelli M, Rahtz M, Riat HS, Sheppard D, Taylor K, Thormann A, Vullo A, Wilder SP, Zadissa A, Birney E, Harrow J, Muffato M, Perry E, Ruffier M, Spudich G, Trevanion SJ, Cunningham F, Aken BL, Zerbino DR, Flicek P. Ensembl 2016. *Nucleic Acids Res*. 2016;44(D1):D710-D716. doi:10.1093/nar/gkv1157.

367. Chiu Y-F, Lee C-Y, Hsu F-C. Multipoint association mapping for longitudinal family data: an application to hypertension phenotypes. *BMC Proc*. 2016;10(Suppl 7):315-320. doi:10.1186/s12919-016-0049-2.

368. Chiu Y-F, Justice AE, Melton PE. Longitudinal analytical approaches to genetic data. *BMC Genet*. 2016;17 Suppl 2(S2):4. doi:10.1186/s12863-015-0312-y.

369. Siffert W, Rosskopf D, Siffert G, Busch S, Moritz A, Erbel R, Sharma AM, Ritz E, Wichmann HE, Jakobs KH, Horsthemke B. Association of a human G-protein β3 subunit variant with hypertension. *Nat Methods*. 1998;18(1):45-48. doi:10.1038/ng0198-45.

370. Siffert W. G protein polymorphisms in hypertension, atherosclerosis, and diabetes. *Annu Rev Med*. 2005;56:17-28. doi:10.1146/annurev.med.56.082103.104625.

371. Tozawa Y. G protein beta3 subunit variant: tendency of increasing susceptibility to hypertension in Japanese. *Blood Press*. 2001;10(3):131-134. doi:10.1080/080370501753182334.

372. Kraja AT, Hunt SC, Rao DC, Dávila-Román VG, Arnett DK, Province MA. Genetics of hypertension and cardiovascular disease and their interconnected pathways: lessons from large studies. *Curr Hypertens Rep*. 2011;13(1):46-54. doi:10.1007/s11906-010-0174-7.

373. Guauque-Olarte S, Messika-Zeitoun D, Droit A, Lamontagne M, Tremblay-Marchand J, Lavoie-Charland E, Gaudreault N, Arsenault BJ, Dubé M-P, Tardif J-C, Body SC, Seidman JG, Boileau C, Mathieu P, Pibarot P, Bossé Y. Calcium signaling pathway genes RUNX2 and CACNA1C are associated with calcific aortic valve disease. *Circ Cardiovasc Genet*. 2015;8(6):812-822. doi:10.1161/CIRCGENETICS.115.001145.

374. Johnson AD, Newton-Cheh C, Chasman DI, Ehret GB, Johnson T, Rose L, Rice K, Verwoert GC, Launer LJ, Gudnason V, Larson MG, Chakravarti A, Psaty BM, Caulfield M, van Duijn CM, Ridker PM, Munroe PB, Levy D, Cohorts for Heart and Aging Research in Genomic Epidemiology Consortium, Global BPgen Consortium, Women's Genome Health Study. Association of hypertension drug target genes with blood pressure and hypertension in 86,588 individuals.

Hypertension. 2011;57(5):903-910. doi:10.1161/HYPERTENSIONAHA.110.158667.

375. Guo L, Lee AA, Rizvi TA, Ratner N, Kirschner LS. The protein kinase A regulatory subunit R1A (Prkar1a) plays critical roles in peripheral nerve development. *J Neurosci*. 2013;33(46):17967-17975. doi:10.1523/JNEUROSCI.0766-13.2013.

376. Stratakis CA, Kirschner LS, Carney JA. Clinical and molecular features of the Carney complex: diagnostic criteria and recommendations for patient evaluation. *J Clin Endocrinol Metab*. 2001;86(9):4041-4046. doi:10.1210/jcem.86.9.7903.

377. Stratakis CA. Mutations of the gene encoding the protein kinase A type I-alpha regulatory subunit (PRKAR1A) in patients with the “complex of spotty skin pigmentation, myxomas, endocrine overactivity, and schwannomas” (Carney complex). *Ann N Y Acad Sci*. 2002;968:3-21.

378. Seidel E, Scholl UI. Genetic mechanisms of human hypertension and their implications for blood pressure physiology. *Physiol Genomics*. 2017;49(11):630-652. doi:10.1152/physiolgenomics.00032.2017.

379. Zheng J, Rao DC, Shi G. An update on genome-wide association studies of hypertension. *Appl Inform*. 2015;10(1):1-20. doi:10.1186/s40535-015-0013-7.

380. Wallace S, Guo DC, Regalado E, Mellor-Crummey L, Bamshad M, Nickerson DA, Dauser R, Hanchard N, Marom R, Martin E, Berka V, Sharina I, Ganesan V, Saunders D, Morris SA, Milewicz DM. Disrupted nitric oxide signaling due to GUCY1A3 mutations increases risk for moyamoya disease, achalasia and hypertension. *Clin Genet*. 2016;90(4):351-360. doi:10.1111/cge.12739.

381. Rippe C, Zhu B, Krawczyk KK, Van Bavel E, Albinsson S, lund JSX, Bakker ENTP, rd KSX. Hypertension reduces soluble guanylyl cyclase expression in the mouse aorta via the Notch signaling pathway. *Sci Rep*. April 2017:1-13. doi:10.1038/s41598-017-01392-1.

382. Erdmann J, Stark K, Esslinger UB, Rumpf PM, Koesling D, de Wit C, Kaiser FJ, Braunholz D, Medack A, Fischer M, Zimmermann ME, Tennstedt S, Graf E, Eck S, Aherrahrou Z, Nahrstaedt J, Willenborg C, Bruse P, Brænne I, Nöthen MM, Hofmann P, Braund PS, Mergia E, Reinhard W, Burgdorf C, Schreiber S, Balmforth AJ, Hall AS, Bertram L, Steinhagen-Thiessen E, Li S-C, März W, Reilly M, Kathiresan S, McPherson R, Walter U, CARDIoGRAM, Ott J, Samani NJ, Strom TM, Meitinger T, Hengstenberg C, Schunkert H. Dysfunctional nitric oxide signalling increases risk of myocardial infarction. *Nature*. 2013;504(7480):432-436. doi:10.1038/nature12722.

383. Wobst J, Rumpf PM, Dang TA, Segura-Puimedon M, Erdmann J, Schunkert H. Molecular variants of soluble guanylyl cyclase affecting cardiovascular risk. *Circ J*. 2015;79(3):463-469. doi:10.1253/circj.CJ-15-0025.

384. Wobst J, Ameln S, Wolf B, Wierer M, Dang TA, Sager HB, Tennstedt S, Hengstenberg C, Koesling D, Friebe A, Braun SL, Erdmann J, Schunkert H, Kessler T. Stimulators of the soluble guanylyl cyclase: promising functional insights from rare coding atherosclerosis-related *GUCY1A3* variants. *Basic Res Cardiol*. 2016;111(4):1-13. doi:10.1007/s00395-016-0570-5.

385. Segura-Puimedon M, Mergia E, Al-Hasani J, Aherrahrou R, Stoelting S, Kremer F, Freyer J, Koesling D, Erdmann J, Schunkert H, de Wit C, Aherrahrou Z. Proatherosclerotic effect of the α1-subunit of soluble guanylyl cyclase by

promoting smooth muscle phenotypic switching. *Am J Pathol*. 2016;186(8):2220-2231. doi:10.1016/j.ajpath.2016.04.010.

386. Kessler T, Wobst J, Wolf B, Eckhold J, Vilne B, Hollstein R, Ameln von S, Dang TA, Sager HB, Moritz Rumpf P, Aherrahrou R, Kastrati A, Björkegren JLM, Erdmann J, Lusis AJ, Civelek M, Kaiser FJ, Schunkert H. Functional characterization of the *GUCY1A3* coronary artery disease risk locus. *Circulation*. 2017;136(5):476-489. doi:10.1161/CIRCULATIONAHA.116.024152.

387. CARDIoGRAMplusC4D Consortium, Deloukas P, Kanoni S, Willenborg C, Farrall M, Assimes TL, Thompson JR, Ingelsson E, Saleheen D, Erdmann J, Goldstein BA, Stirrups K, König IR, Cazier J-B, Johansson Å, Hall AS, Lee J-Y, Willer CJ, Chambers JC, Esko T, Folkersen L, Goel A, Grundberg E, Havulinna AS, Ho WK, Hopewell JC, Eriksson N, Kleber ME, Kristiansson K, Lundmark P, Lyytikäinen L-P, Rafelt S, Shungin D, Strawbridge RJ, Thorleifsson G, Tikkanen E, Van Zuydam N, Voight BF, Waite LL, Zhang W, Ziegler A, Absher D, Altshuler D, Balmforth AJ, Barroso I, Braund PS, Burgdorf C, Claudi-Boehm S, Cox D, Dimitriou M, Do R, DIAGRAM Consortium, CARDIOGENICS Consortium, Doney ASF, Mokhtari El N, Eriksson P, Fischer K, Fontanillas P, Franco-Cereceda A, Gigante B, Groop L, Gustafsson S, Hager J, Hallmans G, Han B-G, Hunt SE, Kang HM, Illig T, Kessler T, Knowles JW, Kolovou G, Kuusisto J, Langenberg C, Langford C, Leander K, Lokki M-L, Lundmark A, McCarthy MI, Meisinger C, Melander O, Mihailov E, Maouche S, Morris AD, Müller-Nurasyid M, MuTHER Consortium, Nikus K, Peden JF, Rayner NW, Rasheed A, Rosinger S, Rubin D, Rumpf MP, Schäfer A, Sivananthan M, Song C, Stewart AFR, Tan S-T, Thorgeirsson G, et al. Large-scale association analysis identifies new risk loci for coronary artery disease. *Nat Methods*. 2013;45(1):25-33. doi:10.1038/ng.2480.

388. Sandberg K, Ji H. Sex differences in primary hypertension. *Biol Sex Differ*. 2012;3(1):7. doi:10.1186/2042-6410-3-7.

389. Russwurm C, Zoidl G, Koesling D, Russwurm M. Dual Acylation of PDE2A Splice Variant 3: targeting to synaptic membranes. *J Biol Chem*. 2009;284(38):25782-25790. doi:10.1074/jbc.M109.017194.

390. Sverrisdottir YB, Green AL, Aziz TZ, Bahuri NFA, Hyam J, Basnayake SD, Paterson DJ. Differentiated baroreflex modulation of sympathetic nerve activity during deep brain stimulation in humans. *Hypertension*. 2014;63(5):1000-1010. doi:10.1161/HYPERTENSIONAHA.113.02970.

391. Sabbah HN, Ilsar I, Zaretsky A, Rastogi S, Wang M, Gupta RC. Vagus nerve stimulation in experimental heart failure. *Heart Fail Rev*. 2011;16(2):171-178. doi:10.1007/s10741-010-9209-z.

392. Smith AA, Taylor T, Wortis SB. Abnormal catechol amine metabolism in familial dysautonomia. *N Engl J Med*. 1963;268(13):705-707. doi:10.1056/nejm196303282681304.

393. Romero JC, Reckelhoff JF. Role of angiotensin and oxidative stress in essential hypertension. *Hypertension*. 1999;34(4):943-949.

394. Catt KJ, Zimmet PZ, Cain MD, Cran E, Best JB, Coghlan JP. Angiotensin II blood-levels in human hypertension. *Lancet*. 1971;297(7697):459-464. doi:10.1016/S0140-6736(71)91085-3.

395. Schiffer S, Pummer S, Witte K, Lemmer B. Cardiovascular regulation in TGR(mREN2)27 rats: 24h variation in plasma catecholamines, angiotensin

peptides, and telemetric heart rate variability. *Chronobiol Int*. 2009;18(3):461-474. doi:10.1081/CBI-100103969.

396. Shinohara K, Kishi T, Hirooka Y, Sunagawa K. Circulating angiotensin II deteriorates left ventricular function with sympathoexcitation via brain angiotensin II receptor. *Physiol Rep*. 2015;3(8):e12514–12. doi:10.14814/phy2.12514.

397. Najafi A, Sequeira V, Kuster DWD, van der Velden J. β-adrenergic receptor signalling and its functional consequences in the diseased heart. *Eur J Clin Invest*. 2016;46(4):362-374. doi:10.1111/eci.12598.

398. Bristow MR. Mechanism of action of beta-blocking agents in heart failure. *Asian-australas J Anim Sci*. 1997;80(11A):L26-L40. doi:10.1016/S0002-9149(97)00846-1.

399. Esler M, Jennings G, Korner P, Willett I, Dudley F, Hasking G, Anderson W, Lambert G. Assessment of human sympathetic nervous-system activity from measurements of norepinephrine turnover. *Hypertension*. 1988;11(1):3-20. doi:10.1161/01.HYP.11.1.3.

400. Bristow MR. Treatment of chronic heart failure with β-adrenergic receptor antagonists: a convergence of receptor pharmacology and clinical cardiology. *Circ Res*. 2011;109(10):1176-1194. doi:10.1161/CIRCRESAHA.111.245092.

401. Wiysonge CS, Bradley HA, Volmink J, Mayosi BM. Cochrane corner: beta-blockers for hypertension. *Heart*. 2018;104(4):282-283. doi:10.1136/heartjnl-2017-311585.

402. Nedergaard OA, Abrahamsen J. Modulation of noradrenaline release by activation of presynaptic beta-adrenoceptors in the cardiovascular system. *Ann N Y Acad Sci*. 1990;604:528-544.

403. Majewski H. Modulation of noradrenaline release through activation of presynaptic β-adrenoreceptors. *J Auton Pharmacol*. 1983;3(1):47-60. doi:10.1111/j.1474-8673.1983.tb00496.x.

404. Misu Y, Kubo T. Presynaptic β-adrenoceptors. *Med Res Rev*. 1986;6(2):197-225. doi:10.1002/med.2610060204.

405. Lokhandwala MF, Eikenburg DC. Presynaptic receptors and alterations in norepinephrine release in spontaneously hypertensive rats. *Life Sci*. 1983;33(16):1527-1542. doi:10.1016/0024-3205(83)90693-8.

406. Adler-Graschinsky E, Langer SZ. Possible role of a beta-adrenoceptor in the regulation of noradrenaline release by nerve stimulation through a positive feed-back mechanism. *Br J Pharmacol*. 1975;53(1):43-50. doi:10.1111/(ISSN)1476-5381.

407. Costa M, Majewski H. Facilitation of noradrenaline release from sympathetic nerves through activation of ACTH receptors, beta-adrenoceptors and angiotensin II receptors. *Br J Pharmacol*. 1988;95(3):993-1001. doi:10.1111/j.1476-5381.1988.tb11730.x.

408. Apparsundaram S, Eikenburg DC. Role of prejunctional beta adrenoceptors in rat cardiac sympathetic neurotransmission. *J Pharmacol Exp Ther*. 1995;272(2):519-526.

409. Berg T. β1-blockers lower norepinephrine release by inhibiting presynaptic, facilitating β1-adrenoceptors in normotensive and hypertensive rats. *Front Neurol*. 2014;5:51. doi:10.3389/fneur.2014.00051.

410. Berg T. Altered β1–3-adrenoceptor influence on α2-adrenoceptor-mediated control of catecholamine release and vascular tension in hypertensive rats. *Front Physiol*. 2015;6:1-12. doi:10.3389/fphys.2015.00120.

411. Finney PA, Donnelly LE, Belvisi MG, Chuang T-T, Birrell M, Harris A, Mak JC, Scorer C, Barnes PJ, Adcock IM, Giembycz MA. Chronic systemic administration of salmeterol to rats promotes pulmonary beta$_2$-adrenoceptor desensitization and down-regulation of G$_{sa}$. *Br J Pharmacol*. 2001;132:1261±1270.

412. Malbon CC. Developmental cell biology: G proteins in development. 2005;6(9):689-701. doi:10.1038/nrm1716.

413. Hoffmann C, Leitz MR, Oberdorf-Maass S, Lohse MJ, Klotz KN. Comparative pharmacology of human beta-adrenergic receptor subtypes--characterization of stably transfected receptors in CHO cells. *Naunyn Schmiedebergs Arch Pharmacol*. 2004;369(2):151-159. doi:10.1007/s00210-003-0860-y.

414. Williams RS, Bishop T. Selectivity of dobutamine for adrenergic receptor subtypes. In vitro analysis by radioligand binding. *J Clin Invest*. 1981;67(6):1703-1711. doi:10.1172/JCI110208.

415. Cullum VA, Farmer JB, Jack D, Levy GP. Salbutamol: a new, selective beta-adrenoceptive receptor stimulant. *Br J Pharmacol*. 1969;35(1):141-151.

416. Ladage D, Schwinger RHG, Brixius K. Cardio-selective beta-blocker: pharmacological evidence and their influence on exercise capacity. *Cardiovasc Ther*. 2013;31(2):76-83. doi:10.1111/j.1755-5922.2011.00306.x.

417. Bardsley EN, Davis H, Ajijola OA, Buckler KJ, Ardell J, Shivkumar K, Paterson DJ. Identification of novel mRNA transcripts in the sympathetic stellate ganglia using RNA sequencing. *The FASEB Journal*. 2018;32(1_supplement):596.4-596.4. doi:10.1096/fasebj.2018.32.1_supplement.596.4.

418. Hein L, Altman JD, Kobilka BK. Two functionally distinct α2-adrenergic receptors regulate sympathetic neurotransmission. *Nature*. 1999;402(6758):181-184. doi:10.1038/46040.

419. Altman JD, Trendelenburg AU, MacMillan L, Bernstein D, Limbird L, Starke K, Kobilka BK, Hein L. Abnormal regulation of the sympathetic nervous system in alpha$_{2A}$-adrenergic receptor knockout mice. *Mol Pharmacol*. 1999;56(1):154-161.

420. Gilsbach R, Schneider J, Lother A, Schickinger S, Leemhuis J, Hein L. Sympathetic alpha$_2$-adrenoceptors prevent cardiac hypertrophy and fibrosis in mice at baseline but not after chronic pressure overload. *Cardiovasc Res*. 2010;86(3):432-442. doi:10.1093/cvr/cvq014.

421. Wiysonge CS, Bradley HA, Volmink J, Mayosi BM, Opie LH. Beta-blockers for hypertension. Cochrane Hypertension Group, ed. *Cochrane Database Syst Rev*. 2017;285(4):2719-2796. doi:10.1002/14651858.CD002003.pub5.

422. Blumenthal SJ, McConnaughey MM, Iams SG. Myocardial adrenergic-receptors and adenylate-cyclase in the developing spontaneously hypertensive rat. *Clin Exp Hypertens A*. 1982;4(6):883-901.

423. Horvath A, Bertherat J, Groussin L, Guillaud-Bataille M, Tsang K, Cazabat L, Libé R, Remmers E, René-Corail F, Faucz FR, Clauser E, Calender A, Bertagna X, Carney JA, Stratakis CA. Mutations and polymorphisms in the gene encoding regulatory subunit type 1-alpha of protein kinase A (PRKAR1A): an update. *Hum Mutat*. 2010;31(4):369-379. doi:10.1002/humu.21178.

424. Kawashima T. The autonomic nervous system of the human heart with special reference to its origin, course, and peripheral distribution. *Anat Embryol*. 2005;209(6):425-438. doi:10.1007/s00429-005-0462-1.

425. Ellison JP, Williams TH. Sympathetic nerve pathways to the human heart, and their variations. *Am J Anat*. 1969;124(2):149-162. doi:10.1002/aja.1001240203.

426. Herring N, Lee C-W, Sunderland N, Wright K, Paterson DJ. Pravastatin normalises peripheral cardiac sympathetic hyperactivity in the spontaneously hypertensive rat. *J Mol Cell Cardiol*. 2011;50(1):99-106. doi:10.1016/j.yjmcc.2010.09.025.

427. Seaford R, Wilkins J, Wright M, Gill C. *Selfhood and the Soul: Essays on Ancient Thought and Literature in Honour of Christopher Gill*. 2017.

428. Esler M. Mental stress and human cardiovascular disease. *Neurosci Biobehav Rev*. 2017;74(Pt B):269-276. doi:10.1016/j.neubiorev.2016.10.011.

429. Esler M, Eikelis N, Schlaich M, Lambert G, Alvarenga M, Dawood T, Kaye D, Barton D, Pier C, Guo L, Brenchley C, Jennings G, Lambert E. Chronic mental stress is a cause of essential hypertension: presence of biological markers of stress. *Clin Exp Pharmacol Physiol*. 2008;35(4):498-502. doi:10.1111/j.1440-1681.2008.04904.x.

430. Brown MJ, Macquin I. Is adrenaline the cause of essential hypertension? *Lancet*. 1981;2(8255):1079-1082.

431. Floras JS. Epinephrine and the genesis of hypertension. *Hypertension*. 1992;19(1):1-18.

432. Blankestijn PJ, Man in't Veld AJ, Tulen J, van den Meiracker AH, Boomsma F, Moleman P, Ritsema van Eck HJ, Derkx FH, Mulder P, Lamberts SJ. Support for adrenaline-hypertension hypothesis: 18 hour pressor effect after 6 hours adrenaline infusion. *Lancet*. 1988;2(8625):1386-1389.

433. Gudmundsdottir H, Strand AH, Høieggen A, Reims HM, Westheim AS, Eide IK, Kjeldsen SE, Os I. Do screening blood pressure and plasma catecholamines predict development of hypertension? Twenty-year follow-up of middle-aged men. *Blood Press*. 2008;17(2):94-103. doi:10.1080/08037050801972923.

434. Misu Y, Kuwahara M, Amano H, Kubo T. Adrenaline as an endogenous agonist for presynaptic beta-adrenoceptors and their relevance to the development of hypertension in spontaneously hypertensive rats. *J Hypertens Suppl*. 1988;6(4):S572-S574.

435. Esler M, Eikelis N, Schlaich M, Lambert G, Alvarenga M, Kaye D, El-Osta A, Guo L, Barton D, Pier C, Brenchley C, Dawood T, Jennings G, Lambert E. Human sympathetic nerve biology: parallel influences of stress and epigenetics in essential hypertension and panic disorder. *Ann N Y Acad Sci*. 2008;1148:338-348. doi:10.1196/annals.1410.064.

436. Esler M, Jennings G, Biviano B, Lambert G, Hasking G. Mechanism of elevated plasma noradrenaline in the course of essential hypertension. *J Cardiovasc Pharmacol*. 1986;8:S39-S43.

437. Kuczenski R. Soluble, membrane-bound, and detergent-solubilized rat striatal tyrosine hydroxylase. pH-dependent cofactor binding. *J Biol Chem*. 1973;248(14):5074-5080.

438. Zigmond RE, Schwarzschild MA, Rittenhouse AR. Acute regulation of tyrosine hydroxylase by nerve activity and by neurotransmitters via phosphorylation. *Annu Rev Neurosci*. 1989;12(1):415-461. doi:10.1146/annurev.ne.12.030189.002215.

439. Kumer SC, Vrana KE. Intricate regulation of tyrosine hydroxylase activity and gene expression. *J Neurochem*. 1996;67(2):443-462.

440. Mestikawy El S, Glowinski J, Hamon M. Tyrosine hydroxylase activation in depolarized dopaminergic terminals - Involvement of Ca^{2+}-dependent phosphorylation. *Nature*. 1983;302(5911):830-832. doi:10.1038/302830a0.

441. Brown MJ, Dollery CT. Adrenaline and hypertension. *Clin Exp Hypertens*. 1984;A6(1-2):539-549. doi:10.3109/10641968409062582.

442. Majewski H, Tung LH, Rand MJ. Adrenaline-induced hypertension in rats. *J Cardiovasc Pharmacol*. 1981;3(1):179-185. doi:10.1242/jcs.188060.

443. Brown MJ, Macquin I. Catecholamine neurotransmitters and the heart. *Acta Medica Scandinavica*. 1982;211(S660):34-39. doi:10.1111/j.0954-6820.1982.tb00358.x.

444. Franco-Morselli R, Elghozi JL, Joly E, Di Giuilio S, Meyer P. Increased plasma adrenaline concentrations in benign essential hypertension. *Br Med J*. 1977;2(6097):1251-1254. doi:10.1136/bmj.2.6097.1251.

445. Johansson M, Rundqvist B, Eisenhofer G, Friberg P. Cardiorenal epinephrine kinetics: evidence for neuronal release in the human heart. *Am J Physiol*. 1997;273(5):H2178-H2185.

446. Majewski H, Tung LH, Rand MJ. Adrenaline activation of prejunctional β-adrenoceptors and hypertension. *J Cardiovasc Pharmacol*. 1982;4(1):99-106. doi:10.1097/00005344-198201000-00016.

447. Rand MJ, Majewski H. Adrenaline Mediates A Positive Feedback Loop in Noradrenergic Transmission: Its Possible Role in Development of Hypertension. *Clin Exp Hypertens A*. 1984;6(1-2):347-370. doi:10.3109/10641968409062570.

448. Pak CH. Plasma adrenaline and noradrenaline concentrations of the spontaneously hypertensive rat. *Jpn Heart J*. 1981;22(6):987-995. doi:10.1536/ihj.22.987.

449. Esler M, Rumantir M, Kaye D, Lambert G. The sympathetic neurobiology of essential hypertension: disparate influences of obesity, stress, and noradrenaline transporter dysfunction? *Am J Hypertens*. 2001;14(6 Pt 2):139S–146S.

450. Kaye DM, Lambert GW, Lefkovits J, Morris M, Jennings G, Esler MD. Neurochemical evidence of cardiac sympathetic activation and increased central nervous system norepinephrine turnover in severe congestive heart failure. *J Am Coll Cardiol*. 1994;23(3):570-578. doi:10.1016/0735-1097(94)90738-2.

451. MacGregor DA, Prielipp RC, Butterworth JF IV, James RL, Royster RL. Relative efficacy and potency of β-adrenoceptor agonists for generating cAMP in human lymphocytes. *Chest*. 1996;109(1):194-200. doi:10.1378/chest.109.1.194.

452. Majewski H, Rand MJ, Tung LH. Activation of prejunctional β-adrenoceptors in rat atria by adrenaline applied exogenously or released as a co-transmitter. *Br J Pharmacol*. 1981;73(3):669-679. doi:10.1111/j.1476-5381.1981.tb16802.x.

453. Westfall TC, Peach MJ, Tittermary V. Enhancement of the electrically induced release of norepinephrine from the rat portal vein: mediation by beta 2-adrenoceptors. *Eur J Pharmacol*. 1979;58(1):67-74.

454. Dahlöf C, Ljung B, Åblad B. Increased noradrenaline release in rat portal vein during sympathetic nerve stimulation due to activation of presynaptic β-adrenoceptors by noradrenaline and adrenaline. *Eur J Pharmacol*. 1978;50(1):75-78. doi:10.1016/0014-2999(78)90255-8.

455. Salpeter SR, Ormiston TM, Salpeter EE. Cardiovascular effects of β-agonists in patients with asthma and COPD: A meta-analysis. *Chest*. 2004;125(6):2309-2321. doi:10.1378/chest.125.6.2309.

456. Sears MR. Adverse effects of β-agonists. *J Allergy Clin Immunol*. 2002;110(6):S322-S328. doi:10.1067/mai.2002.129966.

457. Au DH, Curtis JR, Every NR, McDonell MB, Fihn SD. Association between inhaled β-agonists and the risk of unstable angina and myocardial infarction. *Chest*. 2002;121(3):846-851. doi:10.1378/chest.121.3.846.

458. Rumantir MS, Jennings GL, Lambert GW, Kaye DM, Seals DR, Esler MD. The “adrenaline hypothesis” of hypertension revisited: evidence for adrenaline release from the heart of patients with essential hypertension. *J Hypertens*. 2000;18(6):717-723.

459. Ghazi L, Drawz P. Advances in understanding the renin-angiotensin-aldosterone system (RAAS) in blood pressure control and recent pivotal trials of RAAS blockade in heart failure and diabetic nephropathy. *F1000Res*. 2017;6:297–10. doi:10.12688/f1000research.9692.1.

460. Zhang H, Han GW, Batyuk A, Ishchenko A, White KL, Patel N, Sadybekov A, Zamlynny B, Rudd MT, Hollenstein K, Tolstikova A, White TA, Hunter MS, Weierstall U, Liu W, Babaoglu K, Moore EL, Katz RD, Shipman JM, Garcia-Calvo M, Sharma S, Sheth P, Soisson SM, Stevens RC, Katritch V, Cherezov V. Structural basis for selectivity and diversity in angiotensin II receptors. *Nat Methods*. 2017;544(7650):327-332. doi:10.1038/nature22035.

461. Phillips MI, Speakman EA, Kimura B. Levels of angiotensin and molecular biology of the tissue renin angiotensin systems. *Regul Pept*. 1993;43(1-2):1-20.

462. Balakumar P, Jagadeesh G. A century old renin-angiotensin system still grows with endless possibilities: AT1 receptor signaling cascades in cardiovascular physiopathology. *Cell Signal*. 2014;26(10):2147-2160. doi:10.1016/j.cellsig.2014.06.011.

463. Chow BSM, Allen TJ. Angiotensin II type 2 receptor (AT2R) in renal and cardiovascular disease. *Clin Sci*. 2016;130(15):1307-1326. doi:10.1042/CS20160243.

464. Re R, Bryan SE. Functional intracellular renin-angiotensin systems may exist in multiple tissues. *Clin Exp Hypertens*. 1984;6(10-11):1739-1742. doi:10.3109/10641968409046069.

465. Arata Y, Geshi E, Nomizo A, Aoki S, Katagiri T. Alterations in sarcoplasmic reticulum and angiotensin II receptor type 1 gene expression in spontaneously hypertensive rat hearts. *Jpn Circ J*. 1999;63(5):367-372. doi:10.1253/jcj.63.367.

466. Bachmann S, Peters J, Engler E, Ganten D, Mullins J. Transgenic rats carrying the mouse renin gene-Morphological characterization of a low-renin hypertension model. *Kidney int*. 1992;41(1):24-36. doi:10.1038/ki.1992.4.

467. Crowley SD, Gurley SB, Herrera MJ, Ruiz P, Griffiths R, Kumar AP, Kim H-S, Smithies O, Le TH, Coffman TM. Angiotensin II causes hypertension and cardiac hypertrophy through its receptors in the kidney. *Proc Natl Acad Sci USA*. 2006;103(47):17985-17990. doi:10.1073/pnas.0605545103.

468. Kurabayashi M, Yazaki Y. Downregulation of angiotensin II receptor type 1 in heart failure: a process of adaptation or deterioration? *Circulation*. 1997;95(5):1104-1107. doi:10.1161/01.CIR.95.5.1104.

469. Wang Y, Seto S-W, Golledge J. Angiotensin II, sympathetic nerve activity and chronic heart failure. *Heart Fail Rev*. 2012;19(2):187-198. doi:10.1007/s10741-012-9368-1.

470. De Mello WC, Specht P. Chronic blockade of angiotensin II AT1-receptors increased cell-to-cell communication, reduced fibrosis and improved impulse propagation in the failing heart. *J Renin Angiotensin Aldosterone Syst*. 2006;7(4):201-205. doi:10.3317/jraas.2006.038.

471. Iijima K, Geshi E, Nomizo A, Arata Y, Katagiri T. Alterations in sarcoplasmic reticulum and angiotensin II type 1 receptor gene expression after myocardial infarction in rats. *Jpn Circ J*. 1998;62(6):449-454. doi:10.1253/jcj.62.449.

472. Tan J, Wang H, Leenen FHH. Increases in brain and cardiac AT 1receptor and ACE densities after myocardial infarct in rats. *Am J Physiol Heart Circ Physiol*. 2004;286(5):H1665-H1671. doi:10.1152/ajpheart.00858.2003.

473. Egger M, Domenighetti AA. Adaptive and maladaptive remodeling of cardiomyocyte excitation- contraction coupling by angiotensin II. *Trends Cardiovasc Med*. 2010;20(3):78-85. doi:10.1016/j.tcm.2010.06.001.

474. Sun Y. Intracardiac renin–angiotensin system and myocardial repair/remodeling following infarction. *J Mol Cell Cardiol*. 2010;48(3):483-489. doi:10.1016/j.yjmcc.2009.08.002.

475. van Kats JP, Duncker DJ, Haitsma DB, Schuijt MP, Niebuur R, Stubenitsky R, Boomsma F, Schalekamp MADH, Verdouw PD, Danser AHJ. Angiotensin-converting enzyme inhibition and angiotensin II type 1 receptor blockade prevent cardiac remodeling in pigs after myocardial infarction: role of tissue angiotensin II. *Circulation*. 2000;102(13):1556-1563. doi:10.1161/01.CIR.102.13.1556.

476. Hardwick JC, Ryan SE, Powers EN, Southerland EM, Ardell JL. Angiotensin receptors alter myocardial infarction-induced remodeling of the guinea pig cardiac plexus. *Am J Physiol Regul Integr Comp Physiol*. 2015;309(2):R179-R188. doi:10.1152/ajpregu.00004.2015.

477. Watanabe R, Suzuki J-I, Wakayama K, Maejima Y, Shimamura M, Koriyama H, Nakagami H, Kumagai H, Ikeda Y, Akazawa H, Morishita R, Komuro I, Isobe M. A

peptide vaccine targeting angiotensin II attenuates the cardiac dysfunction induced by myocardial infarction. *Sci Rep*. 2017;7(1):1-13. doi:10.1038/srep43920.

478. Domenighetti AA, Wang Q, Egger M, Richards SM, Pedrazzini T, Delbridge LMD. Angiotensin II-mediated phenotypic cardiomyocyte remodeling leads to age-dependent cardiac dysfunction and failure. *Hypertension*. 2005;46(2):426-432. doi:10.1161/01.HYP.0000173069.53699.d9.

479. Hughes J, Roth RH. Evidence that angiotensin enhances transmitter release during sympathetic nerve stimulation. *Br J Pharmacol*. 1971;41(2):239–&. doi:10.1111/j.1476-5381.1971.tb08025.x.

480. Ma XY, Chapleau MW, Whiteis CA, Abboud FM, Bielefeldt K. Angiotensin selectively activates a subpopulation of postganglionic sympathetic neurons in mice. *Circ Res*. 2001;88(8):787-793. doi:10.1161/hh0801.089542.

481. Berg T. Angiotensin AT_1-α_{2C}-adrenoceptor interaction disturbs α_{2A}-auto-inhibition of catecholamine release in hypertensive rats. *Front Neurol*. 2013;4:70. doi:10.3389/fneur.2013.00070.

482. Schmieder RE. The role of non-haemodynamic factors of the genesis of LVH. *Nephrol Dial Transplant*. 2005;20(12):2610-2612. doi:10.1093/ndt/gfi190.

483. Mazzolai L, Pedrazzini T, Nicoud F, Gabbiani G, Brunner HR, Nussberger J. Increased cardiac angiotensin II levels induce right and left ventricular hypertrophy in normotensive mice. *Hypertension*. 2000;35(4):985-991. doi:10.1161/01.HYP.35.4.985.

484. Mazzolai L, Aubert JF, Brunner HR, Nussberger J, Pedrazzini T. Blood pressure independent cardiac hypertrophy induced by locally activated renin-angiotensin system. *Hypertension*. 1997;30(3):48-48.

485. Osterop APRM, Kofflard MJM, Sandkuijl LA, Cate FJT, Krams R, Schalekamp MADH, Danser AHJ. AT_1 receptor A/C1166 polymorphism contributes to cardiac hypertrophy in subjects with hypertrophic cardiomyopathy. *Hypertension*. 1998;32(5):825-830. doi:10.1161/01.HYP.32.5.825.

486. Harrap SB, Dominiczak AF, Fraser R, Lever AF, Morton JJ, Foy CJ, Watt GCM. Plasma angiotensin II, predisposition to hypertension, and left ventricular size in healthy young adults. *Circulation*. 1996;93(6):1148-1154. doi:10.1161/01.CIR.93.6.1148.

487. Sata M, Fukuda D. Crucial role of renin-angiotensin system in the pathogenesis of atherosclerosis. *J Med Invest*. 2010;57(1,2):12-25. doi:10.2152/jmi.57.12.

488. Paul M, Mehr AP, Kreutz R. Physiology of local renin-angiotensin systems. *Physiol Rev*. 2006;86(3):747-803. doi:10.1152/physrev.00036.2005.

489. Touyz RM. Intracellular mechanisms involved in vascular remodelling of resistance arteries in hypertension: Role of angiotensin II. *Exp Physiol*. 2005;90(4):449-455. doi:10.1113/expphysiol.2005.030080.

490. Nyby MD, Abedi K, Smutko V, Eslami P, Tuck ML. Vascular angiotensin type 1 receptor expression is associated with vascular dysfunction, oxidative stress and inflammation in fructose-fed rats. *Hypertens Res*. 2007;30(5):451-457. doi:10.1291/hypres.30.451.

491. Benigni A, Cassis P, Remuzzi G. Angiotensin II revisited: new roles in inflammation, immunology and aging. *EMBO Mol Med*. 2010;2(7):247-257. doi:10.1002/emmm.201000080.

492. Santos RA, Brosnihan KB, Chappell MC, Pesquero J, Chernicky CL, Greene LJ, Ferrario CM. Converting enzyme activity and angiotensin metabolism in the dog brainstem. *Hypertension*. 1988;11(2 Pt 2):I153-I157.

493. Santos RAS, Simoes e Silva AC, Maric C, Silva DMR, Machado RP, De Buhr I, Heringer-Walther S, Pinheiro SVB, Lopes MT, Bader M, Mendes EP, Lemos VS, Campagnole-Santos MJ, Schultheiss HP, Speth R, Walther T. Angiotensin-(1-7) is an endogenous ligand for the G protein-coupled receptor Mas. *Proc Natl Acad Sci USA*. 2003;100(14):8258-8263. doi:10.1073/pnas.1432869100.

494. Santos RAS, Sampaio WO, Alzamora AC, Motta-Santos D, Alenina N, Bader M, Campagnole-Santos MJ. The ACE2/angiotensin-(1–7)/mas axis of the renin-angiotensin system: focus on angiotensin-(1–7). *Physiol Rev*. 2018;98(1):505-553. doi:10.1152/physrev.00023.2016.

495. Gironacci MM, Vatta M, Rodriguez-Fermepín M, Fernández BE, Peña C. Angiotensin-(1-7) reduces norepinephrine release through a nitric oxide mechanism in rat hypothalamus. *Hypertension*. 2000;35(6):1248-1252. doi:10.1161/01.HYP.35.6.1248.

496. Xing J, Lu J, Li J. Role of angiotensin-(1–7) and Mas-R-nNOS pathways in amplified neuronal activity of dorsolateral periaqueductal gray after chronic heart failure. *Neurosci Lett*. 2014;563:6-11. doi:10.1016/j.neulet.2014.01.025.

497. Rocha NP, Simões e Silva AC, Prestes TRR, Feracin V, Machado CA, Ferreira RN, Teixeira AL, de Miranda AS. RAS in the central nervous system: potential role in neuropsychiatric disorders. *Curr Med Chem*. February 2018. doi:10.2174/0929867325666180226102358.

498. Filho AG, Ferreira AJ, Santos SHS, Neves SRS, Silva Camargos ER, Becker LK, Belchior HA, Dias-Peixoto MF, Pinheiro SVB, Santos RAS. Selective increase of angiotensin(1-7) and its receptor in hearts of spontaneously hypertensive rats subjected to physical training. *Exp Physiol*. 2008;93(5):589-598. doi:10.1113/expphysiol.2007.041293.

499. Lima AM, Xavier CH, Ferreira AJ, Raizada MK, Wallukat G, Velloso EPP, Santos RASD, Fontes MAP. Activation of angiotensin-converting enzyme 2/angiotensin-(1–7)/Mas axis attenuates the cardiac reactivity to acute emotional stress. *Am J Physiol Heart Circ Physiol*. 2013;305(7):H1057-H1067. doi:10.1152/ajpheart.00433.2013.

500. Dias-Peixoto MF, Ferreira AJ, Almeida PWM, Braga VBA, Coutinho DCO, Melo DS, Filho AG, Melo MB, Greco L, Campagnole-Santos MJ, Lima RF, Santos RAS, Guatimosim S. The cardiac expression of Mas receptor is responsive to different physiological and pathological stimuli. *Peptides*. 2012;35(2):196-201. doi:10.1016/j.peptides.2012.03.022.

501. Brosnihan KB, Li P, Ferrario CM. Angiotensin-(1-7) dilates canine coronary arteries through kinins and nitric oxide. *Hypertension*. 1996;27(3):523-528. doi:10.1161/01.HYP.27.3.523.

502. Pörsti I, Bara AT, Busse R, Hecker M. Release of nitric oxide by angiotensin-(1-7) from porcine coronary endothelium: implications for a novel angiotensin receptor. *Br J Pharmacol*. 1994;111(3):652-654. doi:10.1111/j.1476-5381.1994.tb14787.x.

503. Ferrario CM, Chappell MC, Tallant EA, Brosnihan KB, Diz DI. Counterregulatory actions of angiotensin-(1-7). *Hypertension*. 1997;30(3):535-541. doi:10.1161/01.HYP.30.3.535.

504. Aires RD, Santiago LB, Ramalho LZN, Cortes SF, Lemos VS. Mas receptor overexpression increased Ang-(1–7) relaxation response in renovascular hypertensive rat carotid. *Peptides*. 2015;71:250-258. doi:10.1016/j.peptides.2015.08.002.

505. Benter IF, Diz DI, Ferrario CM. Pressor and reflex sensitivity is altered in spontaneously hypertensive rats treated with angiotensin-(1-7). *Hypertension*. 1995;26(6):1138-1144. doi:10.1161/01.HYP.26.6.1138.

506. Britto RR, Santos RAS, Fagundes-Moura CR, Khosla MC, Campagnole-Santos MJ. Role of angiotensin-(1-7) in the modulation of the baroreflex in renovascular hypertensive rats. *Hypertension*. 1997;30(3):549-556. doi:10.1161/01.HYP.30.3.549.

507. Iyer SN, Averill DB, Chappell MC, Yamada K, Allred AJ, Ferrario CM. Contribution of angiotensin-(1-7) to blood pressure regulation in salt-depleted hypertensive rats. *Hypertension*. 2000;36(3):417-422. doi:10.1161/01.HYP.36.3.417.

508. Gironacci MM, Valera MS, Yujnovsky I, Peña C. Angiotensin-(1-7) inhibitory mechanism of norepinephrine release in hypertensive rats. *Hypertension*. 2004;44(5):783-787. doi:10.1161/01.HYP.0000143850.73831.9d.

509. Faria-Silva R, Duarte FV, Santos RAS. Short-term angiotensin(1-7) receptor MAS stimulation improves endothelial function in normotensive rats. *Hypertension*. 2005;46(4):948-952. doi:10.1161/01.HYP.0000174594.17052.33.

510. Jiang F, Yang J, Zhang Y, Dong M, Wang S, Zhang Q, Liu FF, Zhang K, Zhang C. Angiotensin-converting enzyme 2 and angiotensin 1–7: novel therapeutic targets. *Nat Rev Cardiol*. 2014;11(7):413-426. doi:10.1038/nrcardio.2014.59.

511. Abwainy A, Babiker F, Akhtar S, Benter IF. Endogenous angiotensin-(1-7)/Mas receptor/NO pathway mediates the cardioprotective effects of pacing postconditioning. *Am J Physiol Heart Circ Physiol*. 2016;310(1):H104-H112. doi:10.1152/ajpheart.00121.2015.

512. Patel VB, Zhong J-C, Grant MB, Oudit GY. Role of the ACE2/angiotensin 1-7 axis of the renin-angiotensin system in heart failure. *Circ Res*. 2016;118(8):1313-1326. doi:10.1161/CIRCRESAHA.116.307708.

513. van den Meiracker AH, Admiraal PJJ, Janssen JA, Kroodsma JM, de Ronde WAM, Boomsma F, Sissmann J, Blankestijn PJ, Mulder PGM, Man in t Veld AJ, Schalekamp MADH. Hemodynamic and biochemical effects of the AT1 receptor antagonist irbesartan in hypertension. *Hypertension*. 1995;25(1):22-29. doi:10.1161/01.HYP.25.1.22.

514. Hansson L, Lindholm LH, Niskanen L, Lanke J, Hedner T, Niklason A, Luomanmäki K, Dahlöf B, de Faire U, Mörlin C, Karlberg BE, Wester PO, Björck J-E, for the Captopril Prevention Project CAPPP study group. Effect of angiotensin-converting-enzyme inhibition compared with conventional therapy on cardiovascular morbidity and mortality in hypertension: The Captopril Prevention Project (CAPPP) randomised trial. *Lancet*. 1999;353(9153):611-616. doi:10.1016/S0140-6736(98)05012-0.

515. The Heart Outcomes Prevention Evaluation Study Investigators. Effects of an angiotensin-converting-enzyme inhibitor, ramipril, on cardiovascular events in high-risk patients. *N Engl J Med*. 2000;342(3):145-153. doi:10.1056/NEJM200001203420301.

516. The EURopean Trial on Reduction of Cardiac Events with Perindopril in Stable Coronary Artery Disease Invesigators. Efficacy of perindopril in reduction of cardiovascular events among patients with stable coronary artery disease: randomised, double-blind, placebo-controlled, multicentre trial (the EUROPA study). *Lancet*. 2003;362.

517. Rubattu S, Cotugno M, Forte M, Stanzione R, Bianchi F, Madonna M, Marchitti S, Volpe M. Effects of dual angiotensin type 1 receptor/neprilysin inhibition vs. angiotensin type 1 receptor inhibition on target organ injury in the stroke-prone spontaneously hypertensive rat. *J Hypertens*. 2018;36. doi:10.1097/HJH.0000000000001762.

518. Nussberger J, Bohlender J. Pharmacotherapy: optimal blockade of the renin–angiotensin–aldosterone system. *Nat Methods*. 2013;10(4):183-184. doi:10.1038/nrcardio.2013.28.

519. Williams B, MacDonald TM, Morant S, Webb DJ, Sever P, McInnes G, Ford I, Cruickshank JK, Caulfield MJ, Salsbury J, Mackenzie I, Padmanabhan S, Brown MJ, for The British Hypertension Society's PATHWAY Studies Group. Spironolactone versus placebo, bisoprolol, and doxazosin to determine the optimal treatment for drug-resistant hypertension (PATHWAY-2): a randomised, double-blind, crossover trial. *Lancet*. 2015;386(10008):2059-2068. doi:10.1016/S0140-6736(15)00257-3.

520. White WB, Carr AA, Krause S, Jordan R, Roniker B, Oigman W. Assessment of the novel selective aldosterone blocker eplerenone using ambulatory and clinical blood pressure in patients with systemic hypertension. *Am J Cardiol*. 2003;92(1):38-42. doi:10.1016/S0002-9149(03)00461-2.

521. Nussberger J, Brunner DB, Waeber B, Brunner HR. Specific measurement of angiotensin metabolites and in vitro generated angiotensin II in plasma. *Hypertension*. 1986;8(6):476-482. doi:10.1161/01.HYP.8.6.476.

522. Kanehisa M, Furumichi M, Tanabe M, Sato Y, Morishima K. KEGG: new perspectives on genomes, pathways, diseases and drugs. *Nucleic Acids Res*. 2017;45(D1):D353-D361. doi:10.1093/nar/gkw1092.

523. Kanehisa M, Sato Y, Kawashima M, Furumichi M, Tanabe M. KEGG as a reference resource for gene and protein annotation. *Nucleic Acids Res*. 2016;44(D1):D457-D462. doi:10.1093/nar/gkv1070.

524. Masaki H, Kurihara T, Yamaki A, Inomata N, Nozawa Y, Mori Y, Murasawa S, Kizima K, Maruyama K, Horiuchi M, Dzau VJ, Takahashi H, Iwasaka T, Inada M, Matsubara H. Cardiac-specific overexpression of angiotensin II AT2 receptor causes attenuated response to AT1 receptor-mediated pressor and chronotropic effects. *J Clin Invest*. 1998;101(3):527-535. doi:10.1172/JCI1885.

525. Davisson RL, Oliverio MI, Coffman TM, Sigmund CD. Divergent functions of angiotensin II receptor isoforms in the brain. *J Clin Invest*. 2000;106(1):103-106. doi:10.1172/JCI10022.

526. Sakai K, Sigmund CD. Molecular evidence of tissue renin-angiotensin systems: A focus on the brain. *Curr Hypertens Rep*. 2005;7(2):135-140. doi:10.1007/s11906-005-0088-y.

527. Re RN. The intracrine hypothesis and intracellular peptide hormone action. *Bioessays*. 2003;25(4):401-409. doi:10.1002/bies.10248.

528. De Mello WC, Danser AH. Angiotensin II and the heart: on the intracrine renin-angiotensin system. *Hypertension*. 2000;35(6):1183-1188. doi:10.1161/01.HYP.35.6.1183.

529. Esler M. Sympathetic nervous system moves toward center stage in cardiovascular medicine from Thomas Willis to resistant hypertension. *Hypertension*. 2014;63(3):e25-e32. doi:10.1161/HYPERTENSIONAHA.113.02439.

530. Young CN, Davisson RL. Angiotensin-II, the brain, and hypertension: An update. *Hypertension*. 2015;66(5):920-926. doi:doi:10.1161/HYPERTENSIONAHA.115.03624.

531. Sakai K, Chapleau MW, Morimoto S, Cassell MD, Sigmund CD. Differential modulation of baroreflex control of heart rate by neuron- vs. glia-derived angiotensin II. *Physiol Genomics*. 2004;20(1):66-72. doi:10.1152/physiolgenomics.00168.2004.

532. Talaia C, Queiroz G, Pinheiro H, Moura D, Gonçalves J. Involvement of G-protein βγ subunits on the influence of inhibitory α2-autoreceptors on the angiotensin AT1-receptor modulation of noradrenaline release in the rat vas deferens. *Neurochem Int*. 2006;49(7):698-707. doi:10.1016/j.neuint.2006.07.002.

533. Fernandez SF, Huang M-H, Davidson BA, Knight PR, Izzo JL. Modulation of angiotensin II responses in sympathetic neurons by cytosolic calcium. *Hypertension*. 2003;41(1):56-63. doi:10.1161/01.HYP.0000047513.75459.7E.

534. Cox SL, Schelb V, Trendelenburg AU, Starke K. Enhancement of noradrenaline release by angiotensin II and bradykinin in mouse atria: Evidence for cross-talk between $G_{q/11}$ protein- and $G_{i/o}$ protein-coupled receptors. *Br J Pharmacol*. 2000;129(6):1095-1102. doi:10.1038/sj.bjp.0703167.

535. DiBona GF. Nervous kidney: Interaction between renal sympathetic nerves and the renin-angiotensin system in the control of renal function. *Hypertension*. 2000;36(6):1083-1088. doi:10.1161/01.HYP.36.6.1083.

536. Savoia C, Touyz RM, Volpe M, Schiffrin EL. Angiotensin type 2 receptor in resistance arteries of type 2 diabetic hypertensive patients. *Hypertension*. 2007;49(2):341-346. doi:10.1161/01.HYP.0000253968.95136.b8.

537. Ha KS, Yoo KH, Yim HE, Jang GY, Bae IS, Hong YS, Lee JW. Cellular and RAS changes in the hearts of young obese rats. *Pediatr Cardiol*. 2011;32(5):659-666. doi:10.1007/s00246-011-9952-5.

538. Krum H, Lambert E, Windebank E, Campbell DJ, Esler M. Effect of angiotensin II receptor blockade on autonomic nervous system function in patients with essential hypertension. *Am J Physiol Heart Circ Physiol*. 2006;290(4):H1706-H1712. doi:10.1152/ajpheart.00885.2005.

539. Danser AHJ. Cardiac angiotensin II: does it have a function? *Am J Physiol Heart Circ Physiol*. 2010;299(5):H1304-H1306. doi:10.1152/ajpheart.00881.2010.

540. Goldsmith SR. Interactions between the sympathetic nervous system and the RAAS in heart failure. *Curr Heart Fail Rep*. 2004;1(2):45-50. doi:10.1007/s11897-004-0024-5.

541. Barki-Harrington L, Luttrell LM, Rockman HA. Dual inhibition of beta-adrenergic and angiotensin II receptors by a single antagonist: a functional role for receptor-receptor interaction in vivo. *Circulation*. 2003;108(13):1611-1618. doi:10.1161/01.CIR.0000092166.30360.78.

542. Tilley DG. Functional relevance of biased signaling at the angiotensin ii type 1 receptor. *Endocr Metab Immune Disord Drug Targets*. 2011;11(2):99-111.

543. Grant TL, McGrath JC. Interactions between angiotensin-II and alpha-adrenoceptor agonists mediating pressor-responses in the pithed rat. *Br J Pharmacol*. 1988;95(4):1229-1240. doi:10.1111/j.1476-5381.1988.tb11760.x.

544. Liu C-H, Gong Z, Liang Z-L, Liu Z-X, Yang F, Sun Y-J, Ma M-L, Wang Y-J, Ji C-R, Wang Y-H, Wang M-J, Cui F-A, Lin A, Zheng W-S, He D-F, Qu C-X, Xiao P, Liu C-Y, Thomsen ARB, Cahill TJ, Kahsai AW, Yi F, Xiao K-H, Xue T, Zhou Z, Yu X, Sun J-P. Arrestin-biased AT1R agonism induces acute catecholamine secretion through TRPC3 coupling. *Nat Commun*. 2017;8:14335. doi:10.1038/ncomms14335.

545. Saulière A, Bellot M, Paris H, Denis C, Finana F, Hansen JT, Altié M-F, Seguelas MH, Pathak A, Hansen JL, Sénard JM, Galés C. Deciphering biased-agonism complexity reveals a new active AT1 receptor entity. *Nat Chem Biol*. 2012;8(7):622-630. doi:10.1038/nchembio.961.

546. Bellot M, Galandrin S, Boularan C, Matthies HJ, Despas F, Denis C, Javitch J, Mazères S, Sanni SJ, Pons V, Seguelas MH, Hansen JL, Pathak A, Galli A, Sénard JM, Galés C. Dual agonist occupancy of AT_1-R-α_{2C}-AR heterodimers results in atypical G_s -PKA signaling. *Nat Chem Biol*. 2015;11(4):271-279. doi:10.1038/nchembio.1766.

547. Tóth AD, Turu G, Hunyady L, Balla A. Novel mechanisms of G-protein-coupled receptors functions: AT_1angiotensin receptor acts as a signaling hub and focal point of receptor cross-talk. *Best Pract Res Clin Endocrinol Metab*. 2018;32(2):69-82. doi:10.1016/j.beem.2018.02.003.

548. Tóth AD, Gyombolai P, Szalai B, Várnai P, Turu G, Hunyady L. Angiotensin type 1A receptor regulates β-arrestin binding of the β_2-adrenergic receptor via heterodimerization. *Mol Cell Endocrinol*. 2017;442:113-124. doi:10.1016/j.mce.2016.11.027.

549. Lourdes González-Hernández M de, Godínez-Hernández D, Bobadilla-Lugo RA, López-Sánchez P. Angiotensin-II type 1 receptor (AT_1R) and alpha-1D adrenoceptor form a heterodimer during pregnancy-induced hypertension. *Auton Autacoid Pharmacol*. 2010;30(3):167-172. doi:10.1111/j.1474-8673.2009.00446.x.

550. Christensen GL, Knudsen S, Schneider M, Aplin M, Gammeltoft S, Sheikh SP, Hansen JL. AT_1 receptor Gαq protein-independent signalling transcriptionally activates only a few genes directly, but robustly potentiates gene regulation from the β2-adrenergic receptor. *Mol Cell Endocrinol*. 2011;331(1):49-56. doi:10.1016/j.mce.2010.08.004.

551. Kostenis E, Milligan G, Christopoulos A, Sanchez-Ferrer CF, Heringer-Walther S, Sexton PM, Gembardt F, Kellett E, Martini L, Vanderheyden P, Schultheiss HP,

Walther T. G-protein-coupled receptor Mas is a physiological antagonist of the angiotensin II type 1 receptor. *Circulation*. 2005;111(14):1806-1813. doi:10.1161/01.CIR.0000160867.23556.7D.

552. Epelman S, Tang WHW, Chen SY, Van Lente F, Francis GS, Sen S. Detection of soluble angiotensin-converting enzyme 2 in heart failure. *J Am Coll Cardiol*. 2008;52(9):750-754. doi:10.1016/j.jacc.2008.02.088.

553. Ortiz-Pérez JT, Riera M, Bosch X, De Caralt TM, Perea RJ, Pascual J, Soler MJ. Role of circulating angiotensin converting enzyme 2 in left ventricular remodeling following myocardial infarction: a prospective controlled study. *PLoS ONE*. 2013;8(4):e61695. doi:10.1371/journal.pone.0061695.

554. Balligand J. Regulation of cardiac β-adrenergic response by nitric oxide. *Cardiovasc Res*. 1999;43(3):607-620. doi:10.1016/s0008-6363(99)00163-7.

555. Zhang YH, Zhang MH, Sears CE, Emanuel K, Redwood C, El-Armouche A, Kranias EG, Casadei B. Reduced phospholamban phosphorylation is associated with impaired relaxation in left ventricular myocytes from neuronal NO synthase-deficient mice. *Circ Res*. 2008;102(2):242-249. doi:10.1161/CIRCRESAHA.107.164798.

556. Santiago NM, Guimaraes PS, Sirvente RA, Oliveira LAM, Irigoyen MC, Santos RAS, Campagnole-Santos MJ. Lifetime overproduction of circulating angiotensin-(1-7) attenuates deoxycorticosterone acetate-salt hypertension-induced cardiac dysfunction and remodeling. *Hypertension*. 2010;55(4):889-896. doi:10.1161/HYPERTENSIONAHA.110.149815.

557. Botelho-Santos GA, Sampaio WO, Reudelhuber TL, Bader M, Campagnole-Santos MJ, Souza dos Santos RA. Expression of an angiotensin-(1-7)-producing fusion protein in rats induced marked changes in regional vascular resistance. *Am J Physiol Heart Circ Physiol*. 2007;292(5):H2485-H2490. doi:10.1152/ajpheart.01245.2006.

558. Ferreira AJ, Santos R, Almeida AP. Angiotensin-(1-7): cardioprotective effect in myocardial ischemia/reperfusion. *Hypertension*. 2001;38(3):665-668.

559. Grobe JL, Mecca AP, Lingis M, Shenoy V, Bolton TA, Machado JM, Speth RC, Raizada MK, Katovich MJ. Prevention of angiotensin II-induced cardiac remodeling by angiotensin-(1–7). *Am J Physiol Heart Circ Physiol*. 2007;292(2):H736-H742. doi:10.1152/ajpheart.00937.2006.

560. Gomes ERM, Lara AA, Almeida PWM, Guimaraes D, Resende RR, Campagnole-Santos MJ, Bader M, Santos RAS, Guatimosim S. Angiotensin-(1-7) prevents cardiomyocyte pathological remodeling through a nitric oxide/guanosine 3“,5-”cyclic monophosphate-dependent pathway. *Hypertension*. 2009;55(1):153-160. doi:10.1161/HYPERTENSIONAHA.109.143255.

561. Castro CH, Santos RAS, Ferreira AJ, Bader M, Alenina N, Almeida AP. Effects of genetic deletion of angiotensin-(1–7) receptor Mas on cardiac function during ischemia/reperfusion in the isolated perfused mouse heart. *Life Sci*. 2006;80(3):264-268. doi:10.1016/j.lfs.2006.09.007.

562. Zhang F, Hu Y, Xu Q, Ye S. Different effects of angiotensin ii and angiotensin-(1-7) on vascular smooth muscle cell proliferation and migration. *PLoS ONE*. 2010;5(8):e12323-e12326. doi:10.1371/journal.pone.0012323.

563. McCollum LT, Gallagher PE, Ann Tallant E. Angiotensin-(1–7) abrogates mitogen-stimulated proliferation of cardiac fibroblasts. *Peptides*. 2012;34(2):380-388. doi:10.1016/j.peptides.2012.01.020.

564. Freeman EJ, Chisolm GM, Ferrario CM, Tallant EA. Angiotensin-(1-7) inhibits vascular smooth muscle cell growth. *Hypertension*. 1996;28(1):104-108. doi:10.1161/01.HYP.28.1.104.

565. Silva ACSE, Teixeira MM. ACE inhibition, ACE2 and angiotensin-(1–7) axis in kidney and cardiac inflammation and fibrosis. *Pharmacol Res*. 2016;107:154-162. doi:10.1016/j.phrs.2016.03.018.

566. Simões e Silva AC, Silveira KD, Ferreira AJ, Teixeira MM. ACE2, angiotensin-(1-7) and Mas receptor axis in inflammation and fibrosis. *Br J Pharmacol*. 2013;169(3):477-492. doi:10.1111/bph.12159.

567. Jiang T, Gao L, Shi J, Lu J, Wang Y, Zhang Y. Angiotensin-(1-7) modulates renin–angiotensin system associated with reducing oxidative stress and attenuating neuronal apoptosis in the brain of hypertensive rats. *Pharmacol Res*. 2013;67(1):84-93. doi:10.1016/j.phrs.2012.10.014.

568. Jiang T, Gao L, Guo J, Lu J, Wang Y, Zhang Y. Suppressing inflammation by inhibiting the NF-κB pathway contributes to the neuroprotective effect of angiotensin-(1-7) in rats with permanent cerebral ischaemia. *Br J Pharmacol*. 2012;167(7):1520-1532. doi:10.1111/j.1476-5381.2012.02105.x.

569. Lopez Verrilli MA, Pirola CJ, Pascual MM, Dominici FP, Turyn D, Gironacci MM. Angiotensin-(1-7) through AT_2 receptors mediates tyrosine hydroxylase degradation via the ubiquitin-proteasome pathway. *J Neurochem*. 2009;109(2):326-335. doi:10.1111/j.1471-4159.2009.05912.x.

570. Gironacci MM, Adler-Graschinsky E, Pena C, Enero MA. Effects of angiotensin II and angiotensin-(1-7) on the release of [3H]norepinephrine from rat atria. *Hypertension*. 1994;24(4):457-460. doi:10.1161/01.HYP.24.4.457.

571. Gironacci MM, Lorenzo PS, Adler-Graschinsky E. Possible participation of nitric oxide in the increase of norepinephrine release caused by angiotensin peptides in rat atria. *Hypertension*. 1997;29(6):1344-1350. doi:10.1161/01.HYP.29.6.1344.

572. Paton JFR, Kasparov S, Paterson DJ. Nitric oxide and autonomic control of heart rate: a question of specificity. *Trends Neurosci*. 2002;25(12):626-631.

573. Schwarz P, Diem R, Dun NJ, Forstermann U. Endogenous and exogenous nitric oxide inhibits norepinephrine release from rat heart sympathetic nerves. *Circ Res*. 1995;77(4):841-848. doi:10.1161/01.RES.77.4.841.

574. Morimoto S, Cassell MD, Sigmund CD. Glia- and neuron-specific expression of the renin-angiotensin system in brain alters blood pressure, water intake, and salt preference. *J Biol Chem*. 2002;277(36):33235-33241. doi:10.1074/jbc.M204309200.

575. Vaseghi M, Zhou W, Shi J, Ajijola OA, Hadaya J, Shivkumar K, Mahajan A. Sympathetic innervation of the anterior left ventricular wall by the right and left stellate ganglia. *Heart Rhythm*. 2012;9(8):1303-1309. doi:10.1016/j.hrthm.2012.03.052.

576. Rondina MT, Weyrich AS. Targeting phosphodiesterases in anti-platelet therapy. *Handb Exp Pharmacol*. 2012;(210):225-238. doi:10.1007/978-3-642-29423-5_9.

577. Kehler J, Nielsen J. PDE10A inhibitors: novel therapeutic drugs for schizophrenia. *Curr Pharm Des*. 2011;17(2):137-150.

578. Nikolaev V, Zaccolo M. *Microdomains in the Cardiovascular System*. Springer; 2017. doi:10.1007/978-3-319-54579-0.

579. Hendel MD, Collister JP. Contribution of the subfornical organ to angiotensin II-induced hypertension. *Am J Physiol Heart Circ Physiol*. 2005;288(2):H680-H685. doi:10.1152/ajpheart.00823.2004.

580. Jancovski N, Bassi JK, Carter DA, Choong Y-T, Connelly A, Nguyen T-P, Chen D, Lukoshkova EV, Menuet C, Head GA, Allen AM. Stimulation of angiotensin type 1A receptors on catecholaminergic cells contributes to angiotensin-dependent hypertension. *Hypertension*. 2013;62(5):866-871. doi:10.1161/HYPERTENSIONAHA.113.01474.

Appendix

This appendix includes the script used for the DESeq2 analysis and gene lists for GOgroups Cellular Component (CC), Biological Processes (BP), Molecular Function (MF) and KEGG groups.

8.1 Differential Expression Analysis using DESeq2

The following script was applied to analyse the differentially expressed transcripts using the DESeq2 library in R[327] .

```
salmon_countData<as.matrix(read.csv/path_to/sal-
mon_gene_count_matrix.csv",header=TRUE))
rownames(salmon_countData) <- salmon_countData[ , 1]
salmon_countData <- salmon_countData[,-1]

salmon_colData <- as.matrix(read.csv/path_to/salmon_colData.csv",head-
er=TRUE))
rownames(salmon_colData) <- salmon_colData[ , 1]
salmon_colData <- salmon_colData[,-1]

all(rownames(salmon_colData) %in% colnames(salmon_countData))
all(rownames(salmon_colData) == colnames(salmon_countData))

storage.mode(salmon_countData) = "integer"
salmon_dds <- DESeqDataSetFromMatrix(countData = salmon_countData,
colData = salmon_colData, design = ~ condition)

salmon_dds$condition <- relevel(salmon_dds$condition, ref="Wistar")
salmon_dds <- DESeq(salmon_dds)
salmon_res <- results(salmon_dds)
write.csv(as.data.frame(salmon_res), file="salmon_results.csv")
```

8.2 Gene lists for Cellular Component Gene Ontology Group

Table 8.1. Cellular Component Gene Ontology Gene List

Cellular Component GO Description	GO Group Gene List
Neuron Part	*Rp1, Pdgfb, Grik1, Grik2, Wfs1, Snca, Calb1, Adora1, Atcay, Grin2b, Rapgef2, Rab27a, Kif5b, Kif5a, Ptprn2, Cst3, Qdpr, Ptpro, Ascl1, Rab15, Vamp3, Smarca2, Cobl, Bbs4, Ccl2, Ric3, Adcyap1, Bloc1s6, Pde6b, Pfn2, Pabpc1, Hcn1, Dixdc1, Gabra2, Cpne5, Ptpn5, Ak1, Omp, Lin7c, P2rx4, Rnf6, P2rx6, Cnih2, Lamp5, P2rx3, Chrnb4, Rgs8, Ahcyl2, Cacna1c, Oprm1, Kcnh1, Spg7, Kcnab2, Pde11a, Psph, Cxadr, Syngr1, Ybx1, Kcnip4, Pcp4, Cxcr4, Ceacam16, Adcy10, Ddc, Stx3, Tpx2, Sez6l, Gal, Adrb2, Zfyve27, Plxdc1, Grm7, Khsrp, Gnb3, Siah2, Tph1, Vip, Spock1, Palmd, Calca, Synpr, Fam107a, Nr1d1, Slc4a8, Avil, Camk2d, Apba2, Slc4a7, Htr3a, Htr3b, Pcsk5, Pik3r1, Dclk1, Glrb, Ahi1, Gria3, Tmprss5, Tmprss3, Sirt2, Rgs14, Cdh13, Rgs20, Gria2, Pde2a, Gria1, Slc18a3, Slc18a1, Rnf40*
Neuron Projection	*Oprm1, Kcnh1, Spg7, Pdgfb, Kcnab2, Grik1, Wfs1, Grik2, Snca, Psph, Syngr1, Cxadr, Calb1, Adora1, Ybx1, Kcnip4, Atcay, Grin2b, Pcp4, Cxcr4, Rapgef2, Adcy10, Rab27a, Ddc, Stx3, Kif5b, Kif5a, Ptprn2, Tpx2, Qdpr, Cst3, Ptpro, Adrb2, Zfyve27, Grm7, Plxdc1, Khsrp, Vamp3, Siah2, Gnb3, Tph1, Cobl, Ccl2, Spock1, Palmd, Ric3, Adcyap1, Calca, Bloc1s6, Pfn2, Synpr, Fam107a, Nr1d1, Camk2d, Slc4a8, Avil, Pabpc1, Htr3a, Htr3b, Pcsk5, Pik3r1, Hcn1, Dixdc1, Gabra2, Glrb, Cpne5, Ptpn5, Ak1, Omp, Lin7c, Gria3, Rgs14, Sirt2, Cdh13, P2rx4, Rnf6, P2rx6, Cnih2, Gria2, Pde2a, Gria1, Lamp5, P2rx3, Chrnb4, Slc18a3, Rgs8, Ahcyl2, Slc18a1, Cacna1c, Rnf40*
Axon	*Kcnh1, Spg7, Kcnab2, Grik1, Grik2, Snca, Syngr1, Calb1, Adora1, Atcay, Grin2b, Pcp4, Adcy10, Ddc, Stx3, Kif5b, Kif5a, Ptprn2, Tpx2, Cst3, Adrb2, Zfyve27, Grm7, Cobl, Ccl2, Spock1, Adcyap1, Bloc1s6, Calca, Pfn2, Camk2d, Avil, Htr3a, Htr3b, Hcn1, Dixdc1, Gabra2, Ptpn5, Omp, Gria3, Sirt2, P2rx4, Rnf6, Gria2, Pde2a, Gria1, P2rx3, Slc18a3, Slc18a1, Rnf40*
Axon Part	*Kcnh1, Cobl, Spg7, Ccl2, Kcnab2, Grik1, Grik2, Snca, Spock1, Syngr1, Adora1, Calb1, Adcyap1, Bloc1s6, Calca, Pfn2, Grin2b, Camk2d, Hcn1, Dixdc1, Stx3, Kif5b, Ptprn2, Tpx2, Gria3, Sirt2, P2rx4, Gria2, Gria1, Grm7, P2rx3, Slc18a3, Slc18a1, Rnf40*
Terminal Bouton	*Stx3, Grik1, Grik2, Ptprn2, Snca, Gria3, Syngr1, Adora1, Calb1, Adcyap1, Calca, P2rx4, Pfn2, Grin2b, Gria2, Grm7, P2rx3, Slc18a3, Slc18a1*
Axon Terminus	*Hcn1, Dixdc1, Stx3, Ccl2, Grik1, Kcnab2, Grik2, Ptprn2, Snca, Gria3, Syngr1, Calb1, Adora1, Adcyap1, Calca, P2rx4, Pfn2 Grin2b, Gria2, Grm7, P2rx3, Slc18a3, Slc18a1, Rnf40*
Neuronal Cell Body	*Vip, Kcnh1, Oprm1, Cobl, Ccl2, Pdgfb, Grik1, Grik2, Pde11a, Ric3, Calb1, Adora1, Kcnip4, Calca, Nr1d1, Camk2d, Slc4a8, Rapgef2, Adcy10, Htr3a, Htr3b, Pcsk5, Hcn1, Dixdc1, Ddc, Gabra2, Glrb, Cpne5, Kif5a, Ptpn5, Omp, Tpx2, Cst3, Gria3, Sez6l, Tmprss5, Gal, Tmprss3, Sirt2, Ascl1, P2rx4, Adrb2, P2rx6, Gria2, Gria1, P2rx3, Plxdc1, Grm7, Khsrp, Rgs8, Siah2, Cacna1c*
Somatodendritic Compartment	*Oprm1, Kcnh1, Pdgfb, Grik1, Wfs1, Grik2, Pde11a, Calb1, Adora1, Ybx1, Kcnip4, Atcay, Grin2b, Rapgef2, Adcy10, Rab27a, Ddc, Stx3, Kif5a, Cst3, Tpx2, Sez6l, Gal, Ptpro, Ascl1, Adrb2, Zfyve27, Grm7, Plxdc1, Khsrp, Siah2, Gnb3, Vip, Cobl, Ccl2, Palmd, Ric3, Calca, Nr1d1, Camk2d, Slc4a8, Pabpc1, Htr3a, Htr3b, Pcsk5, Hcn1, Dixdc1, Gabra2, Glrb, Cpne5, Ptpn5, Omp, Gria3, Tmprss5, Sirt2, Tmprss3, Rgs14, P2rx4, P2rx6, Cnih2, Gria2, Pde2a, Gria1, Lamp5, P2rx3, Rgs8, Cacna1c*
Perinuclear Region of Cytoplasm	*Kcnh1, Cobl, Osbp, S100a6, Tspan1, Fgfr3, Ccl2, Gsdma, Usp2, Galnt6, Enpp3, Nell1, Snca, Tpd52, Ybx1, Bag5, Agtr2, Fbxw8, Ptges, Hmox1, Camk2d, Mt1, Mmd2, Prkacb, Rapgef2, Adcy10, Traf6, Mx2, Pik3r1, Spp1, Rab8b, Hmgcll1, Kif5b, Kif5a, Ak1, Cst3, Chodl, S100a13, Sirt2, Anxa2, Ppm1f, Cdh13, P2rx4, Loc317165, Chga, Pde2a, Ptgds, Cd34, Fgfr1op, Mt2a, Rab15, Sele*
Neuron Projection Terminus	*Hcn1, Dixdc1, Stx3, Ccl2, Grik1, Kcnab2, Grik2, Ptprn2, Snca, Gria3, Syngr1, Calb1, Adora1, Adcyap1, Calca, P2rx4, Pfn2, Grin2b, Gria2, Grm7, P2rx3, Slc18a3, Slc18a1, Rnf40*
Cell Body	*Oprm1, Kcnh1, Pdgfb, Grik1, Grik2, Pde11a, Cxadr, Adora1, Calb1, Kcnip4, Adcy10, Rapgef2, Ddc, Kif5a, Cst3, Tpx2, Sez6l, Gal, Ascl1, Adrb2, Grm7, Plxdc1, Khsrp, Siah2, Gnb3, Vip, Cobl, Ccl2, Ric3, Calca, Nr1d1, Slc4a8, Camk2d, Htr3a, Htr3b, Pcsk5, Hcn1, Dixdc1, Glrb, Gabra2, Cpne5, Ptpn5, Omp, Gria3, Tmprss5, Sirt2, Tmprss3, P2rx4, P2rx6, Gria2, Gria1, P2rx3, Rgs8, Cacna1c*
Synapse	*Oprm1, Kcnh1, Grik1, Kcnab2, Grik2, Snca, Postn, Cxadr, Syngr1, Calb1, Adora1, Atcay, Prrt2, Grin2b, Rapgef2, Ddc, Stx3, Ptprn2, Ptpro, Adrb2, Grm7, Rab15, Vamp3, Cav3, Ccl2, Spock1, Palmd, Adcyap1, Calca, Pfn2, Synpr, Nr1d1, Lrrtm3, Camk2d, Apba2, Slc4a7 Htr3a, Htr3b, Dnaja3, Dclk1, Hcn1, Gabra2, Glrb, Gabra1, Lin7c, Gria3, Rgs14, P2rx4, Rgs20, P2rx6, Cnih2, Pde2a, Gria2, Gria1, P2rx3, Prkar1a, Chrnb4, Slc18a3, Slc18a1, Cacna1c*
Membrane Bounded Vesicle	*S100a6, Tspan1, S100a8, Efna1, Nit2, Ltbp4, Snca, S100a9, Crabp2, Rab1b, Pgam2, Selenbp1, Calb1, Cd48, Spx, Grin2b, Pacsin3, Slc25a25, St3gal6, Pik3c3, Aif1l, H2afy, Dhx36, Prkacb, Rapgef2, Gng7, Rab27a, Pld3, Dars, Stk25, Kif5b, Gatm, Nudt3, Ptprn2, Qdpr, Cst3, Pdxp, Fbp1, Lypla1, Spire2, Mark3, Mettl7a, Ptpro, Scel, Arpc1b, Rps18, Napepld, Rps14, Rab15, Vamp3, Znhit6, Vps26a, Fxyd3 Gnai3, Fgfr3, Ccl2, Actr3b, Enpp3, Mst1, Snx2, Atp6v1b2, Bloc1s6, Gmppb, Slc11a1, P3h1, Pfn2, Loc501110, Enkur, Osbpl1a, Stx17, Ubash3a, Pabpc1, Slc30a8, Spp1, Ptgr1, Gabra2, Rab8b, Cpne4, Lgals3, Yipf6, Cpne5, Upb1, Ak1, Lin7c, Ak4, Itga4, Upk3a, Acpp, S100a13, Urm1, P2rx4, Col14a1, Fam151a, Lamp5, Fabp3, Slc13a3, Rgd1566265, Gm2a, Myo7b, Sat2, Vps37c, Syngr1, Cxadr, Rps2, Lrrc15, Glb1, Gpx2, Tor3a, Smpdl3b, Nccrp1, Cxcr4, Sema3c, Fam129b, Dpp4, Ahnak, Ddc, Ctsz, Stx3, Clmp, Pfkl, Rph3al, Padi2, Decr1, Pigr, Lmbrd1, Gal, Atp6v1c1, Chga, Sdc1, Evpl, Ptgds, Clic3, Serpinb8, Cybrd1, Gaa, Vopp1, Gnb3, Serpinb3, Carhsp1, Tyrp1 Mal2, Lancl1, Sec14l3, Aldh1a1, Sft2d2, Igsf11, Cbr1, Synpr, C1qtnf3, Tor1b, Galnt16, Apba2, Gp1ba, Pafah1b2, Pga5, Pcsk5, Myof, Cd7, Shmt2, Hist1h2bh, Npr3, Gdpd3, Anxa2, Cdh13, Ywhag, Rgs20, Gria2, Knl1, Gria1, Ptp4a1, Mapk14, Slc18a3, Spata31a5, Slc18a1, Gca, Dmbt1*
Presynapse	*Kcnh1, Ddc, Gabra2, Stx3, Grik1, Grik2, Ptprn2, Snca, Lin7c, Gria3, Syngr1, Adora1, Calb1, Adcyap1, Calca, P2rx4, Pfn2, Synpr, Grin2b, Pde2a, Gria2, Gria1, P2rx3, Grm7, Rab15, Apba2, Slc18a3, Slc18a1, Cacna1c*
Cell Junction	*Oprm1, Osbp, Zc3hav1, Kcnab2, Grik1, Grik2, Snca, Fermt2, Iqgap3, Lmo7, Aqp4, Syngr1, Rps2, Cxadr, Atcay, Bzw1, Grin2b, Prrt2, Hamp, Cxcr4, Aif1l, Fam129b, Rapgef2, Ahnak, Dpp4, Clmp, Stx3, Kif5b, Magi1, Ptprn2, Myh2, Pdxp, Arhgap24, Arpc1b, Sdc1, Rps18 Dcaf6, Evpl, Rps14, Cd99l2, Vamp3, Cav3, Kazn, Hacd3, Itga11, Snx2, Synpr, Marveld2, Lrrtm3, Rpl9, Camk2d, Pabpc1, Htr3a, Plk3r1, Dixdc1, Gabra2, Glrb, Trpc4, Flt1, Gabra1, Ahi1, Lin7c, Gria3, Gjb5, Itga4, Arfip1, Rgs14, Sirt2, Anxa2, Cdh13, P2rx4, Ywhag, P2rx6, Cnih2, Gria2, Gria1, Chrnb4, Perp*

8.3 Gene lists for Biological Processes Gene Ontology Group

Table 8.2a. Biological Processes Gene Ontology Gene List

Biological Processes GO Description	GO Group Gene List
Lipid Metabolic Process	*Pnlip, Pdgfb, Gm2a, Sgpp2, Ormdl1, Adgrf5, Snca, Crabp2, Prkag2, Calb1, Adora1, Auh, St6galnac3, Agpat5, Smpdl3b Ptges, Elovl4, Hmox1, St3gal6, Pik3c3, Prkacb, Cyr61, Pld3, Cyp1a1, Pdpn, Pgap1, Ptprn2, Lypla1, Cbr4, Decr1, Lpcat2, Lpin2, Gal, St6galnac2, Pank2, Adrb2, Napepld, Ptgds, Hrasls, Pla2g7, Hsd11b2, Crot, Cav3, Etfbkmt, Tyrp1, Fgfr3, Hacd3, Hacd1, Aldh1a1, Cbr1, Mtmr1, Nr1d1, Abhd16a, Pafah1b2, Pik3r3, Acaa1a, Acaa1b, Pik3r1, Nr1h3, Ptgr1, Flt1, Cidea, Gdpd3, Daglb, Sirt2, Tmem55b, Rdh12, Cyp4f5, Proca1, Mapk14, Sdr42e1, Fabp3, Acad10, Plcxd2, Retsat*
Response to Organic Substance	*Pdgfb, S100a8, Zc3hav1, Wfs1, Ltbp4, Snca, S100a9, Iqgap3, Aqp4, Postn, Rorb, Calb1, Agtr2, Grin2b, Gata3, St3gal6, Pik3c3, Dhx36, Prkacb, Rapgef2, Mx2, Cyp1a1, Kif5b, Gatm, Snrpn, Ptprn2, Cst3, Ube2j1, Pdxp, Fbp1, Qdpr, Med13, Tox2, Ctdspl2, Vegfb, Ascl1, Arpc1b, Trim32, Hsd11b2, Crot, Cav3, Bbs4, Gclc, Fgfr3, Ccl2, Gcnt2, Grem2, Ccl7, Adcyap Slc11a1, Hcrtr1, Loc501110, Gpr21, Dusp15, Rpl9, Cda, Slc30a8, Traf6, Dnaja3, Spp1, Traf3, Nr1h3, Hcn1, Klf6, Crip1, Card9, Gabra1, Selenot, Ak1, Ptpn5, Crebbp, Mstn, Cidea, Itga4, P2rx4, Rnf6, Ifi27, Gpr35, P2rx6, P2rx3, Chrnb4, Fabp3, Rgs8, Pnlip, Ier2, Oprm1, Fermt2, Psph, Lrrc15, Rps2, Ybx1, Casp6, Cxcr4, Hamp, Ptges, Hmox1, Trim6, Il1rap, Gucy1a3, Cyr61, Ddc, Ptger2, Nol3, Pfkl, Mmp19, Lef1, Padi2, Lmbrd1, Gal, Slit3, Adrb2, Sdc1, Rgd1309362, Zfyve27, Ptgds, Ncoa4, Khsrp, Pmepa1, Cer1, Ffar3, Gdap1, Vom1r90, Rt1-Bb, Calca, Ccl24, Aldh1a1, Cbr1, Nr1d1, Lrrtm3, Gp1ba, Pik3r3, Rnf121, Htr3a, Acaa1a, Htr3b, Myof, Bdh1, Pcsk5, Pik3r1, Shmt2, Glrb, Ltk, Gsta4, Flt1, Stat3, Sirt2, Anxa2, P2ry12, Cdh13, Ywhag, Rgs20, Pde2a, Gria1, Mapk14, Mt2a, Id3, Sele, Rnf40, Dmbt1, Cbs*
Regulation of Blood Pressure	*Bbs4, Edn3, Pdgfb, Ffar3, Postn, Bdkrb2, Npr3, Ptpro, Adora1, Calca, P2rx4, Agtr2, Adrb2, Spx, Id2, Cd34, Hmox1, Hsd11b2, Gucy1a3, Cacna1c, Pcsk5, Pik3r1*
Circulatory System Process	*Vip, Cav3, Bbs4, Edn3, Gclc, Gnai3, Pdgfb, Ffar3, Myl1, Postn, Bdkrb2, Cxadr, Adora1, Adcyap1, Calca, Agtr2, Spx, Cxcr4 Hmox1, Camk2d, Gucy1a3, Kcne5, Pcsk5, Pik3r1, Scn2b, Npr3, Ptpro, Tnni1, Vegfb, P2rx4, Adrb2, Chga, Id2, Pde2a, Cd34, Gaa, Hsd11b2, Cacna1c, Cbs*
Wound Healing	*Oprm1, Cav3, F2rl2, Ccl2, Pdgfb, S100a8, S100a9, Postn, Elk3, Bloc1s6, Igsf10, Slc11a1, Cxcr4, Hmox1, Gp1ba, Myof, Large1, Cyr61, Rab27a, Klf6, Gatm, Pdpn, Myh2, Mstn, Grhl3, Mustn1, Arhgap24, Anxa2, P2ry12, Vegfb, Adrb2, Sdc1, Cd34, Mapk14, Tm4sf4, Dmbt1*
Negative Regulation of Transport	*Oprm1, Cav3, Vip, Edn3, Gnai3, Fam3d, Snca, Adora1, Adcyap1, Calca, Agtr2, Spx, C1qtnf3, Pacsin3, Hamp, Hmox1, Camk2d, Dyrk2, Kcne5, Nr1h3, Lrsam1, C5ar2, Nol3, Lgals3, Pfkl, Ube2j1, Ahi1, Cidea, Lypla1, Lmbrd1, Anxa2, Ppif, P2ry12, Chga, Cnih2, Pde2a, Cd34, Grm7, Vamp3, Slc18a1*
Blood Circulation	*Vip, Cav3, Bbs4, Edn3, Gclc, Gnai3, Pdgfb, Ffar3, Myl1, Postn, Bdkrb2, Cxadr, Adora1, Adcyap1, Calca, Agtr2, Spx, Cxcr4 Hmox1, Camk2d, Gucy1a3, Kcne5, Pcsk5, Pik3r1, Scn2b, Npr3, Ptpro, Tnni1, Vegfb, P2rx4, Adrb2, Chga, Id2, Pde2a, Cd34, Gaa, Hsd11b2, Cacna1c, Cbs*
Heart Contraction	*Cav3, Edn3, Scn2b, Ffar3, Myl1, Cxadr, Adora1, Tnni1, Vegfb, Calca, P2rx4, Chga, Agtr2, Adrb2, Spx, Cxcr4, Gaa, Camk2d, Cacna1c, Kcne5, Pik3r1*
Cell-cell Signalling	*Oprm1, Edn3, Pdgfb, Fam3d, Grik1, Grik2, Ltbp4, Snca, Fermt2, Syngr1, Calb1, Adora1, Agtr2, Csnk2a1, Grin2b, Gata3, Rapgef2, Shc3, Cyr61, Stx3, Kif5b, Csnk1g1, Pfkl, Ptprn2, Rph3al, Lef1, Grhl3, Gal, Ptpro, Sdc1, Adrb2, Cd34, Grm7, Rab15, Vamp3, Serpinb3, Siah2, Rasd2, Vip, Cer1, Ccl2, Fgfr3, Ffar3, Ric3, Adcyap1, Hcrtr1, Pfn2, Gpr21, C1qtnf3, Nr1d1, Apba2, Kcne5, Slc30a8, Htr3a, Htr3b, Dixdc1, Glrb, Gabra1, Rab8b, Selenot, Ptpn5, Omp, Lin7c, Tnfsf9, Cela1, Rgs14, P2rx4, Ywhag, Rgs20, Cnih2, Gria2, Gria1, Mapk14, Slc6a5, P2rx3, Chrnb4, Slc18a3, Cacna1c*
Cellular Response to Chemical Stimulus	*Edn3, Pdgfb, Zc3hav1, S100a8, Wfs1, Ltbp4, Snca, S100a9, Iqgap3, Aqp4, Postn, Rorb, Calb1, Agtr2, Grin2b, Gata3, St3gal6, Rapgef2, C5ar2, Kif5b, Stk25, Cyp1a1, Ptprn2, Fbp1, Pdxp, Cst3, Qdpr, Med13, Ptpro, Ctdspl2, Vegfb, Cd34, Trim32, Cav3, Bbs4, Gcnt2, Gclc, Ccl2, Fgfr3, Mst1, Bdkrb2, Grem2, Ccl7, Adcyap1, Hcrtr1, Gpr21, Dusp15, Rpl9, Traf6, Dnaja3, Spp1, Traf3, Nr1h3, Hcn1, Klf6, Crip1, Gabra1, Selenot, Lgals3, Crebbp, Cidea, Mstn, Itga4, Ppif, P2rx4, Gpr35, Rnf6, Rgs8, Oprm1, Kcnh1, Hp1bp3, Fermt2, Lrrc15, Rps2, Cxadr, Ybx1, Spag16, Wbp2, Bag5, Cxcr4, Pcp4, Hamp, Hmox1, Trim6, Il1rap, Mt1, Adcy10, Cyr61, Ddc, Ptger2, Nol3, Lef1, Padi2, Lmbrd1, Slit3, Ppm1f, Adrb2, Chga, Rgd1309362, Zfyve27, Khsrp, Pla2g7, Pmepa1, Cer1, Ffar3, Abtb2, Rt1-Bb, Calca, Ccl24, Nr1d1, Lrrtm3, Gp1ba, Pik3r3, Rnf121, Htr3a, Htr3b, Myof, Pcsk5, Pik3r1, Ltk, Gsta4, Flt1, Stat3, Sirt2, P2ry12, Cdh13, Ywhag, Rgs20, Pde2a, Id2, Gria1, Mapk14, Mt2a, Slc18a1, Id3, Cbs*
Cellular Lipid Metabolic Process	*Pdgfb, Gm2a, Ormdl1, Sgpp2, Crabp2, Snca, Adgrf5, Auh, St6galnac3, Agpat5, Smpdl3b, Ptges, Elovl4, Hmox1, St3gal6 Pik3c3, Prkacb, Cyr61, Cyp1a1, Pdpn, Pgap1, Lypla1, Cbr4, Decr1, Lpcat2, Lpin2, St6galnac2, Adrb2, Napepld, Ptgds, Hrasls, Pla2g7, Crot, Cav3, Etfbkmt, Tyrp1, Fgfr3, Hacd3, Hacd1, Aldh1a1, Mtmr1, Abhd16a, Acaa1a, Pik3r3, Acaa1b, Pik3r1, Nr1h3, Ptgr1, Flt1, Sirt2, Tmem55b, Daglb, Rdh12, Cyp4f5, Proca1, Mapk14, Fabp3, Acad10, Retsat*
Response to Wounding	*F2rl2, Oprm1, Cav3, Fgfr3, Ccl2, Pdgfb, S100a8, S100a9, Postn, Elk3, Igsf10, Bloc1s6, Slc11a1, Cxcr4, Hmox1, Gp1ba, Myof, Large1, Spp1, Cyr61, Rab27a, Klf6, Nol3, Cyp1a1, Gatm, Pdpn, Myh2, Cst3, Mstn, Grhl3, Mustn1, Arhgap24, Anxa2, P2ry12, Vegfb, Adrb2, Sdc1, Cd34, Mapk14, Id3, Omg, Tm4sf4, Dmbt1*
Defense Response	*Oprm1, S100a8, Zc3hav1, Grik2, Snca, S100a9, Aqp4, Cxadr, Adora1, Tapbp, Gpx2, Casp6, Agtr2, Grin2b, Hist1h2bk, Smpdl3b, Ptges, Hamp, Trim6, Gata3, Hmox1, Defb11, Mx2, Dpp4, Lag3, Gng7, Rab27a, C5ar2, Ptger2, Pdpn, Cst3, Gal, Rt1-A1, Oas1k, Sdc1, Chga, Adrb2, Rgd1309362, Oas1i, Grm7, Trim32, Susd4, Vamp3, Oas1f, Oas1d, Vip, Ccl2, Ffar3, Bdkrb2, Il34, Ccl7, Rt1-Bb, Adcyap1, Calca, Ccl24, Slc11a1, C1qtnf3, Nr1d1, Slc30a8, Dnaja3, Nr1h3, Spp1, Traf3, Hcn1 Lrsam1, Shmt2, Card9, Lgals3, Hist1h2bh, Mstn, Ifi3, Polr3c, Cela1, Sirt2, Stat3, Pde2a, Cyp4f5, Mapk14, Slfn13, Sele*
Trans-synaptic Signalling	*Oprm1, Edn3, Ccl2, Grik1, Grik2, Snca, Ric3, Syngr1, Adora1, Calb1, Adcyap1, Hcrtr1, Pfn2, Gpr21, Grin2b, Apba2, Shc3 Htr3a, Rapgef2, Htr3b, Glrb, Gabra1, Stx3, Kif5b, Ptprn2, Ptpn5, Omp, Rph3al, Lin7c, Rgs14, P2rx4, Adrb2, Ywhag, Cnih2 Gria2, Gria1, P2rx3, Grm7, Slc6a5, Chrnb4, Rab15, Slc18a3, Cacna1c, Rasd2*

Table 8.2b. Biological Processes Gene Ontology Gene List

Biological Processes GO Description	GO Group Gene List
Anterograde Trans-synaptic Signalling	*Oprm1, Edn3, Ccl2, Grik1, Grik2, Snca, Ric3, Syngr1, Adora1, Calb1, Adcyap1, Hcrtr1, Pfn2, Gpr21, Grin2b, Apba2, Shc3, Htr3a, Rapgef2, Htr3b, Glrb, Gabra1, Stx3, Kif5b, Ptprn2, Ptpn5, Omp, Rph3al, Lin7c, Rgs14, P2rx4, Adrb2, Ywhag, Cnih2, Gria2, Gria1, P2rx3, Grm7, Slc6a5, Chrnb4, Rab15, Slc18a3, Cacna1c, Rasd2*
Chemical Synaptic Transmission	*Oprm1, Edn3, Ccl2, Grik1, Grik2, Snca, Ric3, Syngr1, Adora1, Calb1, Adcyap1, Hcrtr1, Pfn2, Gpr21, Grin2b, Apba2, Shc3 Htr3a, Rapgef2, Htr3b, Glrb, Gabra1, Stx3, Kif5b, Ptprn2, Ptpn5, Omp, Rph3al, Lin7c, Rgs14, P2rx4, Adrb2, Ywhag, Cnih2 Gria2, Gria1, P2rx3, Grm7, Slc6a5, Chrnb4, Rab15, Slc18a3, Cacna1c, Rasd2*
Synaptic Signalling	*Oprm1, Edn3, Ccl2, Grik1, Grik2, Snca, Ric3, Syngr1, Adora1, Calb1, Adcyap1, Hcrtr1, Pfn2, Gpr21, Grin2b, Apba2, Shc3 Htr3a, Rapgef2, Htr3b, Glrb, Gabra1, Stx3, Kif5b, Ptprn2, Ptpn5, Omp, Rph3al, Lin7c, Rgs14, P2rx4, Adrb2, Ywhag, Cnih2 Gria2, Gria1, P2rx3, Grm7, Slc6a5, Chrnb4, Rab15, Slc18a3, Cacna1c, Rasd2*
Heart Process	*Cav3, Edn3, Scn2b, Ffar3, Myl1, Cxadr, Adora1, Tnni1, Vegfb, Calca, P2rx4, Chga, Agtr2, Adrb2, Spx, Cxcr4, Gaa, Camk2d, Cacna1c, Kcne5, Pik3r1*
Small Molecule Catabolic Process	*Etfbkmt, Aadat, Cyp1a1, Nudt3, Qdpr, Fbp1, Cbr3, Decr1, Lpin2, Idnk, Glb1, Auh, Amdhd1, Cbr1, Aldh1b1, Tdh, Fabp3, Asrgl1, Aldh4a1, Ahcyl2, Acaa1a, Acaa1b, Acad10, Crot, Cbs*
Catabolic Process	*Pnlip, Gm2a, Wfs1, Pgam2, Pde11a, Adora1, Auh, Glb1, Smpdl3b, Hmox1, Prkacb, Aadat, Pld3, Pfkl, Cyp1a1, Nudt3, Ube2j1, Qdpr, Cst3, Fbp1, Cbr3, Decr1, Lpin2, Adrb2, Napepld, Aldh1b1, Pla2g7, Gaa, Crot, Etfbkmt, Enpp3, Cbr1, Abhd16a, Aldh4a1, Asrgl1, Cda, Pafah1b2, Acaa1a, Rnf121, Acaa1b, Cidea, Sirt2, Idnk, Stat3, Daglb, Amdhd1, Pde2a, Tdh, Fabp3, Ahcyl2, Acad10, Cbs*
Response to Metal Ion	*Kcnh1, Gclc, S100a8, S100a9, Snca, Pgam2, Spag16, Casp6, Grin2b, Ptges, Hamp, Hmox1, Mt1, Slc30a8, Bdh1, Pik3r1, Hcn1, Crip1, Gsta4, Cyp1a1, Gatm, Qdpr, Fbp1, Lef1, Gria3, S100a13, Ppif, Ascl1, Sdc1, Gria2, Id2, Gria1, Mt2a, Cybrd1, Slc18a1*
Regulation of Ion Transport	*Kcnh1, Vip, Cav3, Oprm1, Edn3, Fxyd3, Ccl2, Pdgfb, Kcnab2, Grik1, Wfs1, Snca, Kcnj3, Adora1, Kcnip4, Fxyd7, Adcyap1 Calca, Agtr2, Grin2b, Pacsin3, Cxcr4, Hamp, Camk2d, Htr3a, Kcne5, Htr3b, Ahnak, Hcn1, Trpc4, Nol3, Scn2b, Lgals3, Kif5b, Gal, Ppif, P2ry12, P2rx4, Adrb2, Cnih2, Clic3, Grm7, Cacna1c*
Regulation of System Process	*Vip, Cav3, Oprm1, Edn3, Gnai3, Pdgfb, Ffar3, Cxadr, Adora1, Adcyap1, Calca, Agtr2, C1qtnf3, Spx, Hamp, Camk2d, Gucy1a3, Kcne5, Pik3r1, Nr1h3, Flt1, Rab8b, Nol3, Scn2b, Mstn, Gal, Ptpro, Tnni1, Acpp, P2rx4, Adrb2, Chga, Gpr35, Col14a1, P2rx3, Chrnb4, Gaa, Cacna1c*
Ion transport	*Oprm1, Kcnh1, Edn3, S100a6, Pdgfb, Grik1, Kcnab2, Wfs1, Grik2, Snca, Aqp4, Mfsd2a, Adora1, Kcnip4, Agtr2, Slc25a25, Pacsin3, Grin2b, Hamp, Cxcr4, Lrrc55, Piezo1, Ahnak, Nol3, Scn2b, Kif5b, Pdpn, Gal, Atp6v1c1, Adrb2, Clic3, Grm7, Slc41a3, Crot, Vip, Cav3, Fxyd3, Ccl2, Mfsd3, Enpp3, Bdkrb2, Atp6v1b2, Kcnj3, Fxyd7, Adcyap1, Calca, Slc11a1, Camk2d, Slc4a8, Slc4a7, Slc30a8, Htr3a, Kcne5, Htr3b, Slc39a1, Hcn1, Gabra2, Glrb, Trpc4, Gabra1, Lgals3, Ndufa4l2, Gria3, P2ry12, Ppif, P2rx4, P2rx6, Slc7a3, Cnih2, Gria2, Gria1, Proca1, Slc6a5, P2rx3, Chrnb4, Slco6c1, Fabp3, Slc18a3, Slc13a3, Cacna1c, Slc5a11*
Positive Regulation of Developmental Process	*Oprm1, Rp1, Pdgfb, Nell1, Crabp2, S100a9, Iqgap3, Casp6, Agtr2, Pcp4, Hamp, Cxcr4, Gata3, Hmox1, Il1rap, H2afy, Mmd2, Rapgef2, Cyr61, Stk25, Mief1, Dll3, Lef1, Gal, Vegfb, Ascl1, Rt1-A1, Pdcl3, Adrb2, Slitrk3, Zfyve27, Cd34, Serpinb7, Trim32, Sema4d, Serpinb3, Cav3, Bbs4, Cobl, Fgfr3, Gcnt2, Usp2, Mst1, Il34, Adcyap1, Calca, Ccl24, P3h1, Fbxw8, Gpr21, Lrrtm3, Avil, Traf6, Pik3r1, Dixdc1, Flt1, Ltk, Lgals3, Cpne5, Ptpn5, Ak1, Ahi1, Mustn1, Tnfsf9, Cela1, Rgs14, Sirt2, Rnf112, Ddx56, Id2, Mapk14, Rgs6, Dmbt1*
Leukocyte Chemotaxis	*Edn3, C5ar2, Flt1, Ccl2, S100a8, Lgals3, Pdgfb, S100a9, Mst1, Padi2, Cxadr, Ptpro, Ccl7, Vegfb, Calca, Ccl24, Chga, Pla2g7, Spp1*
Growth	*Osbp, Pdgfb, Wfs1, Crabp2, Postn, Cxadr, N6amt1, Agtr2, Csnk2a1, Slc25a25, Hamp, Gata3, H2afy, Mt1, Sema3c, Large1, Cyr61, Gatm, Fbp1, Lef1, Gal, Slit3, Ppm1f, Adrb2, Zfyve27, Fgfr1op, Trim32, Sema4d, Smarca2, Tm4sf4, Cer1, Cav3, Cobl, Bbs4, Fgfr3, Mst1, Igsf10, P3h1, Gpr21, Fam107a, Lefty2, Camk2d, Apba2, Cda, Dclk1, Spp1, Cpne5, Ahi1, Mstn, Mustn1, Cela1, Raph1, Stat3, Rnf6, Col14a1, Mapk14, Mt2a, Prkar1a, Cirbp, Tmtc3, Cacna1c, Omg, Dmbt1*
Leukocyte Migration	*Edn3, Ccl2, S100a8, Pdgfb, S100a9, Mst1, Cxadr, Adora1, Ccl7, Ccl24, Calca, Gata3, Spp1, C5ar2, Flt1, Lgals3, Padi2, Itga4, Ptpro, P2ry12, Vegfb, Chga, Cd34, Pla2g7, Sele*
Cell Surface Receptor Signalling Pathway	*Edn3, Tspan1, Pdgfb, Grik1, Grik2, Efna1, Ltbp4, Snca, Pgam2, Adora1, Agtr2, Csnk2a1, Grin2b, Gata3, Psenen, Prkacb, Rapgef2, Gng7, C5ar2, Csnk1g1, Dll3, Grhl3, Ptpdc1, Ptpro, Ctdspl2, Vegfb, Ascl1, Trim32, Cav3, Bbs4, Gcnt2, Ccl2, Fgfr3, Gclc, Itga11, Grem2, Ccl7, Gpr21, Dusp15, Ubash3a, Dyrk2, Traf6, Dnaja3, Traf3, Nr1h3, Klf6, Dixdc1, Lgals3, Cidea, Mstn, Itga4, Acpp, P2rx4, Gpr35, P2rx6, Cnih2, P2rx3, Oprm1, Dedd, Adgrf5, Fermt2, Lrrc15, Ybx1, Cxcr4, Trim6, Hmox1, Il1rap, Sema3c, Shc3, Lag3, Cyr61, Nol3, Lef1, Padi2, Pigr, Lmbrd1, Slit3, Siglec1, Adrb2, Sdc1, Zfyve27, Grm7, Chsy1, Siah2, Sema4d, Pmepa1, Cer1, Ccl24, Lrrtm3, Gp1ba, Pik3r3, Pcsk5, Pik3r1, Ltk, Flt1, Ahi1, Birc6, Gria3, Tspan18, Cela1, Rcan2, Tspan17, Sirt2, Rgs14, Stat3, P2ry12, Cdh13, Rgs20, Rnf115, Gria2, Cdh17, Gria1, Mapk14, Perp*
Regulation of Transport	*Edn3, Tspan1, Grik1, S100a8, Pdgfb, Wfs1, S100a9, Snca, Postn, Adora1, Agtr2, Pacsin3, Grin2b, Spx, Gata3, Pik3c3, Rab27a, C5ar2, Scn2b, Kif5b, Ube2j1, Lypla1, Ctdspl2, Cd34, Rab15, Vamp3, Cav3, Fxyd3, Ccl2, Gnai3, Kcnj3, Fxyd7, Adcyap1, P3h1, Slc11a1, Pfn2, Dyrk2, Traf6, Slc30a8, Nr1h3, Hcn1, Trpc4, Rab8b, Lgals3, Ptpn5, Ak1, Cidea, Arfip1, Ppif, P2rx4, Ifi27, Cnih2, Cacna1c, Oprm1, Kcnh1, Kcnab2, Fam3d, Kcnip4, Pcp4, Hamp, Cxcr4, Trim6, Hmox1, Il1rap, Ahnak, Nol3, Pfkl, Mief1, Rph3al, Gal, Lmbrd1, Dnajc27, Sdc1, Adrb2, Chga, Clic3, Grm7, Vip, Ston1, Ffar3, Calca, Nr1d1, C1qtnf3, Camk2d, Htr3a, Kcne5, Pik3r3, Htr3b, Pik3r1, Elmod1, Lrsam1, Ahi1, Anxa2, P2ry12, Cdh13, Rgs20, Pde2a, Mapk14, Slc18a1, Sele*

Table 8.2c. Biological Processes Gene Ontology Gene List

Biological Processes GO Description	GO Group Gene List
Regulation of Heart Contraction	*Cav3, Edn3, Gnai3, Scn2b, Ffar3, Cxadr, Adora1, Calca, P2rx4, Chga, Agtr2, Adrb2, Spx, Gaa, Camk2d, Cacna1c, Kcne5 Pik3r1*
Renal System Process	*Pdgfb, Wfs1, Aqp4, Npr3, Ptpro, Adora1, Agtr2, Adrb2, Spx, Cd34, Chrnb4, Hsd11b2, Cacna1c, Pcsk5*
Positive Regulation of Multicellular Organismal Process	*Oprm1, Edn3, Pdgfb, Zc3hav1, Nell1, Crabp2, S100a9, Iqgap3, Postn, Casp6, Agtr2, Pcp4, Hamp, Cxcr4, Trim6, Gata3, Hmox1, Il1rap, H2afy, Mmd2, Rapgef2, Cyr61, Stk25, Pdpn, Dll3, Lef1, Gal, Ppm1f, Vegfb, Ascl1, Rt1-A1, Pdcl3, Chga, Adrb2, Slitrk3, Zfyve27, Cd34, Serpinb7, Trim32, Serpinb3, Sema4d, Vip, Bbs4, Cobl, Gcnt2, Ccl2, Fgfr3, Ffar3, Usp2, Mst1, Il34, Adcyap1, Calca, Ccl24, P3h1, Slc11a1, Fbxw8, Gpr21, C1qtnf3, Lrrtm3, Camk2d, Avil, Traf6, Pik3r1, Spp1, Dixdc1, Flt1, Card9, Ltk, Rab8b, Lgals3, Cpne5, Ptpn5, Ak1, Ahi1, Mustn1, Polr3c, Tnfsf9, Cela1, Rgs14, Sirt2, Rnf112, Ddx56, Id2, Mapk14, P2rx3, Rgs6, Chrnb4*
Taxis	*Edn3, Ccl2, Pdgfb, S100a8, Efna1, S100a9, Mst1, Cxadr, Ccl7, Calca, Ccl24, Cxcr4, Gata3, Etv1, Sema3c, Etv4, Spp1, Cyr61, C5ar2, Flt1, Stx3, Kif5b, Lgals3, Kif5a, Padi2, Lef1, Ptpro, Slit3, Ppm1f, Vegfb, Cdh13, Chga, Id2, Pla2g7, Cntn4, Sema4d, Gfra3*
Myeloid Leukocyte Migration	*Edn3, C5ar2, Flt1, Ccl2, S100a8, Lgals3, Pdgfb, S100a9, Cxadr, Ptpro, Ccl7, Vegfb, Calca, Ccl24, Chga, Pla2g7, Spp1*

8.4 Gene lists for Molecular Function Gene Ontology Group

Table 8.3. Molecular Function Gene Ontology Gene List

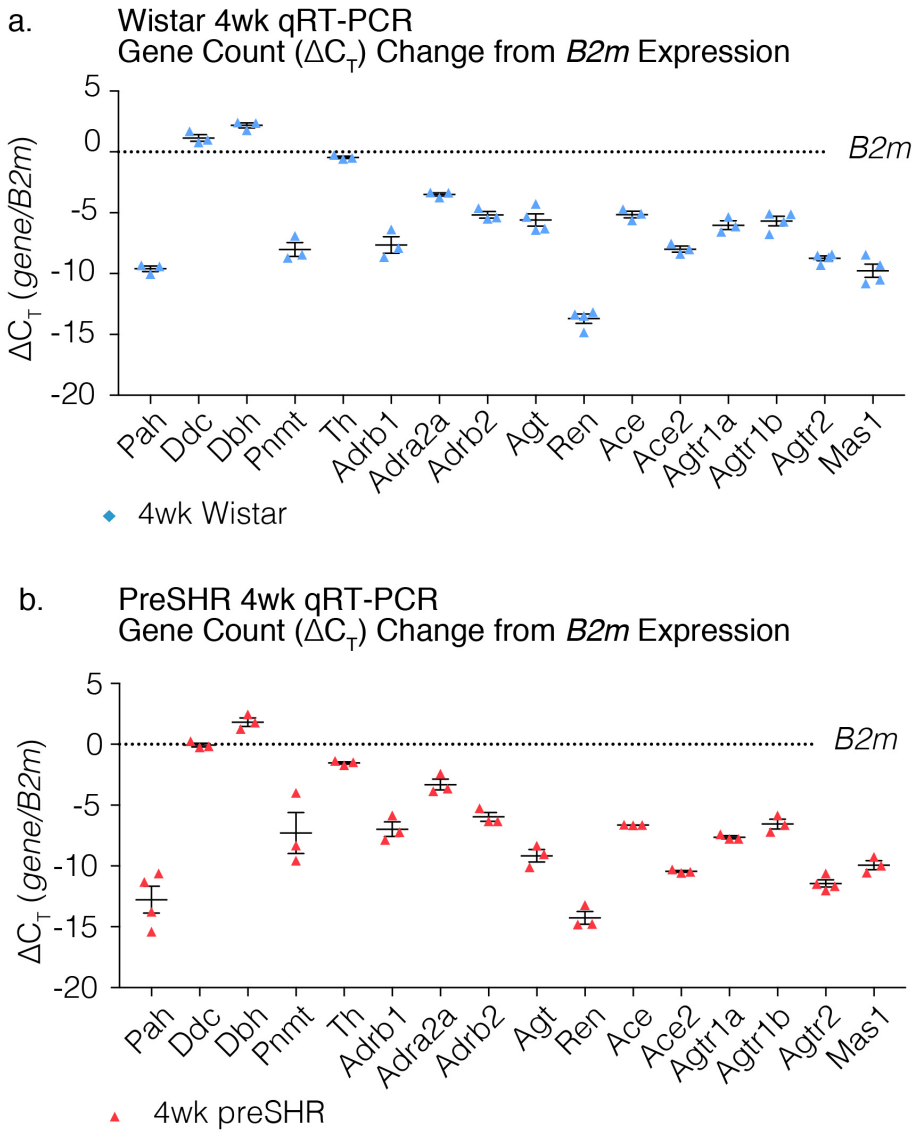
Molecular Function GO Description	GO Group Gene List
Excitatory Extracellular Ligand-Gated Ion Channel Activity	*Glrb, Grik1, Grik2, Gria3, P2rx4, P2rx6, Gria2, Grin2b, Gria1, P2rx3, Chrnb4, Htr3a, Htr3b*
Extracellular Ligand-Gated Ion Channel Activity	*Gabra2, Glrb, Gabra1, Grik1, Grik2, Gria3, P2rx4, P2rx6, Grin2b, Gria2, Gria1, P2rx3, Chrnb4, Htr3a, Htr3b*
Phosphoric Ester Hydrolase Activity	*Styxl1, Sgpp2, Enpp3, Pde11a, Pgam2, Psph, Adora1, Pde6b, Mtmr1, Smpdl3b, Dusp15, Hmox1, Phospho1, Ptpn7, Pld3, Pfkl, Ptprn2, Ptpn5, Pgap1, Pdxp, Fbp1, Lpin2, Gdpd3, Ptpro, Ptpdc1, Tmem55b, Acpp, Ctdspl2, Ppm1f, Napepld, Pde2a Ptp4a1, Plcxd2*
Ligand-Gated Ion Channel Activity	*Hcn1, Gabra2, Glrb, Gabra1, Grik1, Grik2, Gria3, Kcnj3, P2rx4, P2rx6, Grin2b, Gria2, Gria1, P2rx3, Chrnb4, Htr3a, Htr3b*
Ligand-Gated Channel Activity	*Hcn1, Gabra2, Glrb, Gabra1, Grik1, Grik2, Gria3, Kcnj3, P2rx4, P2rx6, Grin2b, Gria2, Gria1, P2rx3, Chrnb4, Htr3a, Htr3b*
Identical Protein Binding	*Kcnh1, S100a6, Pdgfb, Grik1, Grik2, Nell1, Ide, Snca, Prkg2, Psph, Cxadr, Tpd52, Hmox1, Ceacam16, Dpp4, Mtus2, Aadat, Nol3, Pfkl, Stk25, Mief1, Fbp1, Pdxp, Qdpr, Mtpap, Cst3, Dynlt3, Ptpro, Vegfb, Ascl1, Adrb2, Mapk4, Fgfr1op, Grm7 Znhit6, Cer1, Ralyl, Tyrp1, Usp2, Snx2, Daam1, Grem2, Calca, Aldh1a1, Bloc1s6, Slc11a1, C1qtnf3, Tef, Camk2d, Aldh4a1, Cda, Pafah1b2, Slc30a8, Traf6, Hcn1, Shmt2, Flt1, Card9, Gsta4, Yipf6, Ahi1, Cidea, Mstn, Npr3, Arfip1, S100a13, Acpp, Stat3, Cdh13, P2rx6, Gria2, Pde2a, Gria1, Tdg, Omg, Rnf40, Gca, Cbs*
Anion Binding	*Aadat, Ddc, Glrb, Shmt2, Gclc, Stx3, S100a8, Grik1, Snx14, Accs, Crabp2, Snca, S100a9, Egln3, P3h1, Mthfd2, Ptgds, Grin2b, Cd34, Grm7, Fabp3, Rapgef2, Adcy10, Tph1, Sele, Cbs*
Gated Channel Activity	*Oprm1, Kcnh1, Grik1, Kcnab2, Grik2, Kcnj3, Kcnip4, Grin2b, Kcne5, Htr3a, Piezo1, Htr3b, Hcn1, Glrb, Gabra2, Gabra1, Scn2b, Gria3, P2rx4, P2rx6, Gria2, Clic3, Gria1, Grm7, P2rx3, Chrnb4, Cacna1c*
Substrate-Specific Channel Activity	*Kcnh1, Oprm1, Fxyd3, Kcnab2, Grik1, Grik2, Aqp4, Kcnj3, Kcnip4, Fxyd7, Grin2b, Kcne5, Htr3a, Piezo1, Htr3b, Hcn1, Glrb Gabra2, Trpc4, Gabra1, Scn2b, Pdpn, Gria3, P2rx4, P2rx6, Clic3, Gria2, Gria1, Grm7, P2rx3, Chrnb4, Cacna1c*
Carboxylic Acid Binding	*Ddc, Glrb, Shmt2, Stx3, Gclc, Grik1, S100a8, Snca, S100a9, Crabp2, Egln3, P3h1, Grin2b, Ptgds, Grm7, Fabp3, Tph1, Sele*

8.5 Gene lists for KEGG Functional Enrichment Analysis

Table 8.4. KEGG Functional Enrichment Analysis Gene List

KEGG Description	KEGG Function Enrichment Groups Gene List
Retrograde Endocannabinoid Signalling	*Gabra2, Gnai3, Gabra1, Napepld, Gria2, Gria1, Mapk14, Gria3, Prkacb, Gnb3, Cacna1c, Kcnj3, Daglb, Gng7*
Dopaminergic Synapse	*Ddc, Gnai3, Kif5b, Kif5a, Gria3, Kcnj3, Gria2, Grin2b, Gria1, Mapk14, Camk2d, Prkacb, Gnb3, Slc18a1, Cacna1c, Gng7*
Metabolic Pathways	*Pnlip, Alg1, Sat2, Pgam2, Psph, Auh, Glb1, Mthfd2, St6galnac3, Agpat5, Ptges, Pik3c3, St3gal6, Phospho1, Pld3, Aadat, Ddc, Hmgcll1, Gatm, Pfkl, Cyp1a1, Suclg2, Pgap1, Fbp1, Qdpr, Pdxp, Cbr3, Lpcat2, Lpin2, Atp6v1c1, Pank2, Ptgds, Rfk, Aldh1b1, Rrm2, Pla2g7, Gaa, Chsy1, Tph1, Tyrp1, Gclc, Gcnt2, Galnt6, Enpp3, Atp6v1b2, Gmppb, Aldh1a1, Cbr1, Mtmr1, Hpse2, Fut4, Galnt16, Aldh4a1, Cda, Pafah1b2, Galnt18, Acaa1a, Bdh1, Acaa1b, Allc, Shmt2, Ndufa4l2, Upb1, Ak1, Mgat4c, Ak4, Uap1l1, Polr3c, Idnk, Rdh12, Ndufv3, Amdhd1, Ahcyl2, Cbs*
Circadian Entrainment	*Gnai3, Gria3, Prkg2, Kcnj3, Gria2, Grin2b, Gria1, Camk2d, Gucy1a3, Gnb3, Prkacb, Cacna1c, Adcy10, Gng7*

8.6 ΔC_T values for qRT-PCR in Rat Stellate Ganglia



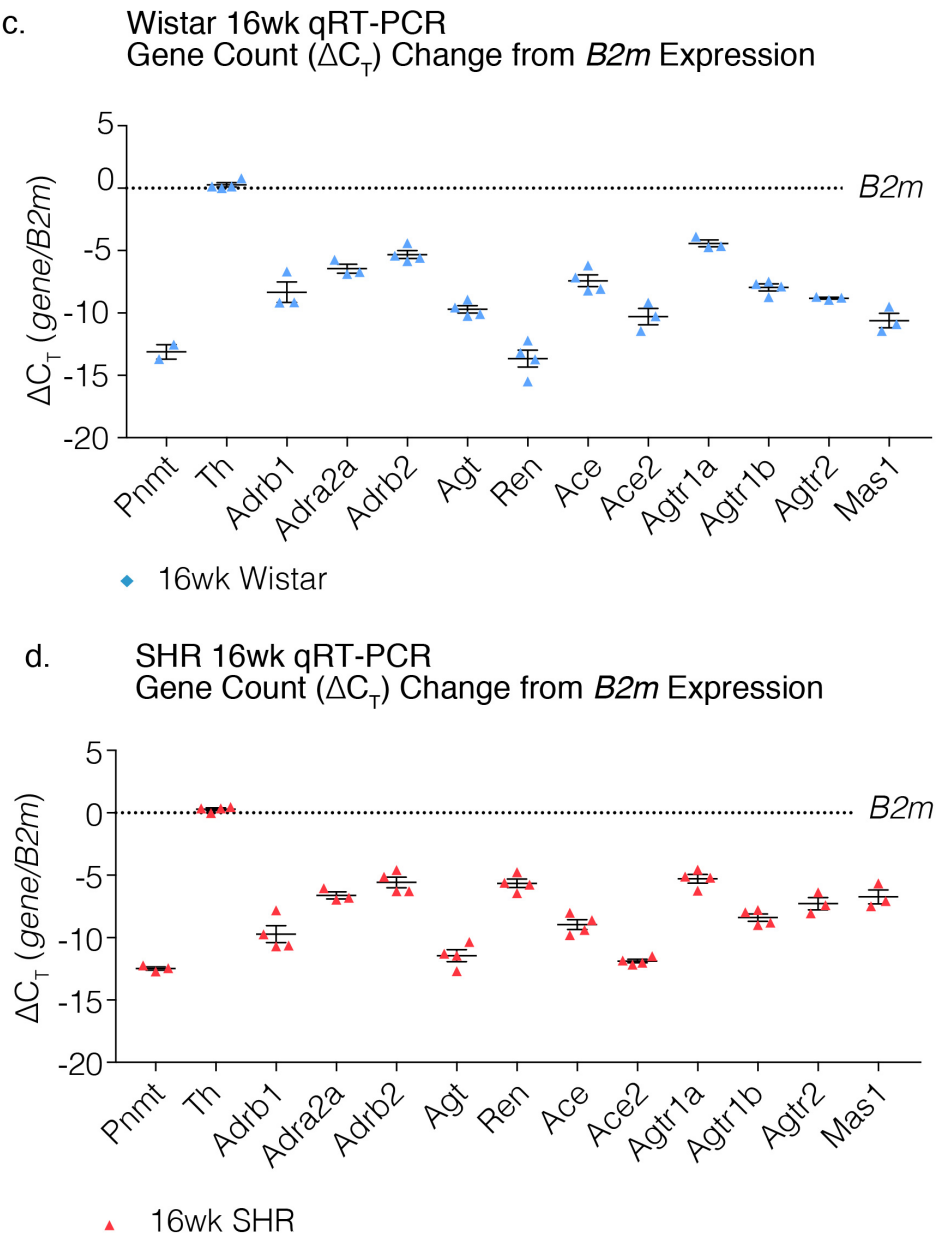


Figure 8.6. ΔC$_T$ values for qRT-PCR in Rat Stellate Ganglia.
Change in expression between *B2m* and genes of interest are shown for four-week Wistar (a), four-week preSHR (b), 16-wk Wistar (c) and 16-wk SHR (d).